TARGETING METABOLIC VULNERABILITIES IN BREAST CANCER SUBTYPES

By

Martin Peter Ogrodzinski

A DISSERTATION

Submitted to
Michigan State University
in partial fulfillment of the requirements
for the degree of

Physiology – Doctor of Philosophy

2020

ABSTRACT

TARGETING METABOLIC VULNERABILITIES IN BREAST CANCER SUBTYPES

By

Martin Peter Ogrodzinski

Breast cancer is a highly prevalent and deadly disease. Globally, it is the most diagnosed cancer in women and is responsible for the most cancer-related deaths among women. Breast cancer is also a remarkably heterogeneous disease, with clear variability in clinical parameters including histological presentation, receptor status, and gene expression patterns that differ between patients. A significant amount of effort has been spent characterizing breast cancer into subtypes, with the main goal of improving patient outcomes by: 1) designing targeted therapies, and 2) improving our ability to determine patient prognosis. While scientists have made significant strides in meeting these goals, we still lack targeted therapies for some subtypes of breast cancer, and current therapies often fail to provide a lasting cure. Thus, additional research is needed to improve patient care. One promising area in breast cancer research is cancer metabolism. Using metabolism as a therapeutic target is rapidly gaining traction, as it is now widely appreciated that cancer cells exhibit significant differences in metabolism compared to normal cells. The primary goal of this dissertation is to study the metabolism of distinct subtypes of breast cancer and identify metabolic vulnerabilities that can be used to effectively treat each subtype.

This thesis will begin with a review of current classification strategies for breast cancer subtypes and knowledge regarding subtype-specific metabolism. It will also

consider modern techniques for targeting breast cancer metabolism for therapeutic benefit. Breast cancer heterogeneity and metabolism are investigated using cell lines and tumors derived from the MMTV-Myc mouse model, which mimics the complexity observed in human disease. Cell lines derived from two histologically defined subtypes, epithelial-mesenchymal transition (EMT) and papillary, are used to establish clear metabolic profiles for each subtype. Metabolic vulnerabilities are identified in glutathione biosynthesis and the tricarboxylic acid cycle in the EMT subtype and nucleotide biosynthesis is determined to be a metabolic weakness in the papillary subtype. It is further shown that pharmacologically targeting each of these metabolic pathways has the greatest effect on reducing proliferation when used against the vulnerable subtype. These *in vitro* findings are then expanded upon by integrating genomic and metabolomic data acquired from *in vivo* tumors. *In vivo* experiments reveal that the EMT and papillary tumors prefer parallel pathways to generate nucleotides, with the EMT subtype preferring to salvage nucleotides while the papillary subtype prefers to produce nucleotides *de novo.* CRISPR/Cas9 gene editing is used to functionally characterize the metabolic effects of targeting nucleotide salvage and *de novo* biosynthesis in the EMT and papillary subtypes, and determine that targeting the preferred pathway of each subtype is most effective at slowing tumor growth.

Overall, this work demonstrates the power of using metabolism as a therapeutic target of breast cancer, and further shows that metabolic vulnerabilities specific to individual subtypes can be used effectively to guide personalized medicine.

This work is dedicated to:
My best friend and greatest supporter: Allie Ogrodzinski

ACKNOWLEDGMENTS

The work shown within this dissertation would not have been possible without an extended network of people who have helped shape me as a person and guided me along the path of growing as a scientist. There are too many individuals to name everyone, but I am nonetheless grateful to each of you for your role in making me the person I am today. I do want to specifically thank my incredibly patient and supportive wife, Allie. I could not have made it this far without your love and support. Thank you for sharing this journey with me.

Thank you to my family, especially my parents Martin and April, who have supported me every step of the way. Thank you to my grandparents, aunts, uncles, cousins, nieces, nephews, and in-laws –there are too many to name, but thank you all for showing me the many faces of success and happiness. Also, thank you to my siblings – Amanda, Emily, Allison, Ana, Elizabeth, Erica, Alexis, Yvonne, Tim, Sam, Joey, and Louis. You have all been so helpful and supportive, I am grateful to each of you. To my brother Sam, having you around these past few years has helped me in countless ways. I look forward to witnessing the rest of your journey as a fellow Spartan.

At Michigan State University I have had the opportunity to learn from a wide range of faculty and students, all of whom have left their marks on my life and research. Most notably I would like to recognize my mentor Dr. Sophia Lunt. Thank you for all your time, patience, and support over the years. From the very beginning you helped me define my passion for research and I am extremely grateful for the opportunities you have given me throughout the start of my scientific career. I am confident that the skills and knowledge I

have gained working with you will help me succeed as a future physician scientist. I also want to thank all the past and present members of the Lunt lab for their support over the years – especially Deanna Broadwater, Elliot Ensink, Dr. Hyllana Medeiros, Dr. Shao Thing Teoh, and Dr. Lei Yu. I could not have asked to be part of a better team. I particularly want to acknowledge Shao, who is always willing to spend time talking about science and has seemingly endless patience when it comes to troubleshooting code or explaining his analytical techniques. I would also like to thank two former members of the Andrechek lab, Dr. Jon Rennhack and Dr. Dan Hollern, for encouraging me to pursue research and providing support over the years.

I am also grateful to have had the opportunity to collaborate on many projects with several labs at Michigan State and other institutions. I am thankful to all the collaborators I have worked with over the years. In particular, I would like to thank Dr. Eran Andrechek, Dr. Paul-Joseph Aspuria, and Dr. Sriram Venneti for the opportunity to contribute to work in their labs. Working with so many different people has been very rewarding, and I am grateful to have been a part of so many different stories.

I also want to give a special thanks to Lauren Aitch and the Aitch foundation for funding my research. I am so honored to have had the opportunity to work with you and your foundation. I would also like to thank the core facilities at Michigan State, without whom much of my work would not have been possible. This includes everyone at campus animal resources, the investigative histopathology laboratory, and the mass spectrometry and metabolomics core.

To the members of my committee: Dr. Eran Andrechek, Dr. Dan Jones, Dr. Karl Olson, and Dr. Hua Xiao – thank you for your valuable feedback and for all the time spent

listening to me talk about my work. I would also like to thank the Physiology program, the College of Human Medicine, and Spectrum Health for their support, funding, and for providing me with the opportunity to earn my degree at Michigan State University.

TABLE OF CONTENTS

LIST OF TABLES

LIST OF FIGURES

KEY TO ABBREVIATIONS

5FU – 5-Fluorouracil

ACL– ATP citrate lyase

ADP – Adenosine diphosphate

AKGDH – Alpha-ketoglutarate dehydrogenase

AKT – Protein kinase B

AMPK – AMP-activated protein kinase

APRT – Adenine phosphoribosyltransferase

ASCT2 – Alanine serine cysteine-preferring transporter 2

ASS – Argininosuccinate synthetase

ATP – Adenosine triphosphate

BMI – Body mass index

BSO – Buthionine sulfoximine

CAF – Cancer associated fibroblasts

CBZ - Carboxybenzyl

cGPD – Cytosolic Glycerol-3-phosphate dehydrogenase 1

CoA – Coenzyme A

CPT1 – Carnitine palmitoyltransferase-1

CTP – Cytidine triphosphate

DAB – Diaminobenzidine

dADP – Deoxyadenosine diphosphate

dAMP – Deoxyadenosine monophosphate

dATP – Deoxyadenosine triphosphate

dCDP – Deoxycytidine diphosphate

dCMP – Deoxycytidine monophosphate

dCTP – Deoxycytidine triphosphate

dGDP – Deoxyguanosine diphosphate

dGMP – Deoxyguanosine monophosphate

dGTP – Deoxyguanosine triphosphate

dUTP – Deoxyuridine triphosphate

DHAP – Dihydroxyacetone phosphate

DMEM – Dulbecco's modified Eagle's Medium

DMSO – Dimethyl sulfoxide

dTDP – Deoxythymidine diphosphate

dTMP – Deoxythymidine monophosphate

dTTP – Deoxythymidine triphosphate

E – Eosin

ECAR – Extracellular acidification rate

EGFR – Epidermal growth factor receptor

EMT – Epithelial-mesenchymal transition

ENT – Equilibrative nucleoside transporter

ER – Estrogen receptor

ESI – Electrospray ionization

ETC – Electron transport chain

FAD – Flavin adenine dinucleotide

FASN – Fatty acid synthase

FBP – Fructose bisphosphate

FDR – False discovery rate

FTSEC – Fallopian tube secretory epithelial cells

G3P – Glycerol-3-phosphate

GCL – Glutamate-cysteine ligase

GCLC – GCL catalytic subunit

GCLM – GCL modifier subunit

GEO – Gene expression omnibus

GMP – Guanosine monophosphate

GPC – Glycerophosphocholine

GS – Glutamine synthetase

GSEA – Gene set enrichment analysis

GSR – Glutathione reductase

GSS – Glutathione synthetase

GTP – Guanosine triphosphate

H – Hematoxylin

HER2 – Human epidermal growth factor receptor 2

HFD – High fat diet

HGSC – High grade serous ovarian cancer

HIF – Hypoxia-inducible factor

IBC – Inflammatory breast cancer

IDP – Inosine diphosphate

IGF-1 – Insulin-like growth factor-1

IHC – Immunohistochemical

IMP – Inosine monophosphate

KM – Kaplan-Meier

KO – Knock out

LC-MS/MS – Liquid chromatography-tandem mass spectrometry

LDH – Lactate dehydrogenase

MCT – Monocarboxylate transporter

mGPD – Mitochondrial G3P dehydrogenase 2

ml - Milliliter

mM – Millimolar

MRM – Multiple reaction monitoring

MTHFD1L – Methylenetetrahydrofolate dehydrogenase 1-like

MTHFD2 – Methylenetetrahydrofolate dehydrogenase 2

mTOR – Mammalian target of rapamycin

MTX – Methotrexate

N – Sample-size

NAD – Nicotinamide adenine dinucleotide oxidized

NADH – Nicotinamide adenine dinucleotide reduced

NADP – Nicotinamide adenine dinucleotide phosphate oxidized

NADPH – Nicotinamide adenine dinucleotide phosphate reduced

nM – Nanomolar

NMR – Nuclear magnetic resonance

NTP – Nucleoside triphosphate

OCR – Oxygen consumption rate

OTC – Ornithine transcarbamylase

PAM50 – Prediction analysis of microarray 50

pAMPK – Phosphorylated AMPK

Pcho – Phosphocholine

PCR – Polymerase chain reaction

PDH – Pyruvate dehydrogenase

PDX – Patient derived xenograft

PHGDH – Phosphoglycerate dehydrogenase

PI3K – Phosphatidylinositol 3-kinase

PKM1 – Pyruvate kinase M1

PKM2 – Pyruvate kinase M2

PPAT – Phosphoribosyl pyrophosphate amidotransferase

PPP – Pentose phosphate pathway

PR – Progesterone receptor

PRPP – Phosphoribosyl pyrophosphate

pS6K – S6 kinase

PSAT1 – Phosphoserine aminotransferase 1

PSC – Puromycin-resistant scramble control

PSPH – Phosphoserine phosphatase

PtdCho – Phosphatidylcholine

PVDF – Polyvinylidene fluoride

qRT-PCR – Quantitative reverse transcription polymerase chain reaction

RFS – Relapse free survival

ROS – Reactive oxygen species

RPMI – Roswell Park Memorial Institute medium

RRM2 – Ribonucleotide reductase M2

S – Supplementary

S6K – S6 kinase

SAM – S-adenosylmethionine

SHMT1 – Serine hydroxymethyltransferase 1

SHMT2 – Serine hydroxymethyltransferase 2

TAC – Transcriptome analysis console

TCA – Tricarboxylic acid

TIDE – Tracking of indels by decomposition

TNBC – Triple negative breast cancer

TUNEL – Terminal deoxynucleotidyl transferase dUTP nick end labeling

TYMS – Thymidylate synthase

UDP – Uridine diphosphate

µl – Microliter

µM - Micromolar

UMP – Uridine monophosphate

UTP – Uridine triphosphate

XMP – Xanthosine monophosphat

CHAPTER 1.

DECIPHERING METABOLIC REWIRING IN BREAST CANCER SUBTYPES

1.1 PREFACE

This chapter is a modified version of a previously published article:

> Ogrodzinski, M. P., Bernard, J. J., & Lunt, S. Y. (2017). Deciphering metabolic rewiring in breast cancer subtypes. *Translational Research*, *189*, 105-122.

1.2 Abstract

Metabolic reprogramming, an emerging hallmark of cancer, is observed in breast cancer. Breast cancer cells rewire their cellular metabolism to meet the demands of survival, proliferation, and invasion. However, breast cancer is a heterogeneous disease, and metabolic rewiring is not uniform. Each subtype of breast cancer displays distinct metabolic alterations. Here, we focus on unique metabolic reprogramming associated with subtypes of breast cancer, as well as common features. Therapeutic opportunities based on subtype-specific metabolic alterations are also discussed. Through this discussion, we aim to provide insight into subtype-specific metabolic rewiring and vulnerabilities that have the potential to better guide therapy and improve outcomes for patients.

1.3 Introduction

Breast cancer remains the leading cause of cancer deaths for women worldwide, and incidence rates are increasing [1]. The heterogeneity of breast cancers makes treatment challenging, as therapies must be tailored to the context of each patient's disease. Effective personalized therapy can only be achieved by considering the clinical manifestations as well as the underlying biology. Current therapeutic strategies largely do not leverage the metabolic reprogramming of breast cancers. Treatment guidelines for women with localized disease in stages I-III focus on surgical removal (breast conserving surgery or mastectomy) and post-surgical radiation, when not contraindicated. Most patients diagnosed with advanced stage III or IV breast cancers undergo treatment regimens including chemotherapy and/or radiation therapy [2,3]. In general, patients with estrogen receptor positive (ER+) breast cancer receive adjuvant endocrine therapy in

addition to chemotherapy in advanced cases; patients with human epidermal growth factor receptor 2 positive (HER2+) breast cancer often receive anti-HER2 therapy combined with chemotherapy; and patients with triple negative breast cancer (TNBC) receive chemotherapy [3]. Many chemotherapy regimens are used in the treatment of breast cancer, and commonly include combinations of cyclophosphamide, methotrexate, 5-fluorouracil, taxanes, and/or anthracyclines [4]. While these compounds have helped many patients, recurrence rates are still high [5], and tumors often develop therapeutic resistance [6]. Therefore, targeting breast cancer-specific metabolic vulnerabilities may be a valuable addition to the clinicians' toolbox for treating patients with breast cancer as an adjuvant therapy, a targeted first-line therapy for triple negative breast cancers, or a second-line therapy in tumors that develop resistance.

Cancer cells rewire their metabolism to support survival, proliferation, and invasion [7-9]. Metabolic rewiring varies significantly between cancers based on genetics and environment [10-12], and may manifest through upregulation of metabolic pathways or through downstream effects of oncogenes [13,14]. A well-known example of metabolic rewiring in cancer is the Warburg effect: while normal differentiated cells increase glycolysis in response to certain environmental cues such as hypoxia, many cancer cells upregulate glycolysis and lactate fermentation regardless of oxygen availability [15]. Cancer cells can also upregulate the tricarboxylic acid (TCA) cycle in the mitochondria to support both energy generation and macromolecule synthesis. The TCA cycle is replenished through upregulated anaplerosis using various carbon sources including glutamine, pyruvate, and branched chain amino acids [16]. Despite the metabolic heterogeneity within and between cancers, most alterations in metabolism support

pathways involving bioenergetics, biosynthesis, and redox balance [10]. These metabolic changes are induced both by alterations in signaling pathways and the tumor microenvironment. Signaling pathways that impact cancer metabolism include phosphatidylinositol 3-kinase (PI3K), Protein Kinase B (Akt), mammalian target of rapamycin (mTOR), hypoxia-inducible factor-1 (HIF-1), sterol regulatory element binding protein, c-Myc, Kras, and p53 [8]. Interestingly, several of these signaling pathways are in turn regulated by metabolic feedback from metabolites including amino acids, fatty acids, α-ketoglutarate, and ATP [17]. Altered metabolite levels in cancer also influence epigenetic modifications. Metabolites such as acetyl-CoA, succinate, fumarate, α-ketoglutarate, and S-adenosylmethionine (SAM) have been shown to participate in epigenetic reprogramming and regulate gene expression [18]. Cellular metabolism plays an integral role in numerous biological processes, and investigation into cancer metabolism can greatly enhance our understanding of cancer biology.

Metabolomics has improved our current understanding of cancer metabolism [19-21]. Metabolomics is the analysis of metabolite levels in biological systems, usually by mass spectrometry or nuclear magnetic resonance (NMR), and is primarily used to investigate three main areas. First, metabolomics has the potential to identify biomarkers for diagnosis and/or monitoring of disease progression [22,23]. While significant validation will be required before clinical application, metabolomic analysis of patient plasma samples may enable the diagnosis of breast cancer and even subtype differentiation without performing a biopsy [24-26]. Second, metabolomics enables the discovery of oncometabolites, which are metabolites that accumulate significantly in tumors due to a specific mutation. Oncometabolites can serve as biomarkers, but also contribute to the

development of malignancy, providing a mechanistic understanding of tumor biology [27]. Oncometabolites include D-2-hydroxyglutarate, which accumulates in tumors with mutant isocitrate dehydrogenase 1 or 2 [28], as well as fumarate and succinate, which accumulate in tumors with mutations in fumarate hydratase and/or succinate dehydrogenase [29]. Third, metabolomics enables the identification of metabolic pathways uniquely upregulated in cancers. One way to accomplish this is through flux studies that measure the incorporation of stable isotope tracers, such as ^{13}C-glucose, into metabolic pathways [30,31]. Upregulated metabolic pathways could represent metabolic vulnerabilities and serve as novel therapeutic targets, or explain mechanisms of drug sensitivity or resistance in cancer [22,32]. Metabolomics will continue to advance our understanding of various metabolic phenotypes in cancers, enabling novel diagnostic and therapeutic approaches.

In this review, we focus on the metabolic variations between breast cancer subtypes. We begin with an overview of the methods for breast cancer classification. Next, we focus on known metabolic differences in each breast cancer subtype. We further discuss the metabolic impacts of hypoxia, a common feature among breast cancer subtypes. We also consider the influence of obesity and diabetes as co-morbidities influencing breast cancer development and progression. Finally, we discuss approaches for targeting metabolism in breast cancer.

1.4 Merging traditional breast cancer subtypes with metabolic profiles

The heterogeneity in breast cancer has led to the development of several classification systems. Breast cancer is commonly classified into subtypes by the following: 1) morphological criteria (e.g., ductal, lobular, invasive, or in situ); 2) expression

of receptors (e.g., ER+, HER2, or triple negative); and 3) intrinsic subtype (e.g., luminal, basal-like, claudin-low) [33,34]. Clinically, breast cancers are commonly categorized by expression of three receptors: the estrogen receptor (ER), progesterone receptor (PR), and human epidermal growth factor receptor 2 (HER2 .[35]. This classification system can help direct targeted treatment regimens, such as endocrine therapy for ER+ breast cancer. Gene expression profiling has enabled further sub-classification of breast cancer into five intrinsic subtypes: luminal A, luminal B, HER2 over-expressing, basal-like, and normal-like [34]. Several methods have been proposed by different groups for characterizing intrinsic subtypes [36,37], culminating in the development of the Prediction Analysis of Microarray 50 (PAM50) [38], a set of 50 genes that is weighted together with clinical variables in a FDA-approved test to categorize patients into intrinsic subtypes, assess a patient's risk of distant recurrence, and direct therapy [39]. While no classification system perfectly captures the full heterogeneity of breast cancers, they provide valuable insights into the underlying biology of breast cancers to help guide treatment and predict the chance of metastasis. Taking subtype-specific metabolic vulnerabilities into account may further improve patient outcomes.

Breast cancer subtypes possess distinct metabolic features that may be exploited for the development of subtype-specific drugs with fewer side effects (summarized in **Table 1**). To begin deciphering the metabolic heterogeneity in breast cancer, we focus on the three major subtypes of breast cancer by receptor status: ER+ breast cancer, HER2+ breast cancer, and triple negative breast cancer. We also include a discussion of inflammatory breast cancer, a rare yet deadly subtype of breast cancer. We first discuss TNBC, the least common yet often the most aggressive form of breast cancer occurring

frequently in younger women. Understanding how cancer subtypes differ metabolically may enable the development of new treatment approaches, improve our understanding of the mechanisms by which drug resistance occurs, and provide new methods for early diagnosis and monitoring of breast cancer [23,32].

1.5 Triple-negative breast cancer

Triple-negative breast cancers (TNBCs) account for ~12% of all breast cancers [40]. The majority of TNBCs can be classified into the basal-like intrinsic subtype, which generally lacks ER and HER2 and express genes observed in basal epithelial cells of the normal breast [34,36-38]. Both triple-negative and basal-like breast cancers occur proportionally more often in younger patients and have worse clinical outcomes [41]. Targeted therapies are currently unavailable due to the lack of ER, PR, and HER2 expression. Thus, developing new therapeutic targets based on metabolic vulnerabilities is especially promising for improving TNBC patient outcomes.

TNBCs generally display the Warburg effect [42], having elevated glucose uptake [43,44] and increased lactate secretion along with upregulated expression of glycolytic genes relative to other breast cancer subtypes [45]. The Warburg effect may support proliferation by increasing the availability of glycolytic intermediates for biosynthetic pathways, and lactate production is required to balance the NAD/NADH ratio to sustain glycolysis [15]. Consistent with the Warburg effect, TNBCs exhibit increased glucose and lactate transporters [46,47] and lactate dehydrogenase (LDH) [48], which generates lactate from the glycolytic end-product pyruvate. The glycolytic rates of TNBCs correlate with proliferation rates and tumor aggressiveness [12]. Upregulated glucose metabolism in TNBCs is due in part to amplification and/or overexpression of the transcription factor

c-Myc (hereafter referred to as Myc), which is overexpressed in basal-like subtypes with lower expression in luminal and HER2+ subtypes [49]. Myc directly activates the glucose transporter GLUT1, as well as genes involved in glycolysis [50] and the lactate dehydrogenase-A gene [51]. Myc has also been shown to upregulate glycolysis by repressing expression of thioredoxin-interacting protein, a potent inhibitor of glucose metabolism.[52] Epidermal growth factor receptor (EGFR) overexpression, frequently observed in TNBC patients and linked with poor clinical outcome [53,54], has also been linked with upregulated aerobic glycolysis in TNBC [55].

Deregulation of Myc also upregulates glutamine metabolism [56], which is increased in TNBCs. Glutamine is a non-essential amino acid that contributes to several metabolic pathways including protein synthesis, nucleotide biosynthesis, and the TCA cycle. Myc upregulates glutamine transporters and the expression of mitochondrial glutaminase, which converts glutamine to glutamate for use in ATP generation and glutathione synthesis [57,58]. Glutaminase expression has been associated with poor prognosis in triple negative breast cancer [59].

Many cancer cells, including TNBCs, display reliance on glutamine, termed glutamine addiction [60,61]. The importance of glutamine in cancer is likely due to its ability to participate in a wide variety of metabolic processes, including protein and lipid biosynthesis, nitrogen donation, glutathione generation, and energy production. Increased glutaminolysis, the process of catabolizing glutamine to fuel metabolic pathways such as the TCA cycle, is also often observed in cancers [62,63]. Breast cancer subtypes express variable levels of enzymes involved in glutaminolysis [64]. Compared to other subtypes, TNBCs display glutamine addiction and increased glutaminolysis, and

are therefore sensitive to glutamine depletion [65]. The glutamine dependence of some TNBCs may be due to the lack of glutamine synthetase (GS), the enzyme that synthesizes glutamine; co-culture with luminal cells that express GS increases the viability of glutamine-dependent basal-like breast cancer cells in glutamine-free media [65]. Most basal-like and claudin-low TNBC cell lines consume more glutamine than luminal breast cancer cell lines and proliferating nontumorigenic cells, but only a subset of the TNBC cell lines are glutamine auxotrophs [66]. Glutamine starvation decreases the abundance of reduced glutathione and NADPH while increasing oxidized glutathione and glucose uptake in glutamine addicted cell lines; these changes are not observed in the ER+ MCF7 breast cancer cell line, where glutamine starvation decreases reduced glutathione levels without affecting NADPH, oxidized glutathione, or glucose uptake [67]. These results suggest that TNBC cell lines display altered glutamine metabolism compared to ER+ breast cancer cell lines. However, caution should be exercised before translating these results to the *in vivo* setting, as the glutamine metabolism of cancer cells *in vitro* may not align with *in vivo* tumor metabolism: lung cancer cell lines derived from primary lung tumors in mice display significant glutamine metabolism in culture and are sensitive to glutaminase inhibition; however, the primary lung tumors *in vivo* do not significantly utilize glutamine and are unaffected by glutaminase inhibition [68]. There is also some controversy surrounding the subtype specificity of altered glutamine metabolism in breast cancer. A study investigating metabolic profiles of tumors from non-treated breast cancer patients found altered glutaminase expression and glutamine levels between metabolic clusters of breast cancer, but these clusters were not distinguishable by receptor status [69]. However, other *in vivo* studies support subtype specific differences in glutamine

metabolism. Increased glutaminase expression has been observed in primary TNBC tumors as compared to other breast cancer subtypes and normal breast tissue, and TNBC cell lines and xenografts display sensitivity to glutaminase inhibitors [70]. Additionally, in a study comparing 75 breast tumors from patients without known distant metastases, TNBC tumors contained a lower level of glutamine than ER/PR/HER2+ tumors [71]. This may be due to the increased glutaminolysis in TNBCs. Knockdown of alanine, serine, cysteine-preferring transporter 2 (ASCT2; SLC1A5), a transporter that mediates uptake of neutral amino acids including glutamine, caused cell death *in vitro* and decreased growth of xenografted cells *in vivo* in triple-negative basal-like breast cancer cells, with minimal impact on luminal breast cancer cells [72]. TNBCs' reliance on glutamine represents one metabolic vulnerability that can be targeted therapeutically, and is further discussed in a later section.

In contrast to the increased uptake of glutamine, TNBCs activate the serine biosynthesis pathway [12]. TNBCs often amplify or overexpress phosphoglycerate dehydrogenase (PHGDH), the rate-limiting enzyme in the serine biosynthesis pathway [73,74]. Microarray analysis of formalin-fixed, paraffin-embedded tissues from TNBC patients revealed that increased PHGDH expression in the tumor and decreased serine hydroxymethyltransferase 1 (SHMT1) expression in the stroma are correlated with poor clinical prognosis [75]. Upregulation of all three genes in the serine biosynthesis pathway, PHGDH, phosphoserine aminotransferase 1 (PSAT1), and phosphoserine phosphatase (PSPH) has been found in TNBC cells highly metastatic to the bone [76]. Myc activity may also at least partially explain this observation, as Myc has been shown to upregulate expression of serine biosynthesis genes [77]. Although it is not clear how upregulation of

the serine biosynthesis pathway benefits cancer cells, upregulated serine metabolism is commonly observed in many cancers, and serine is a precursor to several downstream metabolites that support cancer growth [78,79]. These serine-derived metabolites include folates, sphingolipids, phospholipids, glycine, and cysteine. Glycine and cysteine also contribute to glutathione biosynthesis. Many pathways involving these metabolites are also upregulated in TNBC: higher expression of mitochondrial glycine synthesis enzymes serine hydroxymethyltransferase 2 (SHMT2), methylenetetrahydrofolate dehydrogenase (NADP+ dependent) 2 (MTHFD2), and methylenetetrahydrofolate dehydrogenase (NADP+ dependent) 1-like (MTHFD1L) in breast cancer patients has been associated with greater mortality [80]. Cysteine, a serine-derived amino acid, has also been linked with TNBC. A screen removing individual amino acids across a panel of breast cancer cells revealed that basal-like TNBC cells undergo rapid programmed necrosis following cystine deprivation, while luminal type breast cancer cells are resistant to cystine deprivation [81].

Another amino acid implicated in TNBC is arginine. TNBC cell lines with low expression of enzymes in the arginine biosynthesis pathway, argininosuccinate synthetase (ASS) and ornithine transcarbamylase (OTC), are sensitive to arginine depletion by treatment with recombinant human arginase [82]. This may be due to a reliance on extracellular arginine for synthesis of proteins, polyamines, and nitric oxide. Nitric oxide, which can be produced from arginine by nitric oxide synthase, has been implicated in a number of biological processes involved in cancer progression including angiogenesis, immune system evasion, and metastasis. In breast cancer patients, nitric oxide production has been correlated with advanced disease and poor clinical outcomes

[83]. However, there are inconsistencies in the effect of nitric oxide between TNBC cell lines; TNBC cell line MDA-MB-468, but not TNBC cell line MDA-MB-231, is sensitive to nitric oxide-induced cell death [84]. Nitric oxide actually increases proliferation in MDA-MB-231 cells by upregulating translation of cyclin D1 and ornithine decarboxylase [85]. One study links these distinct metabolic characteristics of TNBC cell lines to ethnic background [84], but it is not clear whether the predominant underlying causes are genetic or environmental. Additionally, not all TNBC cell lines are sensitive to arginine deprivation; several TNBC cell lines express ASS and are also generally resistant to arginine deprivation [86]. Sensitivity to arginine depletion has been reported in several other cancers including acute lymphoblastic T cell leukemia [87], non-Hodgkin's lymphoma [88], acute myeloid leukemia [89], melanoma [90], hepatocellular carcinoma [91], and pancreatic cancer deficient in argininosuccinate synthetase [92].

In addition to altered amino acid metabolism, TNBCs have been shown to increase lipid uptake. Compared to ER+ MCF7 cells, TNBC cell lines MDA-MD-231 and MDA-MB-436 have increased cholesterol uptake and storage along with decreased cholesterol synthesis [93]. Lipids serve as an important energy source, as metastatic TNBC cell lines and transmitochondrial cybrids (rho-zero cells lacking mtDNA fused with enucleated mitochondrial donor cells) [94] with TNBC mitochondria show dependence on fatty acid oxidation for energy production [95]. In Myc-driven TNBC transgenic and patient-derived xenograft models, targeting fatty acid oxidation using etomoxir, an irreversible inhibitor of carnitine palmitoyltransferase-1 (CPT1), significantly decreased *in vivo* tumor growth [96]. CPT1 is required for catabolism of long-chain fatty acids through fatty acid oxidation [97]. Levels of choline, a vitamin involved in phospholipid biosynthesis, have been found to be

higher in tumors from patients with TNBCs compared to patients with ER+/PR+/HER2+ cancers [71]. Distinct alterations in lipid metabolism have also been observed in HER2+ breast cancer, and will be further discussed. Taken together, TNBCs have altered metabolic pathways involving glucose, amino acids, and lipids (**Figure 1A**).

1.6 ER+ breast cancer

ER+ breast cancer is the most common subtype, accounting for ~70% of breast cancers [40]. ER+ breast tumors express genes associated with normal breast luminal cells, and the term “luminal breast cancer” is often used interchangeably with ER+ breast cancer [34]. The luminal/ER+ sub-group can be divided into additional intrinsic groups based on gene expression (e.g., luminal A and luminal B) [33]. Luminal A tumors are generally ER+/HER2-, while luminal B tumors tend to be ER+ and HER2+/- [35]. ER+ breast cancer is associated with a more favorable prognosis than HER2+ and TNBC [98], partially due to the availability of drugs that disrupt estrogen signaling or biosynthesis [99].

Some evidence indicates that unlike TNBCs, ER+ breast cancers may display the *reverse Warburg effect* [100], in which breast cancer cells rely on glycolytic end products such as lactate and pyruvate supplied by neighboring cancer associated fibroblasts (CAFs). Cancer cells promote metabolic rewiring of surrounding stromal cells, such as fibroblasts, into CAFs by promoting a hypoxic environment through hydrogen peroxide secretion [101]. Hydrogen peroxide activates caveolin 1 and hypoxia-inducible factor 1-alpha (HIF-1α), which in turn upregulates aerobic glycolysis to produce lactate [102,103]. To promote secretion of lactate from CAFs, breast cancer cells induce expression of a lactate transporter, monocarboxylate transporter (MCT) 4 in CAFs [104]. Conversely, breast cancer cells have been observed to express MCT1 [104], a transporter for lactate

uptake, to import lactate produced by CAFs [105,106]. Imported lactate can be converted by LDH to pyruvate, which can be utilized as fuel for the TCA cycle. ER+ cancers also exhibit high LDH expression [47]. While the reverse Warburg effect is an interesting concept, experimental evidence is limited. Additional analysis including metabolic profiling and *in vivo* flux analysis would be valuable in confirming these findings.

In addition to the reverse Warburg effect, differences in other metabolic pathways have been observed. A study comparing the metabolism of ER+ to ER- primary breast tumors found glutamate, β-alanine, and 2-hydroxyglutarate to be less abundant in ER+ breast tumors, while glutamine and 3-phosphoglycerate were more abundant [107]. The increased glutamine and decreased glutamate levels can potentially be explained through the differences in glutaminase expression between ER+ and ER- tumors. Glutaminase is overexpressed in TNBCs, as described in the TNBC section [65,59], while ER+ cell lines and tumors have higher expression of glutamine synthetase [65,70]. Thus, ER+ tumors with lower glutaminase and higher glutamine synthetase expression would maintain higher levels of glutamine. Elevated 3-phosphoglycerate may indicate differences in the relative activity of metabolic pathways that produce or utilize this metabolite, such as glycolysis and the serine biosynthesis pathway.

While the efficacy of endocrine therapy supports estrogen's role in stimulating proliferation of ER+ breast cancer cells [108,109], estrogen also has a role in cellular metabolism. Interestingly, estrogen's impact on ER+ breast cancer cell line metabolism depends on available glucose levels. In high glucose conditions (25 mM), estrogen stimulates glycolysis and suppresses the TCA cycle. However, under physiological glucose concentrations (5.5 mM), estrogen instead suppresses glycolysis and stimulates

the TCA cycle through AMP kinase-mediated upregulation of pyruvate dehydrogenase [110]. Under low glucose conditions (2.8 mM), ER+ cell lines are resistant to apoptosis secondary to endoplasmic reticulum stress through regulation of several pathways, including increased autophagy [111]. Estrogen treatment of ER+ breast cancer cell lines has also been shown to alter choline metabolism by decreasing phosphocholine (PCho) and increasing phosphatidylcholine (PtdCho) levels, and inducing the expression of several genes involved in choline metabolism [112]. In human tissues, ER+ samples display a higher PCho/glycerophosphocholine (GPC) ratio versus ER- samples [113]. However, this relationship has not held universally among ER+ cell lines. In another study, stimulation with estrogen increased the PCho/GPC ratio in MCF7 cells, but reduced the PCho/GPC ratio in T47D cells [112]. Estrogen-related receptors, orphan receptors structurally related to estrogen receptors, also impact breast cancer metabolism by modulating expression of genes involved in metabolic pathways such as glycolysis, glutaminolysis, and oxidative phosphorylation [114].

Anti-estrogen therapy using tamoxifen is an effective way to treat some ER+ breast tumors, but tamoxifen treatment fails in 66% of ER+/PR−, 55% of ER−/PR+, and 25% of ER+/PR+ breast cancer patients [105,106]. In addition to other resistance mechanisms [115,116], metabolism may play a role in tamoxifen resistance. For example, tamoxifen resistance has been linked with cholesterol metabolism [117,118]. Increased expression of cholesterol and fatty acid metabolism genes induced by overexpression of the mucin 1 transmembrane glycoprotein predict tamoxifen treatment failure and recurrence in ER+ breast cancer patients treated with tamoxifen [119]. Nucleotide metabolism has also been connected to tamoxifen resistance: elevated expression of ribonucleotide reductase M2

(RRM2), which catalyzes the production of deoxynucleotides, is found in tamoxifen-resistant ER+ patient tumors [120]. Additionally, increased RRM2 expression has been associated with decreased survival in tamoxifen-resistant luminal breast cancer patients [120]. RRM2 was identified as a key contributor to Akt-induced tamoxifen resistance, and genetic or pharmacological inhibition of RRM2 significantly reduces growth of tamoxifen-resistant breast cancer cells *in vitro* and *in vivo* [121]. Compared to other breast cancer subtypes, ER+ breast cancers exhibit distinct metabolic characteristics, including the reverse Warburg effect and decreased glutamine catabolism. These metabolic alterations are summarized in **Figure 1B**. Additionally, estrogen signaling in ER+ breast cancers likely plays an important role in cellular metabolism, and should be considered for future work involving endocrine resistant breast cancers.

1.7 HER2+ breast cancer

Approximately 15% of breast cancers present with amplification and/or overexpression of HER2 [40,122,123]. Two-thirds of HER2+ breast tumors are also ER+. Patients with HER2+ breast cancer have worse outcomes than those with ER+/HER2- breast cancer, and similar or worse outcomes as patients with TNBC [124,125]. Additionally, there is evidence that treatment of ER+ breast cancer with endocrine therapy can increase HER2 expression [126,127]. Drugs that target HER2, such as trastuzumab, are clinically available for treating HER2+ breast cancers [128]. However, trastuzumab is only effective for ~30% of HER2+ patients, and resistance remains a problem [129].

HER2 is a receptor tyrosine kinase which impacts several signaling pathways that mediate metabolism. HER2-affected signaling pathways include the PI3K/Akt/mTOR [130] and MAPK [131] pathways, which regulate metabolic pathways that support cancer

growth, including glycolysis, amino acid metabolism, and lipid biosynthesis. Akt and mTOR activity increase the rate of glycolysis and amino acid uptake through upregulation of glucose and amino acid transporters and metabolic enzymes [132]. HER2+ breast cancers express relatively increased GLUT1 compared with ER+ breast cancers, but lower GLUT1 than TNBCs [47]. HER2+ breast cancers also exhibit high MCT1 and LDH expression [47]. HER2+ breast cancer cell lines display increased glycolytic metabolism both *in vitro* and in mouse xenografts [133]; inhibiting the glycolytic enzyme 6-phosphofructo-2-kinase, which is upregulated in HER2+ breast cancer cell lines, decreases glucose uptake and proliferation of HER2+ breast cancer cells both *in vitro* and *in vivo* [134]. The increased glucose uptake in HER2+ breast cancer cell lines supports lipid biosynthesis, which is important for energy storage as well as the production and maintenance of cell membrane components. The glucose to lipid conversion rate is elevated in HER2+ breast cancer cell lines compared to TNBC cell lines [135]. Glucose fuels *de novo* lipid biosynthesis through mTOR complex-2 mediated upregulation of ATP citrate lyase (ACL) [135], which converts citrate to acetyl CoA to support lipid biosynthesis. HER2 can directly activate a second enzyme in the fatty acid biosynthesis pathway, fatty acid synthase (FASN) [136]. Inhibition of FASN activity has been shown to reduce HER2 expression in breast cancer cells [137]. Thus, HER2+ breast cancers increase *de novo* production of lipids, while TNBCs increase uptake of lipids.

Similar to TNBCs, HER2+ breast cancers display altered glutamine metabolism [64]. The receptor tyrosine kinase EPHA2, which is overexpressed in HER2+ breast cancers, increases glutamine metabolism and promotes lipid accumulation through RhoA GTPase mediated regulation of glutaminase activity in HER2+ breast cancer cell lines

[138]. High glycine and alanine levels have also been reported in HER2+ breast tumors from patients [71]. These results illustrate metabolic alterations that are specific to HER2+ breast cancer (**Figure 1C**), such as increased lipid biosynthesis, as well as characteristics observed in both HER2+ and TNBCs, such as increased glycolysis and glutamine metabolism.

1.8 Inflammatory Breast Cancer

Inflammatory breast cancer (IBC) is a rare subtype of breast cancer that is not represented by a specific histological subtype [139]. IBC is considered locally advanced at diagnosis and presents with redness and swelling of the breast, often without a noticeable lump [140]. While IBC makes up only ~2% of breast cancer cases, it accounts for a disproportionate ~7% of breast cancer mortality, and IBC incidence appears to be increasing over time [141]. Unlike other breast cancers, IBC presents more frequently as HER2+ or TNBC, with proportionally fewer ER+ cases [142,143]. ER expression does not correlate with significantly better prognosis for IBC, but patients with triple negative IBC generally have worse outcomes [143,144]. IBC is an understudied form of breast cancer, and unfortunately insufficient information is available to gain a comprehensive understanding of its metabolic characteristics. One study examining the metabolism of the triple negative IBC-derived SUM149 cell line found that relative to MCF7 (ER+) and MCF-10A (immortalized non-transformed mammary epithelial) cells, SUM149 cells are more glycolytic, converting more glucose to lactate. To fuel their TCA cycle, SUM149 cells predominantly utilize glutamine, and their glutamine metabolism and N-acetylaspartate production is regulated by RhoC GTPase [145]. This study also showed that SUM149 cells have the highest activity of the M2 isoform of pyruvate kinase (PKM2) relative to

MCF7 and MCF-10A cells. Pyruvate kinase catalyzes the final step in glycolysis, converting ADP and phosphoenolpyruvate to ATP and pyruvate. While normal non-proliferating cells express the M1 isoform of pyruvate kinase (PKM1), proliferating cells and all cancer cells studied to date express PKM2 [146-149]. These metabolic characteristics are summarized in **Figure 1D**. This study investigated the IBC SUM149 cell line, which can be additionally sub-classified as basal-like and therefore does not enable discrimination of metabolic features between IBCs and TNBCs. However, it provides the foundation for future work that may enable the development of new treatment options for patients with this rare and deadly subtype of breast cancer.

1.9 Hypoxia, a Common Feature in Breast Cancer Subtypes

In addition to metabolic reprogramming, another hallmark of cancer is the formation of new vasculature to facilitate the transport of nutrients and waste [150]. Many factors contribute to the formation of new vasculature in tumors [151-153], including hypoxia-inducible factors (HIFs) [154]. As the tumor grows, it becomes increasingly dependent on its blood supply to deliver oxygen and macronutrients and to clear waste products. Regions of hypoxia within the tumor promote angiogenesis to enable continued tumor growth and development [153,154].

In breast cancer patients, hypoxia has been associated with poor prognostic factors including lower overall survival, lower disease free survival, and higher risk of developing metastatic disease [155,156]. As many as 40% of invasive breast cancer samples display hypoxic markers [157], and overexpression of HIFs has been found to be generally similar between molecular subtypes of breast cancer [158,159]. However, subtype-specific interactions with hypoxia have been described. Under hypoxia, ER+

MCF7 and T47D breast cancer cell lines decrease expression of the two principal estrogen receptors, ER-α and ER-β [160]. Signaling through ER-α and HIF-1α co-regulates metabolic genes in glycolysis including glyceraldehyde-3-phosphate dehydrogenase, glucose-6-phopsphate isomerase, hexokinase 2, lactate dehydrogenase A, PKM2, and phosphofructokinase [161]. Supplementing hypoxic MCF7 cells with estrogen further increases HIF-1α expression, while treatment with ER-antagonist fulvestrant reduces HIF-1α expression [161]. In ER+ cell lines, fulvestrant treatment also downregulates expression of the glucose transporter GLUT1, which is normally induced in hypoxia [161]. In TNBC cell line MDA-MB-231, fulvestrant treatment has no effect on HIF-1α expression [161].

HIF-1α expression has also been associated with drug resistance in several cancers [162] and may mediate drug resistance in breast cancer. When treated with chemotherapeutics such as paclitaxel, TNBC, ER+/PR+, and HER2+ breast cancer cell lines all increase HIF expression even in normoxic conditions [163]. The relative proportion of breast cancer stem cells increased in the TNBC and ER+/PR+ cell lines, but not in the HER2+ cell line [163]. HIF-1α expression also increases resistance to tamoxifen treatment in ER+ breast cancer cell lines [161].

HIF-1α has been shown to upregulate antioxidant production in response to chemotherapy by inducing glutathione synthesis in TNBC cell lines [164]. This may be mediated through upregulation of metabolic enzymes PHGDH, SHMT2, and MTHFD2, which help promote redox balance in hypoxic conditions by generating mitochondrial NADPH, which is necessary to convert oxidized glutathione to reduced glutathione. In support of this, hypoxia increases PHGDH expression in breast cancer cells [165].

Knockdown of the serine biosynthesis pathway enzyme PHGDH increases mitochondrial reactive oxygen species (ROS) and decreases NADPH levels, inhibiting regeneration of reduced glutathione [165]. Thus, PHGDH knockdown sensitizes breast cancer cell lines to chemotherapy [165]. This is particularly interesting in the context of TNBC, given the previously discussed upregulation of the serine biosynthesis pathway and the importance of glutamine metabolism in glutathione production.

Unlike TNBC cell lines, HER2+ breast cancer cell lines display increased HIF-1α expression even in normoxic conditions, and expression of HIF-1α is essential for HER2+ cancer cell growth *in vivo* and *in vitro* [166]. HER2+ breast cancer cell lines also display better adaptability to growth in hypoxic conditions as compared to TNBC and ER+/PR+ breast cancer cell lines, which may be mediated by the anti-apoptotic protein Mcl-1; knockdown of Mcl-1 resulted in downregulation of both HER2 and HIF-1α in HER2+ breast cancer cell lines [167]. Mcl-1 expression increases in ER+ breast cancer cell lines when treated with estrogen. This effect was blocked through co-treatment with ER antagonists, but no increase in Mcl-1 expression was seen in TNBC cell lines treated with estrogen [168]. These results illustrate the complexity associated with regulation of hypoxia and highlight subtype specific regulatory pathways as promising areas of future investigation.

1.10 Comorbidities and Predisposing Factors: Obesity and Diabetes

Obesity and type 2 diabetes are growing public health problems that impact cancer. In the United States, ~40% of adult women are obese, and the prevalence of obesity in women is increasing [169]. Obesity is defined as having a body mass index (BMI) of 30 or higher and is a risk factor for the development of post-menopausal breast

cancer [170-173]. Both obesity and adult weight gain have been primarily associated with ER+ tumors [174], and BMI is positively associated with tumor diameter in ER+ tumors [175,174], whereas HER2+ tumor diameter is inversely related to BMI [176]. Adipose tissue, once thought to be a passive reservoir for energy storage, is an active endocrine organ secreting growth factors, pro-angiogenic factors, inflammatory cytokines, lipids and hormones, including estrogen [177]. Several epidemiological and clinical studies demonstrate an association between obesity and increased breast tumor size, greater distant metastasis development, and elevated mortality [178-180]. Obese women have 130% higher concentrations of estrogen compared with non-obese women [181]. Elevated estrogen levels are thought to contribute to the link between obesity and breast cancer risk, progression, and mortality [182-184]. Hormone-responsive tumors are more sensitive to the impacts of obesity [185].

Mechanistic studies evaluating the role of cellular metabolism in obesity-associated post-menopausal breast cancers are lacking. It is attractive to speculate that the elevated estrogen levels observed in obesity influence cellular metabolism in breast cancer cells. One study implicates adipocyte-derived lipids in metabolic rewiring. Co-culturing mature 3T3-L1 adipocytes with TNBC MDA-MD-231 or ER+ MCF7 breast cancer cells stimulates lipolysis in neighboring adipocytes, leading to an accumulation of adipocyte-derived fatty acids that are taken up by breast cancer cells to support their proliferation and migration [186]. Adipocytes in the *in vivo* tumor microenvironment have also been shown to release fatty acids that are used by ovarian cancer cells for energy production [187]. Further work is needed to determine how obesity impacts cellular metabolism in post-menopausal breast cancers.

One of the primary complications of obesity is the increased risk of type 2 diabetes. Type 2 diabetes is a disease in which the body's ability to respond to insulin is impaired and results in abnormal systemic metabolism of carbohydrates and glucose. However, there are also abnormalities in cellular metabolism due to the characteristic hyperinsulinemia and hyperglycemia in diabetic patients. Hyperinsulinemia promotes glucose uptake in tumors that are insulin-dependent [188,189]. Insulin and insulin-like growth factor 1 (IGF-1) stimulate macromolecular synthesis and promote the proliferation of MCF7 breast cancer cells *in vitro* [190]. Both insulin and IGF-1 affect estrogen signaling in breast cancer cell lines by activating ER-□ transcriptional activity [191], establishing another molecular link between obesity, diabetes and breast cancer. In addition to its direct metabolic role, the hyperglycemia associated with diabetes can increase production of ROS from mitochondrial respiration. ROS can lead to DNA damage that can increase cell motility and invasiveness in models of breast cancer [192]. Glucose and insulin can both activate mTOR, which promotes many of the complications observed in type 2 diabetes, including cancer [193]. The PI3K/Akt/mTOR pathway is frequently activated in cancers and, in breast cancer cells, contributes to increased cell proliferation, growth factor independence and endocrine resistance [194].

While the complex interactions between obesity, diabetes, cellular metabolism, and cancer are still unclear, several types of breast cancer mouse models have been utilized to decipher the link between obesity, diabetes and tumor progression/metastasis. Historically, many of these studies have focused on either genetic or diet-induced obesity models, and the conclusions drawn from these models vary. In the A^{vy} genetic model of obesity, in which ubiquitous expression of the agouti protein stimulates appetite [195],

mice have a shortened latency to mammary tumor development and an increased tumor incidence [196,197]. In contrast, *Lep^{ob}Lep^{ob}* mice, which have a defect in the appetite suppressing hormone leptin, have reduced spontaneous mammary tumor development compared to lean mice [198]. It is hypothesized that these *Lep^{ob}Lep^{ob}* mice, although obese, do not have an increase in mammary tumor development because leptin promotes breast cancer cell proliferation [199]. In diet-induced obesity models, obesity is induced in transgenic mice prone to mammary tumorigenesis by diets where 30% - 60% of the total caloric intake is from fat. In Balb/c mice with a deficit in p53, a high-fat diet (HFD, 60% kcal from fat) fails to stimulate weight gain but promotes puberty-specific mammary tumor formation [200]. While HFD fed mouse models show different levels of obesity and metabolic syndrome due to genetic background, weight gain is generally implicated in the development of hormonally responsive breast cancers, but the effect on hormone receptor negative tumors is inconsistent [201-204]. Recently, there has been considerable interest in examining the effects of local adipocytes and immune cells in subcutaneous adipose tissue on triple negative breast cancer [205,206]. These types of tumor microenvironment studies will be advantageous for investigating effects of adipose tissue on cellular metabolism as discussed above. While some studies have been performed, many are hypothesis-generating and do not show direct mechanistic causation. Current evidence suggests that estrogen, insulin, and IGF-1 signaling all impact metabolic rewiring. The contribution of these mechanisms *in vivo*, where more complex interactions between breast cancer cells and proximal adipocytes likely occurs, remains to be elucidated.

1.11 Targeting metabolism in breast cancer

Altered metabolic pathways in cancer offer a wide range of drug targets that can be exploited for therapy [207,208]. Anti-metabolite drugs such as methotrexate and 5-flurouracil, which target nucleotide metabolism, have long been used in the treatment of cancers [209], including breast cancer [4]. These drugs cause cell death in all rapidly proliferating cells – including normal cells – by inhibiting RNA and DNA production [210], and therefore cause severe side effects such as neurotoxicity and anemia [211,212]. Targeting metabolic pathways specifically upregulated in cancer cells but not normal cells may allow the development of therapies with fewer adverse side effects compared to current chemotherapy options. Breast cancer therapy can be personalized by targeting upregulated metabolic pathways in a subtype-specific manner, including glycolysis, glutaminolysis, the TCA cycle, one-carbon metabolism, and lipid metabolism. Given the prevalence of glutamine addiction in many cancers, glutaminase inhibitors are being developed and may prove efficacious for treatment of TNBCs. As expected, treatment with glutaminase inhibitors causes an increase in intracellular glutamine levels in TNBC xenografts, but not in ER+ xenografts that do not express high levels of glutaminase [213]. Glutaminase inhibition reduces proliferation in TNBC cells and xenografts by selectively limiting TNBCs' ability to utilize glutamine; treatment with a glutaminase inhibitor decreased glutathione levels in TNBC cells but not in ER+ breast cancer cells [70]. Sensitivity to glutaminase inhibitors can be decreased *in vitro* by supplementing the growth media with pyruvate [214]. Sensitivity to glutaminase inhibitors may be associated with Myc-induced upregulation of glutamine metabolism, as these inhibitors have shown promise in several other Myc-driven cancers including lymphoma [215], hepatocellular

carcinoma [216], and renal cell carcinoma [217]. Targeting the serine biosynthesis pathway may also be effective for TNBC treatment, as knockdown of this pathway has been shown to sensitize TNBC cell lines to chemotherapy [165]. These results highlight the potential utility of drugs that inhibit cancer-specific metabolic vulnerabilities, especially in the treatment of TNBCs, which lack targeted therapies.

As previously discussed, HER2 signaling affects several metabolic pathways. Therefore, drugs targeting the HER2 signaling axis are likely to have metabolic effects. Treatment of HER2+ cell lines with trastuzumab decreases glucose uptake and lactate excretion [218]. Treatment with lapatinib, a receptor tyrosine kinase inhibitor that disrupts HER2 and EGFR signaling, decreases expression of the glucose transporter GLUT4 and to a lesser extent GLUT1 in HER2+ cells [219]. Inhibitors of FASN have also been explored for HER2+ breast cancers due to increased *de novo* lipid biosynthesis observed in this subtype [220]. Treating HER2+ cell lines with FASN inhibitors in combination with trastuzumab synergistically reduces cell viability and enhances cell death [137]. Interestingly, FASN inhibitors sensitize resistant HER2+ cell lines and patient derived xenografts to anti-HER2 compounds [221]. Targeting metabolic pathways specifically upregulated in breast cancer subtypes provide new avenues of therapy while also making existing treatments more effective.

Drugs that are FDA-approved for other diseases could be repurposed to target metabolic vulnerabilities in cancer. One example of this is metformin, a widely-prescribed drug for type 2 diabetes, which has been associated with decreased risk of developing cancer [222]. In addition to stabilizing blood glucose levels in diabetic patients, metformin affects cellular metabolism and may therefore have utility as an anti-cancer agent [223].

Metformin is a weak inhibitor of complex 1 in the mitochondrial electron transport chain, allowing it to disrupt mitochondrial metabolism to inhibit proliferation in cancer cells [224,225]. Treatment of several breast cancer cell lines with metformin decreases phospholipid biosynthesis, which is essential for lipid bilayer formation and proliferation [226]. Metformin has also been shown to disrupt cancer cell energetics in ER+ MCF7 cells, where treatment results in increased glucose consumption, increased lactate production, decreased oxygen consumption, and reduced mitochondrial membrane potential [227]. Taken together, metformin leads to a metabolic shift away from oxidative phosphorylation and the TCA cycle, thereby inhibiting energy production and downstream biosynthetic pathways. Subtype-specific metabolic characteristics and potential anti-metabolites are summarized in **Table 1**. As our understanding of metabolic vulnerabilities in cancer continues to develop, it will be possible to develop more effective, personalized therapies for all breast cancer subtypes.

1.12 Conclusions and Future Directions

Breast cancer subtypes display diverse metabolic phenotypes that contribute to tumor growth, invasiveness, treatment efficacy, and drug resistance. Metabolic studies have revealed alterations in glucose, glutamine, amino acid, and lipid pathways in breast cancer subtypes. TNBCs upregulate aerobic glycolysis, upregulate serine metabolism, and generally display glutamine addiction; ER+ breast cancers rely less on glucose and glutamine uptake, preferring to consume lactate produced by neighboring CAFs; HER2+ breast cancers upregulate fatty acid synthesis while displaying increased glucose and glutamine uptake. The full extent of metabolic reprogramming in all breast cancer subtypes has yet to be elucidated.

While we have made progress in understanding breast cancer metabolism, our understanding of human breast cancer metabolism *in vivo* remains incomplete. Much of the work discussed here has been performed in cancer cell lines, which inadequately model the complex tumor microenvironment in terms of nutrient conditions, cell population (e.g. CAFs, adipocytes, immune cells), or the patient's hormone levels. Similar cell lines occasionally yield inconsistent results, which makes generalization and clinical translation challenging. Genetically engineered mouse models better represent tumor microenvironments, but mouse mammary development and biology is different from that of humans, and most drugs efficacious in mice fail in human clinical trials. Patient-derived xenograft (PDX) models enable studies using human tumors, but require immunodeficient mice that lack key immune components, or humanized mice that may inaccurately recapitulate human physiology. Nevertheless, these model systems remain valuable tools and allow experiments not feasible in humans. Metabolomics in human patients is limited by cost and variables that are difficult to control, such as diet, age, environment, genetic variations, disease progression, and prior treatment. Studies using model systems can establish proof of concept, identify new therapeutic targets, and inform study design for future work involving human patients. Extensive work involving both model systems and patients is required to realize the full potential of targeted therapies based on metabolic vulnerabilities of breast cancer subtypes.

In addition to our incomplete understanding of breast cancer metabolism, our knowledge of normal breast metabolism is limited. Considerable metabolic changes must occur in normal breast tissue during prenatal development, puberty, pregnancy, lactation, involution, and menopause. However, little is known about metabolism during these

processes. Future work is required to characterize metabolism in normal breast tissue during developmental stages and the menstrual cycle. Additional studies are also needed to understand metabolic profiles of localized versus advanced breast cancer and primary versus metastasized disease, as well as metabolic interactions with the immune system.

Metabolomics, in conjunction with genetic engineering and imaging technologies, will allow us to address many of these challenges to further decipher metabolic differences between breast cancer subtypes. We can leverage these tools to determine which metabolic alterations are most relevant in cancer biology to guide drug development and personalized therapy. Targeting metabolic vulnerabilities in breast cancer subtypes has great potential to provide advanced treatment options with fewer side effects, ultimately improving outcomes for breast cancer patients.

1.13 Acknowledgments

We thank Eran Andrechek, Deanna Broadwater, Susan Conrad, Elliot Ensink, Sarah-Maria Fendt, John LaPres, Jonathan Rennhack, Shao Thing Teoh, and Hua Xiao for helpful discussions and critical reading of this manuscript. We also thank breast cancer research patient advocates Valerie Fraser (Inflammatory Breast Cancer International Consortium) and Suzanne Gauvreau. Funding: This work was supported by the AACR-Incyte Corporation NextGen Grant for Transformative Cancer Research, Grant Number 16-20-46-LUNT, and the Office of the Assistant Secretary of Defense for Health Affairs, through the Breast Cancer Research Program, under Award No. W81XWH-15-1-0453.

1.14 Dissertation Goals

Breast cancer heterogeneity provides clear clinical problems, I believe that in order to improve patient outcomes we must continue to improve our understanding of the basic biological processes in cancer, including how cancer cells rewire their metabolism to support proliferation. In recent years targeting cancer-specific metabolism has gained significant attention, and I believe that this idea can be further applied to develop targeted therapies for breast cancer subtypes.

To study this, I have used two histologic subtypes of mammary tumors derived from the MMTV-Myc mouse model, EMT and papillary. Tumors from the MMTV-Myc model are not only extremely heterogenous, they also share common features with human breast cancer and are therefore an ideal model system to study breast cancer heterogeneity. Additionally, while there is significant literature characterizing MMTV-Myc tumors based on gene expression, little work has been performed specifically characterizing the metabolism of tumor subtypes in the MMTV-Myc model. I have therefore sought to fill this gap in knowledge by investigating breast cancer heterogeneity and metabolism using this model system. The central hypothesis of my thesis is: the EMT and papillary subtypes display distinct metabolic profiles, which can be targeted to selectively disrupt subtype-specific metabolic demands. Therefore, the primary goals of this dissertation are: 1) identify metabolic profiles specific to the EMT and papillary subtypes and 2) target relevant metabolic pathways in each subtype to demonstrate subtype-specificity.

I first extracted metabolites from cell lines derived from EMT and papillary tumors and performed isotope labeling studies to identify metabolic differences in each subtype.

A full list of the metabolites examined in this work is in **Table S1**. These analyses revealed the EMT subtype performs more glutathione biosynthesis and has increased TCA cycle metabolism than the papillary subtype, while the papillary subtype has increased nucleotide biosynthesis compared to the EMT subtype. Using this data, metabolism-targeting drugs were selected that inhibit glutathione biosynthesis, the TCA cycle, and nucleotide biosynthesis. When these drugs were used *in vitro* to treat each subtype, it was clear that each subtype was most sensitive to pharmacological inhibition of its preferred metabolic pathway (chapter 3).

I then built upon these findings by integrating metabolomics and genomics analyses of EMT and papillary tumors to identify metabolic preferences for specific pathways of nucleotide biosynthesis, with the papillary subtype preferring *de novo* biosynthesis and the EMT subtype preferring nucleotide salvage. Using gene editing techniques, I targeted both nucleotide biosynthetic pathways in each subtype and demonstrate *in vivo* effects on tumor growth when the preferred metabolic pathway of each subtype is targeted (chapter 4).

My work highlights the exciting potential for using metabolism to develop treatment strategies for subtypes of breast cancer. This work has translational potential, and could inspire additional studies to investigate metabolism as a therapeutic target of cancer.

1.15 APPENDIX

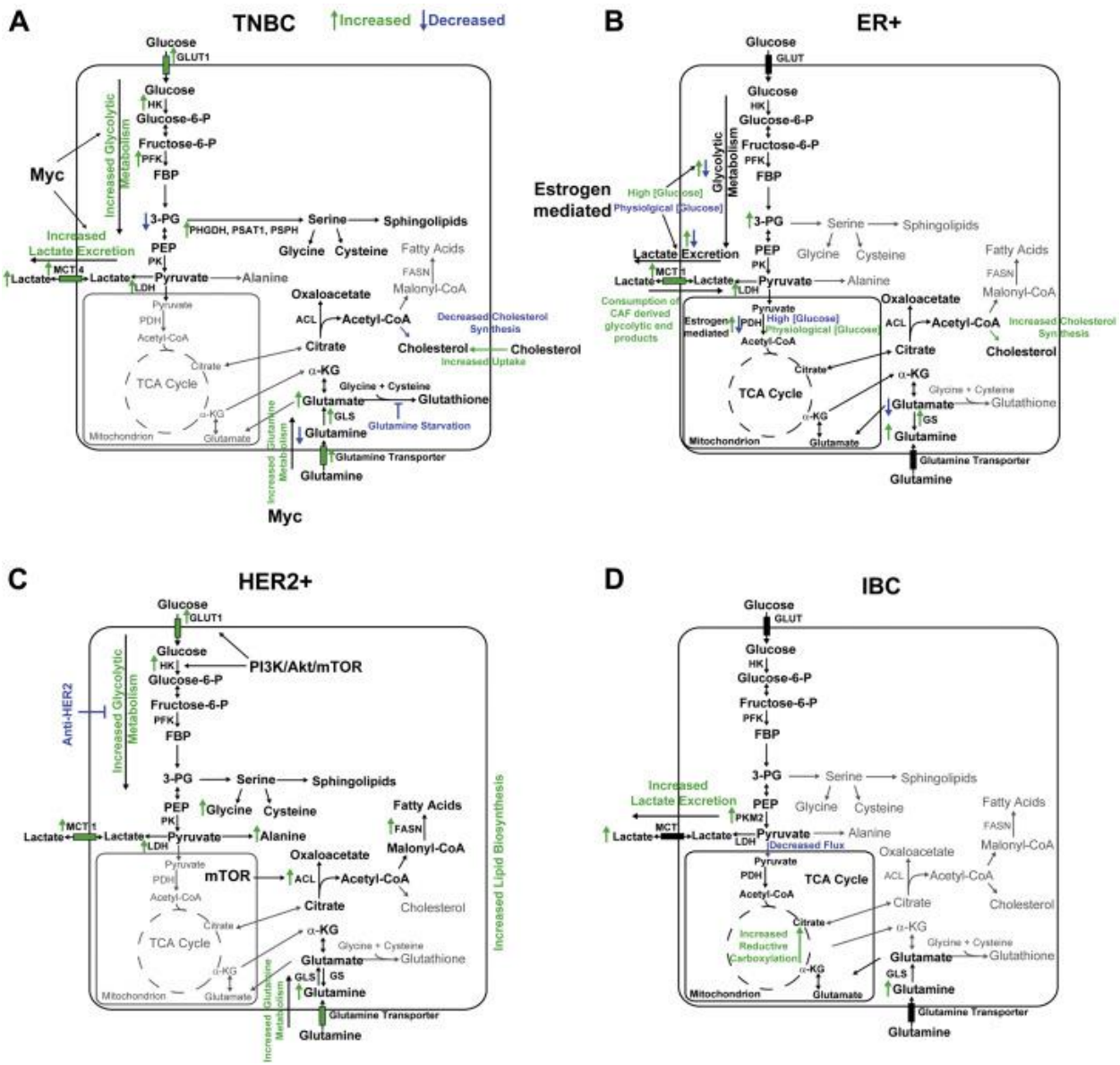

Figure 1.1 Schematic illustration of altered metabolic pathways in breast cancer subtypes. (**A**) Triple negative breast cancer (TNBC); (**B**) Estrogen receptor positive (ER+) breast cancer; (**C**) Human epidermal growth factor receptor 2 positive (HER2+) breast cancer; (**D**) Inflammatory breast cancer (IBC).

		Breast Cancer Subtype			
		ER+		HER2+	TNBC
Clinical features	Prevalence[40]	~70%		~15%	~12%
	Targeted Therapy	Endocrine		Anti-HER2	None
	Intrinsic Subtype[35]	Luminal A (ER+ PR+ HER2-)	Luminal B (ER+ PR+ HER2+/-)	HER2+ (ER- PR- HER2+)	Basal-like* (ER- PR- HER2-)
	Breast Cancer-Specific Survival[41]	84%	87%	52%	75%
Metabolic Alterations	Glycolytic Flux	Context Dependent		Increased	Increased
	Glutamine Catabolism	Decreased		Increased	Increased
	Lipid Metabolism	Increased Cholesterol Biosynthesis		Increased Fatty Acid Biosynthesis	Increased Cholesterol Uptake
	Potential Anti-metabolites	Complex 1 Inhibitors		Fatty Acid Synthase Inhibitors	Glutaminase Inhibitors

*The majority of TNBCs are classified as basal-like.

Table 1.1 Summary of clinical and metabolic features of breast cancer subtypes.

Ionization mode	Metabolite	Parent (m/z)	Product (m/z)	Cone Voltage (V)	Collision Energy (V)	Note
ESI negative	2-3 phosphoglycerate M-0	185.0	97.0	22	16	
ESI negative	2-3 phosphoglycerate M-1	186.0	97.0	22	16	
ESI negative	2-3 phosphoglycerate M-2	187.0	97.0	22	16	
ESI negative	2-3 phosphoglycerate M-3	188.0	97.0	22	16	
ESI negative	Acetoacetyl-CoA_	850.2	766.1	40	30	
ESI negative	Acetyl-CoA	808.0	408.0	40	37	
ESI negative	Aconitate	173.1	84.8	16	13	
ESI negative	Adenine	134.0	106.8	40	21	
ESI negative	ADP	426.1	158.6	34	21	
ESI negative	ADP-glucose	588.0	346.0	34	22	
ESI negative	ADP-ribose	558.1	345.8	50	21	
ESI negative	Alanine	221.9	113.7	28	10	CBZ-Derivatized
ESI negative	Allantoate_and_Carbamoyl_aspartate	175.0	132.0	28	12	
ESI negative	AMP	346.0	79	40	29	
ESI negative	Arginine	306.9	198.8	22	10	CBZ-Derivatized
ESI negative	Asparagine	264.9	112.75	28	10	CBZ-Derivatized
ESI negative	Aspartate M-0 (unlabeled)	265.9	157.7	40	10	CBZ-Derivatized
ESI negative	Aspartate M-1	266.9	158.7	40	10	CBZ-Derivatized
ESI negative	Aspartate M-2	267.9	159.7	40	10	CBZ-Derivatized
ESI negative	Aspartate M-3	268.9	160.7	40	10	CBZ-Derivatized
ESI negative	Aspartate M-4	269.9	161.7	40	10	CBZ-Derivatized
ESI negative	ATP M-0 (unlabeled)	506.0	159.0	16	28	
ESI negative	ATP M-1	507.0	159.0	16	28	
ESI negative	ATP M-2	508.0	159.0	16	28	
ESI negative	ATP M-3	509.0	159.0	16	28	
ESI negative	ATP M-4	510.0	159.0	16	28	
ESI negative	ATP M-5	511.0	159.0	16	28	
ESI negative	ATP M-6	512.0	159.0	16	28	
ESI negative	ATP M-7	513.0	159.0	16	28	
ESI negative	ATP M-8	514.0	159.0	16	28	
ESI negative	ATP M-9	515.0	159.0	16	28	
ESI negative	ATP M-10	516.0	159.0	16	28	
ESI negative	Bisphosphoglycerate	265.0	166.7	16	13	
ESI negative	camphorsulfonate	231.0	79.8	40	25	Internal Standard
ESI negative	CDP	402.0	159.0	28	22	
ESI negative	Citrate+Isocitrate	191.0	110.6	22	13	
ESI negative	CMP	322.1	78.7	34	29	
ESI negative	CMP-N-acetyl-neuraminate	613.0	322.0	40	20	
ESI negative	CoA	766.0	408.0	40	40	

Table S1.1 Full list of analyzed metabolites.

Table S1.1 (cont'd)

ESI negative	CTP	481.8	158.7	10	22	
ESI negative	Cysteine	253.8	145.6	50	10	CBZ-Derivatized
ESI negative	dADP	409.9	158.6	40	28	
ESI negative	dAMP	330.1	194.6	28	21	
ESI negative	dATP	489.9	158.6	46	28	
ESI negative	dCMP	305.9	78.6	50	22	
ESI negative	dCTP	465.8	158.6	10	34	
ESI negative	Deoxyinosine	251.0	135.0	28	19	
ESI negative	Deoxyribose-phosphate	213.0	79.0	28	33	
ESI negative	Deoxyuridine	227.0	184.0	28	12	
ESI negative	dGDP	426.1	158.6	34	21	
ESI negative	dGMP	346.0	79	40	29	
ESI negative	dGTP	505.9	158.6	16	28	
ESI negative	dTDP	400.9	158.7	46	22	
ESI negative	dTMP	321.0	194.5	28	21	
ESI negative	dTTP	480.9	158.7	40	34	
ESI negative	dUMP	307.0	194.5	28	13	
ESI negative	FAD	784.2	436.9	50	29	
ESI negative	FBP M-0 (unlabeled)	339.0	97.0	28	28	
ESI negative	FBP M-1	340	97.0	28	28	
ESI negative	FBP M-2	341.0	97.0	28	28	
ESI negative	FBP M-3	342.0	97.0	28	28	
ESI negative	FBP M-4	343.0	97.0	28	28	
ESI negative	FBP M-5	344.0	97.0	28	28	
ESI negative	FBP M-6	345.0	97.0	28	28	
ESI negative	Flavin_mononucleotide	455.0	213.0	22	19	
ESI negative	Fumarate M-0 (unlabeled)	115.0	71.0	22	5	
ESI negative	Fumarate M-1-0	116.0	71.0	22	5	
ESI negative	Fumarate M-1-1	116.1	72.0	22	5	
ESI negative	Fumarate M-2-1	117.0	72.0	22	5	
ESI negative	Fumarate M-2-2	117.0	73.0	22	5	
ESI negative	Fumarate M-3-2	118.0	73.0	22	5	
ESI negative	Fumarate M-3-3	118.0	74.0	22	5	
ESI negative	Fumarate M-4-3	119.0	74.0	22	5	
ESI negative	GAP+DHAP	169.1	97.0	16	13	
ESI negative	GDP	441.8	343.8	28	16	
ESI negative	Glucono-lactone	177.0	129.0	22	11	
ESI negative	Glucosamine-6-phosphate	258.0	96.6	28	21	
ESI negative	Glutamate M-0 (unlabeled)	279.9	127.7	28	16	CBZ-Derivatized
ESI negative	Glutamate M-1	280.9	128.7	28	16	CBZ-Derivatized

Table S1.1 (cont'd)

ESI negative	Glutamate M-2	281.9	129.7	28	16	CBZ-Derivatized
ESI negative	Glutamate M-3	282.9	130.7	28	16	CBZ-Derivatized
ESI negative	Glutamate M-4	283.9	131.7	28	16	CBZ-Derivatized
ESI negative	Glutamate M-5	284.9	132.7	28	16	CBZ-Derivatized
ESI negative	Glutamine M-0 (unlabeled)	279.0	127.0	28	16	CBZ-Derivatized
ESI negative	Glutamine M-1	280.0	128.0	28	16	CBZ-Derivatized
ESI negative	Glutamine M-2	281.0	129.0	28	16	CBZ-Derivatized
ESI negative	Glutamine M-3	282.0	130.0	28	16	CBZ-Derivatized
ESI negative	Glutamine M-4	283.0	131.0	28	16	CBZ-Derivatized
ESI negative	Glutamine M-5	284.0	132.0	28	16	CBZ-Derivatized
ESI negative	Glutathione_disulfide_oxidized	611.0	306.0	46	21	
ESI negative	Glutathione_reduced	305.9	142.7	40	16	
ESI negative	glycerate	105.0	74.8	22	13	
ESI negative	Glycerol_3-phosphate	170.8	78.7	46	16	
ESI negative	Glycine M-0 (unlabeled)	207.8	99.7	22	10	CBZ-Derivatized
ESI negative	Glycine M-1	208.8	100.7	22	10	CBZ-Derivatized
ESI negative	Glycine M-2	209.8	101.7	22	10	CBZ-Derivatized
ESI negative	GMP	362.1	78.7	34	21	
ESI negative	GTP	521.8	158.7	40	28	
ESI negative	Hexose-phosphate	258.8	96.6	10	16	
ESI negative	histidine	287.9	179.8	22	10	CBZ-Derivatized
ESI negative	Hydroxybutyryl-CoA+Malonyl-CoA	852.2	408.0	40	41	
ESI negative	hypoxanthine	134.8	91.7	34	16	
ESI negative	IDP	427.0	159.0	22	25	
ESI negative	IMP M-0 (unlabeled)	347.2	78.7	34	21	
ESI negative	IMP M-1	348.2	78.7	34	21	
ESI negative	IMP M-2	349.2	78.7	34	21	
ESI negative	IMP M-3	350.2	78.7	34	21	
ESI negative	IMP M-4	351.2	78.7	34	21	
ESI negative	IMP M-5	352.2	78.7	34	21	
ESI negative	IMP M-6	353.2	78.7	34	21	
ESI negative	IMP M-7	354.2	78.7	34	21	
ESI negative	IMP M-8	355.2	78.7	34	21	
ESI negative	IMP M-9	356.2	78.7	34	21	
ESI negative	IMP M-10	357.2	78.7	34	21	
ESI negative	Inosine	267.0	135.0	28	25	
ESI negative	Isoleucine/Leucine	263.9	155.8	10	10	CBZ-Derivatized
ESI negative	Ketoglutarate M-0-0 (unlabeled)	145.0	101.0	22	5	
ESI negative	Ketoglutarate M-1-0	146.0	101.0	22	5	
ESI negative	Ketoglutarate M-1-1	146.0	102.0	22	5	

Table S1.1 (cont'd)

ESI negative	Ketoglutarate M-2-1	147.0	102.0	22	5	
ESI negative	Ketoglutarate M-2-2	147.0	103.0	22	5	
ESI negative	Ketoglutarate M-3-2	148.0	103.0	22	5	
ESI negative	Ketoglutarate M-3-3	148.0	104.0	22	5	
ESI negative	Ketoglutarate M-4-3	149.0	104.0	22	5	
ESI negative	Ketoglutarate M-4-4	149.0	105.0	22	5	
ESI negative	Ketoglutarate M-5-4	150.0	105.0	22	5	
ESI negative	Lactate	88.8	42.7	46	10	
ESI negative	Lysine	413.0	196.8	50	16	CBZ-Derivatized
ESI negative	Malate M-0 (unlabeled)	133.0	115.0	16	16	
ESI negative	Malate M-1	134.0	116.0	16	16	
ESI negative	Malate M-2	135.0	117.0	16	16	
ESI negative	Malate M-3	136.0	118.0	16	16	
ESI negative	Malate M-4	137.1	119.0	16	16	
ESI negative	Methionine	281.8	173.7	22	10	CBZ-Derivatized
ESI negative	n-acetyl-glucosamine	220.1	118.4	16	5	
ESI negative	N-acetyl-glucosamine-1-phosphate	300.0	79.0	22	22	
ESI negative	N-acetyl-neuraminate/sialic acid	308.0	87.0	40	15	
ESI negative	NAD	662.1	540.1	22	22	
ESI negative	NADH	664.2	407.8	46	28	
ESI negative	NADP	742.0	619.6	22	13	
ESI negative	NADPH	744.1	407.8	34	34	
ESI negative	Ornithine	399.0	182.7	40	16	CBZ-Derivatized
ESI negative	Phenylalanine	298.0	147.0	28	27	CBZ-Derivatized
ESI negative	Phosphoenolpyruvate	167.0	78.8	16	13	
ESI negative	Phosphogluconic_acid	274.8	96.7	22	16	
ESI negative	Phosphoserine	183.8	96.7	40	10	
ESI negative	PIPES	301.0	192.8	40	25	Internal Standard
ESI negative	Proline	247.9	139.7	34	10	CBZ-Derivatized
ESI negative	PRPP M-0 (unlabeled)	389.0	291.0	40	18	
ESI negative	PRPP M-1	390.0	292.0	40	18	
ESI negative	PRPP M-2	391.0	293.0	40	18	
ESI negative	PRPP M-3	392.0	294.0	40	18	
ESI negative	PRPP M-4	393.0	295.0	40	18	
ESI negative	PRPP M-5	394.0	296.0	40	18	
ESI negative	Ribose 5-phosphate M-0 (unlabeled)	229.0	96.6	28	21	
ESI negative	Ribose 5-phosphate M-1	230.0	96.6	28	21	
ESI negative	Ribose 5-phosphate M-2	231.0	96.6	28	21	
ESI negative	Ribose 5-phosphate M-3	232.0	96.6	28	21	
ESI negative	Ribose 5-phosphate M-4	233.0	96.6	28	21	

Table S1.1 (cont'd)

ESI negative	Ribose 5-phosphate M-5	234.0	96.6	28	21	
ESI negative	Ribulose-5-phosphate	229.0	96.6	28	21	
ESI negative	Sedoheptulose-phosphate	289.0	97.0	28	25	
ESI negative	Serine M-0	237.8	129.7	16	10	CBZ-Derivatized
ESI negative	Serine M-1	238.8	130.7	16	10	CBZ-Derivatized
ESI negative	Serine M-2	239.8	131.7	16	10	CBZ-Derivatized
ESI negative	Serine M-3	240.8	132.7	16	10	CBZ-Derivatized
ESI negative	Succinate M-0 (unlabeled)	117.0	73.0	28	10	
ESI negative	Succinate M-1-0	118	73.0	28	10	
ESI negative	Succinate M-1-1	118	74.0	28	10	
ESI negative	Succinate M-2-1	119	74.0	28	10	
ESI negative	Succinate M-2-2	119	75.0	28	10	
ESI negative	Succinate M-3-2	120	75.0	28	10	
ESI negative	Succinate M-3-3	120	76.0	28	10	
ESI negative	Succinate M-4-3	121.0	76.0	28	10	
ESI negative	Threonine	251.9	143.7	22	10	CBZ-Derivatized
ESI negative	Tryptophan	336.7	228.7	34	10	CBZ-Derivatized
ESI negative	Tyrosine	313.9	205.8	22	10	CBZ-Derivatized
ESI negative	UDP	402.8	158.4	10	22	
ESI negative	UDP-D-glucose	565.0	323.0	22	22	
ESI negative	UDP-D-glucuronate	579.0	403.0	22	22	
ESI negative	UDP-N-acetyl-glucosamine	606.0	385.0	22	22	
ESI negative	UMP	322.9	78.6	46	28	
ESI negative	Uridine	243.0	199.8	28	13	
ESI negative	UTP M-0 (unlabeled)	483.0	159.0	28	34	
ESI negative	UTP M-1	484.0	159.0	28	34	
ESI negative	UTP M-2	485.0	159.0	28	34	
ESI negative	UTP M-3	486.0	159.0	28	34	
ESI negative	UTP M-4	487.0	159.0	28	34	
ESI negative	UTP M-5	488.0	159.0	28	34	
ESI negative	UTP M-6	489.0	159.0	28	34	
ESI negative	UTP M-7	490.0	159.0	28	34	
ESI negative	UTP M-8	491.0	159.0	28	34	
ESI negative	UTP M-9	492.0	159.0	28	34	
ESI negative	Valine	249.9	141.8	28	12	CBZ-Derivatized
ESI negative	xanthine	151.0	108.0	22	21	
ESI negative	Xanthosine	283.0	151.0	28	22	
ESI negative	XMP	363.0	210.5	34	21	

1.16 REFERENCES

REFERENCES

1. DeSantis C, Howlader N, Cronin KA, Jemal A (2011) Breast Cancer Incidence Rates in U.S. Women Are No Longer Declining. Cancer Epidemiology Biomarkers & Prevention 20 (5):733-739. doi:10.1158/1055-9965.epi-11-0061

2. Miller KD, Siegel RL, Lin CC, Mariotto AB, Kramer JL, Rowland JH, Stein KD, Alteri R, Jemal A (2016) Cancer treatment and survivorship statistics, 2016. CA: a cancer journal for clinicians 66 (4):271-289. doi:10.3322/caac.21349

3. Senkus E, Kyriakides S, Penault-Llorca F, Poortmans P, Thompson A, Zackrisson S, Cardoso F (2013) Primary breast cancer: ESMO Clinical Practice Guidelines for diagnosis, treatment and follow-up†. Annals of Oncology 24 (suppl_6):vi7-vi23. doi:10.1093/annonc/mdt284

4. Anampa J, Makower D, Sparano JA (2015) Progress in adjuvant chemotherapy for breast cancer: an overview. BMC Medicine 13 (1):195. doi:10.1186/s12916-015-0439-8

5. Early Breast Cancer Trialists' Collaborative G (2005) Effects of chemotherapy and hormonal therapy for early breast cancer on recurrence and 15-year survival: an overview of the randomised trials. The Lancet 365 (9472):1687-1717. doi:10.1016/s0140-6736(05)66544-0

6. Gonzalez-Angulo AM, Morales-Vasquez F, Hortobagyi GN (2007) Overview of Resistance to Systemic Therapy in Patients with Breast Cancer. In: Yu D, Hung M-C (eds) Breast Cancer Chemosensitivity. Springer New York, New York, NY, pp 1-22. doi:10.1007/978-0-387-74039-3

7. Vander Heiden MG, DeBerardinis RJ (2017) Understanding the Intersections between Metabolism and Cancer Biology. Cell 168 (4):657-669. doi:10.1016/j.cell.2016.12.039

8. DeBerardinis RJ, Chandel NS (2016) Fundamentals of cancer metabolism. Science Advances 2 (5):e1600200. doi:10.1126/sciadv.1600200

9. Pavlova Natalya N, Thompson Craig B (2016) The Emerging Hallmarks of Cancer Metabolism. Cell Metabolism 23 (1):27-47. doi:10.1016/j.cmet.2015.12.006

10. Cantor JR, Sabatini DM (2012) Cancer Cell Metabolism: One Hallmark, Many Faces. Cancer Discovery 2 (10):881-898. doi:10.1158/2159-8290.cd-12-0345

11. Elia I, Fendt S-M (2016) In vivo cancer metabolism is defined by the nutrient microenvironment. Translational Cancer Research:S1284-S1287

12. Elia I, Schmieder R, Christen S, Fendt SM (2016) Organ-specific cancer metabolism and its potential for therapy. Handbook of Experimental Pharmacology, vol 233. doi:10.1007/164_2015_10

13. Hu J, Locasale JW, Bielas JH, O'Sullivan J, Sheahan K, Cantley LC, Heiden MGV, Vitkup D (2013) Heterogeneity of tumor-induced gene expression changes in the human metabolic network. Nat Biotech 31 (6):522-529. doi:10.1038/nbt.2530 http://www.nature.com/nbt/journal/v31/n6/abs/nbt.2530.html#supplementary-information

14. DeBerardinis RJ, Sayed N, Ditsworth D, Thompson CB (2008) Brick by brick: metabolism and tumor cell growth. Current Opinion in Genetics & Development 18 (1):54-61. doi:http://dx.doi.org/10.1016/j.gde.2008.02.003

15. Lunt SY, Vander Heiden MG (2011) Aerobic glycolysis: meeting the metabolic requirements of cell proliferation. Annu Rev Cell Dev Biol 27:441-464. doi:10.1146/annurev-cellbio-092910-154237

16. Ahn CS, Metallo CM (2015) Mitochondria as biosynthetic factories for cancer proliferation. Cancer & metabolism 3 (1):1. doi:10.1186/s40170-015-0128-2

17. Lorendeau D, Christen S, Rinaldi G, Fendt S-M (2015) Metabolic control of signalling pathways and metabolic auto-regulation. Biology of the Cell 107 (8):251-272. doi:10.1111/boc.201500015

18. Kaelin William G, Jr., McKnight Steven L (2013) Influence of Metabolism on Epigenetics and Disease. Cell 153 (1):56-69. doi:10.1016/j.cell.2013.03.004

19. Wishart D, Mandal R, Stanislaus A, Ramirez-Gaona M (2016) Cancer Metabolomics and the Human Metabolome Database. Metabolites 6 (1):10

20. Patel S, Ahmed S (2015) Emerging field of metabolomics: Big promise for cancer biomarker identification and drug discovery. Journal of Pharmaceutical and Biomedical Analysis 107:63-74. doi:http://dx.doi.org/10.1016/j.jpba.2014.12.020

21. Olivares O, Däbritz JHM, King A, Gottlieb E, Halsey C (2015) Research into cancer metabolomics: Towards a clinical metamorphosis. Seminars in Cell & Developmental Biology 43:52-64. doi:http://dx.doi.org/10.1016/j.semcdb.2015.09.008

22. Spratlin JL, Serkova NJ, Gail Eckhardt S (2009) Clinical Applications of Metabolomics in Oncology: A Review. Clinical cancer research : an official journal of the American Association for Cancer Research 15 (2):431-440. doi:10.1158/1078-0432.CCR-08-1059

23. Armitage EG, Southam AD (2016) Monitoring cancer prognosis, diagnosis and treatment efficacy using metabolomics and lipidomics. Metabolomics 12 (9):146. doi:10.1007/s11306-016-1093-7

24. Fan Y, Zhou X, Xia T-S, Chen Z, Li J, Liu Q, Alolga RN, Chen Y, Lai M-D, Li P, Zhu W, Qi L-W (2016) Human plasma metabolomics for identifying differential metabolites and predicting molecular subtypes of breast cancer. Oncotarget 7 (9):9925-9938. doi:10.18632/oncotarget.7155

25. Bro R, Kamstrup-Nielsen MH, Engelsen SB, Savorani F, Rasmussen MA, Hansen L, Olsen A, Tjønneland A, Dragsted LO (2015) Forecasting individual breast cancer risk using plasma metabolomics and biocontours. Metabolomics 11 (5):1376-1380. doi:10.1007/s11306-015-0793-8

26. Shen J, Yan L, Liu S, Ambrosone CB, Zhao H (2013) Plasma Metabolomic Profiles in Breast Cancer Patients and Healthy Controls: By Race and Tumor Receptor Subtypes. Translational Oncology 6 (6):757-765

27. Yang M, Soga T, Pollard PJ (2013) Oncometabolites: linking altered metabolism with cancer. The Journal of Clinical Investigation 123 (9):3652-3658. doi:10.1172/JCI67228

28. Dang L, White DW, Gross S, Bennett BD, Bittinger MA, Driggers EM, Fantin VR, Jang HG, Jin S, Keenan MC, Marks KM, Prins RM, Ward PS, Yen KE, Liau LM, Rabinowitz

JD, Cantley LC, Thompson CB, Vander Heiden MG, Su SM (2009) Cancer-associated IDH1 mutations produce 2-hydroxyglutarate. Nature 462 (7274):739-744. doi:nature08617 [pii] 10.1038/nature08617

29. Pollard PJ, Brière JJ, Alam NA, Barwell J, Barclay E, Wortham NC, Hunt T, Mitchell M, Olpin S, Moat SJ, Hargreaves IP, Heales SJ, Chung YL, Griffiths JR, Dalgleish A, McGrath JA, Gleeson MJ, Hodgson SV, Poulsom R, Rustin P, Tomlinson IPM (2005) Accumulation of Krebs cycle intermediates and over-expression of HIF1α in tumours which result from germline FH and SDH mutations. Human Molecular Genetics 14 (15):2231-2239. doi:10.1093/hmg/ddi227

30. Buescher JM, Antoniewicz MR, Boros LG, Burgess SC, Brunengraber H, Clish CB, DeBerardinis RJ, Feron O, Frezza C, Ghesquiere B, Gottlieb E, Hiller K, Jones RG, Kamphorst JJ, Kibbey RG, Kimmelman AC, Locasale JW, Lunt SY, Maddocks OD, Malloy C, Metallo CM, Meuillet EJ, Munger J, Noh K, Rabinowitz JD, Ralser M, Sauer U, Stephanopoulos G, St-Pierre J, Tennant DA, Wittmann C, Vander Heiden MG, Vazquez A, Vousden K, Young JD, Zamboni N, Fendt SM (2015) A roadmap for interpreting (13)C metabolite labeling patterns from cells. Curr Opin Biotechnol 34:189-201. doi:10.1016/j.copbio.2015.02.003

31. Lane AN, Fan TWM (2017) NMR-based Stable Isotope Resolved Metabolomics in systems biochemistry. Archives of Biochemistry and Biophysics. doi:http://dx.doi.org/10.1016/j.abb.2017.02.009

32. Shajahan-Haq AN, Cheema MS, Clarke R (2015) Application of Metabolomics in Drug Resistant Breast Cancer Research. Metabolites 5 (1):100-118. doi:10.3390/metabo5010100

33. Sørlie T, Perou CM, Tibshirani R, Aas T, Geisler S, Johnsen H, Hastie T, Eisen MB, van de Rijn M, Jeffrey SS, Thorsen T, Quist H, Matese JC, Brown PO, Botstein D, Lønning PE, Børresen-Dale AL (2001) Gene expression patterns of breast carcinomas distinguish tumor subclasses with clinical implications. Proc Natl Acad Sci U S A 98. doi:10.1073/pnas.191367098

34. Perou CM, Sorlie T, Eisen MB, van de Rijn M, Jeffrey SS, Rees CA, Pollack JR, Ross DT, Johnsen H, Akslen LA, Fluge O, Pergamenschikov A, Williams C, Zhu SX, Lonning PE, Borresen-Dale A-L, Brown PO, Botstein D (2000) Molecular portraits of human breast tumours. Nature 406 (6797):747-752. doi:http://www.nature.com/nature/journal/v406/n6797/suppinfo/406747a0_S1.html

35. Dai X, Li T, Bai Z, Yang Y, Liu X, Zhan J, Shi B (2015) Breast cancer intrinsic subtype classification, clinical use and future trends. American Journal of Cancer Research 5 (10):2929-2943

36. Sørlie T, Tibshirani R, Parker J, Hastie T, Marron JS, Nobel A, Deng S, Johnsen H, Pesich R, Geisler S, Demeter J, Perou CM, Lønning PE, Brown PO, Børresen-Dale A-L, Botstein D (2003) Repeated observation of breast tumor subtypes in independent gene expression data sets. Proceedings of the National Academy of Sciences 100 (14):8418-8423. doi:10.1073/pnas.0932692100

37. Hu Z, Fan C, Oh DS, Marron JS, He X, Qaqish BF (2006) The molecular portraits of breast tumors are conserved across microarray platforms. BMC Genomics 7. doi:10.1186/1471-2164-7-96

38. Parker JS, Mullins M, Cheang MC, Leung S, Voduc D, Vickery T, Davies S, Fauron C, He X, Hu Z, Quackenbush JF, Stijleman IJ, Palazzo J, Marron JS, Nobel AB, Mardis E, Nielsen TO, Ellis MJ, Perou CM, Bernard PS (2009) Supervised risk predictor of breast cancer based on intrinsic subtypes. J Clin Oncol 27. doi:10.1200/jco.2008.18.1370

39. Liu MC, Pitcher BN, Mardis ER, Davies SR, Friedman PN, Snider JE, Vickery TL, Reed JP, DeSchryver K, Singh B, Gradishar WJ, Perez EA, Martino S, Citron ML, Norton L, Winer EP, Hudis CA, Carey LA, Bernard PS, Nielsen TO, Perou CM, Ellis MJ, Barry WT (2016) PAM50 gene signatures and breast cancer prognosis with adjuvant anthracycline- and taxane-based chemotherapy: correlative analysis of C9741 (Alliance). Npj Breast Cancer 2:15023. doi:10.1038/npjbcancer.2015.23 http://www.nature.com/articles/npjbcancer201523#supplementary-information

40. Howlader N, Altekruse SF, Li CI, Chen VW, Clarke CA, Ries LAG, Cronin KA (2014) US Incidence of Breast Cancer Subtypes Defined by Joint Hormone Receptor and HER2 Status. JNCI Journal of the National Cancer Institute 106 (5):dju055. doi:10.1093/jnci/dju055

41. Foulkes WD, Smith IE, Reis-Filho JS (2010) Triple-Negative Breast Cancer. New England Journal of Medicine 363 (20):1938-1948. doi:doi:10.1056/NEJMra1001389

42. Kim S, Kim DH, Jung W-H, Koo JS (2013) Metabolic phenotypes in triple-negative breast cancer. Tumor Biology 34 (3):1699-1712. doi:10.1007/s13277-013-0707-1

43. Koo HR, Park JS, Kang KW, Cho N, Chang JM, Bae MS, Kim WH, Lee SH, Kim MY, Kim JY, Seo M, Moon WK (2014) ^{18}F-FDG uptake in breast cancer correlates with immunohistochemically defined subtypes. European Radiology 24 (3):610-618. doi:10.1007/s00330-013-3037-1

44. Groheux D, Giacchetti S, Moretti J-L, Porcher R, Espié M, Lehmann-Che J, de Roquancourt A, Hamy A-S, Cuvier C, Vercellino L, Hindié E (2011) Correlation of high ^{18}F-FDG uptake to clinical, pathological and biological prognostic factors in breast cancer. European Journal of Nuclear Medicine and Molecular Imaging 38 (3):426-435. doi:10.1007/s00259-010-1640-9

45. Palaskas N, Larson SM, Schultz N, Komisopoulou E, Wong J, Rohle D, Campos C, Yannuzzi N, Osborne JR, Linkov I, Kastenhuber ER, Taschereau R, Plaisier SB, Tran C, Heguy A, Wu H, Sander C, Phelps ME, Brennan C, Port E, Huse JT, Graeber TG, Mellinghoff IK (2011) ^{18}F-Fluorodeoxy-glucose Positron Emission Tomography Marks MYC-Overexpressing Human Basal-Like Breast Cancers. Cancer Research 71 (15):5164-5174. doi:10.1158/0008-5472.can-10-4633

46. Choi J, Kim DH, Jung WH, Koo JS (2013) Metabolic interaction between cancer cells and stromal cells according to breast cancer molecular subtype. Breast Cancer Research 15 (5):R78. doi:10.1186/bcr3472

47. Doyen J, Trastour C, Ettore F, Peyrottes I, Toussant N, Gal J, Ilc K, Roux D, Parks SK, Ferrero JM, Pouysségur J (2014) Expression of the hypoxia-inducible monocarboxylate transporter MCT4 is increased in triple negative breast cancer and correlates independently with clinical outcome. Biochemical and Biophysical Research Communications 451 (1):54-61. doi:http://dx.doi.org/10.1016/j.bbrc.2014.07.050

48. McCleland ML, Adler AS, Shang Y, Hunsaker T, Truong T, Peterson D, Torres E, Li L, Haley B, Stephan J-P, Belvin M, Hatzivassiliou G, Blackwood EM, Corson L, Evangelista M, Zha J, Firestein R (2012) An Integrated Genomic Screen Identifies LDHB as an Essential Gene for Triple-Negative Breast Cancer. Cancer Research 72 (22):5812-5823. doi:10.1158/0008-5472.can-12-1098

49. Van Dang C, Xu J, Chen Y, Olopade OI (2010) MYC and Breast Cancer. Genes & Cancer 1 (6):629-640. doi:10.1177/1947601910378691

50. Osthus RC, Shim H, Kim S, Li Q, Reddy R, Mukherjee M, Xu Y, Wonsey D, Lee LA, Dang CV (2000) Deregulation of Glucose Transporter 1 and Glycolytic Gene Expression by c-Myc. Journal of Biological Chemistry 275 (29):21797-21800. doi:10.1074/jbc.C000023200

51. Shim H, Dolde C, Lewis BC, Wu C-S, Dang G, Jungmann RA, Dalla-Favera R, Dang CV (1997) c-Myc transactivation of LDH-A: Implications for tumor metabolism and growth. Proceedings of the National Academy of Sciences 94 (13):6658-6663

52. Shen L, O'Shea JM, Kaadige MR, Cunha S, Wilde BR, Cohen AL, Welm AL, Ayer DE (2015) Metabolic reprogramming in triple-negative breast cancer through Myc suppression of TXNIP. Proceedings of the National Academy of Sciences 112 (17):5425-5430. doi:10.1073/pnas.1501555112

53. Nakai K, Hung M-C, Yamaguchi H (2016) A perspective on anti-EGFR therapies targeting triple-negative breast cancer. American Journal of Cancer Research 6 (8):1609-1623

54. Costa R, Shah AN, Santa-Maria CA, Cruz MR, Mahalingam D, Carneiro BA, Chae YK, Cristofanilli M, Gradishar WJ, Giles FJ (2017) Targeting Epidermal Growth Factor Receptor in triple negative breast cancer: New discoveries and practical insights for drug development. Cancer Treatment Reviews 53:111-119. doi:http://dx.doi.org/10.1016/j.ctrv.2016.12.010

55. Lim S-O, Li C-W, Xia W, Lee H-H, Chang S-S, Shen J, Hsu JL, Raftery D, Djukovic D, Gu H, Chang W-C, Wang H-L, Chen M-L, Huo L, Chen C-H, Wu Y, Sahin A, Hanash SM, Hortobagyi GN, Hung M-C (2016) EGFR Signaling Enhances Aerobic Glycolysis in Triple-Negative Breast Cancer Cells to Promote Tumor Growth and Immune Escape. Cancer Research 76 (5):1284-1296. doi:10.1158/0008-5472.can-15-2478

56. Dang Chi V (2012) *MYC* on the Path to Cancer. Cell 149 (1):22-35. doi:10.1016/j.cell.2012.03.003

57. Wise DR, DeBerardinis RJ, Mancuso A, Sayed N, Zhang X-Y, Pfeiffer HK, Nissim I, Daikhin E, Yudkoff M, McMahon SB, Thompson CB (2008) Myc regulates a transcriptional program that stimulates mitochondrial glutaminolysis and leads to glutamine addiction. Proceedings of the National Academy of Sciences 105 (48):18782-18787. doi:10.1073/pnas.0810199105

58. Gao P, Tchernyshyov I, Chang TC, Lee YS, Kita K, Ochi T, Zeller KI, De Marzo AM, Van Eyk JE, Mendell JT, Dang CV (2009) c-Myc suppression of miR-23a/b enhances mitochondrial glutaminase expression and glutamine metabolism. Nature 458 (7239):762-765. doi:10.1038/nature07823

59. Kim JY, Heo S-H, Choi SK, Song IH, Park IA, Kim Y-A, Park HS, Park SY, Bang WS, Gong G, Lee HJ (2017) Glutaminase expression is a poor prognostic factor in node-positive triple-negative breast cancer patients with a high level of tumor-infiltrating lymphocytes. Virchows Archiv:1-9. doi:10.1007/s00428-017-2083-5

60. Wise DR, Thompson CB (2010) Glutamine Addiction: A New Therapeutic Target in Cancer. Trends in biochemical sciences 35 (8):427-433. doi:10.1016/j.tibs.2010.05.003

61. Hensley CT, Wasti AT, DeBerardinis RJ (2013) Glutamine and cancer: cell biology, physiology, and clinical opportunities. The Journal of Clinical Investigation 123 (9):3678-3684. doi:10.1172/JCI69600

62. Yang L, Venneti S, Nagrath D (2017) Glutaminolysis: A Hallmark of Cancer Metabolism. Annual Review of Biomedical Engineering. doi:10.1146/annurev-bioeng-071516-044546

63. McKeehan WL (1982) Glycolysis, glutaminolysis and cell proliferation. Cell Biol Int Rep 6 (7):635-650

64. Kim S, Kim DH, Jung W-H, Koo JS (2013) Expression of glutamine metabolism-related proteins according to molecular subtype of breast cancer. Endocrine-Related Cancer 20 (3):339-348. doi:10.1530/erc-12-0398

65. Kung H-N, Marks JR, Chi J-T (2011) Glutamine Synthetase Is a Genetic Determinant of Cell Type–Specific Glutamine Independence in Breast Epithelia. PLOS Genetics 7 (8):e1002229. doi:10.1371/journal.pgen.1002229

66. Timmerman Luika A, Holton T, Yuneva M, Louie Raymond J, Padró M, Daemen A, Hu M, Chan Denise A, Ethier Stephen P, van ‘t Veer Laura J, Polyak K, McCormick F, Gray Joe W (2013) Glutamine Sensitivity Analysis Identifies the xCT Antiporter as a Common Triple-Negative Breast Tumor Therapeutic Target. Cancer Cell 24 (4):450-465. doi:10.1016/j.ccr.2013.08.020

67. Cetinbas NM, Sudderth J, Harris RC, Cebeci A, Negri GL, Yılmaz ÖH, DeBerardinis RJ, Sorensen PH (2016) Glucose-dependent anaplerosis in cancer cells is required for cellular redox balance in the absence of glutamine. Scientific Reports 6:32606. doi:10.1038/srep32606

68. Davidson Shawn M, Papagiannakopoulos T, Olenchock Benjamin A, Heyman Julia E, Keibler Mark A, Luengo A, Bauer Matthew R, Jha Abhishek K, O'Brien James P, Pierce Kerry A, Gui Dan Y, Sullivan Lucas B, Wasylenko Thomas M, Subbaraj L, Chin Christopher R, Stephanopolous G, Mott Bryan T, Jacks T, Clish Clary B, Vander Heiden Matthew G (2016) Environment Impacts the Metabolic Dependencies of Ras-Driven Non-Small Cell Lung Cancer. Cell Metabolism 23 (3):517-528. doi:https://doi.org/10.1016/j.cmet.2016.01.007

69. Haukaas TH, Euceda LR, Giskeødegård GF, Lamichhane S, Krohn M, Jernström S, Aure MR, Lingjærde OC, Schlichting E, Garred Ø, Due EU, Mills GB, Sahlberg KK, Børresen-Dale A-L, Bathen TF, The Oslo Breast Cancer C (2016) Metabolic clusters of breast cancer in relation to gene- and protein expression subtypes. Cancer & Metabolism 4:12. doi:10.1186/s40170-016-0152-x

70. Gross MI, Demo SD, Dennison JB, Chen L, Chernov-Rogan T, Goyal B, Janes JR, Laidig GJ, Lewis ER, Li J, MacKinnon AL, Parlati F, Rodriguez MLM, Shwonek PJ, Sjogren EB, Stanton TF, Wang T, Yang J, Zhao F, Bennett MK (2014) Antitumor Activity of the Glutaminase Inhibitor CB-839 in Triple-Negative Breast Cancer. Molecular Cancer Therapeutics 13 (4):890. doi:10.1158/1535-7163.MCT-13-0870

71. Cao MD, Lamichhane S, Lundgren S, Bofin A, Fjøsne H, Giskeødegård GF, Bathen TF (2014) Metabolic characterization of triple negative breast cancer. BMC Cancer 14:941. doi:10.1186/1471-2407-14-941

72. van Geldermalsen M, Wang Q, Nagarajah R, Marshall AD, Thoeng A, Gao D, Ritchie W, Feng Y, Bailey CG, Deng N, Harvey K, Beith JM, Selinger CI, O'Toole SA, Rasko JEJ, Holst J (2016) ASCT2/SLC1A5 controls glutamine uptake and tumour growth in triple-negative basal-like breast cancer. Oncogene 35 (24):3201-3208. doi:10.1038/onc.2015.381

73. Possemato R, Marks KM, Shaul YD, Pacold ME, Kim D, Birsoy K, Sethumadhavan S, Woo H-K, Jang HG, Jha AK, Chen WW, Barrett FG, Stransky N, Tsun Z-Y, Cowley GS, Barretina J, Kalaany NY, Hsu PP, Ottina K, Chan AM, Yuan B, Garraway LA, Root DE, Mino-Kenudson M, Brachtel EF, Driggers EM, Sabatini DM (2011) Functional genomics reveal that the serine synthesis pathway is essential in breast cancer. Nature 476(7360):346-350.

doi:http://www.nature.com/nature/journal/v476/n7360/abs/nature10350.html#supplementary-information

74. Locasale JW, Grassian AR, Melman T, Lyssiotis CA, Mattaini KR, Bass AJ, Heffron G, Metallo CM, Muranen T, Sharfi H, Sasaki AT, Anastasiou D, Mullarky E, Vokes NI, Sasaki M, Beroukhim R, Stephanopoulos G, Ligon AH, Meyerson M, Richardson AL, Chin L, Wagner G, Asara JM, Brugge JS, Cantley LC, Vander Heiden MG (2011) Phosphoglycerate dehydrogenase diverts glycolytic flux and contributes to oncogenesis. Nature genetics 43 (9):869-874. doi:10.1038/ng.890

75. Noh S, Kim DH, Jung WH, Koo JS (2014) Expression levels of serine/glycine metabolism-related proteins in triple negative breast cancer tissues. Tumor Biology 35 (5):4457-4468

76. Pollari S, Käkönen S-M, Edgren H, Wolf M, Kohonen P, Sara H, Guise T, Nees M, Kallioniemi O (2011) Enhanced serine production by bone metastatic breast cancer cells stimulates osteoclastogenesis. Breast cancer research and treatment 125 (2):421-430

77. Sun L, Song L, Wan Q, Wu G, Li X, Wang Y, Wang J, Liu Z, Zhong X, He X, Shen S, Pan X, Li A, Wang Y, Gao P, Tang H, Zhang H (2015) cMyc-mediated activation of serine biosynthesis pathway is critical for cancer progression under nutrient deprivation conditions. Cell Res 25 (4):429-444. doi:10.1038/cr.2015.33

78. Mattaini KR, Sullivan MR, Vander Heiden MG (2016) The importance of serine metabolism in cancer. The Journal of Cell Biology 214 (3):249-257. doi:10.1083/jcb.201604085

79. Amelio I, Cutruzzolá F, Antonov A, Agostini M, Melino G (2014) Serine and glycine metabolism in cancer. Trends in Biochemical Sciences 39 (4):191-198. doi:https://doi.org/10.1016/j.tibs.2014.02.004

80. Jain M, Nilsson R, Sharma S, Madhusudhan N, Kitami T, Souza AL, Kafri R, Kirschner MW, Clish CB, Mootha VK (2012) Metabolite Profiling Identifies a Key Role for Glycine in Rapid Cancer Cell Proliferation. Science 336 (6084):1040-1044. doi:10.1126/science.1218595

81. Tang X, Ding CK, Wu J, Sjol J, Wardell S, Spasojevic I, George D, McDonnell DP, Hsu DS, Chang JT, Chi JT (2016) Cystine addiction of triple-negative breast cancer associated with EMT augmented death signaling. Oncogene. doi:10.1038/onc.2016.394

82. Wang Z, Shi X, Li Y, Fan J, Zeng X, Xian Z, Wang Z, Sun Y, Wang S, Song P, Zhao S, Hu H, Ju D (2014) Blocking autophagy enhanced cytotoxicity induced by recombinant human arginase in triple-negative breast cancer cells. Cell Death Dis 5:e1563. doi:10.1038/cddis.2014.503

83. Korde Choudhari S, Chaudhary M, Bagde S, Gadbail AR, Joshi V (2013) Nitric oxide and cancer: a review. World Journal of Surgical Oncology 11 (1):118. doi:10.1186/1477-7819-11-118

84. Martinez L, Thames E, Kim J, Chaudhuri G, Singh R, Pervin S (2016) Increased sensitivity of African American triple negative breast cancer cells to nitric oxide-induced mitochondria-mediated apoptosis. BMC Cancer 16:559. doi:10.1186/s12885-016-2547-z

85. Pervin S, Singh R, Hernandez E, Wu G, Chaudhuri G (2007) Nitric Oxide in Physiologic Concentrations Targets the Translational Machinery to Increase the Proliferation of Human Breast Cancer Cells: Involvement of Mammalian Target of Rapamycin/eIF4E Pathway. Cancer Research 67 (1):289-299. doi:10.1158/0008-5472.can-05-4623

86. Long Y, Tsai W-B, Wang D, Hawke DH, Savaraj N, Feun LG, Hung M-C, Chen HHW, Kuo MT (2017) Argininosuccinate synthetase 1 (ASS1) is a common metabolic marker of chemosensitivity for targeted arginine- and glutamine-starvation therapy. Cancer Letters 388:54-63. doi:https://doi.org/10.1016/j.canlet.2016.11.028

87. Hernandez CP, Morrow K, Lopez-Barcons LA, Zabaleta J, Sierra R, Velasco C, Cole J, Rodriguez PC (2010) Pegylated arginase I: a potential therapeutic approach in T-ALL. Blood 115 (25):5214-5221. doi:10.1182/blood-2009-12-258822

88. Zeng X, Li Y, Fan J, Zhao H, Xian Z, Sun Y, Wang Z, Wang S, Zhang G, Ju D (2013) Recombinant human arginase induced caspase-dependent apoptosis and autophagy in non-Hodgkin/'s lymphoma cells. Cell Death Dis 4:e840. doi:10.1038/cddis.2013.359

89. Tanios R, Bekdash A, Kassab E, Stone E, Georgiou G, Frankel AE, Abi-Habib RJ (2013) Human recombinant arginase I(Co)-PEG5000 [HuArgI(Co)-PEG5000]-induced arginine depletion is selectively cytotoxic to human acute myeloid leukemia cells. Leukemia Research 37 (11):1565-1571. doi:http://dx.doi.org/10.1016/j.leukres.2013.08.007

90. Sugimura K, Ohno T, Kusuyama T, Azuma I (1992) High sensitivity of human melanoma cell lines to the growth inhibitory activity of mycoplasmal arginine deiminase in vitro. Melanoma Res 2 (3):191-196

91. Cheng PN-M, Lam T-L, Lam W-M, Tsui S-M, Cheng AW-M, Lo W-H, Leung Y-C (2007) Pegylated Recombinant Human Arginase (rhArg-peg5,000mw) Inhibits the In vitro and In vivo Proliferation of Human Hepatocellular Carcinoma through Arginine Depletion. Cancer Research 67 (1):309-317. doi:10.1158/0008-5472.can-06-1945

92. Bowles TL, Kim R, Galante J, Parsons CM, Virudachalam S, Kung H-J, Bold RJ (2008) Pancreatic cancer cell lines deficient in argininosuccinate synthetase are sensitive to arginine deprivation by arginine deiminase. International Journal of Cancer 123 (8):1950-1955. doi:10.1002/ijc.23723

93. Antalis CJ, Arnold T, Rasool T, Lee B, Buhman KK, Siddiqui RA (2010) High ACAT1 expression in estrogen receptor negative basal-like breast cancer cells is associated with LDL-induced proliferation. Breast Cancer Research and Treatment 122 (3):661-670. doi:10.1007/s10549-009-0594-8

94. Vithayathil SA, Ma Y, Kaipparettu BA (2012) Transmitochondrial Cybrids: Tools for Functional Studies of Mutant Mitochondria. In: Wong PDL-JC (ed) Mitochondrial Disorders: Biochemical and Molecular Analysis. Humana Press, Totowa, NJ, pp 219-230. doi:10.1007/978-1-61779-504-6_15

95. Park Jun H, Vithayathil S, Kumar S, Sung P-L, Dobrolecki Lacey E, Putluri V, Bhat Vadiraja B, Bhowmik Salil K, Gupta V, Arora K, Wu D, Tsouko E, Zhang Y, Maity S, Donti Taraka R, Graham Brett H, Frigo Daniel E, Coarfa C, Yotnda P, Putluri N, Sreekumar A, Lewis Michael T, Creighton Chad J, Wong L-Jun C, Kaipparettu Benny A (2016) Fatty Acid Oxidation-Driven Src Links Mitochondrial Energy Reprogramming and Oncogenic Properties in Triple-Negative Breast Cancer. Cell Reports 14 (9):2154-2165. doi:10.1016/j.celrep.2016.02.004

96. Camarda R, Zhou AY, Kohnz RA, Balakrishnan S, Mahieu C, Anderton B, Eyob H, Kajimura S, Tward A, Krings G, Nomura DK, Goga A (2016) Inhibition of fatty acid oxidation as a therapy for MYC-overexpressing triple-negative breast cancer. Nat Med 22 (4):427-432. doi:10.1038/nm.4055

http://www.nature.com/nm/journal/v22/n4/abs/nm.4055.html#supplementary-information

97. Bonnefont J-P, Djouadi F, Prip-Buus C, Gobin S, Munnich A, Bastin J (2004) Carnitine palmitoyltransferases 1 and 2: biochemical, molecular and medical aspects. Molecular Aspects of Medicine 25 (5–6):495-520. doi:http://dx.doi.org/10.1016/j.mam.2004.06.004

98. Onitilo AA, Engel JM, Greenlee RT, Mukesh BN (2009) Breast Cancer Subtypes Based on ER/PR and Her2 Expression: Comparison of Clinicopathologic Features and Survival. Clinical Medicine & Research 7 (1-2):4-13. doi:10.3121/cmr.2009.825

99. Pearson OH, Manni A, Arafah B, uddin M (1982) Antiestrogen Treatment of Breast Cancer: An Overview. Cancer Research 42 (8 Supplement):3424s

100. Pavlides S, Whitaker-Menezes D, Castello-Cros R, Flomenberg N, Witkiewicz AK, Frank PG, Casimiro MC, Wang C, Fortina P, Addya S, Pestell RG, Martinez-Outschoorn UE, Sotgia F, Lisanti MP (2009) The reverse Warburg effect: Aerobic glycolysis in cancer associated fibroblasts and the tumor stroma. Cell Cycle 8 (23):3984-4001. doi:10.4161/cc.8.23.10238

101. Martinez-Outschoorn UE, Lin Z, Trimmer C, Flomenberg N, Wang C, Pavlides S, Pestell RG, Howell A, Sotgia F, Lisanti MP (2011) Cancer cells metabolically "fertilize" the tumor microenvironment with hydrogen peroxide, driving the Warburg effect. Cell Cycle 10 (15):2504-2520. doi:10.4161/cc.10.15.16585

102. Martinez-Outschoorn UE, Trimmer C, Lin Z, Whitaker-Menezes D, Chiavarina B, Zhou J, Wang C, Pavlides S, Martinez-Cantarin MP, Capozza F, Witkiewicz AK, Flomenberg N, Howell A, Pestell RG, Caro J, Lisanti MP, Sotgia F (2010) Autophagy in cancer associated fibroblasts promotes tumor cell survival. Cell Cycle 9 (17):3515-3533. doi:10.4161/cc.9.17.12928

103. Martinez-Outschoorn UE, Pavlides S, Whitaker-Menezes D, Daumer KM, Milliman JN, Chiavarina B, Migneco G, Witkiewicz AK, Martinez-Cantarin MP, Flomenberg N, Howell A, Pestell RG, Lisanti MP, Sotgia F (2010) Tumor cells induce the cancer

associated fibroblast phenotype via caveolin-1 degradation: implications for breast cancer and DCIS therapy with autophagy inhibitors. Cell Cycle 9. doi:10.4161/cc.9.12.12048

104. Whitaker-Menezes D, Martinez-Outschoorn UE, Lin Z, Ertel A, Flomenberg N, Witkiewicz AK, Birbe R, Howell A, Pavlides S, Gandara R, Pestell RG, Sotgia F, Philp NJ, Lisanti MP (2011) Evidence for a stromal-epithelial “lactate shuttle” in human tumors. Cell Cycle 10 (11):1772-1783. doi:10.4161/cc.10.11.15659

105. Clarke R, Liu MC, Bouker KB, Gu Z, Lee RY, Zhu Y, Skaar TC, Gomez B, O'Brien K, Wang Y, Hilakivi-Clarke LA (2003) Antiestrogen resistance in breast cancer and the role of estrogen receptor signaling. Oncogene 22 (47):7316-7339

106. Harris JR, Lippman ME, Morrow M (1996) Diseases of the Breast. Wolters Kluwer Health, Philadelphia, US

107. Budczies J, Brockmöller SF, Müller BM, Barupal DK, Richter-Ehrenstein C, Kleine-Tebbe A, Griffin JL, Orešič M, Dietel M, Denkert C, Fiehn O (2013) Comparative metabolomics of estrogen receptor positive and estrogen receptor negative breast cancer: alterations in glutamine and beta-alanine metabolism. Journal of Proteomics 94:279-288. doi:http://dx.doi.org/10.1016/j.jprot.2013.10.002

108. Russo J, Russo IH (2006) The role of estrogen in the initiation of breast cancer. J Steroid Biochem Mol Biol 102. doi:10.1016/j.jsbmb.2006.09.004

109. Duffy MJ (2006) Estrogen Receptors: Role in Breast Cancer. Critical Reviews in Clinical Laboratory Sciences 43 (4):325-347. doi:10.1080/10408360600739218

110. O'Mahony F, Razandi M, Pedram A, Harvey BJ, Levin ER (2012) Estrogen Modulates Metabolic Pathway Adaptation to Available Glucose in Breast Cancer Cells. Molecular Endocrinology 26 (12):2058-2070. doi:10.1210/me.2012-1191

111. Krętowski R, Borzym-Kluczyk M, Stypułkowska A, Brańska-Januszewska J, Ostrowska H, Cechowska-Pasko M (2016) Low glucose dependent decrease of apoptosis and induction of autophagy in breast cancer MCF-7 cells. Molecular and Cellular Biochemistry 417 (1):35-47. doi:10.1007/s11010-016-2711-4

112. Jia M, Andreassen T, Jensen L, Bathen TF, Sinha I, Gao H, Zhao C, Haldosen L-A, Cao Y, Girnita L, Moestue SA, Dahlman-Wright K (2016) Estrogen Receptor α Promotes Breast Cancer by Reprogramming Choline Metabolism. Cancer Research 76 (19):5634-5646. doi:10.1158/0008-5472.can-15-2910

113. Grinde MT, Skrbo N, Moestue SA, Rødland EA, Borgan E, Kristian A, Sitter B, Bathen TF, Børresen-Dale A-L, Mælandsmo GM, Engebraaten O, Sørlie T, Marangoni E, Gribbestad IS (2014) Interplay of choline metabolites and genes in patient-derived breast cancer xenografts. Breast Cancer Research 16 (1):R5. doi:10.1186/bcr3597

114. Deblois G, Giguere V (2013) Oestrogen-related receptors in breast cancer: control of cellular metabolism and beyond. Nature reviews Cancer 13 (1):27-36

115. Musgrove EA, Sutherland RL (2009) Biological determinants of endocrine resistance in breast cancer. Nat Rev Cancer 9 (9):631-643

116. Osborne CK, Schiff R (2011) Mechanisms of Endocrine Resistance in Breast Cancer. Annual Review of Medicine 62 (1):233-247. doi:10.1146/annurev-med-070909-182917

117. Poirot M, Silvente-Poirot S, Weichselbaum RR (2012) Cholesterol metabolism and resistance to tamoxifen. Current Opinion in Pharmacology 12 (6):683-689. doi:http://dx.doi.org/10.1016/j.coph.2012.09.007

118. Lloyd SM, Arnold J, Sreekumar A (2015) Metabolomic profiling of hormone-dependent cancers: a bird's eye view. Trends in Endocrinology & Metabolism 26 (9):477-485. doi:10.1016/j.tem.2015.07.001

119. Pitroda SP, Khodarev NN, Beckett MA, Kufe DW, Weichselbaum RR (2009) MUC1-induced alterations in a lipid metabolic gene network predict response of human breast cancers to tamoxifen treatment. Proceedings of the National Academy of Sciences 106 (14):5837-5841. doi:10.1073/pnas.0812029106

120. Putluri N, Maity S, Kommangani R, Creighton CJ, Putluri V, Chen F, Nanda S, Bhowmik SK, Terunuma A, Dorsey T, Nardone A, Fu X, Shaw C, Sarkar TR, Schiff R, Lydon JP, O'Malley BW, Ambs S, Das GM, Michailidis G, Sreekumar A (2014) Pathway-Centric Integrative Analysis Identifies RRM2 as a Prognostic Marker in Breast Cancer

Associated with Poor Survival and Tamoxifen Resistance. Neoplasia (New York, NY) 16 (5):390-402. doi:10.1016/j.neo.2014.05.007

121. Shah KN, Mehta KR, Peterson D, Evangelista M, Livesey JC, Faridi JS (2014) AKT-Induced Tamoxifen Resistance Is Overturned by RRM2 Inhibition. Molecular Cancer Research 12 (3):394-407. doi:10.1158/1541-7786.mcr-13-0219

122. Slamon DJ, Clark GM, Wong SG, Levin WJ, Ullrich A, McGuire WL (1987) Human breast cancer: correlation of relapse and survival with amplification of the HER-2/neu oncogene. Science 235 (4785):177

123. Slamon DJ, Godolphin W, Jones LA, Holt JA, Wong SG, Keith DE (1989) Studies of the HER-2/neu proto-oncogene in human breast and ovarian cancer. Science 244. doi:10.1126/science.2470152

124. Wirapati P, Sotiriou C, Kunkel S, Farmer P, Pradervand S, Haibe-Kains B, Desmedt C, Ignatiadis M, Sengstag T, Schütz F, Goldstein DR, Piccart M, Delorenzi M (2008) Meta-analysis of gene expression profiles in breast cancer: toward a unified understanding of breast cancer subtyping and prognosis signatures. Breast Cancer Research 10 (4):R65. doi:10.1186/bcr2124

125. Carey LA, Perou CM, Livasy CA, et al. (2006) Race, breast cancer subtypes, and survival in the carolina breast cancer study. JAMA : the journal of the American Medical Association 295 (21):2492-2502. doi:10.1001/jama.295.21.2492

126. Martin L-A, Farmer I, Johnston SRD, Ali S, Marshall C, Dowsett M (2003) Enhanced Estrogen Receptor (ER) α, ERBB2, and MAPK Signal Transduction Pathways Operate during the Adaptation of MCF-7 Cells to Long Term Estrogen Deprivation. Journal of Biological Chemistry 278 (33):30458-30468. doi:10.1074/jbc.M305226200

127. Flågeng MH, Haugan Moi LL, Dixon JM, Geisler J, Lien EA, Miller WR, Lønning PE, Mellgren G (2009) Nuclear receptor co-activators and HER-2/neu are upregulated in breast cancer patients during neo-adjuvant treatment with aromatase inhibitors. British Journal of Cancer 101 (8):1253-1260. doi:10.1038/sj.bjc.6605324

128. Romond EH, Perez EA, Bryant J, Suman VJ, Geyer CEJ, Davidson NE, Tan-Chiu E, Martino S, Paik S, Kaufman PA, Swain SM, Pisansky TM, Fehrenbacher L, Kutteh LA,

Vogel VG, Visscher DW, Yothers G, Jenkins RB, Brown AM, Dakhil SR, Mamounas EP, Lingle WL, Klein PM, Ingle JN, Wolmark N (2005) Trastuzumab plus Adjuvant Chemotherapy for Operable HER2-Positive Breast Cancer. New England Journal of Medicine 353 (16):1673-1684. doi:doi:10.1056/NEJMoa052122

129. Vu T, Claret FX (2012) Trastuzumab: Updated Mechanisms of Action and Resistance in Breast Cancer. Frontiers in oncology 2:62. doi:10.3389/fonc.2012.00062

130. Moasser MM (2007) The oncogene HER2; Its signaling and transforming functions and its role in human cancer pathogenesis. Oncogene 26 (45):6469-6487. doi:10.1038/sj.onc.1210477

131. Roberts PJ, Der CJ (2007) Targeting the Raf-MEK-ERK mitogen-activated protein kinase cascade for the treatment of cancer. Oncogene 26 (22):3291-3310

132. Plas DR, Thompson CB (2005) Akt-dependent transformation: there is more to growth than just surviving. Oncogene 24 (50):7435-7442. doi:1209097 [pii] 10.1038/sj.onc.1209097

133. Walsh AJ, Cook RS, Manning HC, Hicks DJ, Lafontant A, Arteaga CL, Skala MC (2013) Optical metabolic imaging identifies glycolytic levels, sub-types and early treatment response in breast cancer. Cancer research 73 (20):6164-6174. doi:10.1158/0008-5472.CAN-13-0527

134. O'Neal J, Clem A, Reynolds L, Dougherty S, Imbert-Fernandez Y, Telang S, Chesney J, Clem BF (2016) Inhibition of 6-phosphofructo-2-kinase (PFKFB3) suppresses glucose metabolism and the growth of HER2+ breast cancer. Breast Cancer Research and Treatment 160 (1):29-40. doi:10.1007/s10549-016-3968-8

135. Chen Y, Qian J, He Q, Zhao H, Toral-Barza L, Shi C, Zhang X, Wu J, Yu K (2016) mTOR complex-2 stimulates acetyl-CoA and de novo lipogenesis through ATP citrate lyase in HER2/PIK3CA-hyperactive breast cancer. Oncotarget 7 (18)

136. Jin Q, Yuan LX, Boulbes D, Baek JM, Wang YN, Gomez-Cabello D, Hawke DH, Yeung SC, Lee MH, Hortobagyi GN, Hung MC, Esteva FJ (2010) Fatty acid synthase phosphorylation: a novel therapeutic target in HER2-overexpressing breast cancer cells. Breast Cancer Research : BCR 12 (6):R96-R96. doi:10.1186/bcr2777

137. Menendez JA, Vellon L, Mehmi I, Oza BP, Ropero S, Colomer R, Lupu R (2004) Inhibition of fatty acid synthase (FAS) suppresses HER2/neu (erbB-2) oncogene overexpression in cancer cells. Proceedings of the National Academy of Sciences of the United States of America 101 (29):10715-10720. doi:10.1073/pnas.0403390101

138. Youngblood VM, Kim LC, Edwards DN, Hwang Y, Santapuram PR, Stirdivant SM, Lu P, Ye F, Brantley-Sieders DM, Chen J (2016) The Ephrin-A1/EPHA2 Signaling Axis Regulates Glutamine Metabolism in HER2-Positive Breast Cancer. Cancer Research 76 (7):1825-1836. doi:10.1158/0008-5472.can-15-0847

139. van Uden DJP, van Laarhoven HWM, Westenberg AH, de Wilt JHW, Blanken-Peeters CFJM (2015) Inflammatory breast cancer: An overview. Critical Reviews in Oncology / Hematology 93 (2):116-126. doi:10.1016/j.critrevonc.2014.09.003

140. Robertson FM, Bondy M, Yang W, Yamauchi H, Wiggins S, Kamrudin S, Krishnamurthy S, Le-Petross H, Bidaut L, Player AN, Barsky SH, Woodward WA, Buchholz T, Lucci A, Ueno N, Cristofanilli M (2010) Inflammatory Breast Cancer: The Disease, the Biology, the Treatment. CA: a cancer journal for clinicians 60 (6):351-375. doi:10.3322/caac.20082

141. Hance KW, Anderson WF, Devesa SS, Young HA, Levine PH (2005) Trends in Inflammatory Breast Carcinoma Incidence and Survival: The Surveillance, Epidemiology, and End Results Program at the National Cancer Institute. Journal of the National Cancer Institute 97 (13):966-975. doi:10.1093/jnci/dji172

142. Parton M, Dowsett M, Ashley S, Hills M, Lowe F, Smith IE (2004) High incidence of HER-2 positivity in inflammatory breast cancer. The Breast 13 (2):97-103. doi:http://dx.doi.org/10.1016/j.breast.2003.08.004

143. Masuda H, Brewer TM, Liu DD, Iwamoto T, Shen Y, Hsu L, Willey JS, Gonzalez-Angulo AM, Chavez-MacGregor M, Fouad TM, Woodward WA, Reuben JM, Valero V, Alvarez RH, Hortobagyi GN, Ueno NT (2014) Long-term treatment efficacy in primary inflammatory breast cancer by hormonal receptor- and HER2-defined subtypes. Annals of Oncology 25 (2):384-391. doi:10.1093/annonc/mdt525

144. Liu J, Chen K, Jiang W, Mao K, Li S, Kim MJ, Liu Q, Jacobs LK (2017) Chemotherapy response and survival of inflammatory breast cancer by hormone receptor- and HER2-defined molecular subtypes approximation: an analysis from the National Cancer

Database. Journal of Cancer Research and Clinical Oncology 143 (1):161-168. doi:10.1007/s00432-016-2281-6

145. Wynn ML, Yates JA, Evans CR, Van Wassenhove LD, Wu ZF, Bridges S, Bao L, Fournier C, Ashrafzadeh S, Merrins MJ, Satin LS, Schnell S, Burant CF, Merajver SD (2016) RhoC GTPase Is a Potent Regulator of Glutamine Metabolism and N-Acetylaspartate Production in Inflammatory Breast Cancer Cells. Journal of Biological Chemistry 291 (26):13715-13729. doi:10.1074/jbc.M115.703959

146. Anastasiou D, Yu Y, Israelsen WJ, Jiang J-K, Boxer MB, Hong BS, Tempel W, Dimov S, Shen M, Jha A, Yang H, Mattaini KR, Metallo CM, Fiske BP, Courtney KD, Malstrom S, Khan TM, Kung C, Skoumbourdis AP, Veith H, Southall N, Walsh MJ, Brimacombe KR, Leister W, Lunt SY, Johnson ZR, Yen KE, Kunii K, Davidson SM, Christofk HR, Austin CP, Inglese J, Harris MH, Asara JM, Stephanopoulos G, Salituro FG, Jin S, Dang L, Auld DS, Park H-W, Cantley LC, Thomas CJ, Vander Heiden MG (2012) Pyruvate kinase M2 activators promote tetramer formation and suppress tumorigenesis. Nat Chem Biol 8 (10):839-847. doi:http://www.nature.com/nchembio/journal/v8/n10/abs/nchembio.1060.html#supplementary-information

147. Christofk HR, Vander Heiden MG, Harris MH, Ramanathan A, Gerszten RE, Wei R, Fleming MD, Schreiber SL, Cantley LC (2008) The M2 splice isoform of pyruvate kinase is important for cancer metabolism and tumour growth. Nature 452 (7184):230-233. doi:nature06734 [pii] 10.1038/nature06734

148. Mazurek S (2011) Pyruvate kinase type M2: A key regulator of the metabolic budget system in tumor cells. The International Journal of Biochemistry & Cell Biology 43 (7):969-980. doi:http://dx.doi.org/10.1016/j.biocel.2010.02.005

149. Lunt SY, Muralidhar V, Hosios AM, Israelsen WJ, Gui DY, Newhouse L, Ogrodzinski M, Hecht V, Xu K, Acevedo PN, Hollern DP, Bellinger G, Dayton TL, Christen S, Elia I, Dinh AT, Stephanopoulos G, Manalis SR, Yaffe MB, Andrechek ER, Fendt SM, Vander Heiden MG (2015) Pyruvate kinase isoform expression alters nucleotide synthesis to impact cell proliferation. Mol Cell 57 (1):95-107. doi:10.1016/j.molcel.2014.10.027

150. Hanahan D, Weinberg RA (2011) Hallmarks of cancer: the next generation. Cell 144 (5):646-674. doi:10.1016/j.cell.2011.02.013

151. Baeriswyl V, Christofori G (2009) The angiogenic switch in carcinogenesis. Seminars in Cancer Biology 19 (5):329-337. doi:http://dx.doi.org/10.1016/j.semcancer.2009.05.003

152. Ravi R, Mookerjee B, Bhujwalla ZM, Sutter CH, Artemov D, Zeng Q, Dillehay LE, Madan A, Semenza GL, Bedi A (2000) Regulation of tumor angiogenesis by p53-induced degradation of hypoxia-inducible factor 1α. Genes & Development 14 (1):34-44. doi:10.1101/gad.14.1.34

153. Pugh CW, Ratcliffe PJ (2003) Regulation of angiogenesis by hypoxia: role of the HIF system. Nat Med 9 (6):677-684

154. Schito L, Semenza GL (2016) Hypoxia-Inducible Factors: Master Regulators of Cancer Progression. Trends in Cancer 2 (12):758-770. doi:http://dx.doi.org/10.1016/j.trecan.2016.10.016

155. Dales J-P, Garcia S, Meunier-Carpentier S, Andrac-Meyer L, Haddad O, Lavaut M-N, Allasia C, Bonnier P, Charpin C (2005) Overexpression of hypoxia-inducible factor HIF-1α predicts early relapse in breast cancer: Retrospective study in a series of 745 patients. International Journal of Cancer 116 (5):734-739. doi:10.1002/ijc.20984

156. Schindl M, Schoppmann SF, Samonigg H, Hausmaninger H, Kwasny W, Gnant M, Jakesz R, Kubista E, Birner P, Oberhuber G (2002) Overexpression of Hypoxia-inducible Factor 1α Is Associated with an Unfavorable Prognosis in Lymph Node-positive Breast Cancer. Clinical Cancer Research 8 (6):1831-1837

157. Lundgren K, Holm C, Landberg G (2007) Hypoxia and breast cancer: prognostic and therapeutic implications. Cell Mol Life Sci 64. doi:10.1007/s00018-007-7390-6

158. Yehia L, Boulos F, Jabbour M, Mahfoud Z, Fakhruddin N, El-Sabban M (2015) Expression of HIF-1α and Markers of Angiogenesis Are Not Significantly Different in Triple Negative Breast Cancer Compared to Other Breast Cancer Molecular Subtypes: Implications for Future Therapy. PLOS ONE 10 (6):e0129356. doi:10.1371/journal.pone.0129356

159. van der Groep P, van Diest PJ, Smolders YHCM, Ausems MGEM, van der Luijt RB, Menko FH, Bart J, de Vries EGE, van der Wall E (2013) HIF-1α Overexpression in Ductal

Carcinoma In Situ of the Breast in BRCA1 and BRCA2 Mutation Carriers. PLoS ONE 8 (2):e56055. doi:10.1371/journal.pone.0056055

160. Wolff M, Kosyna FK, Dunst J, Jelkmann W, Depping R (2017) Impact of hypoxia inducible factors on estrogen receptor expression in breast cancer cells. Archives of Biochemistry and Biophysics 613:23-30. doi:http://dx.doi.org/10.1016/j.abb.2016.11.002

161. Yang J, AlTahan A, Jones DT, Buffa FM, Bridges E, Interiano RB, Qu C, Vogt N, Li J-L, Baban D, Ragoussis J, Nicholson R, Davidoff AM, Harris AL (2015) Estrogen receptor-α directly regulates the hypoxia-inducible factor 1 pathway associated with antiestrogen response in breast cancer. Proceedings of the National Academy of Sciences 112 (49):15172-15177. doi:10.1073/pnas.1422015112

162. Rohwer N, Cramer T (2011) Hypoxia-mediated drug resistance: Novel insights on the functional interaction of HIFs and cell death pathways. Drug Resistance Updates 14 (3):191-201. doi:10.1016/j.drup.2011.03.001

163. Samanta D, Gilkes DM, Chaturvedi P, Xiang L, Semenza GL (2014) Hypoxia-inducible factors are required for chemotherapy resistance of breast cancer stem cells. Proceedings of the National Academy of Sciences 111 (50):E5429-E5438. doi:10.1073/pnas.1421438111

164. Lu H, Samanta D, Xiang L, Zhang H, Hu H, Chen I, Bullen JW, Semenza GL (2015) Chemotherapy triggers HIF-1–dependent glutathione synthesis and copper chelation that induces the breast cancer stem cell phenotype. Proceedings of the National Academy of Sciences of the United States of America 112 (33):E4600-E4609. doi:10.1073/pnas.1513433112

165. Samanta D, Park Y, Andrabi SA, Shelton LM, Gilkes DM, Semenza GL (2016) PHGDH Expression Is Required for Mitochondrial Redox Homeostasis, Breast Cancer Stem Cell Maintenance, and Lung Metastasis. Cancer Research 76 (15):4430

166. Whelan KA, Schwab LP, Karakashev SV, Franchetti L, Johannes GJ, Seagroves TN, Reginato MJ (2013) The Oncogene HER2/neu (ERBB2) Requires the Hypoxia-inducible Factor HIF-1 for Mammary Tumor Growth and Anoikis Resistance. Journal of Biological Chemistry 288 (22):15865-15877. doi:10.1074/jbc.M112.426999

167. Bashari MH, Fan F, Vallet S, Sattler M, Arn M, Luckner-Minden C, Schulze-Bergkamen H, Zörnig I, Marme F, Schneeweiss A, Cardone MH, Opferman JT, Jäger D, Podar K (2016) Mcl-1 confers protection of Her2-positive breast cancer cells to hypoxia: therapeutic implications. Breast Cancer Research 18 (1):26. doi:10.1186/s13058-016-0686-4

168. Schacter JL, Henson ES, Gibson SB (2014) Estrogen regulation of anti-apoptotic Bcl-2 family member Mcl-1 expression in breast cancer cells. PLoS One 9. doi:10.1371/journal.pone.0100364

169. Flegal KM, Kruszon-Moran D, Carroll MD, Fryar CD, Ogden CL (2016) Trends in obesity among adults in the united states, 2005 to 2014. JAMA : the journal of the American Medical Association 315 (21):2284-2291. doi:10.1001/jama.2016.6458

170. Cleary MP, Maihle NJ (1997) The role of body mass index in the relative risk of developing premenopausal versus postmenopausal breast cancer. Proceedings of the Society for Experimental Biology and Medicine 216 (1):28-43

171. Trentham-Dietz A, Newcomb PA, Storer BE, Longnecker MP, Baron J, Greenberg ER, Willett WC (1997) Body size and risk of breast cancer. American Journal of Epidemiology 145 (11):1011-1019

172. Huang Z, Hankinson SE, Colditz GA, Stampfer MJ, Hunter DJ, Manson JE, Hennekens CH, Rosner B, Speizer FE, Willett WC (1997) Dual effects of weight and weight gain on breast cancer risk. JAMA : the journal of the American Medical Association 278 (17):1407-1411

173. McTiernan A (2000) Associations between energy balance and body mass index and risk of breast carcinoma in women from diverse racial and ethnic backgrounds in the US. Cancer 88 (S5):1248-1255

174. Ahn J, Schatzkin A, Lacey JV, Albanes D, Ballard-Barbash R, Adams KF, Kipnis V, Mouw T, Hollenbeck AR, Leitzmann MF (2007) Adiposity, adult weight change, and postmenopausal breast cancer risk. Archives of Internal Medicine 167 (19):2091-2102

175. Ove Mæhle B, Tretli S, Skjærven R, Thorsen T (2001) Premorbid body weight and its relations to primary tumour diameter in breast cancer patients; its dependence on

estrogen and progesteron receptor status. Breast cancer research and treatment 68 (2):159-169

176. Van Mieghem T, Leunen K, Pochet N, De Moor B, De Smet F, Amant F, Berteloot P, Timmerman D, Bempt IV, Drijkoningen R (2007) Body mass index and HER-2 overexpression in breast cancer patients over 50 years of age. Breast cancer research and treatment 106 (1):127-133

177. Font-Burgada J, Sun B, Karin M (2016) Obesity and Cancer: The Oil that Feeds the Flame. Cell Metabolism 23 (1):48-62. doi:10.1016/j.cmet.2015.12.015

178. Osman MA, Hennessy BT (2015) Obesity Correlation With Metastases Development and Response to First-Line Metastatic Chemotherapy in Breast Cancer. Clinical Medicine Insights Oncology 9:105-112. doi:10.4137/CMO.S32812

179. Haakinson DJ, Leeds SG, Dueck AC, Gray RJ, Wasif N, Stucky C-CH, Northfelt DW, Apsey HA, Pockaj B (2012) The Impact of Obesity on Breast Cancer: A Retrospective Review. Annals of Surgical Oncology 19 (9):3012-3018. doi:10.1245/s10434-012-2320-8

180. Ewertz M, Jensen M-B, Gunnarsdóttir KÁ, Højris I, Jakobsen EH, Nielsen D, Stenbygaard LE, Tange UB, Cold S (2011) Effect of Obesity on Prognosis After Early-Stage Breast Cancer. Journal of Clinical Oncology 29 (1):25-31. doi:10.1200/jco.2010.29.7614

181. McTiernan A, Rajan KB, Tworoger SS, Irwin M, Bernstein L, Baumgartner R, Gilliland F, Stanczyk FZ, Yasui Y, Ballard-Barbash R (2003) Adiposity and Sex Hormones in Postmenopausal Breast Cancer Survivors. Journal of Clinical Oncology 21 (10):1961-1966. doi:10.1200/jco.2003.07.057

182. Bernstein L, Ross RK (1992) Endogenous hormones and breast cancer risk. Epidemiologic reviews 15 (1):48-65

183. Eliassen AH, Missmer SA, Tworoger SS, Hankinson SE (2006) Endogenous steroid hormone concentrations and risk of breast cancer: does the association vary by a woman's predicted breast cancer risk? Journal of Clinical Oncology 24 (12):1823-1830

184. Cleary MP, Grossmann ME (2009) Obesity and breast cancer: the estrogen connection. Endocrinology 150 (6):2537-2542

185. Carmichael AR (2006) Review article: Obesity as a risk factor for development and poor prognosis of breast cancer. BJOG: An International Journal of Obstetrics & Gynaecology 113 (10):1160-1166. doi:10.1111/j.1471-0528.2006.01021.x

186. Balaban S, Shearer RF, Lee LS, van Geldermalsen M, Schreuder M, Shtein HC, Cairns R, Thomas KC, Fazakerley DJ, Grewal T, Holst J, Saunders DN, Hoy AJ (2017) Adipocyte lipolysis links obesity to breast cancer growth: adipocyte-derived fatty acids drive breast cancer cell proliferation and migration. Cancer & Metabolism 5 (1):1. doi:10.1186/s40170-016-0163-7

187. Nieman KM, Kenny HA, Penicka CV, Ladanyi A, Buell-Gutbrod R, Zillhardt MR, Romero IL, Carey MS, Mills GB, Hotamisligil GS (2011) Adipocytes promote ovarian cancer metastasis and provide energy for rapid tumor growth. Nat Med 17. doi:10.1038/nm.2492

188. Algire C, Amrein L, Bazile M, David S, Zakikhani M, Pollak M (2011) Diet and tumor LKB1 expression interact to determine sensitivity to anti-neoplastic effects of metformin in vivo. Oncogene 30 (10):1174-1182

189. Venkateswaran V, Haddad AQ, Fleshner NE, Fan R, Sugar LM, Nam R, Klotz LH, Pollak M (2007) Association of diet-induced hyperinsulinemia with accelerated growth of prostate cancer (LNCaP) xenografts. Journal of the National Cancer Institute 99 (23):1793-1800

190. Osborne CK, Bolan G, Monaco ME, Lippman ME (1976) Hormone responsive human breast cancer in long-term tissue culture: effect of insulin. Proceedings of the National Academy of Sciences 73 (12):4536-4540

191. Lorincz A, Sukumar S (2006) Molecular links between obesity and breast cancer. Endocrine-related cancer 13 (2):279-292

192. Tessari P, Cecchet D, Cosma A, Puricelli L, Millioni R, Vedovato M, Tiengo A (2011) Insulin resistance of amino acid and protein metabolism in type 2 diabetes. Clinical Nutrition 30 (3):267-272

193. Blagosklonny M (2013) TOR-centric view on insulin resistance and diabetic complications: perspective for endocrinologists and gerontologists. Cell death & disease 4 (12):e964

194. Brachmann SM, Hofmann I, Schnell C, Fritsch C, Wee S, Lane H, Wang S, Garcia-Echeverria C, Maira S-M (2009) Specific apoptosis induction by the dual PI3K/mTor inhibitor NVP-BEZ235 in HER2 amplified and PIK3CA mutant breast cancer cells. Proceedings of the National Academy of Sciences 106 (52):22299-22304

195. Wolff GL, Roberts DW, Mountjoy KG (1999) Physiological consequences of ectopic agouti gene expression: the yellow obese mouse syndrome. Physiol Genomics 1 (3):151-163

196. Heston WE, Vlahakis G (1961) Influence of the Ay gene on mammary-gland tumors, hepatomas, and normal growth in mice. Journal of the National Cancer Institute 26:969-983

197. Heston WE, Vlahakis G (1968) C3H-Avy--a high hepatoma and high mammary tumor strain of mice. Journal of the National Cancer Institute 40 (6):1161-1166

198. Heston WE, Vlahakis G (1962) Genetic obesity and neoplasia. Journal of the National Cancer Institute 29:197-209

199. Hu X, Juneja SC, Maihle NJ, Cleary MP (2002) Leptin--a growth factor in normal and malignant breast cells and for normal mammary gland development. Journal of the National Cancer Institute 94 (22):1704-1711

200. Zhu Y, Aupperlee MD, Zhao Y, Tan YS, Kirk EL, Sun X, Troester MA, Schwartz RC, Haslam SZ (2016) Pubertal and adult windows of susceptibility to a high animal fat diet in Trp53-null mammary tumorigenesis. Oncotarget 7 (50):83409-83423. doi:10.18632/oncotarget.13112

201. Cleary MP, Grande JP, Maihle NJ (2004) Effect of high fat diet on body weight and mammary tumor latency in MMTV-TGF-alpha mice. Int J Obes Relat Metab Disord 28 (8):956-962. doi:10.1038/sj.ijo.0802664

202. Cleary MP, Grande JP, Juneja SC, Maihle NJ (2004) Diet-induced obesity and mammary tumor development in MMTV-neu female mice. Nutrition and cancer 50 (2):174-180. doi:10.1207/s15327914nc5002_7

203. Dogan S, Hu X, Zhang Y, Maihle NJ, Grande JP, Cleary MP (2007) Effects of high-fat diet and/or body weight on mammary tumor leptin and apoptosis signaling pathways in MMTV-TGF-alpha mice. Breast cancer research : BCR 9 (6):R91. doi:10.1186/bcr1840

204. Khalid S, Hwang D, Babichev Y, Kolli R, Altamentova S, Koren S, Goodwin PJ, Ennis M, Pollak M, Sonenberg N, Fantus IG (2010) Evidence for a tumor promoting effect of high-fat diet independent of insulin resistance in HER2/Neu mammary carcinogenesis. Breast cancer research and treatment 122 (3):647-659. doi:10.1007/s10549-009-0586-8

205. Hefetz-Sela S, Scherer PE (2013) Adipocytes: impact on tumor growth and potential sites for therapeutic intervention. Pharmacol Ther 138 (2):197-210. doi:10.1016/j.pharmthera.2013.01.008

206. Tan J, Buache E, Chenard MP, Dali-Youcef N, Rio MC (2011) Adipocyte is a non-trivial, dynamic partner of breast cancer cells. Int J Dev Biol 55 (7-9):851-859. doi:10.1387/ijdb.113365jt

207. Vander Heiden MG (2011) Targeting cancer metabolism: a therapeutic window opens. Nat Rev Drug Discov 10 (9):671-684

208. Vernieri C, Casola S, Foiani M, Pietrantonio F, de Braud F, Longo V (2016) Targeting Cancer Metabolism: Dietary and Pharmacologic Interventions. Cancer Discovery. doi:10.1158/2159-8290.cd-16-0615

209. DeVita VT, Chu E (2008) A History of Cancer Chemotherapy. Cancer Research 68 (21):8643

210. Longley DB, Harkin DP, Johnston PG (2003) 5-Fluorouracil: mechanisms of action and clinical strategies. Nat Rev Cancer 3 (5):330-338. doi:10.1038/nrc1074

211. Verstappen CCP, Heimans JJ, Hoekman K, Postma TJ (2003) Neurotoxic Complications of Chemotherapy in Patients with Cancer. Drugs 63 (15):1549-1563. doi:10.2165/00003495-200363150-00003

212. Groopman JE, Itri LM (1999) Chemotherapy-Induced Anemia in Adults: Incidence and Treatment. JNCI: Journal of the National Cancer Institute 91 (19):1616-1634. doi:10.1093/jnci/91.19.1616

213. Zhou R, Pantel AR, Li S, Lieberman BP, Ploessl K, Choi H, Blankemeyer E, Lee H, Kung HF, Mach RH, Mankoff DA (2017) ^{18}F(2S,4R)4-Fluoroglutamine PET Detects Glutamine Pool Size Changes in Triple-Negative Breast Cancer in Response to Glutaminase Inhibition. Cancer Research

214. Christen S, Lorendeau D, Schmieder R, Broekaert D, Metzger K, Veys K, Elia I, Buescher Joerg M, Orth Martin F, Davidson Shawn M, Grünewald Thomas Georg P, De Bock K, Fendt S-M (2016) Breast Cancer-Derived Lung Metastases Show Increased Pyruvate Carboxylase-Dependent Anaplerosis. Cell Reports 17 (3):837-848. doi:http://dx.doi.org/10.1016/j.celrep.2016.09.042

215. Le A, Lane Andrew N, Hamaker M, Bose S, Gouw A, Barbi J, Tsukamoto T, Rojas Camilio J, Slusher Barbara S, Zhang H, Zimmerman Lisa J, Liebler Daniel C, Slebos Robbert JC, Lorkiewicz Pawel K, Higashi Richard M, Fan Teresa WM, Dang Chi V (2012) Glucose-Independent Glutamine Metabolism via TCA Cycling for Proliferation and Survival in B Cells. Cell Metabolism 15 (1):110-121. doi:https://doi.org/10.1016/j.cmet.2011.12.009

216. Xiang Y, Stine ZE, Xia J, Lu Y, O'Connor RS, Altman BJ, Hsieh AL, Gouw AM, Thomas AG, Gao P, Sun L, Song L, Yan B, Slusher BS, Zhuo J, Ooi LL, Lee CGL, Mancuso A, McCallion AS, Le A, Milone MC, Rayport S, Felsher DW, Dang CV (2015) Targeted inhibition of tumor-specific glutaminase diminishes cell-autonomous tumorigenesis. The Journal of Clinical Investigation 125 (6):2293-2306. doi:10.1172/JCI75836

217. Shroff EH, Eberlin LS, Dang VM, Gouw AM, Gabay M, Adam SJ, Bellovin DI, Tran PT, Philbrick WM, Garcia-Ocana A, Casey SC, Li Y, Dang CV, Zare RN, Felsher DW (2015) MYC oncogene overexpression drives renal cell carcinoma in a mouse model through glutamine metabolism. Proceedings of the National Academy of Sciences 112 (21):6539-6544. doi:10.1073/pnas.1507228112

218. Cheyne RW, Trembleau L, McLaughlin A, Smith TAD (2011) Changes in 2-fluoro-2-deoxy-d-glucose incorporation, hexokinase activity and lactate production by breast cancer cells responding to treatment with the anti-HER-2 antibody trastuzumab. Nuclear Medicine and Biology 38 (3):339-346. doi:http://dx.doi.org/10.1016/j.nucmedbio.2010.09.005

219. Acharya S, Xu J, Wang X, Jain S, Wang H, Zhang Q, Chang C-C, Bower J, Arun B, Seewaldt V, Yu D (2016) Downregulation of GLUT4 contributes to effective intervention of estrogen receptor-negative/HER2-overexpressing early stage breast disease progression by lapatinib. American Journal of Cancer Research 6 (5):981-995

220. Zhang J-S, Lei J-P, Wei G-Q, Chen H, Ma C-Y, Jiang H-Z (2016) Natural fatty acid synthase inhibitors as potent therapeutic agents for cancers: A review. Pharmaceutical Biology 54 (9):1919-1925. doi:10.3109/13880209.2015.1113995

221. Blancafort A, Giró-Perafita A, Oliveras G, Palomeras S, Turrado C, Campuzano Ò, Carrión-Salip D, Massaguer A, Brugada R, Palafox M, Gómez-Miragaya J, González-Suárez E, Puig T (2015) Dual Fatty Acid Synthase and HER2 Signaling Blockade Shows Marked Antitumor Activity against Breast Cancer Models Resistant to Anti-HER2 Drugs. PLoS ONE 10 (6):e0131241. doi:10.1371/journal.pone.0131241

222. Evans JMM, Donnelly LA, Emslie-Smith AM, Alessi DR, Morris AD (2005) Metformin and reduced risk of cancer in diabetic patients. BMJ : British Medical Journal 330 (7503):1304-1305. doi:10.1136/bmj.38415.708634.F7

223. Coyle C, Cafferty FH, Vale C, Langley RE (2016) Metformin as an adjuvant treatment for cancer: a systematic review and meta-analysis. Annals of Oncology 27 (12):2184-2195. doi:10.1093/annonc/mdw410

224. Sacco F, Calderone A, Castagnoli L, Cesareni G (2016) The cell-autonomous mechanisms underlying the activity of metformin as an anticancer drug. Br J Cancer 115 (12):1451-1456. doi:10.1038/bjc.2016.385

225. Fendt S-M, Bell EL, Keibler MA, Davidson SM, Wirth GJ, Fiske B, Mayers JR, Schwab M, Bellinger G, Csibi A, Patnaik A, Blouin MJ, Cantley LC, Guarente L, Blenis J, Pollak MN, Olumi AF, Vander Heiden MG, Stephanopoulos G (2013) Metformin Decreases Glucose Oxidation and Increases the Dependency of Prostate Cancer Cells

on Reductive Glutamine Metabolism. Cancer Research 73 (14):4429-4438. doi:10.1158/0008-5472.can-13-0080

226. Smith TAD, Phyu SM (2016) Metformin Decouples Phospholipid Metabolism in Breast Cancer Cells. PLOS ONE 11 (3):e0151179. doi:10.1371/journal.pone.0151179

227. Zakikhani M, Bazile M, Hashemi S, Javeshghani S, Avizonis D, Pierre JS, Pollak MN (2012) Alterations in Cellular Energy Metabolism Associated with the Antiproliferative Effects of the ATM Inhibitor KU-55933 and with Metformin. PLOS ONE 7 (11):e49513. doi:10.1371/journal.pone.0049513

CHAPTER 2.

METFORMIN INDUCES DISTINCT BIOENERGETIC AND METABOLIC PROFILES IN SENSITIVE VERSUS RESISTANT HIGH GRADE SEROUS OVARIAN CANCER AND NORMAL FALLOPIAN TUBE SECRETORY EPITHELIAL CELLS

2.1 PREFACE

Though this chapter does not directly relate to the work in this thesis it was included as a case study illustrating cancer-specific effects of metabolism-targeting drugs, and the application of metabolomics to investigate potential mechanisms of cancer-specific therapeutic response.

This chapter has been previously published as:

> Hodeib, M.*, Ogrodzinski, M. P.*, Vergnes, L., Reue, K., Karlan, B. Y., Lunt, S. Y., & Aspuria, P. J. P. (2018). Metformin induces distinct bioenergetic and metabolic profiles in sensitive versus resistant high grade serous ovarian cancer and normal fallopian tube secretory epithelial cells. *Oncotarget*, *9*(3), 4044.
>
> *Co-first authors

2.2 Abstract

Metformin is a widely used agent for the treatment of diabetes and infertility, however, it has been found to have anti-cancer effects in a variety of malignancies including high grade serous ovarian cancer (HGSC). Studies describing the mechanisms by which metformin affects HGSC are ongoing, but detailed analysis of its effect on the cellular metabolism of both HGSC cells and their precursor, normal fallopian tube secretory epithelial cells (FTSECs), is lacking. We addressed the effects of metformin and the more potent biguanide, phenformin, on HGSC cell lines and normal immortalized FTSECs. Cell proliferation assays identified that FTSECs and a subset of HGSC cell lines are relatively resistant to the anti-proliferative effects of metformin. Bioenergetic and metabolomic analyses were used to metabolically differentiate the metformin-sensitive and metformin-resistant cell lines. Bioenergetically, biguanides elicited a significant decrease in mitochondrial respiration in all HGSC cells and FTSECs. However, biguanides had a greater effect on mitochondrial respiration in metformin sensitive cells. Metabolomic analysis revealed that metformin and phenformin generally induce similar changes in metabolic profiles. Biguanide treatment led to a significant increase in NADH in FTSECs and HGSC cells. Interestingly, biguanide treatment induced changes in the levels of mitochondrial shuttle metabolites, glycerol-3-phopshate (G3P) and aspartate, specifically in HGSC cell lines and not in FTSECs. Greater alterations in G3P or aspartate levels were also found in metformin sensitive cells relative to metformin resistant cells. These data identify bioenergetic and HGSC-specific metabolic effects that correlate with metformin sensitivity and novel metabolic avenues for possible therapeutic intervention.

2.3 Introduction

Ovarian cancer remains the leading cause of gynecologic cancer-related death in women despite widespread efforts to improve surgical procedures and therapeutic targets [1]. In 2015, 21,290 new ovarian cancer diagnoses were made in the United States, and >66% (14,180) of these women died of the disease [2]. High grade serous carcinoma (HGSC) accounts for over half of ovarian cancers and carries the worst overall prognosis [1]. Standard treatment for ovarian cancer involves surgical debulking with the goal of no gross residual disease, followed by combination platinum and taxane chemotherapy. Despite advances there have been only modest improvements in the overall 5- and 10-year relative survival rates which remain 46% and 35%, respectively [1]. Repurposing low-toxicity drugs may help improve the progression free and overall survival rates [1]. Also, understanding the mechanism of how low toxicity drugs affect cancer cells may reveal additional therapeutic targets.

Metformin, a biguanide drug with a low toxicity profile, has been widely used to treat diabetes and fertility [3,4]. In 2005, Evans et al reported a reduced incidence of cancer in diabetic patients receiving metformin, which led to recognition of the drug in cancer-related research [4]. Another large prospective study found that diabetic women treated with metformin have a lower risk of dying of most invasive cancers compared to non-metformin users [5]. Metformin and phenformin, two biguanide drugs traditionally used to treat diabetes, have now been associated with improved survival rates in many different cancer types including non-small cell lung, breast and ovarian cancers [6-8]. Due to safety concerns, phenformin has been removed from the pharmaceutical market for use in humans [9]. However, recent studies have shown that phenformin treatment may

have some utility in treating cancer with a shorter treatment schedule that reduces the risk of severe side effects [6].

As anti-diabetic medications, biguanides primarily act as insulin sensitizers, decrease blood glucose levels, and reduce gluconeogenesis in the liver [10]. Both increased levels of insulin and glucose have been associated with tumor growth and poor overall prognosis in different cancer types [10]. Therefore, the ability of biguanides to lower both glucose and insulin levels may indirectly contribute to its anti-tumor effects. In addition to these indirect effects, biguanides are also posited to directly affect cancer cell proliferation via inhibition of Complex I within the electron transport chain [11]. Indeed, it was recently found that metformin accumulates in tumors and induces metabolic changes similar to that seen in vitro [12]. The bioenergetic stress induced by metformin inhibits proliferation and was largely thought to be mTOR dependent [13,14]. However, metformin inhibition of mTOR has been shown to vary between different studies and cell types, with no correlation to its anti-proliferative effects [12,15].

Preclinical studies focusing on the effect of metformin on HGSC have identified its anti-proliferative effects [12,16,8]. These data and epidemiological evidence have led to clinical trials assessing the use of metformin in both neoadjuvant and post-surgical settings for HGSC [12,17]. However, a molecular characterization of cell lines widely used to study HGSC revealed that they are, in fact, not likely to represent the disease [18]. Also, growing evidence has pointed to the fallopian tube secretory epithelial cells (FTSEC) as the origin of HGSC [19]. FTSECs have not been metabolically characterized, and their response to biguanides are unknown. Extensive metabolic characterization of HGSC cells has also not been reported. Therefore, to assess the metabolic and potential

anti-proliferative effect of biguanides in HGSC, we performed bioenergetic and metabolomic analysis on a panel of clinically relevant HGSC lines and normal cell of origin controls. We find that a subset of HGSC cell lines as well as normal FTSECs are relatively resistant to the anti-proliferative effects of metformin. Also, these effects do not correlate with the ability of metformin to inhibit AMPK/mTOR signaling. Bioenergetic analysis revealed that metformin sensitivity largely correlated with a greater inhibition of oxygen consumption rate. Also, metabolomic analysis identified specific alterations in HGSC cells versus normal FTSECs that also correlate with metformin sensitivity.

2.4 Results

2.4.1 Biguanides inhibit HGSC cell proliferation.

We examined the effect of metformin and phenformin on normal FTSEC and HGSC proliferation in 2-D growth conditions. We analyzed a panel of HGSC cell lines (CAOV3, FUOV1, OV90, OVCAR4, OVCAR433, and TYKNU), which were previously characterized as suitable HGSC models given their genetic makeup (i.e. TP53 mutation, copy-number profile, and low frequency of non-synonymous mutations in protein-coding genes) [19]. Normal TERT-immortalized fallopian tube non-ciliated epithelium cell lines, FNE1 and FNE2, were used as normal controls [20]. Normal FTSECs and HGSCs were treated with either metformin, phenformin, or vehicle control (**Figure 1**). In FTSECs, metformin treatment led to a modest growth inhibition (~30-40%), while phenformin completely inhibited cell proliferation (**Figure 1A & 1D**). In HGSCs, phenformin also significantly inhibited cell proliferation (**Figures 1B & 1C**). However, metformin treatment of HGSC cell lines revealed two subgroups; Metformin-sensitive (TYKNU, OV90, and OVCAR433) and metformin-resistant (OVCAR4 and FUOV1) (**Figure 2B-D**). Metformin

completely inhibited the cell proliferation of metformin-sensitive cells (**Figure 1B & 1D**), while metformin-resistant cells responded similarly to normal FTSECs, with OVCAR4 being slightly more sensitive (**Figure 1C & 1D**).

We also assessed the effect of metformin and phenformin on anchorage independent 3D growth. Cells were grown in ultra-low attachment plates for 24 hours to form cellular aggregates and then treated with metformin, phenformin, or vehicle. As expected, FNE1 and FNE2 were unable to survive anchorage-independent conditions (**Figure 2A**). However, all HGSC cell lines formed stable cell aggregates and continued to survive after 6 days (**Figure 2B & 2C**). Cells were less proliferative in 3D conditions compared to 2D conditions (**Figures 1 & 2**). Generally, cell lines that were highly proliferative in 2D (TYKNU, OV90, and OV433) were also more proliferative than other cells in 3D (**Figure 1 & 2**). The effects of metformin in 3D were similar to those observed in 2D; the growth of TYKNU, OV90, and OVCAR433 was significantly inhibited by metformin, whereby OVCAR4 and FUOV1 were not (**Figure 2B-D**). We noticed that the 3D growth of metformin resistant cells was significantly slower than that of the metformin sensitive cells (**Figure 2E**). Indeed, there was a statistically significant (p-value = .0037) inverse relationship between metformin resistance and 3D cell proliferation rate (**Figure 2F**). These data indicate that normal FTSECs and a subset of HGSC cell lines are relatively metformin resistant.

2.4.2 Phenformin, but not metformin, has an inhibitory effect on phospho-S6K levels via the upregulation of REDD1.

The effect of biguanide treatment on proliferation in other cell types has been primarily described through inhibition of mTOR activation via the upregulation of AMPK

activity or REDD1, both well-established mTOR inhibitors [6,14,13]. To identify possible differences between metformin-resistant and metformin-sensitive cells, we examined the effects of biguanides on the mTOR signaling pathway in FTSEC and HGSC cells. Both biguanides induced AMPK Thr172 phosphorylation (pAMPK) only in the metformin-resistant lines (OVCAR4 and FUOV1) (**Figure 3**). Phenformin, but not metformin, also induced pAMPK in FNE1 (**Figure 3**). We further performed time course experiments addressing the effect of metformin and a potent inducer of AMPK, AICAR, in the metformin-sensitive, OV90, and metformin-resistant, FUOV1, cell lines. Metformin induced a subtle increase in pAMPK in OV90 after 6 hours which decreased significantly by 48 h (**Figure S1A**). This is juxtaposed to the dramatic and sustained increase of pAMPK in FUOV1 cells (**Figure S1A**). AICAR was able to induce phospho-AMPK levels in both cell lines, however to a much lesser extent in OV90 (**Figure S1A**). Metformin sensitivity also did not correlate with the expression of the upstream modulator of AMPK activity, LKB1, nor the expression of the metformin transporter, OCT1 (**Figure S1B&C**). Western blot analysis of REDD1 found that both biguanides induced REDD1 protein levels in all HGSC cells, while only phenformin treatment led to elevated levels of REDD1 in normal FTSEC cells (**Figure 3**). We determined whether REDD1 was also transcriptionally upregulated by performing qRT-PCR analysis. Indeed, both biguanides induced similar levels of REDD1 mRNA in HGSC cells but not in normal FTSECs (**Figure S2**). We then assessed mTOR activity via the phosphorylation status of the mTOR downstream target, S6 kinase (S6K), by western blot. Phenformin significantly decreased phospho-S6 kinase (pS6K) levels in all cell lines, indicating mTOR inhibition (**Figure 3**). In contrast, metformin decreased pS6K levels in only two cell lines, TYKNU (metformin-

sensitive) and FUOV1 (metformin-resistant) (**Figure 3**). Therefore, these data suggest that phenformin is a more potent inhibitor of mTOR activity than metformin, even at doses where metformin has anti-proliferative effects. Together, these data are in line with other studies that suggest upregulation of pAMPK, REDD1, and inhibition of mTOR activity does not correlate with metformin sensitivity in cancer cell lines [15,12]. It also indicates that the anti-proliferative effects of metformin may be at least partially attributable to mechanisms other than mTOR inhibition.

2.4.3 HGSC cell lines have altered bioenergetic profiles compared to normal FTSECs.

Since the effects of metformin could not be fully explained by mTOR inhibition, we sought to characterize the metabolic and bioenergetic effects of biguanide treatment. We initially profiled the baseline bioenergetic activities of FTSECs and HGSC cell lines utilizing the Seahorse bioanalyzer to assess oxygen consumption rate (OCR), a key indicator of mitochondrial activity and cellular respiration, as well as the extracellular acidification rate (ECAR), an indicator of glycolysis. Analysis of the baseline OCR revealed that HGSC cell lines display a significantly increased OCR relative to normal cells (**Figure 4A**). In addition, most HGSC cell lines, except OVCAR4 and OV90, have an increased baseline ECAR relative to normal cells (**Figure 4B**). These data imply that HGSC cells have elevated cellular respiration and increased glycolysis as compared to their cell of origin counterparts.

Since HGSC cells displayed significantly elevated OCR and ECAR, we determined whether these cells were functioning at their maximal respiratory and glycolytic capacities. FCCP, a mitochondrial uncoupler, induces maximal respiration by transporting protons

across the mitochondrial membrane leading to depolarization of the membrane potential and rapid consumption of O2. This maximal OCR is used in conjunction with basal OCR to calculate spare respiratory capacity. FNE1 and FNE2 mitochondria were functioning at 80% and 67% capacity with 20% and 37% spare respiratory capacity, respectively (**Figure 4C**). While a few HGSC cell lines (FUOV1, OVCAR433, and TYKNU) were functioning at near maximal capacity (>90% capacity, <10% spare respiratory capacity), other HGSC cell lines (OV90, OVCAR4) were functioning at significantly lower (<70% capacity, >30% spare respiratory capacity), or similar capacities relative to normal (**Figure 1C**). Therefore, no general trend in spare respiratory capacity could be identified between metformin-resistant cells, metformin-sensitive cells, and normal controls. To calculate maximal glycolytic capacity, oligomycin, an ATP synthase inhibitor, was used to induce a bioenergetic shift towards glycolysis (maximal ECAR). Similar to spare respiratory capacity, there were no significant differences between HGSC and control cells in spare glycolytic capacities (**Figure 1D**).

We further assessed other facets of mitochondrial function including the percentage of respiration devoted to ATP production (ATP-coupled), proton leak (ATP-uncoupled), and non-mitochondrial respiration. OCR measurements during sequential treatment of cell lines with oligomycin (ATP synthase inhibitor) and rotenone/myxothiazol (Complex I and III inhibitors, respectively) allow for these parameters to be defined. Normal cell lines, FNE1 and FNE2, have greater than 60% of their total respiration dedicated to ATP synthesis (**Figure 1E**). However, all HGSC cell lines tested demonstrate significantly less ATP-coupled OCR than controls with the majority of their respiration being allocated towards uncoupled and non-mitochondrial respiration (**Figure 1E**). This

phenomenon of elevated non-ATP-coupled respiration in cancer versus normal cells has also been observed in breast cancer [21]. Altogether these data suggest that HGSC cells are more bioenergetic, while contributing a smaller fraction of their total respiration towards ATP-synthesis compared to normal cells.

2.4.4 Biguanides significantly inhibit oxygen consumption while increasing glycolysis in both normal FTSECs and HGSC cells that can be exploited in low glucose conditions.

To assess the effects of metformin and phenformin on mitochondrial function, cell lines were incubated for 24 hours with either metformin, phenformin, or vehicle control prior to Seahorse bioanalysis. Treatment with metformin or phenformin significantly decreased respiration (>70% of control OCR) in both HGSC and normal cells at similar levels. However, the metformin-resistant cells (OVCAR4 and FUOV1), still had a significantly higher OCR (>10%) than the metformin-sensitive cells (<10%) (**Figure 5A**). This implies that oxidative phosphorylation is less inhibited in metformin-resistant cells as compared to metformin-sensitive cells. Therefore, metformin and phenformin decrease overall oxygen consumption and utilization for ATP-synthesis. Biguanides are also more potent in affecting these processes in metformin-sensitive cells versus metformin-resistant cells.

Previous studies have shown that metformin inhibition of oxygen consumption leads to a subsequent compensatory increase in aerobic glycolysis to compensate for the energy deficit in some cell lines [22,23]. Therefore, we examined the effect of metformin and phenformin on the ECAR of HGSC and normal cells. Both FNE1 and FNE2 had significant ECAR increases upon treatment of metformin or phenformin relative to control

(**Figure 5B**). Most HGSC cell lines also had elevated ECAR upon metformin treatment except FUOV1 (**Figure 5B**). Similarly, phenformin treatment increased ECAR in most HGSC cell lines except TYKNU and FUOV1 (**Figure 5B**). These data confirm previous reports that metformin and phenformin generally inhibit oxygen consumption, but the induction of aerobic glycolysis is governed by other factors [23,22]. Also, under these conditions, these bioenergetic effects do not discriminate between metformin-sensitive and metformin-resistant cells.

A previous study in ovarian cancer indicated that metformin resistance can be overcome by reducing glucose concentration, thereby demonstrating the inhibitory effect of hyperglycemia on the actions of metformin [16]. To address whether glucose served as a protective molecule in metformin resistant cells, we cultured FUOV1 and OVCAR4 cells in media with standard (10 mM) or low (0.1 mM) glucose concentrations and treated cells with metformin, phenformin, or control. There was no significant difference in cell proliferation between untreated glucose and low glucose media after 6 days (**Figure 6A & 6B**). However, metformin and phenformin treatment significantly inhibited proliferation in both cell lines under low glucose conditions compared to standard media (**Figure 6A & 6B**). These data further support the previous study that adequate levels of glucose are required for biguanide resistant cells to survive.

2.4.5 Metabolomic analysis of metformin and phenformin treatment reveals cancer cell specific metabolite fluctuations.

Due to the significant effect of biguanides on mitochondrial function, we were interested in examining the effect of biguanides on central carbon metabolism. We performed metabolomic analysis on both normal FTSECs and all HGSC cell lines (**Figure**

7, Figure S3, Table S1) Similar to a previous study, metformin and phenformin generally induce similar metabolic changes in all cell lines tested (**Figure 7A, Figure S3, Table S1**) [7]. Treatment with either molecule induced significantly elevated levels of NADH relative to controls in both HGSC and normal FTSEC cells, consistent with Complex I inhibition by biguanides (**Figure 7A, Figure S3, Table S1**). In general, biguanide treatment of most cell lines including FNE2 cells also resulted in the depletion of tricarboxylic acid (TCA) cycle intermediates citrate and α-ketoglutarate (**Figure S3 and Table S1**). Treatment with biguanides also caused variable depletion of nucleotide triphosphates between cell lines depending on the specific treatment. Treatment with phenformin caused relative depletion of adenosine triphosphate (ATP), cytidine triphosphate (CTP), and uridine triphosphate (UTP) in OVCAR433 and TYKNU, but not of other NTPs in FUOV1 or OV90. Treatment with metformin caused depletion of CTP specifically in FNE2 and FUOV1, as well as depletion of UTP in OV90, OVCAR44, and TYKNU. Neither treatment caused a significant depletion of guanosine triphosphate (GTP) in any of the cell lines studied (**Figure S3 and Table S1**). The only metabolite specifically and significantly altered in metformin-sensitive cells versus metformin-resistant cells was the nucleoside deoxyuridine (**Figure S4**). Interestingly, we identified biguanide-induced alterations that were particular to all HGSC cells tested and not normal FTSECs. Specifically, in HGSC cells, metformin and phenformin treatment caused a significant elevation in glycerol-3-phosphate (G3P) and a decrease in aspartate levels relative to controls (**Figure 7A&B**). Interestingly, the metformin-sensitive cell lines generally displayed greater effects on either G3P accumulation or aspartate depletion than the metformin-resistant cell lines, especially OVCAR433 (**Figure 7A&B**). G3P is primarily involved in the glycerol-phosphate shuttle,

which in addition to the malate-aspartate shuttle, allows the movement of electrons from cytosolic NADH to the mitochondria for entry into the electron transport chain (**Figure 8A&B**) [24]. The metabolite data suggests that the glycerol-phosphate and malate-aspartate shuttle are perturbed by biguanides thereby leading to an accumulation of G3P and depletion of aspartate. Given that this effect does not occur in the normal FTSECs and is more pronounced in metformin-sensitive cells, it appears that biguanide treatment may specifically affect these mitochondrial shuttles in HGSC cells.

2.4.6 Aspartate and pyruvate supplementation rescue the anti-proliferative effects of metformin on cell growth.

Given that metformin treatment results in a significant decrease in aspartate levels, we tested whether supplementation of cells with aspartate would rescue the anti-proliferative effects. We treated cells simultaneously with either control, aspartate (100 uM), metformin (10 mM), or both aspartate and metformin for 72 h and assessed cell proliferation (**Figure 9A**). Treatment with aspartate alone had significant effects on the growth of all HGSC cell lines tested (**Figure 9A**). Aspartate had a minimal and non-significant effect on the growth of normal FTSEC cell lines (**Figure 9A**). Combinatorial treatment of all cell lines tested with aspartate and metformin resulted in a diminished effect of metformin, bringing cell viability close to control levels (**Figure 9A**). Therefore, aspartate supplementation diminishes the metformin effect as previously reported [15].

Previous studies have also shown that providing an alternative carbon source such as pyruvate can overcome the effects of metformin in cancer cell lines [15]. We also treated cells with either control, pyruvate (1 mM), metformin (10 mM), or both pyruvate and metformin for 72 h and assessed cell proliferation. Strikingly, pyruvate treatment had

a significantly positive effect on the growth of all normal FTSEC and HGSC cell lines (**Figure 9B**). Also, pyruvate significantly diminished the effect of metformin on all cell lines, greater than the effect of aspartate (**Figure 9B**). This is in line with the report from Gui et al that pyruvate is a more powerful suppressant of metformin's ability to inhibit cell growth.

2.5 Discussion

Multiple studies in different cancers have demonstrated that metformin and phenformin have a wide-ranging impact on cancer metabolism [7,21,22]. In a Src-inducible model of breast cancer, both biguanides were found to deplete TCA cycle intermediates as expected from Complex I inhibition [7]. Similar results were found using isolated mitochondria from breast cancer cell lines illustrating that biguanides indeed directly affect mitochondrial function [21]. Biguanide inhibition of TCA cycle activity was also found in NSCLC and colon cancer cell lines [22]. Interestingly, analysis of the effects of biguanides on breast cancer stem cells yielded a different metabolic profile; levels of all ribonucleotide and nucleotide triphosphates (NTPs) were significantly decreased, but no effects were seen on the TCA cycle [7]. In line with these results, we found that biguanides elicited similar effects on metabolites in the TCA cycle and/or NTPs in the HGSC cell lines tested (**Figure S3**). In addition, this is the first study that characterizes the bioenergetics and metabolism of immortalized FTSECs, the purported cell of origin of HGSC [19]. Given that previous biguanide studies on ovarian cancer have not included FTSECs, we were able to identify metabolic effects induced by biguanides that were seen only in transformed HGSC cells. The most significant of these effects was the perturbation of metabolites involved with mitochondrial shuttles, the G3P and malate-aspartate shuttle

(**Figure 7A**). Since NADH is unable to cross the mitochondrial membrane, shuttles exist to transfer electrons from cytosolic NADH to the electron transport chain (ETC) via the reduction of other molecules that can cross into the mitochondria. Mechanistically, the G3P shuttle functions in the following manner: Cytosolic G3P dehydrogenase 1 (cGPD) converts dihydroxyacetone phosphate (DHAP) to G3P by oxidizing NADH to NAD+. G3P is then converted back to DHAP by mitochondrial G3P dehydrogenase 2 (mGPD) to produce FADH2 that donates its electrons to the ETC (**Figure 8A**). The malate-aspartate shuttle utilizes malate and aspartate as electron carriers that are shuttled between the cytosol and mitochondria via exchange transporters (**Figure 8B**). These systems appear to be perturbed by biguanides in transformed HGSC cells as evidenced by elevated levels of G3P and depletion of aspartate. Interestingly, mGPD was found to be a direct target of biguanide inhibition in rats [25]. Whether biguanides inhibit the G3P and malate-aspartate shuttles directly in human cells has not been determined.

Recent evidence has shown that metformin accumulates within ovarian tumors and induces aspartate depletion [12]. This and other studies have posited that metformin prevents the mitochondria from adaptive nutrient utilization since metformin treatment can be rescued by providing alternative fuel sources such as pyruvate or increased amounts of glucose [12,16,15]. We have also confirmed the protective effect supplementation of glucose, aspartate, and pyruvate has against metformin (**Figure 6 and 9**). One caveat of our study is that cells were grown in RPMI media containing supraphysiologic levels of glucose (10 mM vs ~1-5mM) and higher levels of metformin (10 mM) than cells in vivo would be exposed to. However, the metabolomic changes upon metformin treatment seen in our in vitro data overlap significantly with the changes seen in other in vivo studies,

thereby suggesting translatability of our results [12,16,15]. Since biguanide treatment of most HGSC cell lines resulted in depleted nucleotides, increases in glycolysis (as shown by lactate and ECAR), and significant inhibition of ATP-linked OCR, it follows that there is an increased need for glucose to provide the carbons required to replenish nucleotides and ATP via the pentose-phosphate shunt and glycolysis, respectively. Therefore, the ability of metformin to lower blood glucose levels and directly inhibit adaptive nutrient utilization in cancer cells imply a multi-faceted mechanism explaining the efficacy of this anti-tumor agent.

In summary, our study characterizes the metabolic and anti-proliferative effects of biguanides on HGSC cells and its cell of origin, FTSECs. Biguanides significantly inhibit the ETC and accumulate NADH in all cell lines implying that biguanides are also able to enter normal FTSEC cells and act on its direct target, Complex I. However, the anti-proliferative effects of metformin, but not phenformin, are HGSC cell specific and do not correlate with inhibition of mTOR activity. Metabolomic analysis revealed HGSC specific alterations in the levels of mitochondrial shuttle metabolites, aspartate and G3P, thereby illustrating that these processes are of particular importance, and possibly overactive in cancer cells. Alterations in these metabolites also correlate well with the anti-proliferative efficacy of metformin. The activity of these shuttles in HGSC cells versus normal FTSECs have not been described and are worth investigating. Further detailed analysis of the metabolic pathways perturbed in biguanide sensitive cells (i.e. deoxyuridine metabolism) as well as resistance mechanisms in metformin resistant cells may reveal additional metabolic therapeutic targets. Additionally, since this study identifies that metformin induces deleterious effects specifically in HGSC cells not seen in normal FTSECs and its

low toxicity profile, its use as a preventative measure for HGSC should be taken into consideration.

2.6 Methods

2.6.1 Cell lines and reagents

FUOV1, OVCAR4, OV90, OVCAR433, and TYKNU were obtained as previously described [26]. FNE1 and FNE2 (TERT-immortalized normal FTSECs) were a kind gift from Dr. Tan Ince (University of Miami) [20]. Metformin, phenformin, and ultra-low attachment plates were obtained from Sigma-Aldrich. HGSC cells were grown in RPMI 1640 + 10% FBS + 1% penicillin/streptomycin. FNE1 and FNE2 were grown in FOMI media [20] then switched to RPMI 1640 + 10% FBS + 1% penicillin/streptomycin 72 hours prior to assays.

2.6.2 Mitochondrial function and glycolysis

$2x10^4$ cells were plated into 24 well XF plates (Seahorse bioscience). Oxygen consumption rate (OCR) and extracellular acidification rate (ECAR) were measured using an XF24 Extracellular Flux Analyzer (Seahorse Bioscience) in unbuffered DMEM assay medium supplemented with 1 mM pyruvate, 2 mM glutamine and 11 mM glucose. OCR and ECAR were measured before and after the sequential addition of 0.5 µM oligomycin, 0.5 µM FCCP and 1 µM of rotenone/myxothiazol. Values were normalized to protein concentration using a Bradford assay (Bio-Rad). Mitochondrial respiration was calculated as the difference between total and rotenone/myxothiazol rates. Maximal respiration was the response to FCCP. ATP-linked respiration was the oligomycin-sensitive respiration

while uncoupled respiration was the difference between oligomycin and rotenone/myxothiazol rates.

2.6.3 Cell proliferation assay

$1x10^3$ HGSC cells/well were seeded in triplicate on a 96-well plate and treated with metformin (1 mM or 10 mM), phenformin (100µM or 1 mM), aspartate (100 uM), pyruvate (1 mM) or vehicle control (RPMI). To assess cellular viability, cells were subjected to the CelltiterGlo assay (Promega). Luminescence was read on a GloMax luminometer.

2.6.4 Spheroid formation assay

$1x10^3$ HGSC cells/well were seeded in triplicate in an ultra-low attachment 96-well plate and incubated overnight. Next day cells were treated with indicated doses of metformin, phenformin, or control for 72 hours. Viability was assessed by CelltiterGlo 3D assay.

2.6.5 Western blot analysis

Western blot was performed as previously described [27]. Briefly, cell lysates were collected in RIPA buffer supplemented with protease inhibitor cocktail and phosSTOP (Roche) and phosphatase inhibitor cocktail (Roche). 30 µg of pre-cleared cell lysate and 4x laemmli buffer were boiled for 10 minutes. Boiled lysates were run on a 4-20% gradient gel (BioRad) and transferred to a PVDF membrane. After blocking in 5% milk/TBS-T, blots were incubated overnight with primary antibody towards AMPK (Cell Signaling), phospho-AMPK (Cell Signaling), REDD1 (Protein Tech), S6K (Cell Signaling), phospho-S6K (Cell Signaling), LKB1 (Santa Cruz) and β-actin (Sigma Aldrich). Blots were washed with TBS-T and incubated with secondary antibodies. Blots were scanned using the LiCOR Odyssey system.

2.6.6 qRT-PCR analysis

RNA extraction was performed using the RNeasy Mini Kit (Qiagen). RNA was reverse transcribed to cDNA using the Quantitect Reverse Transcription Kit (Qiagen). For qRT-PCR, 50 ng of cDNA was mixed with primers towards REDD1 (Forward 5'-ACAGTTCTAGATGGAAGACC-3', Reverse 5'-ACAGTTCTAGATGGAAGACC-3' or RPL32 (Forward 5'-GTGCAACAAATCTTAC-TGTG, Reverse 5'-CTGCCTACTCATTTTCTTCAC).

2.6.7 Metabolite extraction and analysis

Cells were cultured in 6-well plates with or without metformin (10 μM) or phenformin (1 μM) treatment for 24 hours, and extracted at 80% confluency. Medium was aspirated, and each well was washed with 2 ml saline (pH 7.5). Saline was aspirated, and cells were quenched with 500 μl of -75°C HPLC-grade methanol in each well. After adding 200 μl of HPLC-grade water to each well, cells were scraped with a cell lifter. All contents of each well were collected in a 1.7-ml microcentrifuge tube. Chloroform (500 μl at −20°C) was added to each tube and vortexed for 10 min at 4°C. Extracts were centrifuged at 17,000 × g for 15 min at 4°C. The upper aqueous phase containing polar metabolites was collected in a separate microcentrifuge tube and evaporated under a stream of nitrogen. Metabolites were resuspended in 100 μl of HPLC-grade water immediately before analysis by mass spectrometry. The metabolites were analyzed using a Waters Xevo TQ-S mass spectrometer coupled to an H-Class UPLC system. Metabolites were separated by polarity using a Supelco Ascentis Express C18 column (2.7 μm particle size, 5 cm × 2.1 mm). LC parameters are as follows: autosampler temperature, 5 °C; injection volume, 5 μl; column temperature, 50 °C; flow rate over 11 min: t = 0, 0.4 ml min−1; t = 2, 0.3 ml

min−1; t = 3, 0.25 ml min−1; t = 5, 0.15 ml min−1; t = 9, 0.4 ml min−1; t = 11, 0.4 ml min−1. The LC solvents were solvent A: 10 mM tributylamine and 15 mM acetic acid in 97:3 water:methanol (pH 4.95); and solvent B: methanol. Elution from the column was performed over 11 min with the following gradient: t = 0, 0% B; t = 1, 0% B; t = 2, 20% B; t = 3, 20% B; t = 5, 55% B; t = 8, 95% B; t = 8.5, 95% B, t = 9, 0% B; t = 11, 0% B. Mass spectra were acquired using negative-mode electrospray ionization operating in multiple reaction monitoring (MRM) mode. The capillary voltage was 3,000 V, and cone voltage was 50 V. Nitrogen was used as cone gas and desolvation gas, with flow rates of 150 l h−1 and 600 l h−1, respectively. The source temperature was 150 °C, and desolvation temperature was 500 °C. Argon was used as collision gas at a manifold pressure of 4.3 × 10-3 mbar. Collision energies and source cone potentials were optimized for each MRM transition using Waters QuanOptimize software. Data analysis was performed using MAVEN [28,29]. Metabolite measurements were normalized by cell counts.

2.7 Acknowledgments

We thank members of the Women's Cancer Program at Cedars-Sinai Medical Center for their thoughtful input and insight in completion of this manuscript. We would also like to thank Dr. Tan Ince (U. of Miami) for providing the normal immortalized FTSEC cell lines, FNE1 and FNE2. The work of P.J.P.A. is supported by the Ovarian Cancer Research Fund Alliance Program Project Grant. The work of K.R. is supported by the National Center for Research Resources Grant S10RR026744. The work of S.Y.L. and M.O. is supported by Office of the Assistant Secretary of Defense for Health Affairs, through the Breast Cancer Research Program, under Award No. W81XWH-15-1-0453.

S.Y.L. is also supported by 2016 AACR-Incyte Corporation NextGen Grant for Transformative Cancer Research, Grant Number 16-20-46-LUNT.

2.8 Author Contributions

P.J.P.A. initiated and oversaw the entire study design and execution. M.H. and P.J.P.A performed the proliferation assays and helped with the bioenergetic and metabolomics experiments. L.V. and K.R. performed and helped interpret the bioenergetic experiments. B.Y.K helped with data analysis and interpretation. M.P.O. and S.Y.L. performed and helped interpret the metabolomics data. All authors helped with manuscript preparation.

2.9 APPENDIX

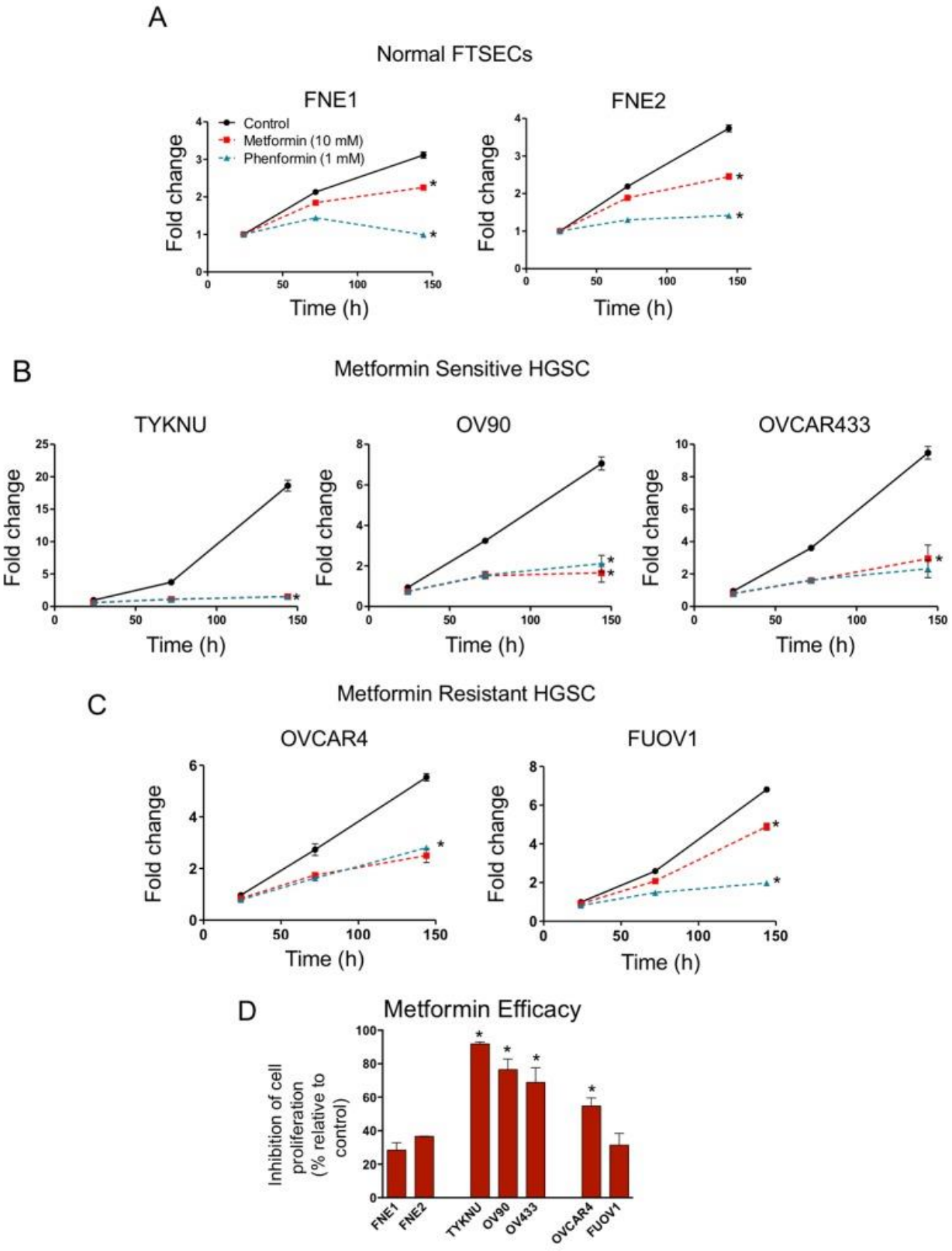

Figure 2.1 The effects of biguanides on 2-D cell proliferation of HGSC and normal FTSEC cell lines. (**A**) Normal FTSECs, (**B**) metformin sensitive and (**C**) metformin resistant cells grown

Figure 2.1 (cont'd)

in 2-D were treated with the indicated doses of metformin, phenformin, or vehicle control at 24 h for 5 days. Cell proliferation was assessed at indicated time points by Celltiter Glo. Proliferation is displayed relative to vehicle control at 24h. (**D**) Metformin efficacy calculated based on metformin treatment relative to control after 5 days of treatment. *denotes significant inhibition relative to control treatment (p-value <.01).

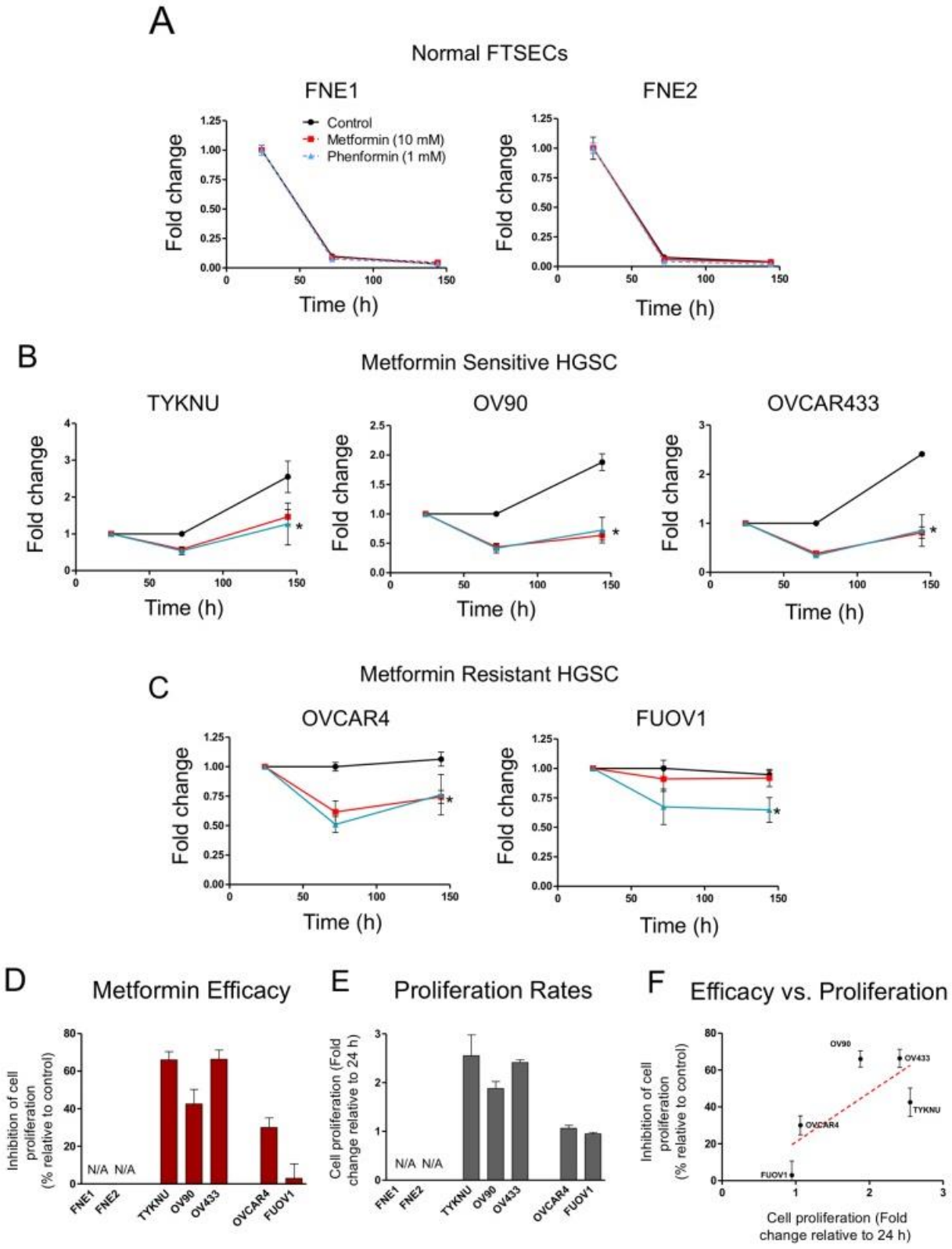

Figure 2.2 The effects of biguanides on 3-D cell proliferation of HGSC and normal FTSEC cell lines. (**A**) Normal FTSECs, (**B**) metformin sensitive and (**C**) relatively metformin resistant

Figure 2.2 (cont'd)

cells grown in ultra-low attachment 3D conditions. Cell proliferation was assessed at indicated time points by Celltiter Glo 3D. Proliferation is displayed relative to vehicle control at 24h. (**D**) Metformin efficacy calculated based on metformin treatment divided by control treatment at 5 days of treatment. (**E**) Proliferation at 6 days relative to 24 h. (F) Plot of metformin efficacy versus cell proliferation rates. Dotted red line is best-fit trend line of all data points and statistically significant to be non-zero (p-value <0.01). *denotes significant inhibition relative to control treatment (p-value <0.01).

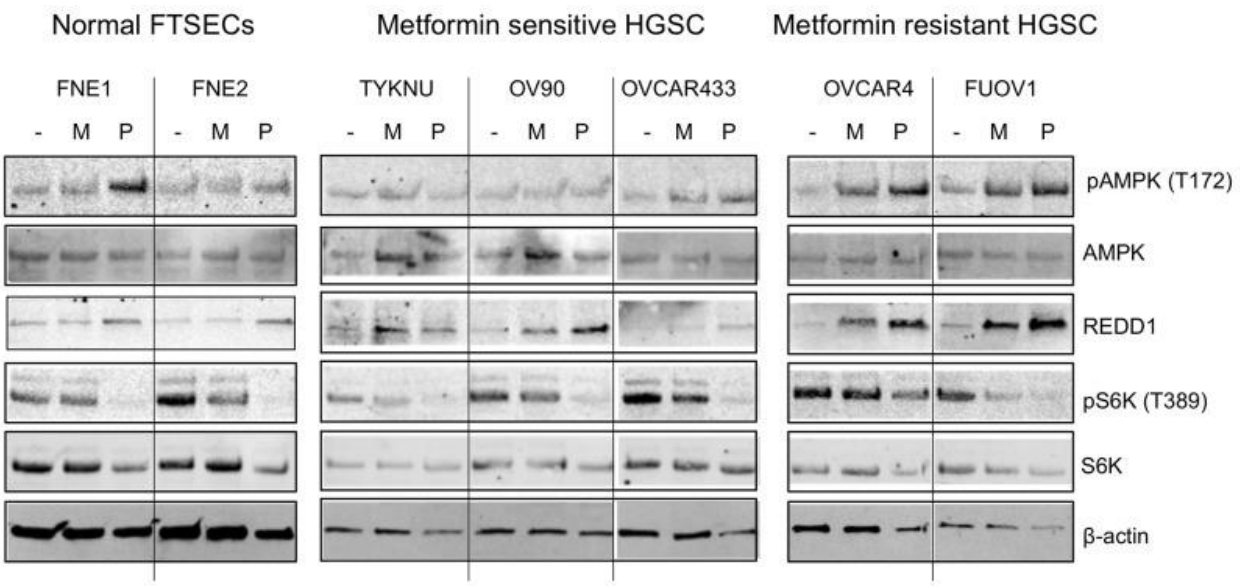

Figure 2.3 The effects of biguanides on mTOR signaling in HGSC and normal FTSEC cell lines. Cell lines were treated with metformin (10 mM), phenformin (1 mM), or vehicle control for 24 hours. Western blot analysis of phospho-AMPK (T172), AMPK, phospho-S6K (T389), S6K, REDD1, and β-actin as a loading control.

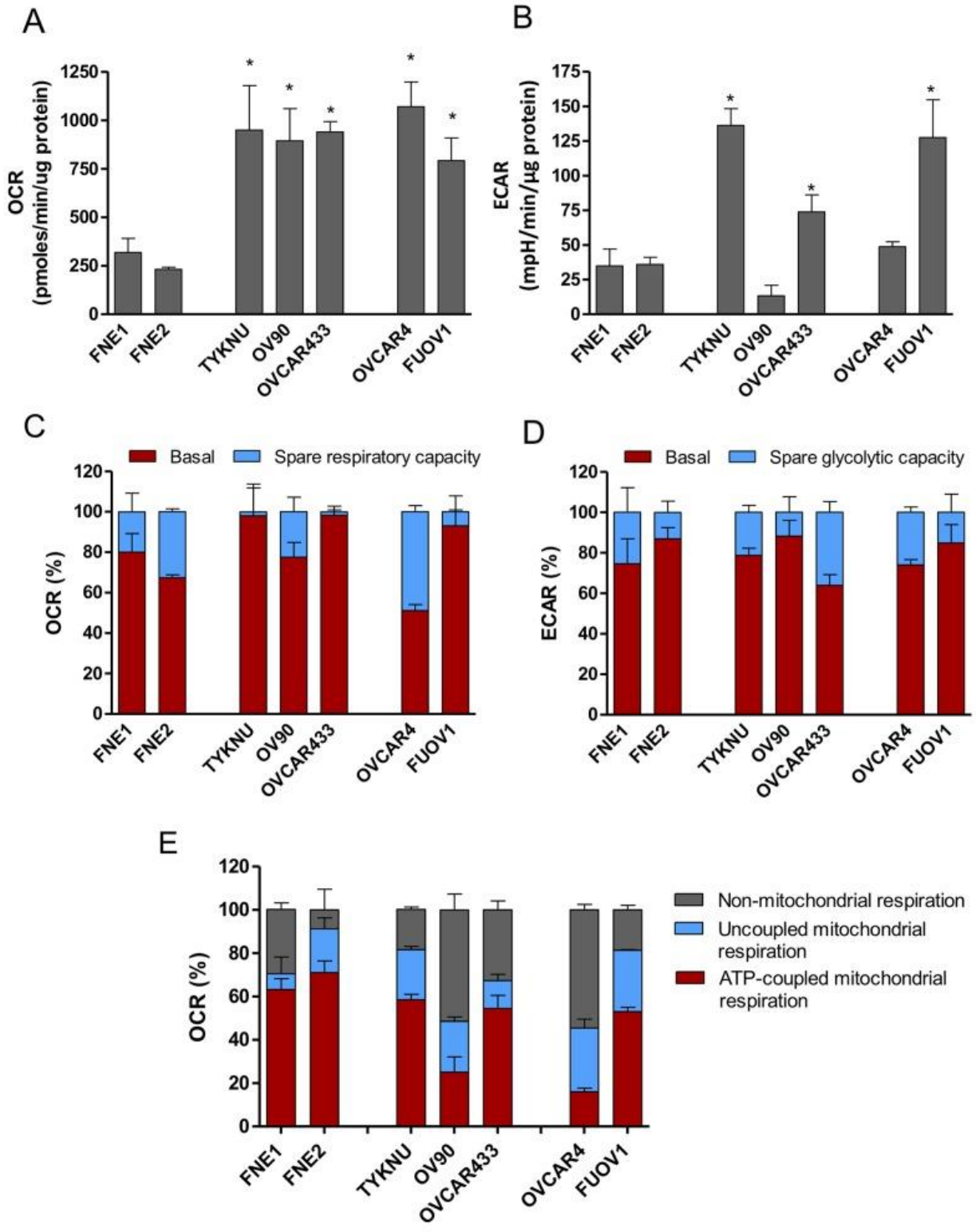

Figure 2.4 Bioenergetic analysis of HGSC and normal FTSEC cell lines. (**A-E**) Oxygen Consumption Rate (OCR) (**A, C, E**) and Extracellular Acidification Rate (ECAR) (**B & D**) measurements were obtained using an extracellular flux analyzer (Seahorse Bioscience).

Figure 2.4 (cont'd)

Basal OCR (**A**) and ECAR (**B**) rates were obtained prior to addition of Oligomycin A to derive Spare Glycolytic Capacity (**D**) and ATP-coupled OCR (**E**), and FCCP to uncouple mitochondria for maximal OCR. (**C**) Spare respiratory capacity was calculated by taking the difference between the maximal OCR and basal OCR. Percentages are relative to maximal respiration. (**D**) Spare Glycolytic Capacity was derived by taking the difference between maximal ECAR and basal ECAR. Percentages are relative to maximal ECAR. (**E**) Non-mitochondrial respiration was calculated as the residual OCR after treatment with Rotenone/myxothiazol that inhibits Complex I. Uncoupled mitochondrial respiration was calculated as the difference between OCR following Oligomycin A treatment and OCR following Rotenone/myxothiazol treatment. All three values are shown as percentages relative to baseline OCR.

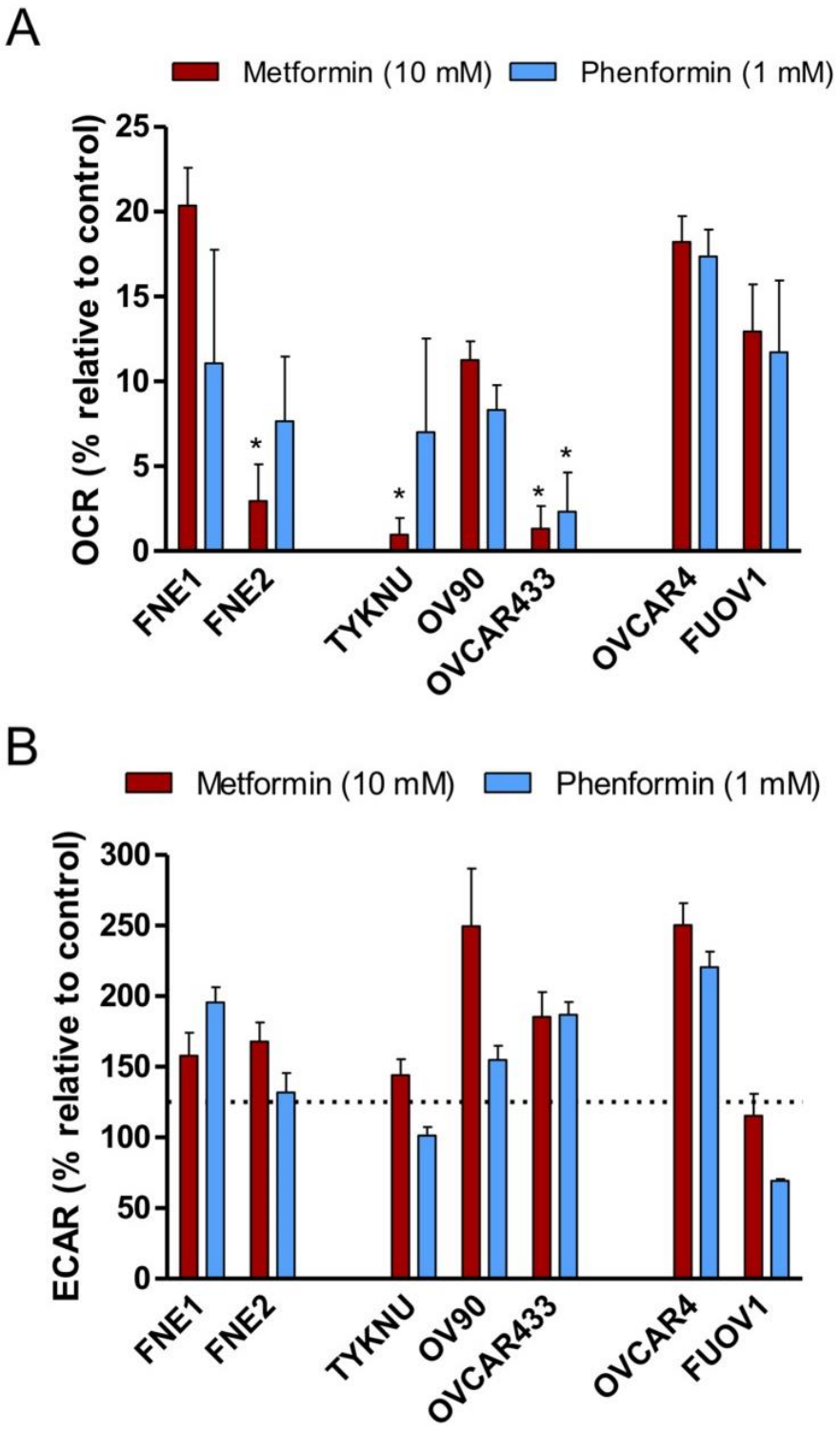

Figure 2.5 The effects of biguanides on the bioenergetics profiles of HGSC and normal FTSEC cell lines. (**A-B**) Cells were treated with Metformin (10 mM), Phenformin (1 mM), or control vehicle for 24 hours prior to analysis by the extracellular flux analyzer. (**A**) Basal OCR relative to control treated cells. * denotes p-value < 0.05 as determined by Tukey's multiple

Figure 2.5 (cont'd)

comparison test. (**B**) Basal ECAR relative to control treated cells. Dotted line indicates the level of a statistically significant change in ECAR (p-value < 0.01).

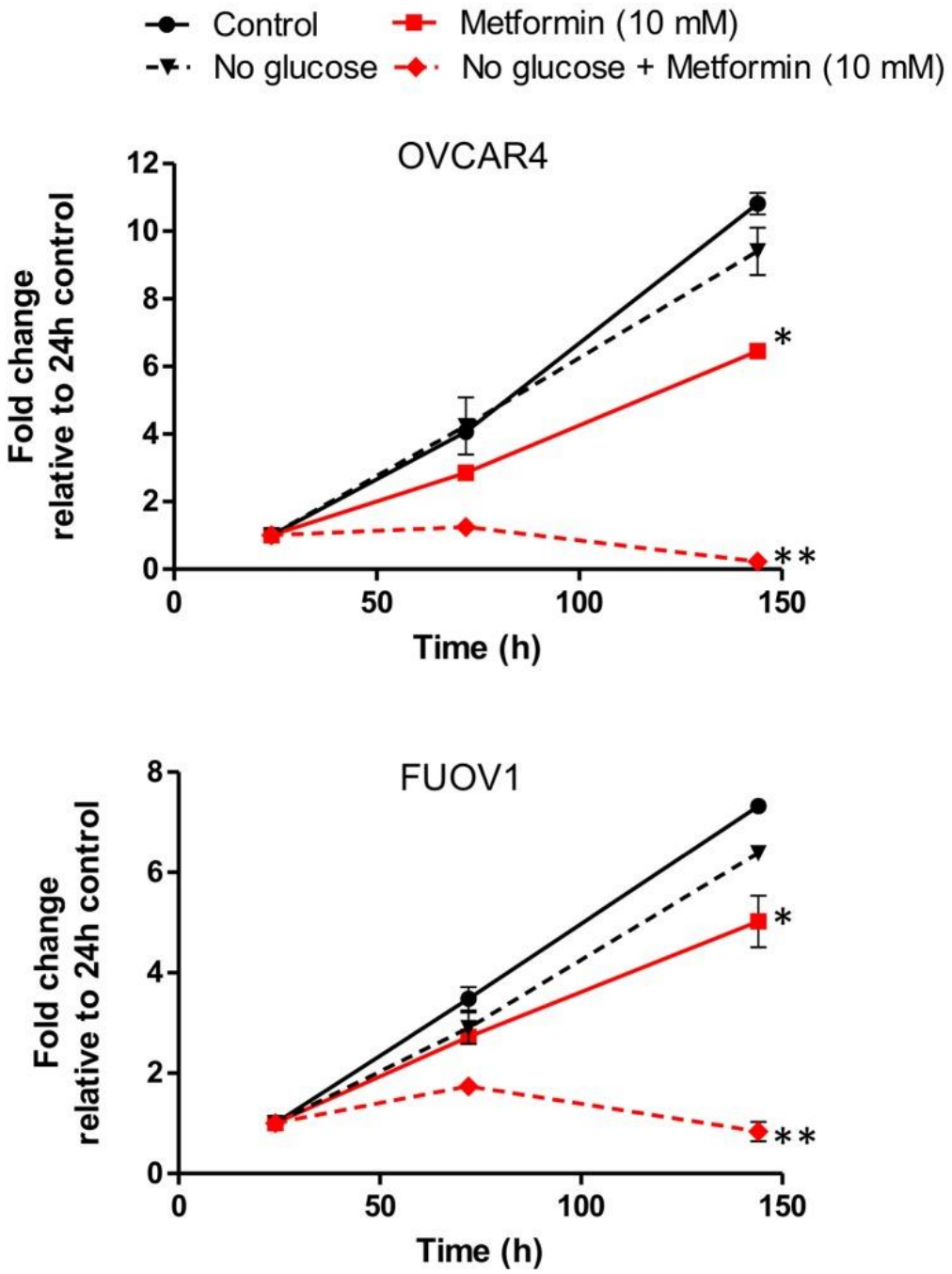

Figure 2.6 Glucose deprivation sensitizes metformin resistant cell lines FUOV1 and OVCAR4 to metformin treatment. Cells were grown in standard glucose or limited glucose conditions were treated with vehicle or metformin (10 mM). Cell proliferation was assessed at 24 h, 72h, and 144 h. Proliferation is depicted relative to 24 h for each treatment. * denotes p-value < 0.01 relative to control. ** denotes p-value <0.01 relative to metformin in standard glucose media.

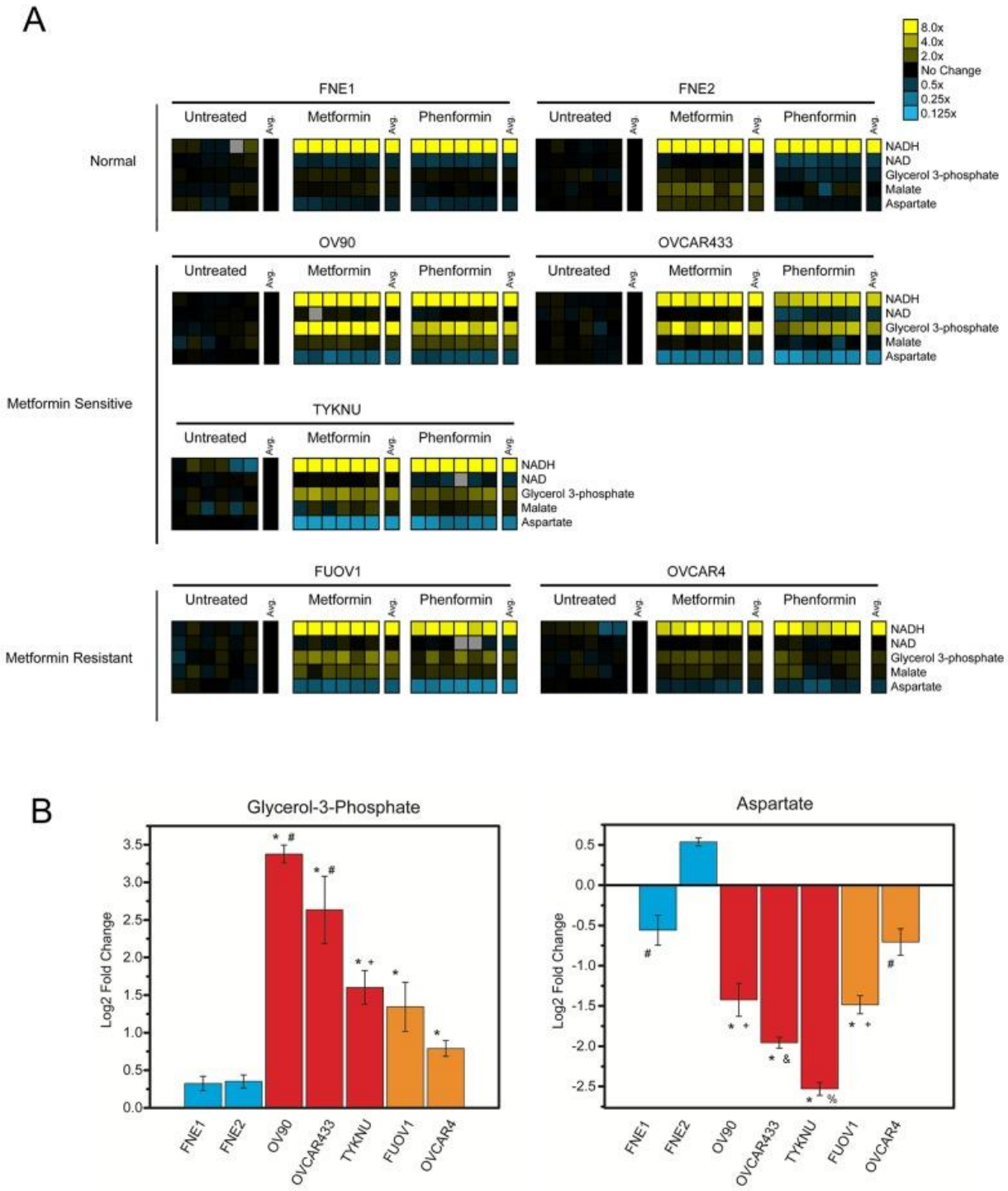

Figure 2.7 The cancer-specific effects of biguanides on mitochondrial shuttle metabolites. (**A**) Metabolite analysis. Cells were treated with metformin (10 mM), phenformin (1 mM), or vehicle control for 24 hours and subjected to targeted mass spectrometry analysis. Metformin and phenformin treatments shown relative to untreated control. Yellow and blue boxes indicate increased or decreased levels relative to control, respectively. Data normalized by cell number. Complete metabolite changes located in Figure S2.2. (**B**) Quantification of G3P and aspartate fold changes induced by metformin treatment. Values listed as log2 fold change in metabolite

Figure 2.7 (cont'd)

abundance for metformin treated versus control normal FTSECs (blue), metformin-sensitive (red), and metformin-resistant (orange) cells. For G3P: *p-value < 0.05 vs normal cell lines by Games-Howell test, #p-value < 0.05 vs TYKNU, FUOV1, and OVCAR4 by Games-Howell test, +p-value < 0.05 vs OVCAR4 by Games-Howell test. For aspartate: *p-value < 0.05 vs normal cell liens by Games-Howell test, #p-value < 0.05 vs FNE2 by Games-Howell test, +p-value < 0.05 vs OVCAR4 by Games-Howell test, &p-value < 0.05 vs OV90, FUOV1, and OVCAR4 by Games-Howell test, and %p-value < 0.05 vs OV90, OVCAR433, FUOV1, and OVCAR4 by Games-Howell test.

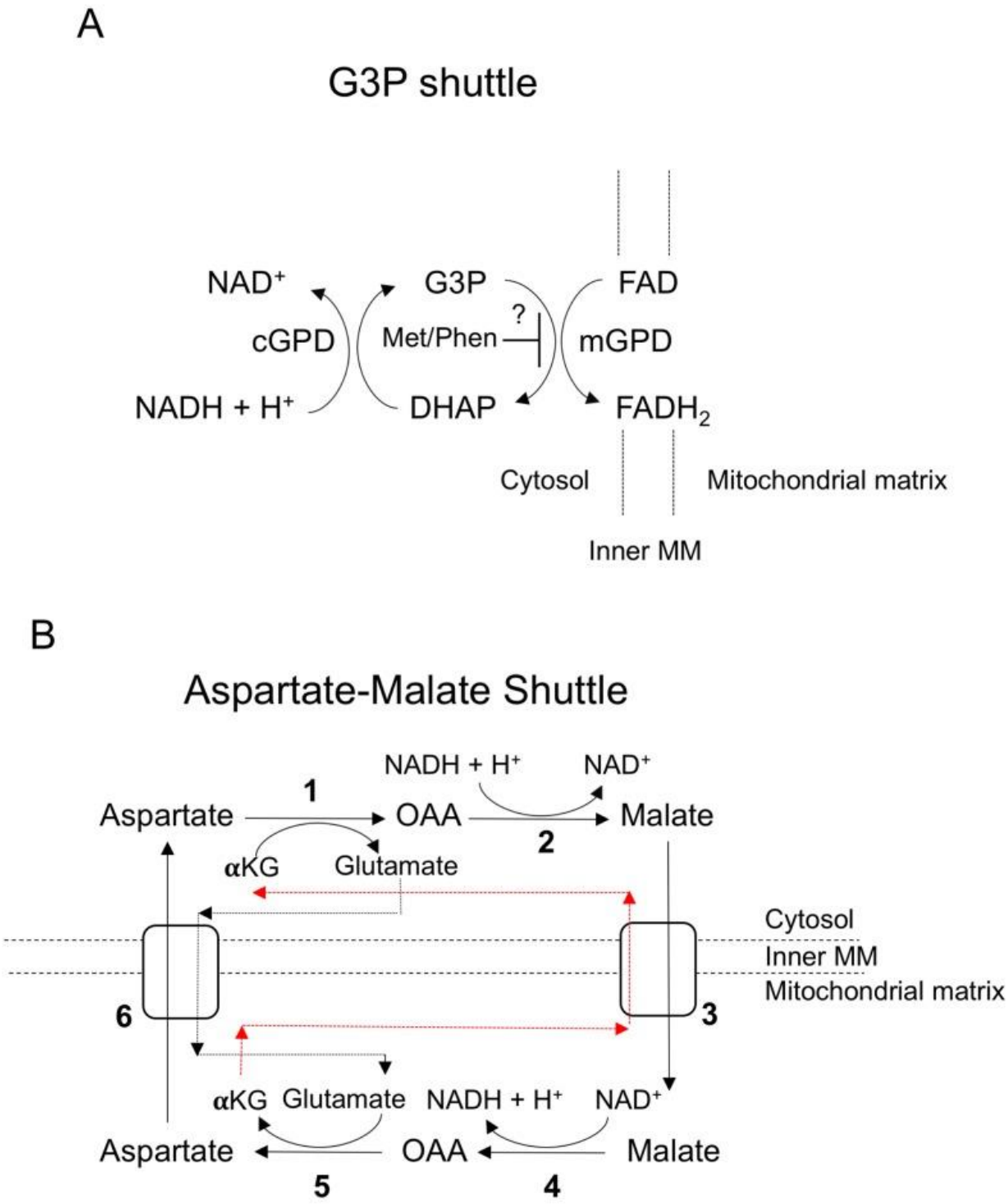

Figure 2.8 Mitochondrial shuttles. (**A**) The glycerol-3-phosphate shuttle. cGPD = cytosolic glycerol-3-phosphate dehydrogenase, mGPD – mitochondrial glycerol-3-phosphate dehydrogenase. **(B)** The malate-aspartate shuttle. Numbers indicate the following enzymes and transporters: (1) Cytosolic aspartate aminotransferase (2) Malate dehydrogenase 1 (3) Malate-alpha-ketoglutarate antiporter (4) Malate dehydrogenase 2 (5) Mitochondrial aspartate

Figure 2.8 (cont'd)

aminotransferase (6) Glutamate-aspartate antiporter. Black and red dashed lines indicate the flow of α-ketoglutarate and glutamate between the cytosol and mitochondrial space.

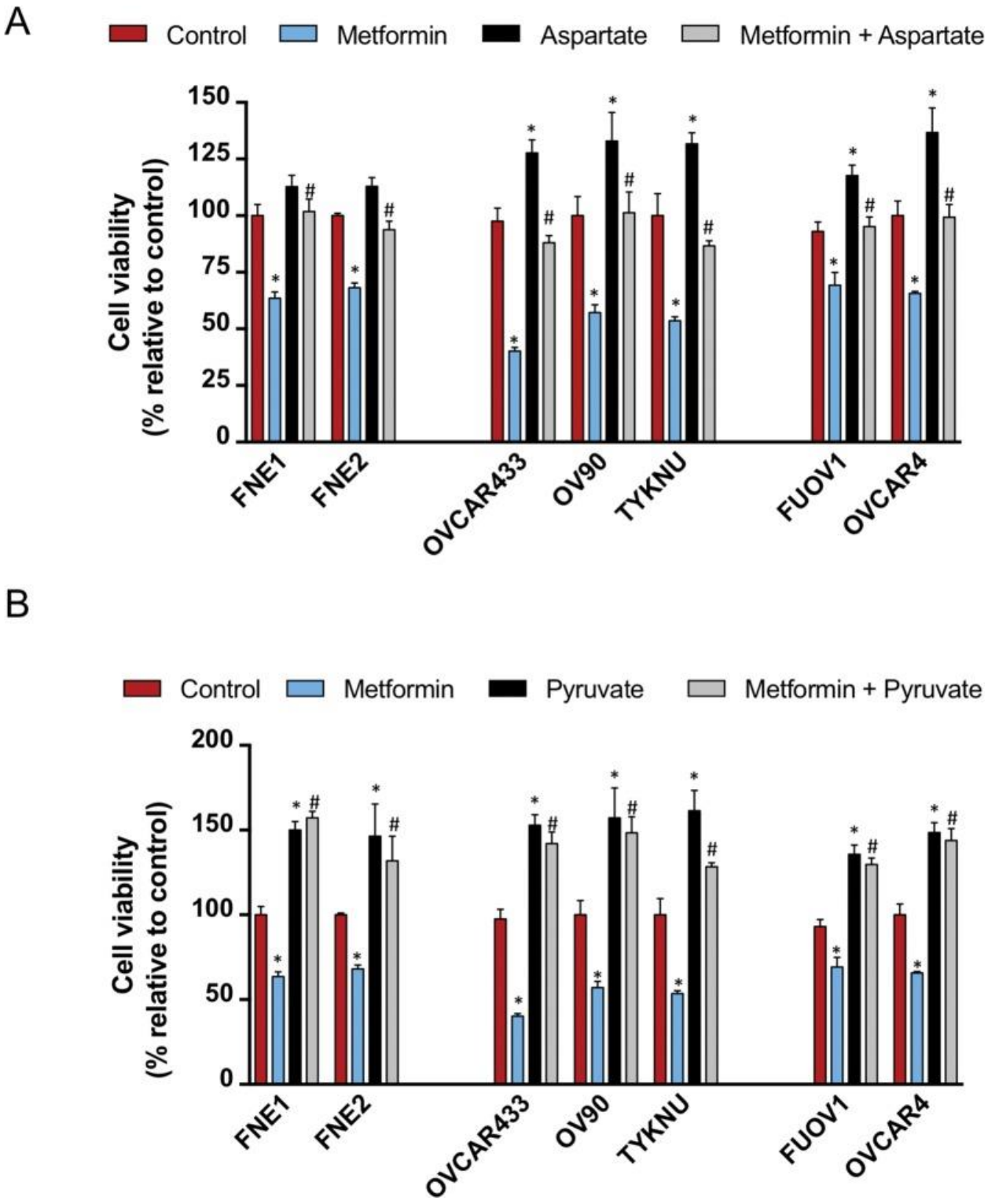

Figure 2.9 Aspartate and pyruvate supplementation inhibits the effects of metformin on cell proliferation. Cells were seeded and after 24 h were treated with either control, metformin (10 mM) with or without **(A)** aspartate (100 uM) or **(B)** pyruvate (1 mM). Cell proliferation was assessed after an additional 72 h by Celltiter Glo. Proliferation is displayed relative to vehicle

Figure 2.9 (cont'd)

control. * denotes p-value < 0.01 relative to control. # denotes p-value < 0.01 relative to metformin treatment.

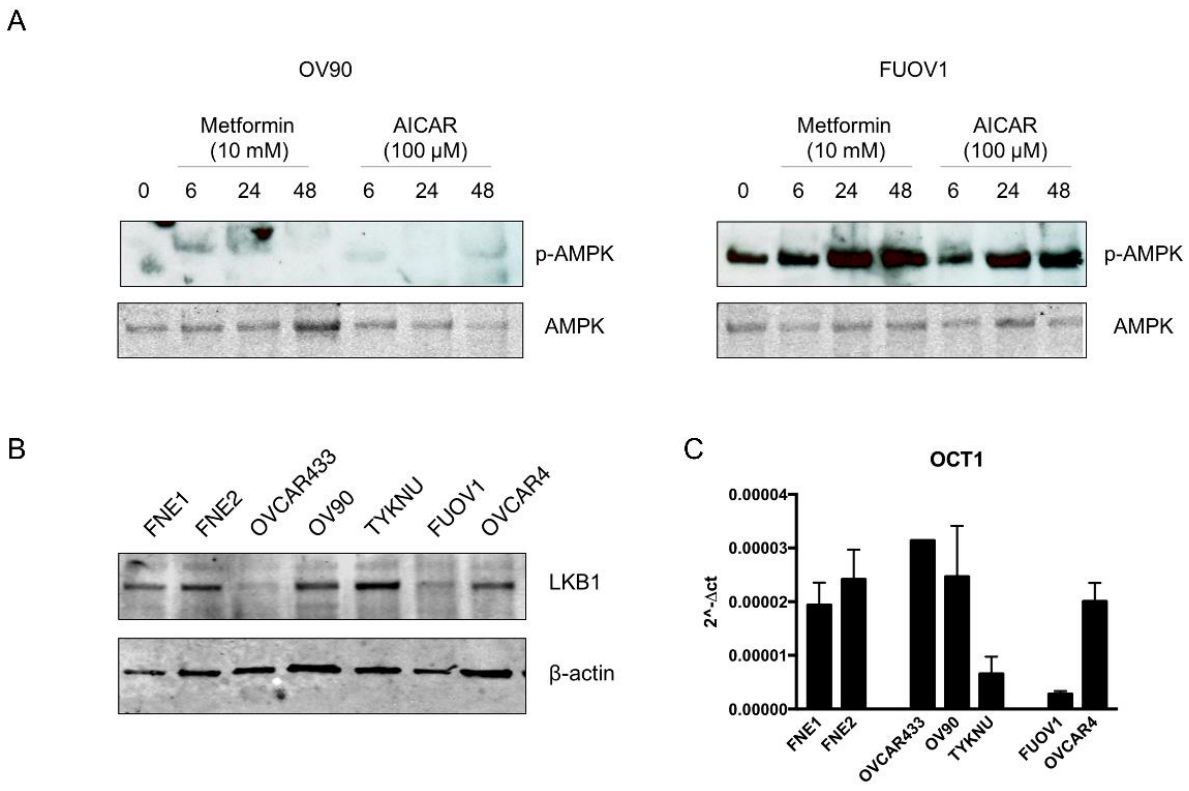

Figure S2.1 Expression levels of phospho-AMPK, AMPK, LKB1, and OCT1. (A) Time course of metformin (10 mM) and AICAR (100 uM) treatment on OV90 and FUOV1. Cells were seeded and 24 hours later treated with either control, metformin, or AICAR and harvested at indicated time points. Western blot analysis for pAMPK and AMPK was performed. **(B)** Western blot analysis of LKB1 in untreated cell lines. β-actin was used as a loading control. **(C)** qRT-PCR analysis of OCT1. RPL32 transcript was used for normalization between samples.

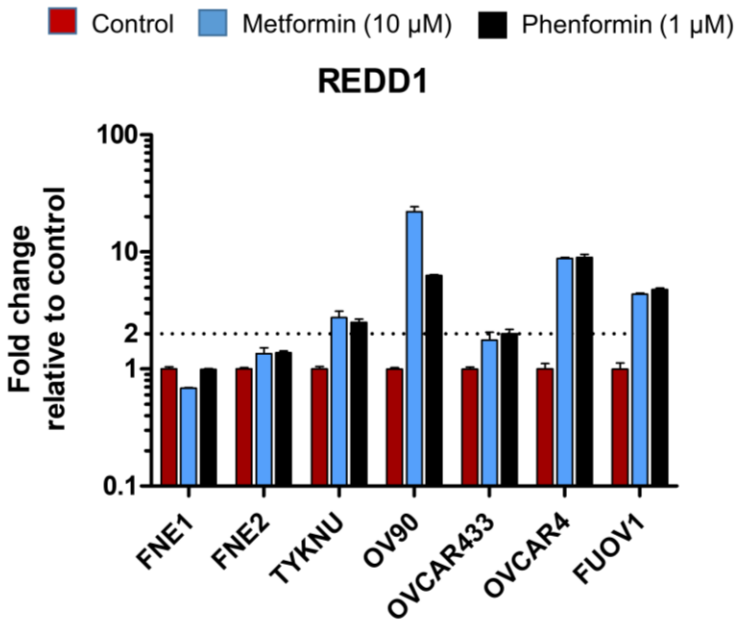

Figure S2.2 The effects of biguanides on REDD1 transcription in HGSC and normal FTSEC cell lines. qRT-PCR analysis of REDD1. Fold change of each treatment shown relative to vehicle control. Dotted line indicates statistically significant upregulation (>2-fold change of a student t-test p-value < 0.01). RPL32 transcript was used for normalization between samples.

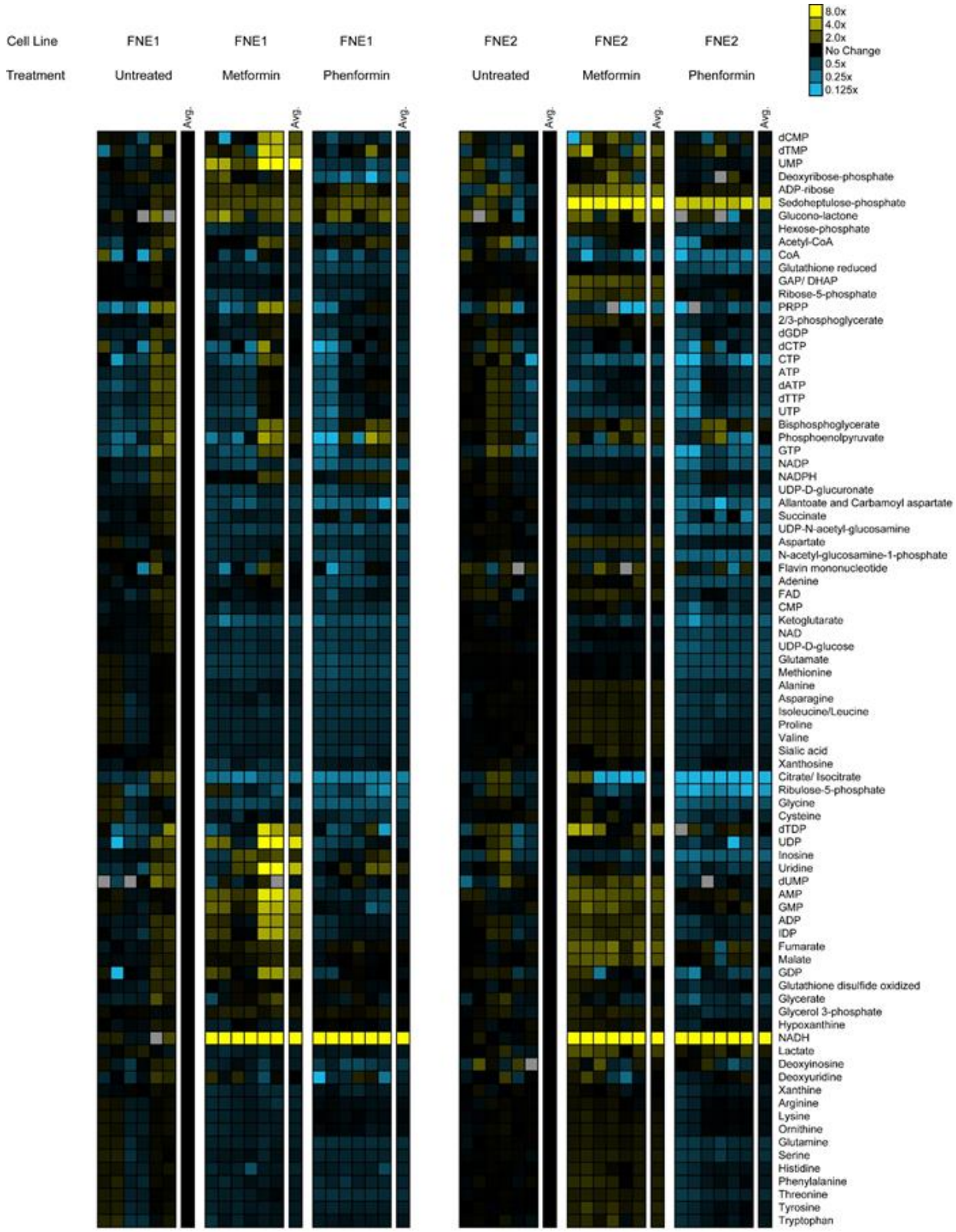

Figure S2.3 Profiles of intracellular metabolites in HGSC and normal FTSEC cell lines treated with metformin (10 mM), phenformin (1 mM), or vehicle control for 24 hours. Relative

Figure S2.3 (cont'd)

levels are expressed as the log ratio of the normalized signal intensity in drug treated cells to the normalized signal intensity in the vehicle control for each cell line. Yellow and blue boxes indicate increased or decreased levels relative to control, respectively. Signal intensity was also normalized by cell number.

Figure S2.3 (cont'd)

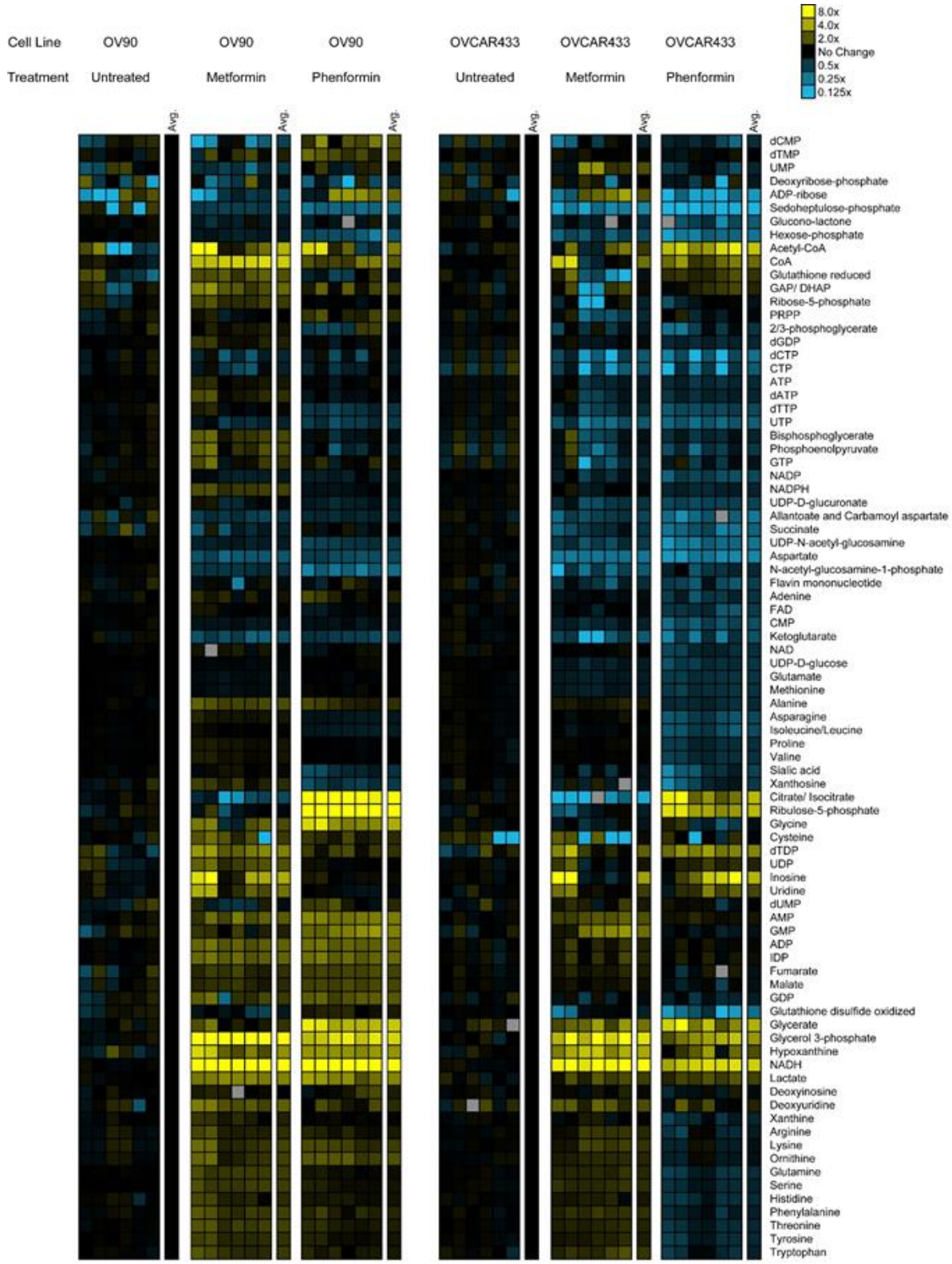

Figure S2.3 (cont'd)

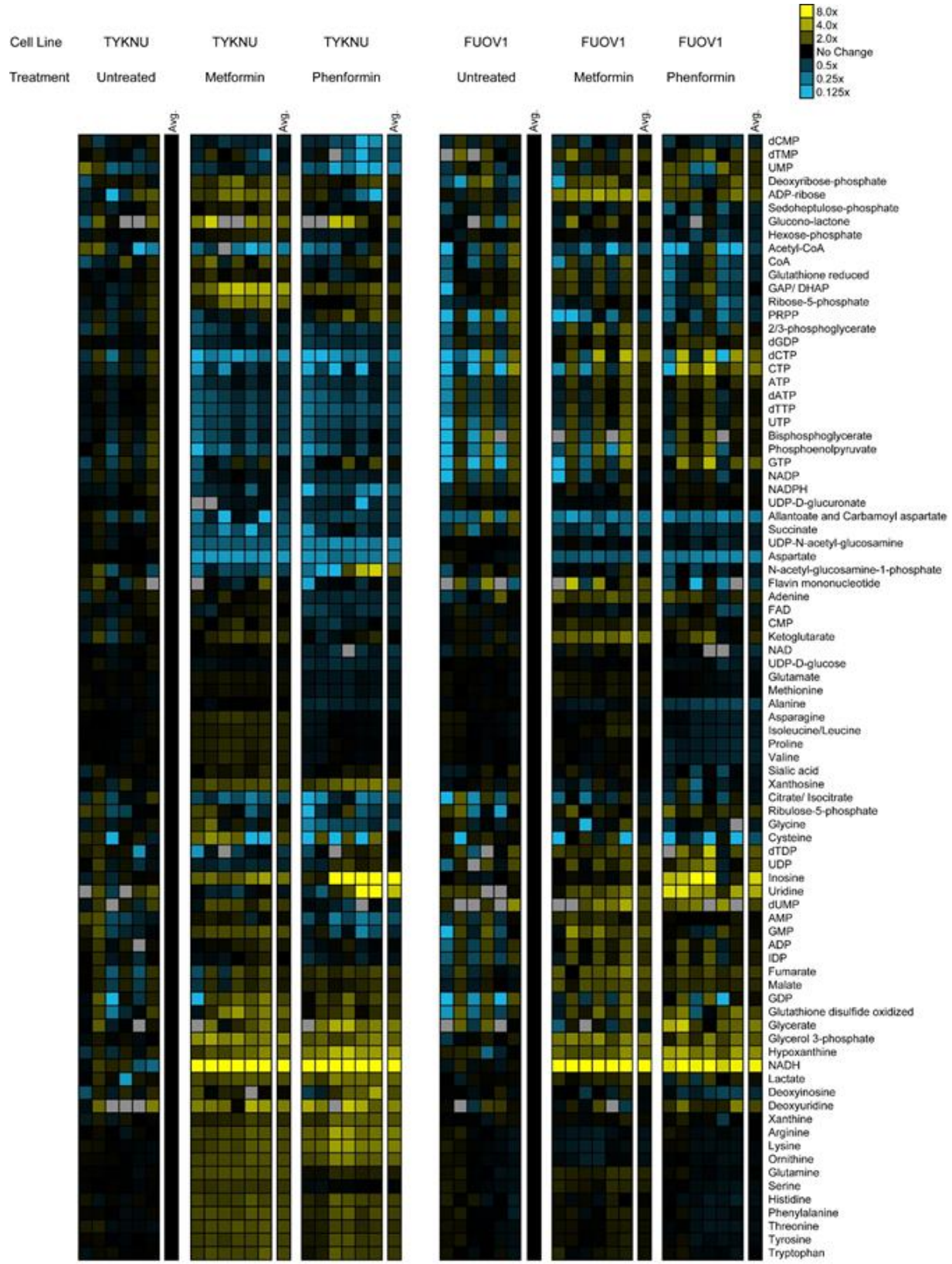

Figure S2.3 (cont'd)

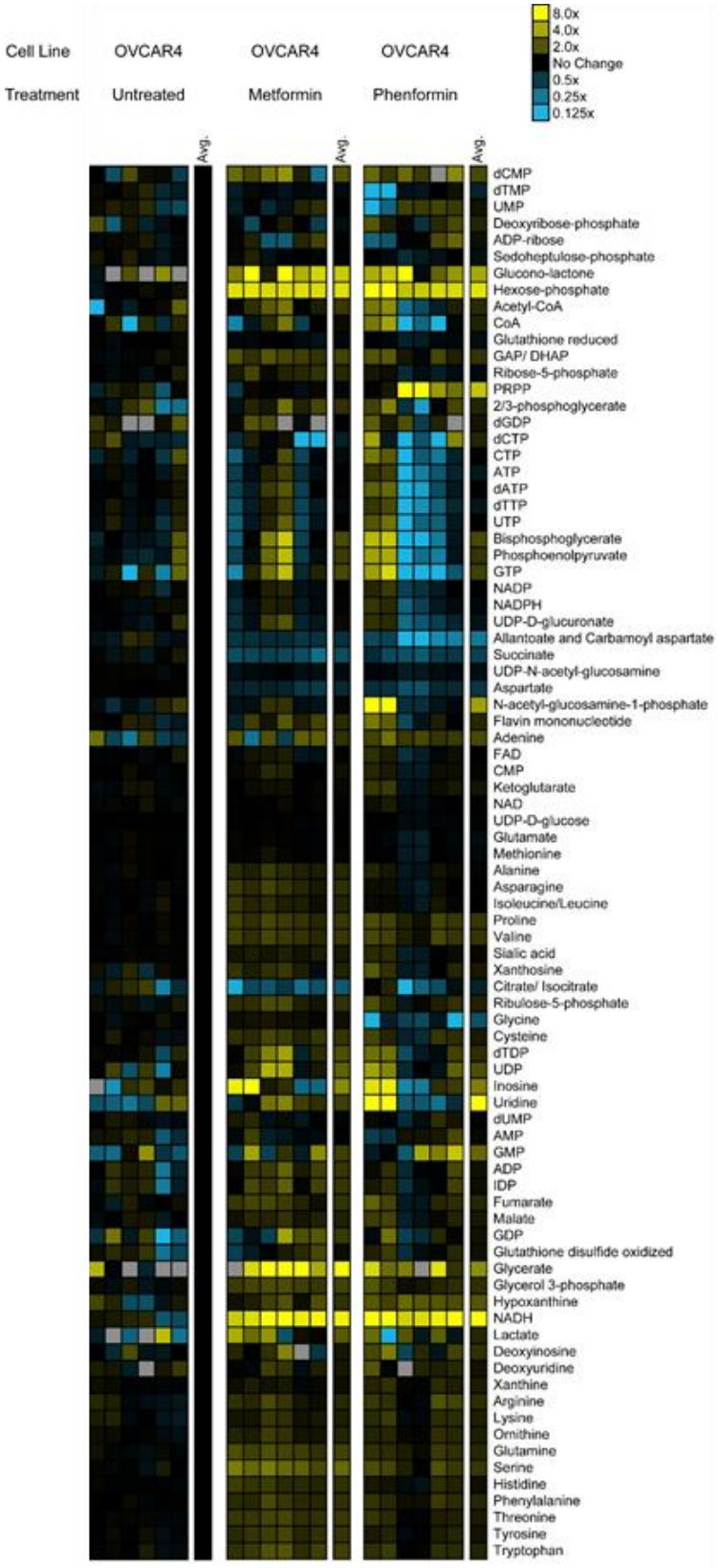

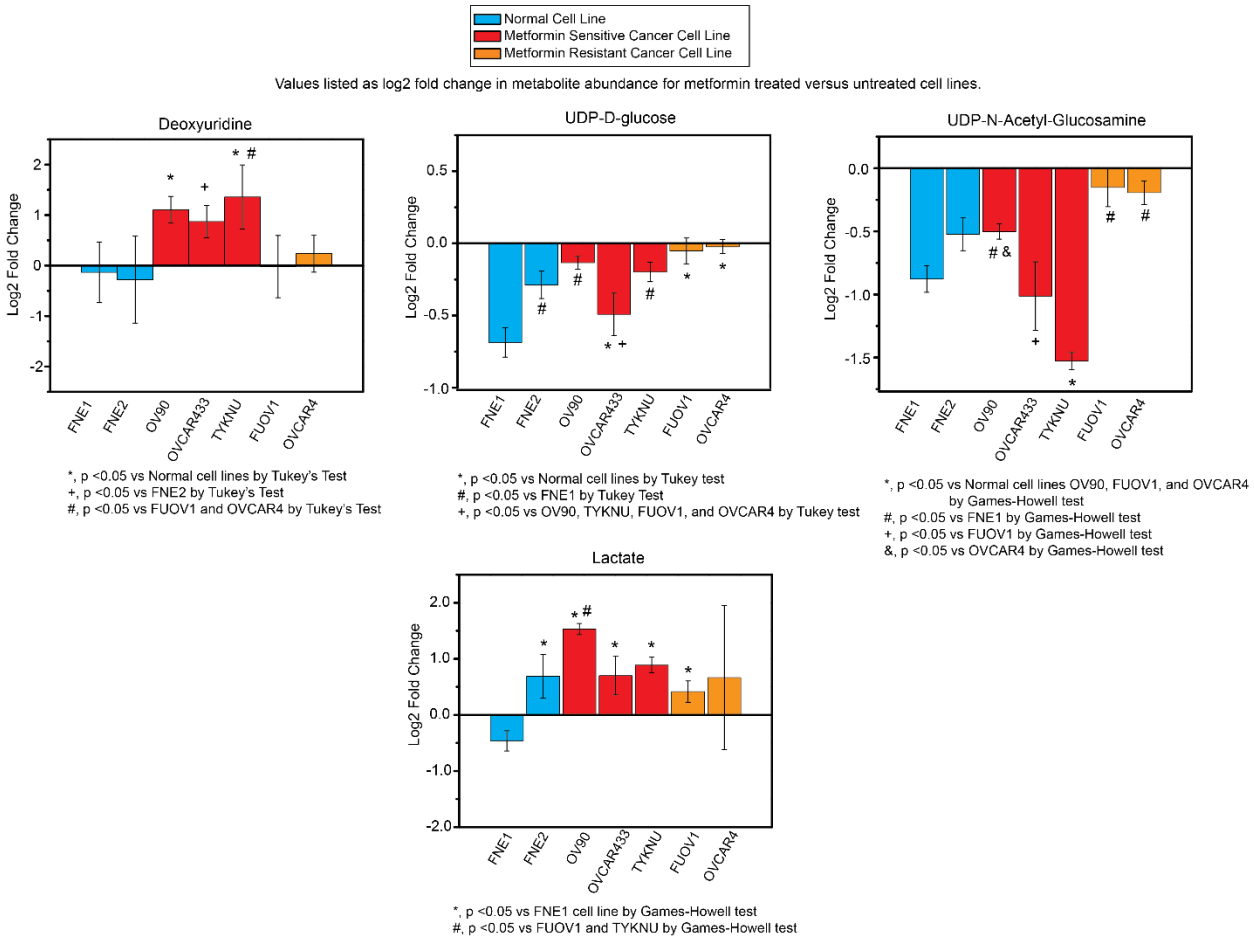

Figure S2.4 Quantification of metabolite changes induced by metformin treatment. Values listed as log2 fold change in metabolite abundance for metformin treated versus control normal FTSECs (blue), metformin-sensitive (red), and metformin-resistant (orange) cells. For statistical analysis, Tukey's or Games-Howell test were used as indicated.

P <0.05	FNE1			
	Metformin vs Untreated		Phenformin vs Untreated	
Metabolite	Log2 Fold Change	P value	Log2 Fold Change	P value
NADH	4.4902	*0.0061*	4.2490	*0.0075*
NAD	-0.6813	0.0185	-0.8820	0.0092
Glycerol 3-phosphate	0.3924	*0.0266*	0.2343	0.0486
Malate	0.2420	0.2825	0.0047	0.9079
Aspartate	-0.5302	0.1708	-0.6692	0.0842
	FNE2			
	Metformin vs Untreated		Phenformin vs Untreated	
Metabolite	Log2 Fold Change	P value	Log2 Fold Change	P value
NADH	4.494289061	0.0000	3.6370	0.0001
NAD	-0.101470172	0.1558	-0.9366	0.0005
Glycerol 3-phosphate	0.382418975	*0.2179*	-0.5175	0.0725
Malate	1.057864281	0.0000	-0.3026	*0.5113*
Aspartate	0.561138602	0.0003	-0.3300	0.0502
	FUOV1			
	Metformin vs Untreated		Phenformin vs Untreated	
Metabolite	Log2 Fold Change	P value	Log2 Fold Change	P value
NADH	3.395786607	0.0000	3.0850	0.0001
NAD	0.334880408	0.1038	-0.3422	0.0169
Glycerol 3-phosphate	1.566685751	0.0010	1.3479	0.0022
Malate	0.651628165	0.2183	0.5430	0.1789
Aspartate	-1.462037971	0.0009	-2.1237	0.0003
	OV90			
	Metformin vs Untreated		Phenformin vs Untreated	
Metabolite	Log2 Fold Change	P value	Log2 Fold Change	P value
NADH	3.757570572	0.0000	3.1531	0.0000
NAD	0.307160273	0.0026	-0.0304	*0.7715*
Glycerol 3-phosphate	3.410913476	0.0001	2.6432	0.0004
Malate	0.516719894	0.2069	0.8732	*0.0423*
Aspartate	-1.337253238	0.0007	-1.1686	0.0002
	OVCAR433			
	Metformin vs Untreated		Phenformin vs Untreated	
Metabolite	Log2 Fold Change	P value	Log2 Fold Change	P value
NADH	3.178679596	0.0000	2.5394	0.0001
NAD	0.069937314	0.2330	-0.7969	0.0048
Glycerol 3-phosphate	3.023537598	0.0000	1.8847	0.0034
Malate	0.252118946	0.1661	-0.1458	0.4038
Aspartate	-1.935654182	0.0001	-2.2291	0.0005
	TYKNU			
	Metformin vs Untreated		Phenformin vs Untreated	
Metabolite	Log2 Fold Change	P value	Log2 Fold Change	P value
NADH	5.308543537	*0.0199*	4.5557	*0.0270*
NAD	0.113864922	0.5758	-0.3706	0.0282
Glycerol 3-phosphate	1.705783431	0.0007	1.1858	0.0066
Malate	0.656276305	0.0202	0.4576	0.6225
Aspartate	-2.515199139	0.0000	-2.0590	0.0003
	TYKNU			
	Metformin vs Untreated		Phenformin vs Untreated	
Metabolite	Log2 Fold Change	P value	Log2 Fold Change	P value
NADH	5.167365698	*0.0088*	4.4671	*0.0121*
NAD	0.005032679	0.4857	-0.7342	0.0086
Glycerol 3-phosphate	1.496715468	0.0001	0.9878	0.0020
Malate	-0.312588339	0.5175	0.3273	0.0468
Aspartate	-2.544860804	0.0000	-2.1172	0.0002
	OVCAR4			
	Metformin vs Untreated		Phenformin vs Untreated	
Metabolite	Log2 Fold Change	P value	Log2 Fold Change	P value
NADH	3.1787	0.0000239	2.5394	0.0000782
NAD	0.0699	0.2329909	-0.7969	0.0048083
Glycerol 3-phosphate	3.0235	0.0000142	1.8847	0.0034068
Malate	0.2521	0.1661287	-0.1458	0.4038247
Aspartate	-1.9357	0.0000972	-2.2291	0.000474

Table S2.1 Statistical analysis of metabolic profiles shown in Figures 2.7, S2.2, and S2.3. Student's *t*-test was used to determine significance. If assumption of homoscedasticity was not

Table S2.1 (cont'd)

met, Welch's *t*-test was used instead (indicated in italics). Statistically significant differences ($p < 0.05$) are highlighted in green and underlined.

2.10 REFERENCES

REFERENCES

1. Bowtell DD, Bohm S, Ahmed AA, Aspuria PJ, Bast RC, Jr., Beral V, Berek JS, Birrer MJ, Blagden S, Bookman MA, Brenton JD, Chiappinelli KB, Martins FC, Coukos G, Drapkin R, Edmondson R, Fotopoulou C, Gabra H, Galon J, Gourley C, Heong V, Huntsman DG, Iwanicki M, Karlan BY, Kaye A, Lengyel E, Levine DA, Lu KH, McNeish IA, Menon U, Narod SA, Nelson BH, Nephew KP, Pharoah P, Powell DJ, Jr., Ramos P, Romero IL, Scott CL, Sood AK, Stronach EA, Balkwill FR (2015) Rethinking ovarian cancer II: reducing mortality from high-grade serous ovarian cancer. Nature reviews Cancer 15 (11):668-679. doi:10.1038/nrc4019

2. Siegel RL, Miller KD, Jemal A (2015) Cancer statistics, 2015. CA: a cancer journal for clinicians 65 (1):5-29. doi:10.3322/caac.21254

3. Nestler JE (2008) Metformin in the treatment of infertility in polycystic ovarian syndrome: an alternative perspective. Fertil Steril 90 (1):14-16. doi:10.1016/j.fertnstert.2008.04.073

4. Evans JM, Donnelly LA, Emslie-Smith AM, Alessi DR, Morris AD (2005) Metformin and reduced risk of cancer in diabetic patients. Bmj 330 (7503):1304-1305. doi:10.1136/bmj.38415.708634.F7

5. Gong Z, Aragaki AK, Chlebowski RT, Manson JE, Rohan TE, Chen C, Vitolins MZ, Tinker LF, LeBlanc ES, Kuller LH, Hou L, LaMonte MJ, Luo J, Wactawski-Wende J (2016) Diabetes, metformin and incidence of and death from invasive cancer in postmenopausal women: Results from the women's health initiative. International journal of cancer 138 (8):1915-1927. doi:10.1002/ijc.29944

6. Shackelford DB, Abt E, Gerken L, Vasquez DS, Seki A, Leblanc M, Wei L, Fishbein MC, Czernin J, Mischel PS, Shaw RJ (2013) LKB1 inactivation dictates therapeutic response of non-small cell lung cancer to the metabolism drug phenformin. Cancer cell 23 (2):143-158. doi:10.1016/j.ccr.2012.12.008

7. Janzer A, German NJ, Gonzalez-Herrera KN, Asara JM, Haigis MC, Struhl K (2014) Metformin and phenformin deplete tricarboxylic acid cycle and glycolytic intermediates during cell transformation and NTPs in cancer stem cells. Proceedings of the National Academy of Sciences of the United States of America 111 (29):10574-10579. doi:10.1073/pnas.1409844111

8. Shank JJ, Yang K, Ghannam J, Cabrera L, Johnston CJ, Reynolds RK, Buckanovich RJ (2012) Metformin targets ovarian cancer stem cells in vitro and in vivo. Gynecologic oncology 127 (2):390-397. doi:10.1016/j.ygyno.2012.07.115

9. Rena G, Pearson ER, Sakamoto K (2013) Molecular mechanism of action of metformin: old or new insights? Diabetologia 56 (9):1898-1906. doi:10.1007/s00125-013-2991-0

10. Pernicova I, Korbonits M (2014) Metformin--mode of action and clinical implications for diabetes and cancer. Nature reviews Endocrinology 10 (3):143-156. doi:10.1038/nrendo.2013.256

11. Wheaton WW, Weinberg SE, Hamanaka RB, Soberanes S, Sullivan LB, Anso E, Glasauer A, Dufour E, Mutlu GM, Budigner GS, Chandel NS (2014) Metformin inhibits mitochondrial complex I of cancer cells to reduce tumorigenesis. eLife 3:e02242. doi:10.7554/eLife.02242

12. Liu X, Romero IL, Litchfield LM, Lengyel E, Locasale JW (2016) Metformin Targets Central Carbon Metabolism and Reveals Mitochondrial Requirements in Human Cancers. Cell metabolism 24 (5):728-739. doi:10.1016/j.cmet.2016.09.005

13. Ben Sahra I, Regazzetti C, Robert G, Laurent K, Le Marchand-Brustel Y, Auberger P, Tanti JF, Giorgetti-Peraldi S, Bost F (2011) Metformin, independent of AMPK, induces mTOR inhibition and cell-cycle arrest through REDD1. Cancer research 71 (13):4366-4372. doi:10.1158/0008-5472.CAN-10-1769

14. Nair V, Sreevalsan S, Basha R, Abdelrahim M, Abudayyeh A, Rodrigues Hoffman A, Safe S (2014) Mechanism of metformin-dependent inhibition of mammalian target of rapamycin (mTOR) and Ras activity in pancreatic cancer: role of specificity protein (Sp)

transcription factors. The Journal of biological chemistry 289 (40):27692-27701. doi:10.1074/jbc.M114.592576

15. Gui DY, Sullivan LB, Luengo A, Hosios AM, Bush LN, Gitego N, Davidson SM, Freinkman E, Thomas CJ, Vander Heiden MG (2016) Environment Dictates Dependence on Mitochondrial Complex I for NAD+ and Aspartate Production and Determines Cancer Cell Sensitivity to Metformin. Cell metabolism 24 (5):716-727. doi:10.1016/j.cmet.2016.09.006

16. Litchfield LM, Mukherjee A, Eckert MA, Johnson A, Mills KA, Pan S, Shridhar V, Lengyel E, Romero IL (2015) Hyperglycemia-induced metabolic compensation inhibits metformin sensitivity in ovarian cancer. Oncotarget 6 (27):23548-23560. doi:10.18632/oncotarget.4556

17. Febbraro T, Lengyel E, Romero IL (2014) Old drug, new trick: repurposing metformin for gynecologic cancers? Gynecologic oncology 135 (3):614-621. doi:10.1016/j.ygyno.2014.10.011

18. Domcke S, Sinha R, Levine DA, Sander C, Schultz N (2013) Evaluating cell lines as tumour models by comparison of genomic profiles. Nature communications 4:2126. doi:10.1038/ncomms3126

19. Perets R, Drapkin R (2016) It's Totally Tubular....Riding The New Wave of Ovarian Cancer Research. Cancer research 76 (1):10-17. doi:10.1158/0008-5472.CAN-15-1382

20. Merritt MA, Bentink S, Schwede M, Iwanicki MP, Quackenbush J, Woo T, Agoston ES, Reinhardt F, Crum CP, Berkowitz RS, Mok SC, Witt AE, Jones MA, Wang B, Ince TA (2013) Gene expression signature of normal cell-of-origin predicts ovarian tumor outcomes. PLoS One 8 (11):e80314. doi:10.1371/journal.pone.0080314

21. Andrzejewski S, Gravel SP, Pollak M, St-Pierre J (2014) Metformin directly acts on mitochondria to alter cellular bioenergetics. Cancer & metabolism 2:12. doi:10.1186/2049-3002-2-12

22. Griss T, Vincent EE, Egnatchik R, Chen J, Ma EH, Faubert B, Viollet B, DeBerardinis RJ, Jones RG (2015) Metformin Antagonizes Cancer Cell Proliferation by Suppressing Mitochondrial-Dependent Biosynthesis. PLoS biology 13 (12):e1002309. doi:10.1371/journal.pbio.1002309

23. Liu X, Chhipa RR, Pooya S, Wortman M, Yachyshin S, Chow LM, Kumar A, Zhou X, Sun Y, Quinn B, McPherson C, Warnick RE, Kendler A, Giri S, Poels J, Norga K, Viollet B, Grabowski GA, Dasgupta B (2014) Discrete mechanisms of mTOR and cell cycle regulation by AMPK agonists independent of AMPK. Proceedings of the National Academy of Sciences of the United States of America 111 (4):E435-444. doi:10.1073/pnas.1311121111

24. Menzies KJ, Zhang H, Katsyuba E, Auwerx J (2016) Protein acetylation in metabolism - metabolites and cofactors. Nature reviews Endocrinology 12 (1):43-60. doi:10.1038/nrendo.2015.181

25. Madiraju AK, Erion DM, Rahimi Y, Zhang XM, Braddock DT, Albright RA, Prigaro BJ, Wood JL, Bhanot S, MacDonald MJ, Jurczak MJ, Camporez JP, Lee HY, Cline GW, Samuel VT, Kibbey RG, Shulman GI (2014) Metformin suppresses gluconeogenesis by inhibiting mitochondrial glycerophosphate dehydrogenase. Nature 510 (7506):542-546. doi:10.1038/nature13270

26. Taylor-Harding B, Aspuria P-J, Agadjanian H, Cheon D-J, Mizuno T, Greenberg D, Allen JR, Spurka L, Funari V, Spiteri E, Wang Q, Orsulic S, Walsh C, Karlan BY, Wiedemeyer WR (2015) Cyclin E1 and RTK/RAS signaling drive CDK inhibitor resistance via activation of E2F and ETS. Oncotarget 6 (2):696-714

27. Aspuria PJ, Lunt SY, Varemo L, Vergnes L, Gozo M, Beach JA, Salumbides B, Reue K, Wiedemeyer WR, Nielsen J, Karlan BY, Orsulic S (2014) Succinate dehydrogenase inhibition leads to epithelial-mesenchymal transition and reprogrammed carbon metabolism. Cancer Metab 2:21. doi:10.1186/2049-3002-2-21

28. Clasquin MF, Melamud E, Rabinowitz JD (2012) LC-MS Data Processing with MAVEN: A Metabolomic Analysis and Visualization Engine. In: Current Protocols in Bioinformatics. John Wiley & Sons, Inc. doi:10.1002/0471250953.bi1411s37

29. Melamud E, Vastag L, Rabinowitz JD (2010) Metabolomic Analysis and Visualization Engine for LC−MS Data. Analytical Chemistry 82 (23):9818-9826. doi:10.1021/ac1021166

CHAPTER 3.

METABOLOMIC PROFILING OF MOUSE MAMMARY TUMOR-DERIVED CELL LINES REVEALS TARGETED THERAPY OPTIONS FOR CANCER SUBTYPES

3.1 PREFACE

This chapter is a modified version of a primary research manuscript currently under revision at *Cellular Oncology.*

3.2 Abstract

Purpose: Breast cancer is a heterogeneous disease with several subtypes that currently do not have targeted therapy options. Metabolomics has the potential to uncover novel targeted treatment strategies by identifying metabolic pathways required for cancer cells to survive and proliferate.

Methods: The metabolic profiles of two histologically distinct breast cancer subtypes from the MMTV-Myc mouse model, epithelial-mesenchymal-transition (EMT) and papillary, were investigated using mass spectrometry-based metabolomics methods. Based on metabolic profiles, drugs most likely to be effective against each subtype were selected and tested.

Results: The EMT and papillary subtypes display different metabolic preferences. Compared to the papillary subtype, the EMT subtype demonstrated increased glutathione and TCA cycle metabolism, while the papillary subtype had increased nucleotide biosynthesis compared to the EMT subtype. Targeting these distinct metabolic pathways effectively inhibited cancer cell proliferation in a subtype-specific manner.

Conclusions: These results demonstrate the feasibility of metabolic profiling to develop novel personalized therapy strategies for different subtypes of breast cancer.

3.3 Introduction

Breast cancer is a heterogeneous disease with subtypes that vary by morphology, receptor status, and gene expression profiles [1,2]. This diversity impacts treatment, as one therapeutic strategy will not work for all patients. Targeted therapies include endocrine therapy for patients with estrogen receptor positive (ER+) breast cancer, as well as monoclonal antibodies/inhibitors against human epidermal growth factor receptor

2 (HER2) for HER2+ breast cancer [3]. Unfortunately, targeted therapies are not available for every breast cancer subtype, and drug resistance and relapse remain problematic [4,5]. Therefore, it is critical to identify additional therapeutic targets for all subtypes of breast cancer, and investigating cancer metabolism has the potential to meet this need [6].

Cancer cells exhibit metabolic differences compared to normal cells, and dysregulated metabolism is considered to be a hallmark of cancer [7]. Central carbon metabolism, which includes pathways such as glycolysis, the tricarboxylic acid (TCA) cycle, the pentose phosphate pathway (PPP), and amino acid metabolism, is dysregulated in cancer cells and fuels survival and proliferation [8]. Previous work has shown that metabolic dysregulation can be specific to different subtypes of breast cancer. For example, HER2+ and triple negative breast cancer (TNBC) have been shown to upregulate glutaminolysis compared to ER+ breast cancer [9,10], and TNBC cell lines and xenograft models are sensitive to glutaminase inhibition [11,12]. Differential utilization of metabolic pathways between subtypes of cancer therefore represent potential targets that can be leveraged to develop novel treatment strategies.

The diversity observed in human breast cancer can be modeled by the MMTV-Myc mouse model [13]. MMTV-Myc mice develop mammary tumors that display heterogeneity in both histology and gene expression [14]. Histological subtypes of the MMTV-Myc model have previously been correlated with human subtypes based on global gene expression [15,16]. For example, MMTV-Myc epithelial-mesenchymal-transition (EMT) tumors correspond to the claudin-low subtype of human breast cancer, a subtype which currently has no targeted therapy options and is generally associated with a poor

prognosis [17]. Compared to MMTV-Myc EMT tumors, MMTV-Myc papillary tumors do not correlate strongly with one particular subtype of human breast cancer based on gene expression signatures; instead, the MMTV-Myc papillary tumors correlate moderately with several breast cancer subtypes including luminal and basal breast cancer [15,16]. However, the MMTV-Myc papillary tumors display increased Myc signaling pathway activity [14], which is also amplified in 15.7% of human breast cancers and is more common in high grade tumors and the basal-like subtype [18]. While the MMTV-Myc EMT tumors are initially induced by Myc, they lose Myc pathway activation due to the epithelial tissue-specificity of the MMTV promoter [14]. Thus, the papillary tumors provide a better model for studying human breast cancer with Myc amplification. As a transcription factor, Myc affects numerous biological processes including metabolism [19,20]. Notably, Myc expression regulates several genes in glucose, amino acid, and nucleotide metabolism [21-23]. Therefore, investigating metabolism of the MMTV-Myc model system may reveal metabolic features common to human cancer and could present new targeted therapeutic options.

Here, we present a study investigating the metabolic profiles of two histologically distinct breast cancer subtypes, EMT and papillary, from the MMTV-Myc mouse model. Cell lines were derived from primary EMT and papillary tumors, and polar metabolites were extracted and analyzed using an optimized liquid chromatography tandem mass spectrometry (LC-MS/MS) method to measure a wide range of metabolites [24]. Based on metabolic profiles, drugs most likely to be effective against each subtype were selected and tested. We found that, compared to the papillary subtype, the EMT subtype demonstrated increased glutathione and TCA cycle metabolism, while the papillary

subtype had increased nucleotide biosynthesis compared to the EMT subtype. Targeting each of these distinct metabolic pathways effectively inhibited cancer cell proliferation in a subtype-specific manner. These results demonstrate the potential utility for metabolic profiling to identify drug targets that can be used to develop novel personalized therapeutic strategies for different subtypes of breast cancer.

3.4 Results

3.4.1 Relative metabolite levels between histologically distinct subtypes of MMTV-Myc mouse mammary tumors define metabolic pathways of interest.

To determine metabolic profiles of histologically distinct mouse mammary tumor subtypes, polar metabolites were extracted from tumor-derived cell lines and quantitated using LC-MS/MS. We found metabolites involved in several central carbon metabolic pathways to be differentially abundant between EMT and papillary tumor-derived cell lines (**Figure 1; Figure S1; and Table S1**).

In the EMT subtype, both oxidized and reduced forms of glutathione, a key metabolite in redox homeostasis, are elevated (**Figure 1B**). Increased levels of both reduced and oxidized glutathione imply that the EMT subtype has elevated glutathione biosynthetic activity. This could reflect a greater dependency on glutathione biosynthesis in the EMT cells and targeting glutathione biosynthesis would therefore be more effective against the EMT subtype. Metabolites increased in the papillary subtype include fructose bisphosphate (FBP; glycolysis); acetyl-CoA (TCA cycle); ribulose-5-phopsphate and ribose-5-phosphate (PPP); and adenosine diphosphate (ADP) and adenosine triphosphate (ATP; nucleotide metabolism; **Figure 1B**). Additional analysis using isotope

labeling is required to determine whether metabolites are present at higher levels due to higher production or lower consumption.

3.4.2 Isotope labeling through the TCA cycle is increased in the EMT subtype.

Elevated acetyl-CoA and FBP levels in the papillary subtype (**Figure 1B**) could be explained by either increased glycolytic activity or decreased TCA cycle activity, since these pathways contribute to the production or consumption of these metabolites, respectively. To further investigate these relative metabolic pathway activities, we performed stable isotope labeling using ^{13}C-glucose and ^{13}C-glutamine. Isotope labeling studies show the rate at which these metabolites are incorporated into different metabolic pathways, enabling comparison of relative metabolic pathway activities between samples. Isotope labeling patterns complement metabolic pool size measurements to reveal more complete metabolic profiles.[25] We find the papillary subtype has proportionally lower abundance of ^{13}C-labeled glycolysis and TCA cycle intermediates from ^{13}C-glucose compared to the EMT subtype (**Figure 2; Table S2**). Therefore, the increased abundance of FBP and acetyl-CoA in the papillary cells are likely due to decreased TCA cycle activity in this subtype compared to the EMT cells. Notably, the labeled fraction of 2/3 phosphoglycerate (66% in EMT vs. 56% in papillary), alpha-ketoglutarate (40% in EMT vs. 28% in papillary), succinate (73% in EMT vs. 42% in papillary), fumarate (54% in EMT vs. 33% in papillary), and malate (44% in EMT vs. 32% in papillary) are each higher in the EMT cells when ^{13}C-glucose is used as the labeled carbon source (**Table S2)**. When ^{13}C-glutamine is used as the labeled carbon source, most TCA cycle metabolites do not demonstrate a significant difference in labeling between the EMT and papillary cells (**Figure S2; Table S3**). These results indicate that

EMT cells increase glucose flux through the TCA cycle to a greater degree than papillary cells. Thus, targeting the TCA cycle is likely to be more effective in the EMT subtype compared to the papillary subtype.

3.4.3 Isotope labeling into nucleotide biosynthesis is elevated in the papillary subtype.

Compared to the EMT cells, the papillary cells exhibit increased levels of nucleotides ADP and ATP, as well as ribulose-5-phosphate and ribose-5-phosphate, two intermediates in the PPP (**Figure 1B**). To determine whether these measurements reflect increased nucleotide production or decreased nucleotide consumption, we applied the same isotope labeling techniques described above. Nucleotides can be generated through *de novo* biosynthesis or salvage pathways. Several carbon sources contribute to the formation of purine and pyrimidine rings during *de novo* biosynthesis. Purine carbons are derived from glycine (2 carbons), formate (2 carbons), and bicarbonate (1 carbon). Pyrimidine carbons are derived from aspartate (3 carbons, predominately from glutamine metabolism) and bicarbonate (1 carbon) [23]. Salvage pathways recycle intermediates scavenged from the environment or produced from RNA and DNA degradation to generate nucleotides, and these pathways require less energy per produced nucleotide compared to *de novo* biosynthesis. The carbon sources for purine and pyrimidine nucleotides are highlighted in **Figure 3A,B**.

Isotope labeling studies show that the papillary cells have higher *de novo* nucleotide biosynthesis compared to the EMT cells (**Figure 3C,D; Tables S2-3**). When cells are fed ^{13}C-glucose, the M-5 isotopologue of inosine monophosphate (IMP) and ATP can be derived from either *de novo* or salvage pathways, while all other isotopologues of

IMP and ATP (M-1 to M-4 and M-6 to M-10, referred to as M-Other in **Figure 3C**) can only be derived through *de novo* biosynthetic pathways (**Figure 3A**). As shown in **Figure 3C** and **Table S2**, M-Other is higher in the papillary cells for both IMP (23% in papillary vs. 19% in EMT) and ATP (19% in papillary vs. 15% in EMT). Further, ^{13}C-glutamine labeling shows increased levels of the M3 isotopologue of uridine triphosphate (UTP) in the papillary cells (23% in papillary vs. 17% in EMT; **Figure 3D; Table S3**) – this isotopologue can also only be derived from *de novo* biosynthesis (**Figure 3B**). Therefore, the papillary cells demonstrate increased *de novo* biosynthesis of both purine and pyrimidine nucleotides compared to the EMT cells. Notably, we find no difference between EMT and papillary cells in ^{13}C-glucose labeling into ribose-5-phosphate, serine, and glycine as well as ^{13}C-glutamine labeling into aspartate (**Figure S3**), which indicates that increased nucleotide biosynthesis in the papillary cells is not simply due to greater abundance of labeled precursors for these pathways. Increased *de novo* nucleotide biosynthesis could reflect a preference to utilize this metabolic pathway to generate nucleotides in the papillary subtype. This would indicate targeting *de novo* nucleotide biosynthesis is likely to be more effective in the papillary subtype.

3.4.4 Relative metabolic pathway activity correlates with drug response.

To test whether metabolism-targeting drugs impact cell proliferation in a subtype-specific manner, cell proliferation was determined in the presence of metabolism-targeting compounds. Compounds were chosen based on our initial findings that the EMT subtype increased glutathione biosynthesis and TCA cycle metabolism, while the papillary subtype increased *de novo* nucleotide biosynthesis. The three selected compounds were: 1) Buthionine sulfoximine (BSO), an inhibitor of glutamate-cysteine

ligase (GCL) in glutathione biosynthesis [26]; 2) CPI-613, which targets pyruvate dehydrogenase (PDH) and alpha-ketoglutarate dehydrogenase (AKGDH) in the TCA cycle [27,28]; and 3) 5-Fluorouracil (5FU) which is an inhibitor of thymidylate synthase (TYMS) in *de novo* nucleotide biosynthesis (**Figure S4**) [29,30].

We found that targeting each distinct metabolic feature inhibits breast cancer cell proliferation in a subtype-specific manner. Since the EMT cells display increased levels of both oxidized and reduced glutathione compared to papillary cells (**Figure 1B**), we reasoned they should be more sensitive to glutathione biosynthesis inhibition. As expected, targeting glutathione biosynthesis with BSO was more effective at inhibiting proliferation of the EMT cells vs. the papillary cells (**Figure 4A-B**). Consistently, the IC_{50} for this compound was significantly lower for the EMT cells (34 µM) vs. the papillary cells (49 µM; *p* value <0.0001; **Figure S5A, D**). We also evaluated the relative expression of these targets using qRT-PCR (**Figure S6)**. For glutathione metabolism, we measured the expression of two subunits of GCL, GCL catalytic subunit (GCLC) and GCL modifier subunit (GCLM), as well as glutathione synthetase (GSS) and glutathione reductase (GSR). We found lower expression of GCLC and GSS in the EMT subtype vs. the papillary subtype (**Figure S6)**. Lower expression of the catalytic subunit GCLC in EMT cells may explain the increased sensitivity of these cells to inhibition by BSO. On the other hand, expression of the modifier subunit GCLM was higher in EMT cells (trending towards significance with *p* value 0.0573; **Figure S6**). Since the GCLM subunit increases catalytic activity of the GCL complex [31,32], higher GCLM expression may explain the increased glutathione biosynthesis observed in EMT cells (**Figure 1**).

The EMT cells also have higher TCA cycle activity compared to the papillary cells (**Figure 2**) and should therefore be more sensitive to TCA cycle inhibition. Indeed, targeting TCA cycle metabolism with CPI-613 was more effective in the EMT vs. papillary cells (**Figure 4C-D**); the IC_{50} for this compound was also significantly lower for the EMT (123 μM) vs. the papillary cells (153 μM; *p* value <0.0001; **Figure S5B, D**). Separate mechanisms have been described for the inhibitory effect of CPI-613 on PDH [27] and AKGDH [28]. We found that the EMT subtype has higher expression of the E1 subunit of PDH compared to the papillary subtype, while the papillary subtype has higher expression of each subunit of the AKGDH complex (**Figure S6)**. Higher PDH expression in EMT cells is consistent with the observation that these cells display higher rates of TCA cycle intermediates labeling from ^{13}C-glucose (**Figure 2**) but not from ^{13}C-glutamine (**Figure S2**). Thus, the higher sensitivity of EMT cells to CPI-613 is likely due to an increased dependence on PDH activity.

Finally, the papillary subtype demonstrates increased *de novo* nucleotide biosynthesis (**Figure 3**) and should therefore be most sensitive to compounds which target nucleotide biosynthesis. Indeed, we find that targeting nucleotide metabolism with 5FU was most effective at inhibiting proliferation of the papillary cells vs. the EMT cells (**Figure 4E-F**); the IC_{50} for this compound was significantly lower for the papillary cells (397 nM) vs. the EMT cells (1359 nM; *p* value <0.0001; **Figure S5C-D**). TYMS expression was similar between the EMT and papillary cells (**Figure S6)**, indicating that the differences in nucleotide metabolism in these cells are not regulated at the gene expression level. These results illustrate how metabolic profiles can be used to identify therapeutic targets for subtypes of breast cancer and highlight the potential to predict

whether a specific cancer subtype will most respond to a given treatment strategy based on metabolic profiles.

3.5 Discussion

In this study, we demonstrate the utility of targeting subtype-specific metabolic profiles to inhibit cancer cell proliferation. Using a combination of unlabeled and isotope-labeled mass-spectrometry-based metabolomics techniques, we developed comprehensive metabolic profiles of two histologically distinct breast cancer subtypes derived from the MMTV-Myc mouse model. We further leveraged these metabolic profiles to identify therapeutic targets for each subtype, and demonstrate that inhibiting cancer cell metabolism is most effective when tailored to the underlying metabolic profile of the cancer in question. This approach, when translated to human disease, has the potential to improve patient outcomes, as it will lead to development of novel metabolic drugs for cancer subtypes that currently lack targeted therapies. This may be particularly relevant for the EMT subtype, as it has been correlated with the claudin-low subtype of breast cancer in humans [15], a subtype which generally carries a poor prognosis and currently lacks targeted therapeutic options [17].

In recent years, there has been growing interest in taking advantage of altered metabolism in cancer for treatment [33-35]. Our findings demonstrate that vulnerabilities identified through metabolic profiling are effective therapeutic targets. Each compound we tested demonstrates a significantly lower IC_{50} value in either the EMT or papillary subtype, clearly corresponding with the metabolic profile of each subtype. Of the three compounds evaluated in this study, 5FU is currently approved as a chemotherapeutic agent, and is used to treat a variety of malignancies [30]. BSO has demonstrated utility

as a sensitizing agent in pre-clinical models of anti-endocrine therapy resistant ER+ breast cancer [36], and in multiple myeloma treated concurrently with the chemotherapeutic melphalan [37]. More recently, BSO has shown promise in early clinical trials as a chemosensitizing agent in combination with melphalan for treatment of pediatric neuroblastoma [38,39]. Finally, CPI-613 is being investigated as a component in combination therapies for several malignancies including colorectal cancer [40], small cell lung cancer [41], and pancreatic cancer [42]. Our findings support investigating these compounds to treat specific subtypes of breast cancer, as each tested compound demonstrates some degree of inhibition regardless of subtype. Moreover, our findings provide an additional rationale for subtype-specific drug selection based on the underlying metabolism of the cancer cells in question, as the drug sensitivity for the EMT and papillary cells directly correlates with the metabolic profile of each subtype.

Our results may also in part explain why some cancer patients do not respond to a given metabolism-targeting therapy. For example, 5FU as a monotherapy to treat metastatic colorectal cancer demonstrates a response rate of only 10-20% [43], indicating a significant proportion of patients fail to respond to 5FU therapy. Response rates are better when 5FU is used in combination therapies to treat metastatic breast cancer, with response rates of 40-80% depending on the specific combination therapy [43]. In such cases, it is possible the metabolic profile of the poor responder's cancer differs significantly from the metabolic profile of a cancer that responds well to treatment. Our study demonstrates that 5FU will be most effective in cancer subtypes that upregulate *de novo* nucleotide biosynthesis. This may be particularly relevant for cancers with elevated Myc activity, since Myc regulates the expression of numerous genes in nucleotide

biosynthesis including TYMS [23], the primary target of 5FU. Increased Myc expression has been observed in TNBC compared to hormone receptor positive breast cancer [44], and patients with TNBC have better response rates to neoadjuvant chemotherapy regimens that contain 5FU [45]. Further, Myc overexpression in hepatocellular carcinoma has recently been shown to decrease both oxidized and reduced glutathione levels in tumor tissue by downregulating glutathione biosynthesis genes [46]. Our findings support this in breast cancer, as the papillary cells, which have relatively higher Myc activity, demonstrate decreased glutathione levels compared to EMT cells [14]. This is consistent with papillary cells being less sensitive to BSO treatment. Thus, breast cancers with increased Myc expression may be less likely to respond to therapies that target glutathione biosynthesis, and breast cancers that lack Myc overexpression may respond favorably to glutathione biosynthesis inhibitors. Other metabolic features associated with increased Myc signaling, such as increased glutaminolysis [47,11] and fatty acid metabolism [48], are also under investigation as potential therapeutic targets. Therefore, metabolomic analysis of patient samples could provide clinicians with additional prognostic information to guide treatment plans, ultimately improving patient outcomes while decreasing unnecessary side effects by avoiding ineffective treatment regimens.

3.6 Methods

3.6.1 Primary mouse tumors

All animal use was performed in accordance with institutional and federal guidelines. Primary MMTV-Myc EMT and MMTV-Myc papillary tumors were acquired as a gift from Dr. Eran Andrechek and have been previously described [14]. Tumors were sectioned, formalin-fixed, and paraffin embedded for histological examination with

hematoxylin and eosin staining. Tumor derived cell lines were established by mechanical dissociation of primary tumors using scissors, followed by culturing tumor pieces in cell culture media [49].

3.6.2 Cell lines and culture conditions

EMT and papillary tumor derived cell lines were cultured in Dulbecco's Modified Eagle Medium (DMEM Corning, Corning, New York 10-017-CM) with 25 mM glucose without sodium pyruvate supplemented with 2 mM glutamine (Corning, 25-005-CI) 10% heat-inactivated fetal bovine serum (MilliporeSigma, Burlington Massachusetts, 12306C), and 1% penicillin and streptomycin (Corning, 30-002-CI). Cells were maintained at 37°C with 5% CO_2.

3.6.3 Metabolic profiling

Unlabeled, targeted metabolomics was performed as previously described [24]. Briefly, cells were seeded in 6-well tissue culture plates at 50,000 cells/well and cultured for 48 hours. Cells were washed with saline (VWR, Radnor, Pennsylvania, 16005-092) and metabolism was quenched with addition of cold methanol. The final metabolite extraction solvent ratios were methanol:water:chloroform (5:2:5). The polar phase was collected and dried under a stream of nitrogen gas. The dried metabolites were then resuspended in HPLC-grade water for analysis. LC-MS analysis was performed with ion-pairing reverse phase chromatography using an Ascentis Express column (C18, 5 cm x 2.1 mm, 2.7 µm, MilliporeSigma, 53822-U) and a Waters Xevo TQ-S triple quadrupole mass spectrometer. Mass spectra were acquired using negative mode electrospray ionization operating in multiple reaction monitoring (MRM) mode. Peak processing was

performed using MAVEN [50] and data for each sample was normalized to the mean signal intensity for all metabolites in the analysis. Metabolites were grouped by relationship to metabolic pathways. Heatmaps were generated using Cluster 3.0 [51] and exported using Java Treeview [52].

3.6.4 Isotope labeling studies

For isotope labeling experiments, DMEM without glucose or glutamine was prepared from powder (MilliporeSigma, D5030) and supplemented with either $^{13}C_6$-glucose (Cambridge Isotope Laboratories, Tewksbury, Massachusetts, CLM-1396) and unlabeled glutamine (MilliporeSigma, G8540) or unlabeled glucose (Fisher Scientific, Hampton, New Hampshire, D16) and $^{13}C_5$-glutamine (Cambridge Isotope Laboratories, CLM-1822). Cells were then seeded and cultured as described above. Prior to metabolite extraction, media was switched to isotope containing media and samples were collected at T = 0 (unlabeled) and 240 minutes. Metabolite extraction and analysis were performed as above. Labeling data was corrected for natural isotope abundance using IsoCor [53].

3.6.5 Cell proliferation and drug response studies

Cells were seeded at a density of 20,000 cells/well in 12-well tissue culture plates and treated with either vehicle (DMSO, MilliporeSigma, D4540) or the indicated drugs. CPI-613 (Cayman Chemical, Ann Arbor, Michigan, 16981), buthionine sulfoximine (Cayman Chemical, 14484), and 5-fluorouracil (TCI, Tokyo, Japan, F0151). Cells were counted daily for 3 days using a Nexcelom Cellometer Auto T4 cell counter and viable cells were determined using trypan blue exclusion (VWR, 45000-717). Proliferation

inhibition was determined using the ratio of the drug treated cell count at day 3 to the vehicle treated cell count at day 3.

3.6.6 qRT-PCR studies

Cells were seeded in 6-well tissue culture plates at 50,000 cells/well and cultured for 48 hours. Total RNA was extracted from the cells using the RNeasy Mini Kit (Qiagen, 74104), and on-column DNase digestion performed using DNase I (Qiagen, 79254). cDNA was prepared using LunaScript™ RT SuperMix Kit (New England Biolabs, E3010S). Real-time PCR was performed using Luna® Universal qPCR Master Mix (New England Biolabs, M3003S) on an Applied Biosystems StepOnePlus™ Real-Time PCR system with the following conditions: 10 min at 55 °C, 1 min at 95 °C followed by 40 cycles at 95 °C for 10 s and 60 °C for 1 min. Gene expression values were normalized to control gene Tbp and verified against an additional control gene Actb. The primer sequences used for real-time PCR are listed in **Table S4**.

3.6.7 Statistical analyses

Statistical analyses were performed using unpaired Student's t-test except where otherwise noted. *p* values were adjusted in R using the p.adjust() function to account for multiple testing using the Benjamini-Hochberg procedure. All error bars presented are standard deviation. IC_{50} values and statistical analysis of drug response were calculated using nonlinear regression performed by GraphPad Prism.

3.7 Acknowledgments

The authors thank Deanna Broadwater, Elliot Ensink, Hyllana Medeiros, and Lei Yu for helpful discussions and critical reading of this manuscript. The authors thank Eran

Andrechek for providing primary MMTV-Myc EMT and MMTV-Myc papillary tumors. The authors also thank the MSU Mass Spectrometry and Metabolomics Core and the MSU Investigative HistoPathology Laboratory.

3.8 Author contributions

MPO performed metabolic profiling, isotope labeling studies, cell culture, drug response studies, experimental design and data analysis. STT performed gene expression studies and assisted with interpretation of results. SYL conceived, designed, and supervised the study. All authors contributed to writing the manuscript and have critically read, edited, and approved the manuscript.

3.9 APPENDIX

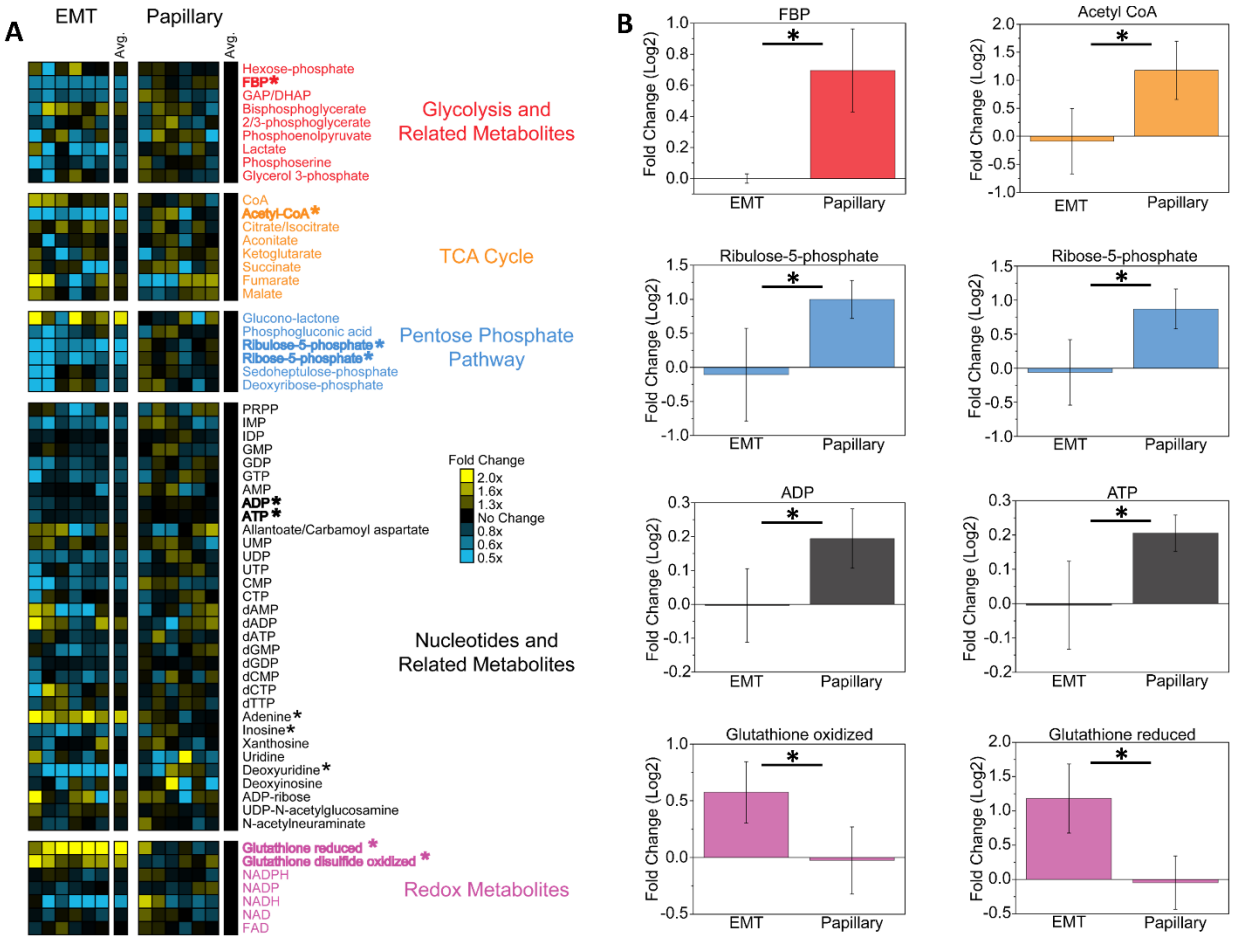

Figure 3.1 Metabolite pool sizes are different between EMT and papillary tumor derived cell lines. (**A**) Heatmap indicating relative metabolite differences between EMT and papillary tumor derived cell lines. Yellow and blue boxes indicate increased or decreased metabolite levels relative to the average of the papillary subtype, respectively. Metabolites with statistically significant differences (*p* value < 0.05) are bolded and marked with asterisks (*). (**B**) Representative bar graphs of metabolites of interest between EMT and papillary subtypes. Data are displayed as means ± S.D., N = 6

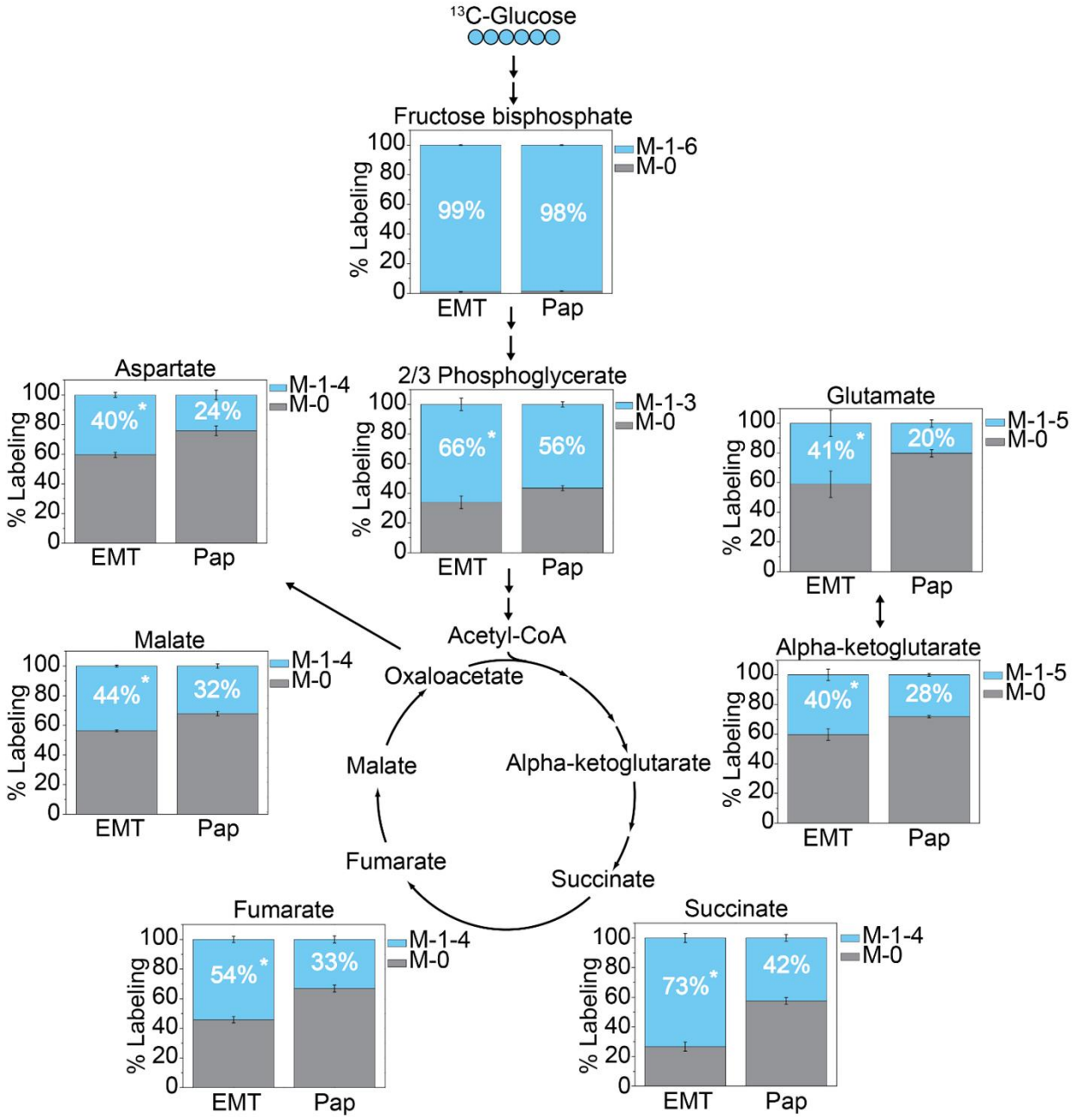

Figure 3.2 ^{13}C-Isotope labeling from glucose into the TCA cycle is significantly higher in the EMT subtype. Grey boxes represent the unlabeled (M-0 isotopologue) proportion for each metabolite. Blue boxes represent the sum of all potential labeled isotopologues (M-1 through M-*X*, where *X* represents the total number of carbons in the metabolite) for each metabolite. Data are displayed as means ± S.D., N = 3 (*p value < 0.05)

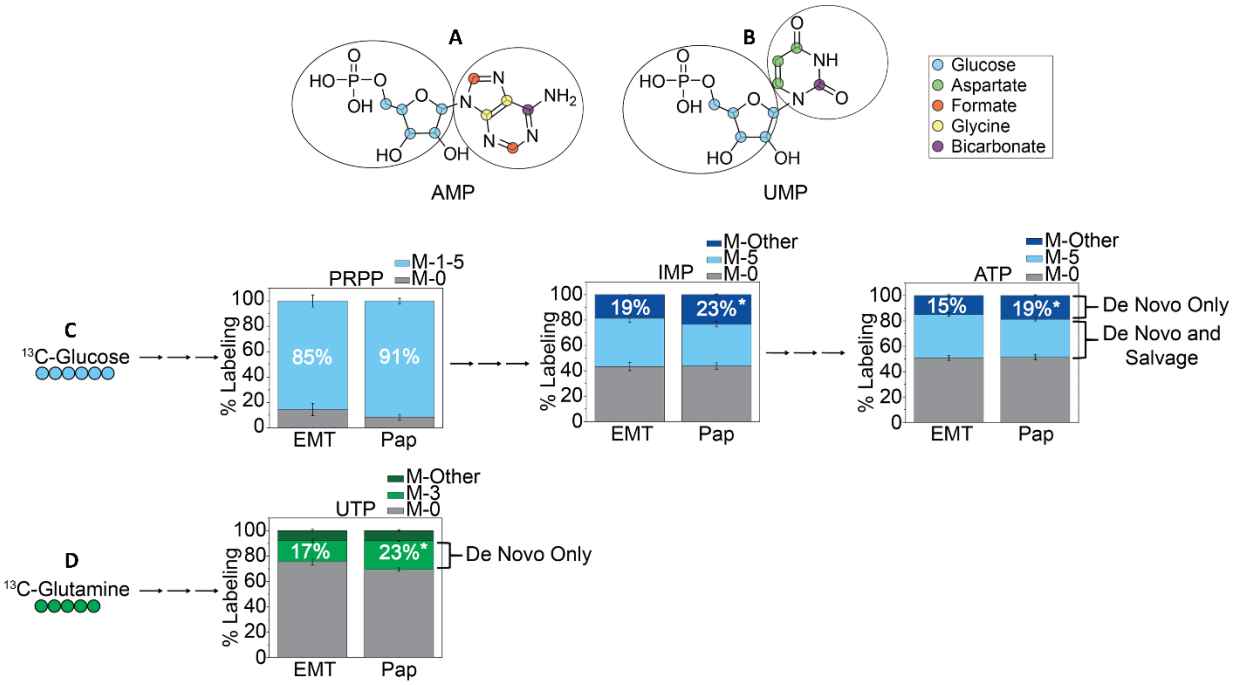

Figure 3.3 ^{13}C-Isotope incorporation from glucose and glutamine into nucleotide biosynthesis is higher in the papillary subtype. Molecular diagrams of (**A**) purine nucleotide AMP and (**B**) pyrimidine nucleotide UMP with carbon sources highlighted as colored circles. The 5 carbon ribose sugar of both (**A,B** left circle) is derived from glucose metabolism. Isotopologues of this mass (M-5) reflect both salvaged nucleotides and nucleotides produced by *de novo* biosynthetic pathways when ^{13}C-glucose is administered. The 5 carbons comprising the purine ring of AMP (**A**, right circle) are derived from glycine, formate, and bicarbonate, all three of which can also be derived from glucose metabolism. Therefore, when ^{13}C-glucose is administered isotopologues of other masses (M-1 to M-4 and M-6 to M-10, referred to as M-Other) reflect only purine production by *de novo* biosynthesis. The 4 carbon comprising the pyrimidine ring of UMP (**B**, right circle) are derived from bicarbonate and aspartate. Aspartate is predominantly derived from glutamine metabolism and provides 3 carbons to UMP; therefore, when ^{13}C-glutamine is administered, M-3 isotopologues reflect *de novo* UMP biosynthesis. (**C**) ^{13}C-Glucose labeling into PRPP, IMP, and ATP. (**D**) ^{13}C-Glutamine labeling into UTP. Grey boxes represent the unlabeled proportion for each metabolite. Colored boxes represent isotopologues for each metabolite and are sorted based on carbon source. Data are displayed as means ± S.D., N = 3 (*p value < 0.05)

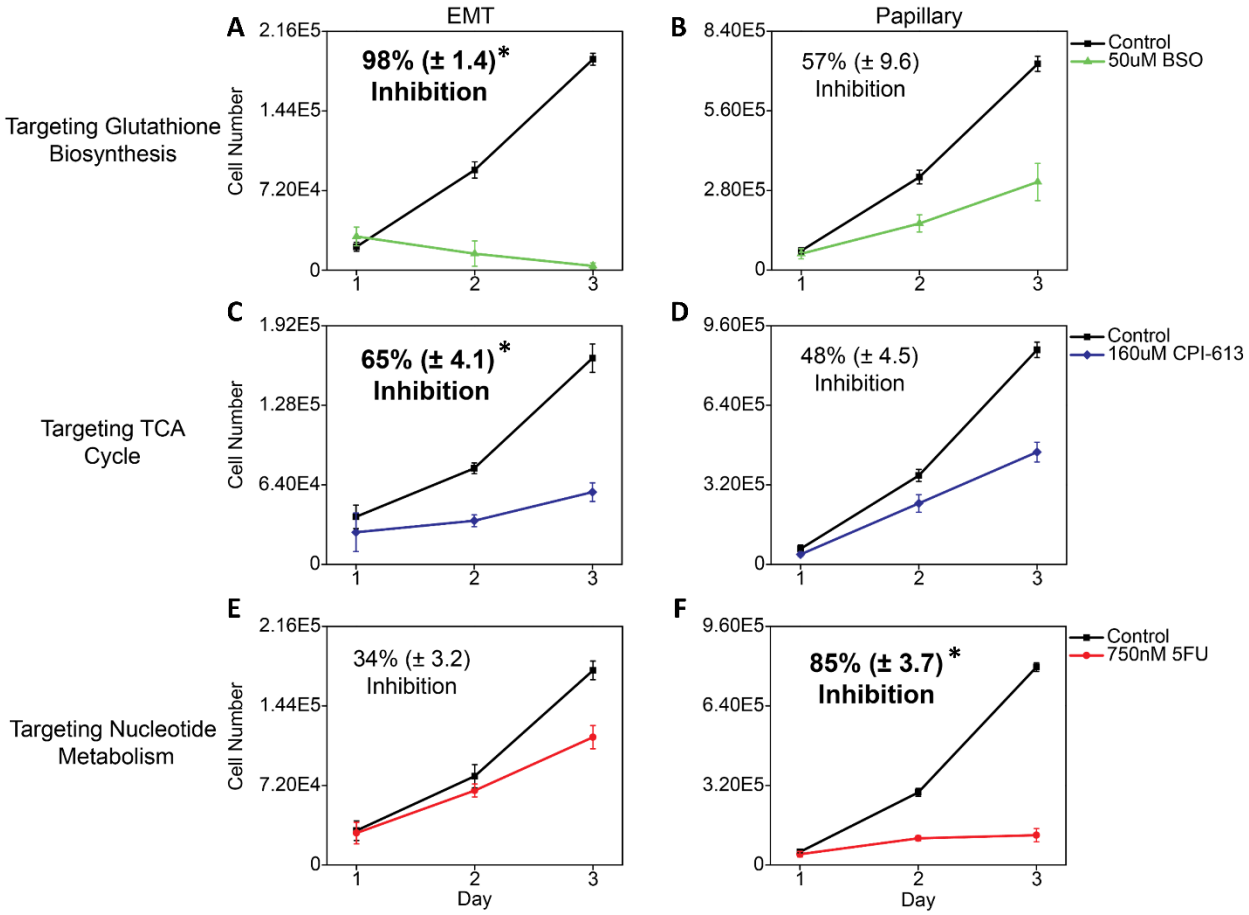

Figure 3.4 Metabolism targeting drugs have subtype-specific effects on cell proliferation. Targeting glutathione biosynthesis has a greater effect on (**A**) EMT compared to (**B**) papillary cells. Targeting the TCA cycle also has a greater effect on (**C**) EMT compared to (**D**) papillary cells. Targeting nucleotide metabolism has less effect on (**E**) EMT compared to (**F**) papillary cells. Bolded values indicate the subtype most affected by each compound. Data are displayed as means ± S.D., N = 3 (*p value < 0.01)

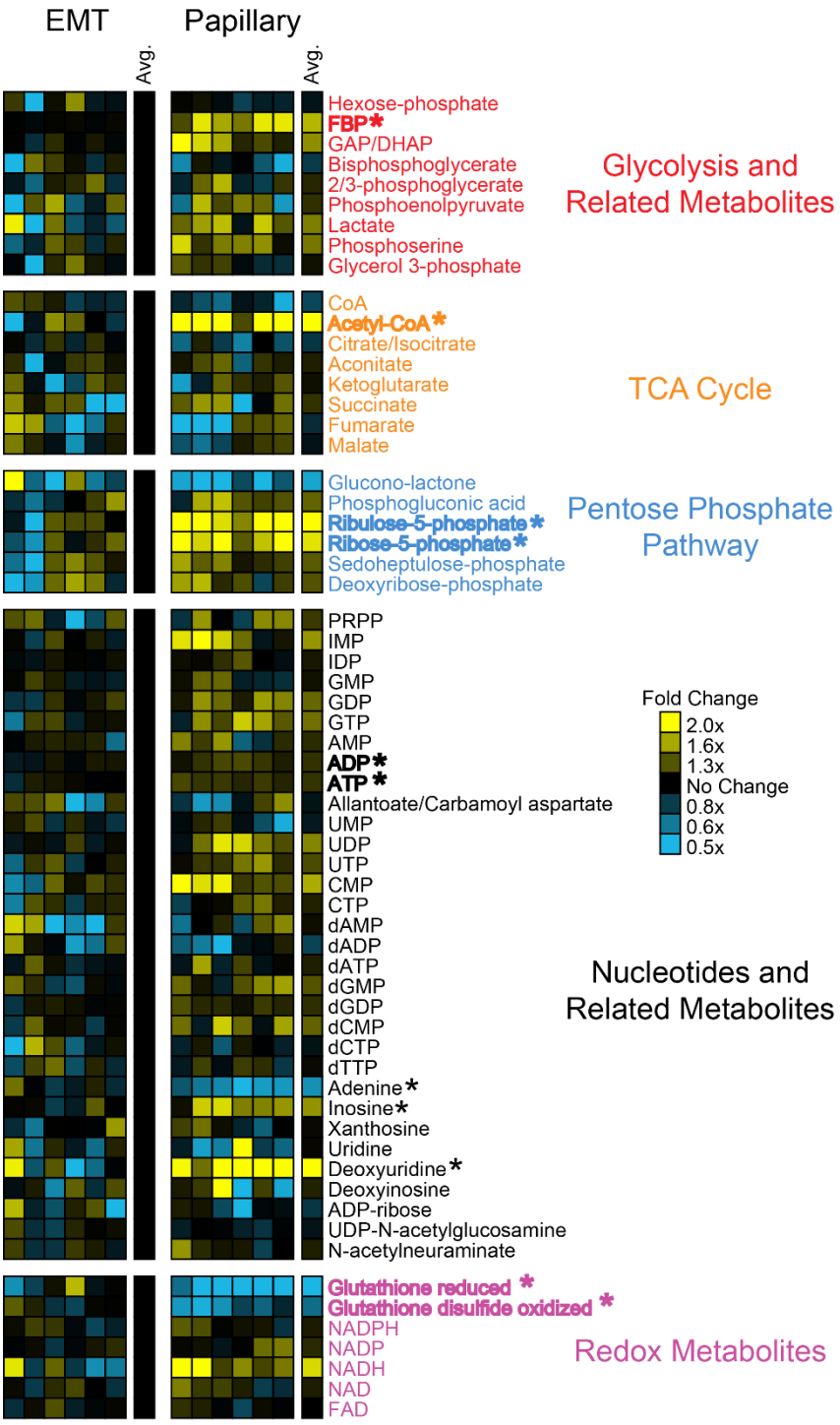

Figure S3.1 Heatmap indicating relative metabolite differences between EMT and papillary tumor derived cell lines. This data is identical to Figure 1A, except the data has been normalized to the EMT subtype. Therefore, yellow and blue boxes indicate increased or decreased metabolite levels relative to the average of the EMT subtype, respectively. Metabolites with statistically significant differences (p value < 0.05) are bolded and marked with asterisks (*).

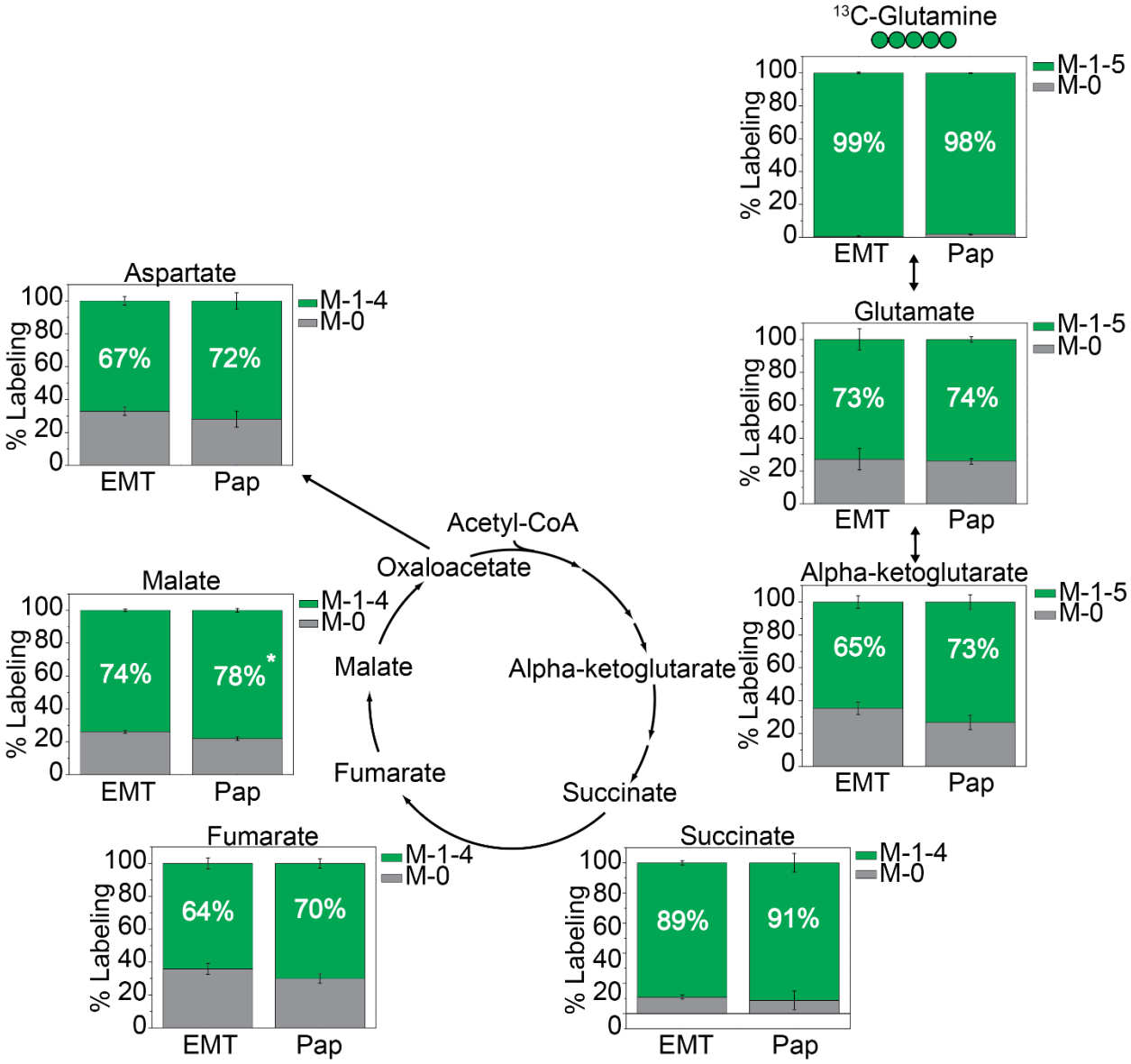

Figure S3.2 ^{13}C-Isotope labeling from glutamine into the TCA cycle is similar between subtypes. Grey boxes represent the unlabeled proportion for each metabolite. Green boxes represent the sum of all potential isotopologues for each metabolite. Data are displayed as means ± S.D., N = 3 (Statistically significant differences (*p* value < 0.05) are marked with asterisks (*)

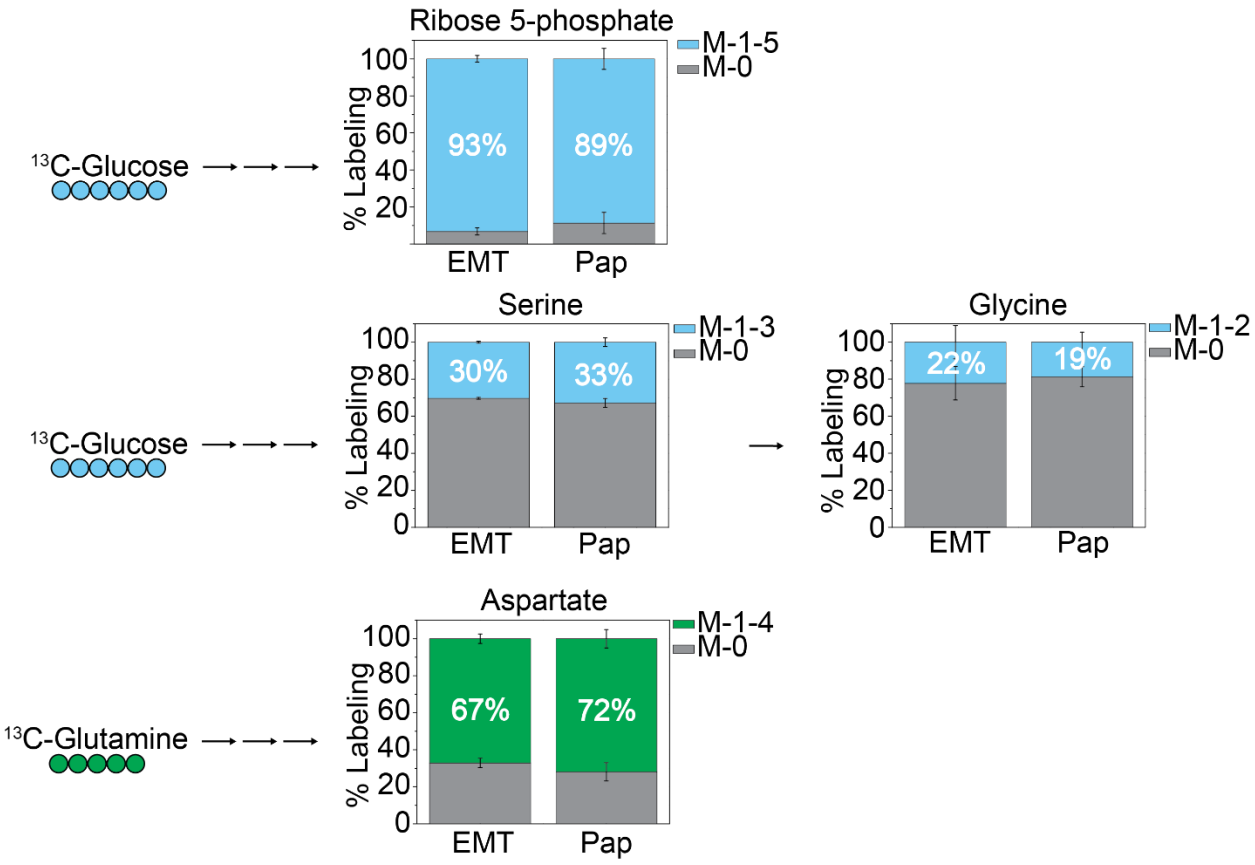

Figure S3.3 ^{13}C-Isotope labeling from glucose into ribose 5-phospahte, serine, and glycine and from glutamine into aspartate is similar between subtypes. Grey boxes represent the unlabeled proportion for each metabolite. Colored boxes represent isotopologues for each metabolite and are sorted based on carbon source. Data are displayed as means ± S.D., N = 3 (Statistically significant differences (*p* value < 0.05) are marked with asterisks (*)

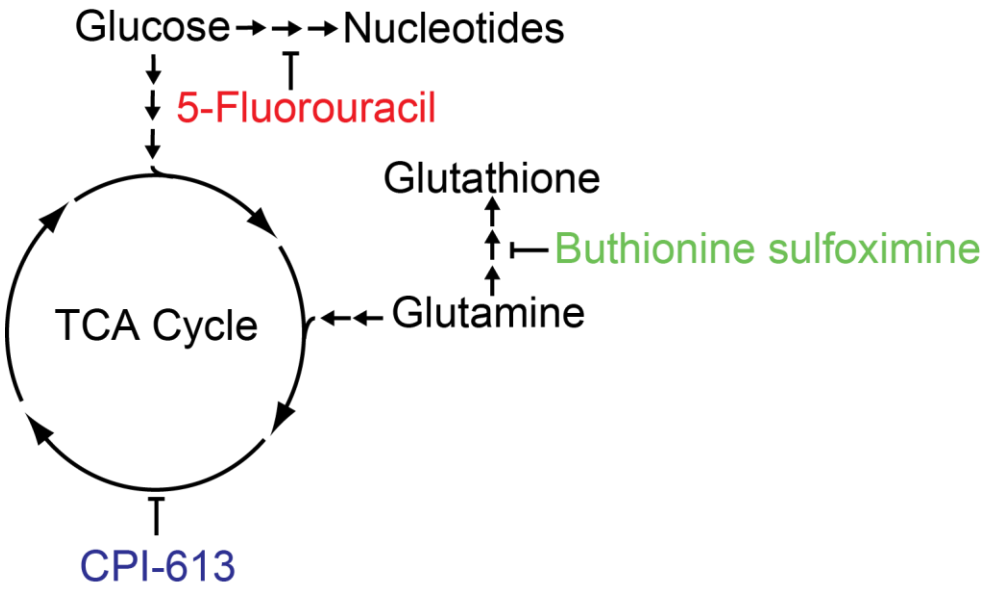

Figure S3.4 Schematic overview of metabolism targeting drugs and affected pathways. Compounds were chosen based on the metabolic differences identified in the EMT and papillary subtypes. Buthionine sulfoximine targets glutamate-cysteine ligase in glutathione biosynthesis, CPI-613 targets pyruvate dehydrogenase and alpha-ketoglutarate dehydrogenase in the TCA cycle, and 5-fluorouracil targets thymidylate synthase in nucleotide biosynthesis

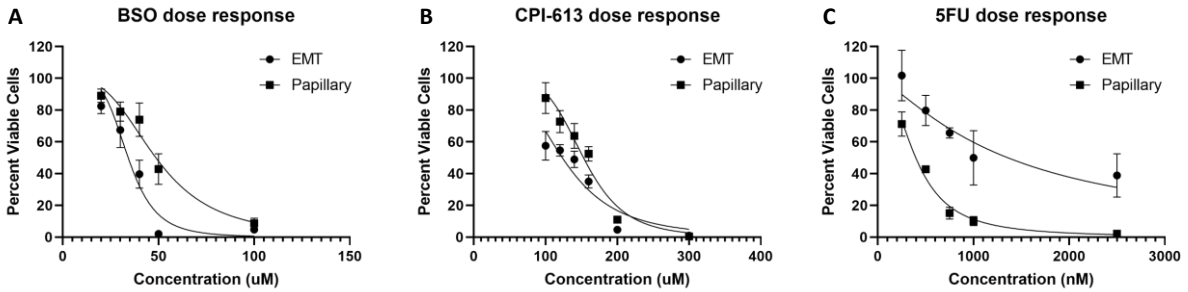

D	BSO			CPI-613			5FU		
	IC50 (uM)	95% CI (uM)	p-value	IC50 (uM)	95% CI (uM)	p-value	IC50 (nM)	95% CI (nM)	p-value
EMT	34.19	31.06 to 37.13	<0.0001	123.4	112.8 to 132.7	<0.0001	1359	981.1 to 2218	<0.0001
Papillary	48.66	44.56 to 53.89		152.9	146.4 to 159.9		397	362.9 to 431.5	

Figure S3.5 Dose response curves for metabolism targeting drugs. (**A**) Buthionine sulfoximine (BSO) and (**B**) CPI-613 demonstrate greater effects on the EMT subtype. (**C**) 5-fluorouracil (5-FU) demonstrates a greater effect on the papillary subtype. (**D**) Data are means ± S.D. (n=3)

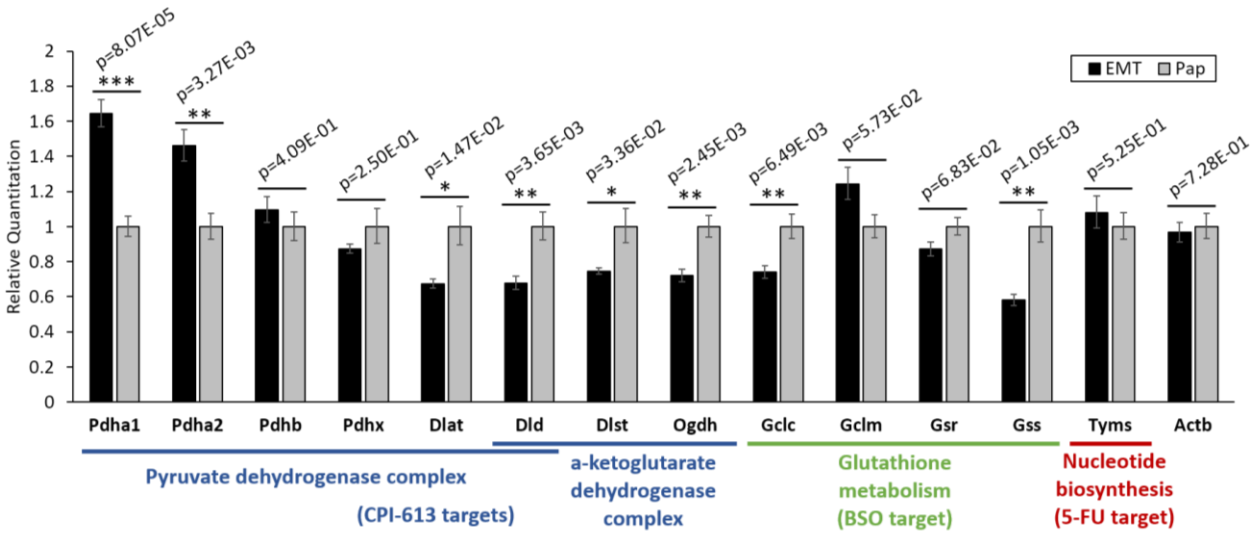

Figure S3.6 qRT-PCR measurement of gene expression in targeted pathways. Gene expression values were normalized to control gene Tbp and expressed relative to papillary subtype cells (Pap). Quantitation values shown are averages of 6 replicates (3 cell culture replicates × 2 PCR plate replicates). Error bars represent standard error of the mean. *P* values were calculated from ΔC_T values using Welch's t-test. *: $p < 0.05$, **: $p < 0.01$; ***: $p < 0.001$. ΔC_T: real-time PCR cycle threshold difference between gene of interest and control gene.

Metabolite	EMT Average	EMT STDEV	Pap Average	Pap STDEV	P-value	Adjusted p-value
2+3-phosphoglycerate	-0.2	0.4	0.4	0.4	5.61E-01	7.40E-01
Acetyl-CoA	-1.3	0.6	0.6	0.5	2.60E-03	2.72E-02
Aconitate	-0.2	0.5	0.4	0.3	5.38E-01	7.40E-01
Adenine	0.8	0.3	0.3	0.3	7.19E-04	2.50E-02
ADP	-0.2	0.1	0.1	0.1	6.14E-03	3.46E-02
ADP-ribose	0.2	0.7	1.6	1.5	4.50E-01	7.15E-01
Allantoate_and_Carbamoyl_aspartate	0.0	0.7	0.6	0.6	8.63E-01	9.22E-01
AMP	-0.2	0.3	0.5	0.4	5.32E-01	7.40E-01
ATP	-0.2	0.1	0.1	0.1	4.11E-03	2.72E-02
Bisphosphoglycerate	0.3	0.5	0.4	0.4	3.03E-01	5.53E-01
Citrate+Isocitrate	0.3	0.2	0.3	0.3	7.17E-02	2.02E-01
CMP	-0.7	0.5	0.4	0.4	2.06E-02	8.51E-02
CoA	0.4	0.3	0.2	0.3	4.38E-02	1.36E-01
CTP	-0.2	0.4	0.3	0.3	4.73E-01	7.34E-01
dADP	0.3	0.6	0.6	0.6	2.95E-01	5.53E-01
dAMP	-0.3	0.9	0.6	0.5	5.88E-01	7.59E-01
dATP	-0.1	0.2	0.3	0.3	5.17E-01	7.40E-01
dCMP	-0.4	0.3	0.4	0.4	8.53E-02	2.20E-01
dCTP	0.0	0.6	0.3	0.2	9.98E-01	9.98E-01
Deoxyinosine	-0.2	0.4	0.7	0.8	9.79E-01	9.98E-01
Deoxyribose-phosphate	-0.5	1.0	0.6	0.4	2.62E-01	5.07E-01
Deoxyuridine	-1.5	0.8	0.6	0.5	3.93E-03	2.72E-02
dGDP	-0.2	0.1	0.1	0.1	2.34E-02	9.06E-02
dGMP	-0.4	0.3	0.3	0.3	9.86E-02	2.26E-01
dTTP	-0.1	0.4	0.2	0.2	7.26E-01	8.55E-01
FAD	0.0	0.2	0.2	0.2	9.90E-01	9.98E-01
FBP	-0.7	0.0	0.2	0.3	1.31E-03	2.70E-02
Fumarate	0.0	1.0	1.0	0.9	7.14E-01	8.55E-01
GAP+DHAP	-0.6	0.1	0.3	0.4	1.83E-02	8.10E-02
GDP	-0.4	0.2	0.3	0.2	1.51E-02	7.19E-02
Glucono-lactone	0.6	1.0	0.7	0.6	1.49E-01	3.29E-01
Glutathione_disulfide_oxidized	0.6	0.3	0.3	0.3	4.38E-03	2.72E-02
Glutathione_reduced	1.2	0.5	0.4	0.4	8.05E-04	2.50E-02
Glycerol_3-phosphate	-0.1	0.5	0.3	0.3	6.38E-01	8.07E-01
GMP	-0.1	0.2	0.3	0.3	7.51E-01	8.62E-01
GTP	-0.5	0.4	0.4	0.3	5.40E-02	1.60E-01
Hexose-phosphate	0.0	0.6	0.3	0.2	8.90E-01	9.35E-01
IDP	-0.1	0.1	0.1	0.2	2.16E-01	4.45E-01
IMP	-0.6	0.2	0.4	0.5	2.94E-02	1.01E-01
Inosine	-0.6	0.2	0.3	0.3	3.39E-03	2.72E-02
Ketoglutarate	-0.1	0.5	0.5	0.5	8.02E-01	9.01E-01
Lactate	-0.7	0.8	0.5	0.3	9.71E-02	2.26E-01
Malate	0.1	0.4	0.4	0.4	6.96E-01	8.55E-01
Nacetylneuraminate	-0.1	0.2	0.3	0.3	5.04E-01	7.40E-01
NAD	-0.1	0.2	0.3	0.3	5.39E-01	7.40E-01
NADH	-1.0	0.7	0.6	0.6	3.37E-02	1.10E-01
NADP	-0.2	0.2	0.2	0.2	2.23E-01	4.46E-01
NADPH	-0.1	0.2	0.2	0.2	4.40E-01	7.15E-01
Phosphoenolpyruvate	-0.4	1.0	0.6	0.6	5.49E-01	7.40E-01
Phosphogluconic_acid	-0.4	0.4	0.4	0.3	9.83E-02	2.26E-01
Phosphoserine	-0.5	0.4	0.2	0.3	2.78E-02	1.01E-01
PRPP	-0.3	0.6	0.5	0.4	4.02E-01	7.12E-01
Ribose-5-phosphate	-1.0	0.5	0.4	0.3	2.32E-03	2.72E-02
Ribulose-5-phosphate	-1.1	0.7	0.4	0.3	4.21E-03	2.72E-02
Sedoheptulose-phosphate	-0.5	0.9	0.4	0.2	2.08E-01	4.44E-01
Succinate	-0.4	0.8	1.1	1.1	8.29E-01	9.01E-01
UDP	-0.5	0.1	0.4	0.4	1.25E-02	6.48E-02
UDPNacetylglucosamine	0.1	0.2	0.2	0.1	4.31E-01	7.15E-01
UMP	0.1	0.2	0.2	0.4	4.29E-01	7.15E-01
Uridine	-0.1	0.5	0.8	0.8	7.30E-01	8.55E-01
UTP	-0.3	0.4	0.2	0.2	8.33E-02	2.20E-01
Xanthosine	-0.1	0.4	0.4	0.3	8.21E-01	9.01E-01

Table S3.1 Metabolite abundance with statistical significance. Data presented relative to the average of the papillary subtype as depicted in Figure 1A. Data represent means and S.D. of 3

Table S3.1 (cont'd)

replicates. Bold values indicate Welch's t-test was used. Highlighted values are statistically significant with adjusted *p* value < 0.05

Metabolite	EMT Average (%)	EMT STDEV	Papillary Average (%)	Papillary STDEV	P-value	Adjusted p-value
2-3 phosphoglycerate M-0	33.9	4.2	43.5	1.7	2.21E-02	4.06E-02
2-3 phosphoglycerate M-1-3	66.1	4.2	56.5	1.7	2.21E-02	4.06E-02
Aspartate M-0	59.6	1.8	75.9	3.2	1.57E-03	6.48E-03
Aspartate M-1-4	40.4	1.8	24.1	3.2	1.57E-03	6.48E-03
ATP M-0	50.9	2.0	51.3	2.0	7.94E-01	8.18E-01
ATP M-5	34.1	1.4	29.9	1.4	2.11E-02	4.06E-02
ATP M-Other	15.0	0.7	18.8	0.6	2.04E-03	7.49E-03
FBP M-0	1.1	0.2	1.4	0.2	6.58E-02	1.03E-01
FBP M-1-6	98.9	0.2	98.6	0.2	6.59E-02	1.03E-01
Fumarate M-0	45.8	2.1	66.9	2.4	3.31E-04	1.82E-03
Fumarate M-1-4	54.2	2.1	33.1	2.4	3.31E-04	1.82E-03
Glutamate M-0	58.9	8.9	79.8	2.5	1.74E-02	3.82E-02
Glutamate M-1-5	41.1	8.9	20.2	2.5	1.74E-02	3.82E-02
Glycine M-0	77.8	9.0	81.3	5.4	5.92E-01	6.30E-01
Glycine M-1-2	22.2	9.0	18.7	5.4	5.92E-01	6.30E-01
IMP M-0	43.4	3.3	43.8	2.6	8.80E-01	8.80E-01
IMP M-5	38.0	3.3	32.9	2.1	8.42E-02	1.26E-01
IMP M-Other	18.6	0.0	23.4	0.6	4.79E-03	**1.44E-02**
Ketoglutarate M-0	59.8	3.9	71.9	0.8	6.14E-03	1.56E-02
Ketoglutarate M-1-5	40.2	3.9	28.1	0.8	6.14E-03	1.56E-02
Malate M-0	56.3	0.6	67.9	1.5	2.19E-04	1.81E-03
Malate M-1-4	43.7	0.6	32.1	1.5	2.19E-04	1.81E-03
PRPP M-0	14.4	4.8	8.4	2.2	1.18E-01	1.62E-01
PRPP M-1-5	85.6	4.8	91.6	2.2	1.18E-01	1.62E-01
Ribose 5-phosphate M-0	6.8	1.9	11.3	5.7	2.57E-01	3.03E-01
Ribose 5-phosphate M-1-5	93.2	1.9	88.7	5.7	2.57E-01	3.03E-01
Serine M-0	69.7	0.5	67.2	2.4	1.53E-01	1.94E-01
Serine M-1-3	30.3	0.5	32.8	2.4	1.53E-01	1.94E-01
Succinate M-0	26.7	3.1	57.6	2.3	1.53E-04	1.81E-03
Succinate M-1-4	73.3	3.1	42.4	2.3	1.53E-04	1.81E-03
UTP M-0	54.8	2.7	53.0	2.2	4.15E-01	4.72E-01
UTP M-5	29.2	3.2	35.1	1.6	4.50E-02	7.81E-02
UTP M-Other	16.0	0.9	11.9	0.6	2.77E-03	9.13E-03

Table S3.2 ^{13}C-Isotope percent labeling from glucose with statistical significance. Data represent means and S.D. of 3 replicates. Bold values indicate Welch's t-test was used. Highlighted values are statistically significant with adjusted *p* value < 0.05

Metabolite	EMT Average	EMT STDEV	Papillary Average	Papillary STDEV	P-value	Adjusted p-value
Aspartate M-0	32.9	2.5	28.1	4.9	2.10E-01	2.97E-01
Aspartate M-1-4	67.1	2.5	71.9	4.9	2.10E-01	2.97E-01
Fumarate M-0	35.8	3.4	29.9	2.8	8.14E-02	1.38E-01
Fumarate M-1-4	64.2	3.4	70.1	2.8	8.14E-02	1.38E-01
Glutamate M-0	27.2	6.5	25.9	1.7	7.59E-01	7.71E-01
Glutamate M-1-5	72.8	6.5	74.1	1.7	7.59E-01	7.71E-01
Glutamine M-0	0.6	0.5	1.8	0.3	1.55E-02	5.28E-02
Glutamine M-1-5	99.4	0.5	98.2	0.3	1.55E-02	5.28E-02
Ketoglutarate M-0	35.4	3.8	26.8	4.5	6.37E-02	1.35E-01
Ketoglutarate M-1-5	64.6	3.8	73.2	4.5	6.36E-02	1.35E-01
Malate M-0	26.0	0.8	22.0	1.0	5.91E-03	3.36E-02
Malate M-1-4	74.0	0.8	78.0	1.0	5.92E-03	3.36E-02
Succinate M-0	11.0	1.4	8.8	6.2	5.84E-01	7.09E-01
Succinate M-1-4	89.0	1.4	91.2	6.2	5.84E-01	7.09E-01
UTP M-0	75.6	2.5	69.5	1.4	2.08E-02	5.88E-02
UTP M-3	16.7	1.6	22.6	0.5	3.31E-03	3.36E-02
UTP M-Other	7.7	1.0	8.0	0.9	7.71E-01	7.71E-01

Table S3.3 ^{13}C-Isotope percent labeling from glutamine with statistical significance. Data represent means and S.D. of 3 replicates. Highlighted values are statistically significant with adjusted *p* value < 0.05

Primer	Sequence
Dlat FWD	5'-AGGCAAAATCATGTGGTTGACGTC
Dlat REV	5'-TCCACCCTGGAACTCATGAGGC
Dld FWD	5'-TGCTGACACAGATGGCATGGTG
Dld REV	5'-GATAAGGTCGGATGCGCATGGC
Dlst FWD	5'-AGCTCGGCACAAGGATGCTTTC
Dlst REV	5'-TCACTGCATTTACAACAGGCTGC
Gclc FWD	5'-ACATGAAAGTGGCCCAGAAGCG
Gclc REV	5'-TCCAGGAAATACCCCTTCCTTCCC
Gclm FWD	5'-GCAGCTGTATCAGTGGGCACAG
Gclm REV	5'-GCCTCAGAGAGCAGTTCTTTCGG
Gsr FWD	5'-GGGCTCACTGAAGACGAAGCTG
Gsr REV	5'-TGTGAATGCCAACCACCTTTTCC
Gss FWD	5'-AGGAATTGCTTGCTACGGCCTG
Gss REV	5'-TCACCAGTGTTGTTCCCTGTCTG
Ogdh FWD	5'-TGTCTGGTATGCTGGCCGAGAC
Ogdh REV	5'-TGAATGCGTCCAGGTCAAAGGC
Pdha1 FWD	5'-ACCCTGGAGTAAGCTACCGCAC
Pdha1 REV	5'-CTCAGGATCAGCCGTGGCAAAC
Pdha2 FWD	5'-GGCTCATGGCTTCTGCTACACG
Pdha2 REV	5'-TACAGGCAAAAGCCACACCAGC
Pdhb FWD	5'-TCTGCGCACCATCAGACCAATG
Pdhb REV	5'-GCAGGGCCTTCCATAATTCTGGC
Pdhx FWD	5'-AATCCAGACCAGCCTCAGCTCC
Pdhx REV	5'-ATGTACCCGCTGCATTCGGTTG
Tyms FWD	5'-TTGCCAGCTATGCTCTGCTCAC
Tyms REV	5'-GGTCTTGGTTCTCGCTGTAGCTG
Actb FWD	5'-TTCCAGCCTTCCTTCTTGGGTATGG
Actb REV	5'-ATGGTGCTAGGAGCCAGAGCAG
Tbp FWD	5'-CAGGGCGCCATGACTCCTGGAATT
Tbp REV	5'-GCTACTGCCTGCTGTTGTTGCT

Table S3.4 qRT-PCR primer sequences.

3.10 REFERENCES

REFERENCES

1. Perou CM, Sorlie T, Eisen MB, van de Rijn M, Jeffrey SS, Rees CA, Pollack JR, Ross DT, Johnsen H, Akslen LA, Fluge O, Pergamenschikov A, Williams C, Zhu SX, Lonning PE, Borresen-Dale AL, Brown PO, Botstein D (2000) Molecular portraits of human breast tumours. Nature 406 (6797):747-752. doi:10.1038/35021093

2. Sørlie T, Perou CM, Tibshirani R, Aas T, Geisler S, Johnsen H, Hastie T, Eisen MB, van de Rijn M, Jeffrey SS, Thorsen T, Quist H, Matese JC, Brown PO, Botstein D, Lønning PE, Børresen-Dale A-L (2001) Gene expression patterns of breast carcinomas distinguish tumor subclasses with clinical implications. Proceedings of the National Academy of Sciences of the United States of America 98 (19):10869-10874. doi:10.1073/pnas.191367098

3. Senkus E, Kyriakides S, Penault-Llorca F, Poortmans P, Thompson A, Zackrisson S, Cardoso F (2013) Primary breast cancer: ESMO Clinical Practice Guidelines for diagnosis, treatment and follow-up†. Annals of Oncology 24 (suppl_6):vi7-vi23. doi:10.1093/annonc/mdt284

4. Early Breast Cancer Trialists' Collaborative G (2005) Effects of chemotherapy and hormonal therapy for early breast cancer on recurrence and 15-year survival: an overview of the randomised trials. The Lancet 365 (9472):1687-1717. doi:10.1016/s0140-6736(05)66544-0

5. Gonzalez-Angulo AM, Morales-Vasquez F, Hortobagyi GN (2007) Overview of Resistance to Systemic Therapy in Patients with Breast Cancer. In: Yu D, Hung M-C (eds) Breast Cancer Chemosensitivity. Springer New York, New York, NY, pp 1-22. doi:10.1007/978-0-387-74039-3

6. Ogrodzinski MP, Bernard JJ, Lunt SY (2017) Deciphering metabolic rewiring in breast cancer subtypes. Transl Res 189:105-122. doi:10.1016/j.trsl.2017.07.004

7. Hanahan D, Weinberg RA (2011) Hallmarks of cancer: the next generation. Cell 144 (5):646-674. doi:10.1016/j.cell.2011.02.013

8. Lunt SY, Vander Heiden MG (2011) Aerobic glycolysis: meeting the metabolic requirements of cell proliferation. Annu Rev Cell Dev Biol 27:441-464. doi:10.1146/annurev-cellbio-092910-154237

9. Kung H-N, Marks JR, Chi J-T (2011) Glutamine Synthetase Is a Genetic Determinant of Cell Type–Specific Glutamine Independence in Breast Epithelia. PLOS Genetics 7 (8):e1002229. doi:10.1371/journal.pgen.1002229

10. Kim S, Kim DH, Jung W-H, Koo JS (2013) Expression of glutamine metabolism-related proteins according to molecular subtype of breast cancer. Endocrine-Related Cancer 20 (3):339-348. doi:10.1530/erc-12-0398

11. Gross MI, Demo SD, Dennison JB, Chen L, Chernov-Rogan T, Goyal B, Janes JR, Laidig GJ, Lewis ER, Li J, MacKinnon AL, Parlati F, Rodriguez MLM, Shwonek PJ, Sjogren EB, Stanton TF, Wang T, Yang J, Zhao F, Bennett MK (2014) Antitumor Activity of the Glutaminase Inhibitor CB-839 in Triple-Negative Breast Cancer. Molecular Cancer Therapeutics 13 (4):890. doi:10.1158/1535-7163.MCT-13-0870

12. Lampa M, Arlt H, He T, Ospina B, Reeves J, Zhang B, Murtie J, Deng G, Barberis C, Hoffmann D, Cheng H, Pollard J, Winter C, Richon V, Garcia-Escheverria C, Adrian F, Wiederschain D, Srinivasan L (2017) Glutaminase is essential for the growth of triple-negative breast cancer cells with a deregulated glutamine metabolism pathway and its suppression synergizes with mTOR inhibition. PLOS ONE 12 (9):e0185092. doi:10.1371/journal.pone.0185092

13. Stewart TA, Pattengale PK, Leder P (1984) Spontaneous mammary adenocarcinomas in transgenic mice that carry and express MTV/myc fusion genes. Cell 38 (3):627-637. doi:10.1016/0092-8674(84)90257-5

14. Andrechek ER, Cardiff RD, Chang JT, Gatza ML, Acharya CR, Potti A, Nevins JR (2009) Genetic heterogeneity of Myc-induced mammary tumors reflecting diverse phenotypes including metastatic potential. Proceedings of the National Academy of Sciences 106 (38):16387-16392. doi:10.1073/pnas.0901250106

15. Hollern DP, Andrechek ER (2014) A genomic analysis of mouse models of breast cancer reveals molecular features of mouse models and relationships to human breast cancer. Breast Cancer Research : BCR 16 (3):R59-R59. doi:10.1186/bcr3672

16. Hollern DP, Swiatnicki MR, Andrechek ER (2018) Histological subtypes of mouse mammary tumors reveal conserved relationships to human cancers. PLoS genetics 14 (1)

17. Prat A, Parker JS, Karginova O, Fan C, Livasy C, Herschkowitz JI, He X, Perou CM (2010) Phenotypic and molecular characterization of the claudin-low intrinsic subtype of breast cancer. Breast Cancer Research 12 (5):R68. doi:10.1186/bcr2635

18. Deming SL, Nass SJ, Dickson RB, Trock BJ (2000) C-myc amplification in breast cancer: a meta-analysis of its occurrence and prognostic relevance. British Journal of Cancer 83 (12):1688-1695. doi:10.1054/bjoc.2000.1522

19. Dang CV (1999) c-Myc target genes involved in cell growth, apoptosis, and metabolism. Molecular and cellular biology 19 (1):1-11. doi:10.1128/mcb.19.1.1

20. Dang CV, O'Donnell KA, Zeller KI, Nguyen T, Osthus RC, Li F (2006) The c-Myc target gene network. Semin Cancer Biol 16 (4):253-264. doi:10.1016/j.semcancer.2006.07.014

21. Wahlstrom T, Henriksson MA (2015) Impact of MYC in regulation of tumor cell metabolism. Biochim Biophys Acta 1849 (5):563-569. doi:10.1016/j.bbagrm.2014.07.004

22. Stine ZE, Walton ZE, Altman BJ, Hsieh AL, Dang CV (2015) MYC, metabolism, and cancer. Cancer discovery 5 (10):1024-1039. doi:10.1158/2159-8290.CD-15-0507

23. Lane AN, Fan TW-M (2015) Regulation of mammalian nucleotide metabolism and biosynthesis. Nucleic acids research 43 (4):2466-2485. doi:10.1093/nar/gkv047

24. Ogrodzinski MP, Teoh ST, Yu L, Broadwater D, Ensink E, Lunt SY (2019) Measuring the Nutrient Metabolism of Adherent Cells in Culture. In: Fendt SM, Lunt S (eds) Methods Mol Biol, vol 1862. Methods Mol Biol. Humana Press, New York, NY, Metabolic Signaling. Methods Mol Biol, pp 37-52. doi:10.1007/978-1-4939-8769-6_3

25. Buescher JM, Antoniewicz MR, Boros LG, Burgess SC, Brunengraber H, Clish CB, DeBerardinis RJ, Feron O, Frezza C, Ghesquiere B, Gottlieb E, Hiller K, Jones RG, Kamphorst JJ, Kibbey RG, Kimmelman AC, Locasale JW, Lunt SY, Maddocks OD, Malloy

C, Metallo CM, Meuillet EJ, Munger J, Noh K, Rabinowitz JD, Ralser M, Sauer U, Stephanopoulos G, St-Pierre J, Tennant DA, Wittmann C, Vander Heiden MG, Vazquez A, Vousden K, Young JD, Zamboni N, Fendt SM (2015) A roadmap for interpreting (13)C metabolite labeling patterns from cells. Curr Opin Biotechnol 34:189-201. doi:10.1016/j.copbio.2015.02.003

26. Griffith OW, Meister A (1979) Potent and specific inhibition of glutathione synthesis by buthionine sulfoximine (Sn-butyl homocysteine sulfoximine). Journal of Biological Chemistry 254 (16):7558-7560

27. Zachar Z, Marecek J, Maturo C, Gupta S, Stuart SD, Howell K, Schauble A, Lem J, Piramzadian A, Karnik S (2011) Non-redox-active lipoate derivates disrupt cancer cell mitochondrial metabolism and are potent anticancer agents in vivo. Journal of molecular medicine 89 (11):1137. doi:10.1007/s00109-011-0785-8

28. Stuart SD, Schauble A, Gupta S, Kennedy AD, Keppler BR, Bingham PM, Zachar Z (2014) A strategically designed small molecule attacks alpha-ketoglutarate dehydrogenase in tumor cells through a redox process. Cancer & metabolism 2 (1):4-4. doi:10.1186/2049-3002-2-4

29. Cohen SS, Flaks JG, Barner HD, Loeb MR, Lichtenstein J (1958) The mode of action of 5-fluorouracil and its derivatives. Proceedings of the National Academy of Sciences of the United States of America 44 (10):1004. doi:10.1073/pnas.44.10.1004

30. Longley DB, Harkin DP, Johnston PG (2003) 5-Fluorouracil: mechanisms of action and clinical strategies. Nat Rev Cancer 3 (5):330-338. doi:10.1038/nrc1074

31. McConnachie LA, Mohar I, Hudson FN, Ware CB, Ladiges WC, Fernandez C, Chatterton-Kirchmeier S, White CC, Pierce RH, Kavanagh TJ (2007) Glutamate cysteine ligase modifier subunit deficiency and gender as determinants of acetaminophen-induced hepatotoxicity in mice. Toxicological Sciences 99 (2):628-636

32. Backos DS, Fritz KS, McArthur DG, Kepa JK, Donson AM, Petersen DR, Foreman NK, Franklin CC, Reigan P (2013) Glycation of glutamate cysteine ligase by 2-deoxy-d-ribose and its potential impact on chemoresistance in glioblastoma. Neurochemical research 38 (9):1838-1849

33. Luengo A, Gui DY, Vander Heiden MG (2017) Targeting metabolism for cancer therapy. Cell chemical biology 24 (9):1161-1180. doi:10.1016/j.chembiol.2017.08.028

34. Martinez-Outschoorn UE, Peiris-Pages M, Pestell RG, Sotgia F, Lisanti MP (2017) Cancer metabolism: a therapeutic perspective. Nat Rev Clin Oncol 14 (1):11-31. doi:10.1038/nrclinonc.2016.60

35. Zhao Y, Butler EB, Tan M (2013) Targeting cellular metabolism to improve cancer therapeutics. Cell Death Dis 4 (3):e532. doi:10.1038/cddis.2013.60

36. Lewis-Wambi JS, Kim HR, Wambi C, Patel R, Pyle JR, Klein-Szanto AJ, Jordan VC (2008) Buthionine sulfoximine sensitizes antihormone-resistant human breast cancer cells to estrogen-induced apoptosis. Breast Cancer Research 10 (6):R104. doi:10.1186/bcr2208

37. Tagde A, Singh H, Kang M, Reynolds C (2014) The glutathione synthesis inhibitor buthionine sulfoximine synergistically enhanced melphalan activity against preclinical models of multiple myeloma. Blood cancer journal 4 (7):e229. doi:10.1038/bcj.2014.45

38. Anderson CP, Matthay KK, Perentesis JP, Neglia JP, Bailey HH, Villablanca JG, Groshen S, Hasenauer B, Maris JM, Seeger RC (2015) Pilot study of intravenous melphalan combined with continuous infusion L-S, R-buthionine sulfoximine for children with recurrent neuroblastoma. Pediatric blood & cancer 62 (10):1739-1746. doi:10.1002/pbc.25594

39. Villablanca JG, Volchenboum SL, Cho H, Kang MH, Cohn SL, Anderson CP, Marachelian A, Groshen S, Tsao-Wei D, Matthay KK (2016) A Phase I New Approaches to Neuroblastoma Therapy Study of Buthionine Sulfoximine and Melphalan With Autologous Stem Cells for Recurrent/Refractory High-Risk Neuroblastoma. Pediatric blood & cancer 63 (8):1349-1356. doi:10.1002/pbc.25994

40. Lima CMSPR, Alistar AT, Desnoyers RJ, Sorscher S, Yacoub GH, Dressler EVM, Pardee TS, Grant SC, Luther S, Butler D, Ogburn O, Strickland K, Pasche B (2019) A phase I clinical trial of fluorouracil (5-FU) + devimistat (CPI-613) combination in previously treated patients (pts) with metastatic colorectal cancer (MCR). Journal of Clinical Oncology 37 (15_suppl):e15054-e15054. doi:10.1200/JCO.2019.37.15_suppl.e15054

41. Lycan TW, Pardee TS, Petty WJ, Bonomi M, Alistar A, Lamar ZS, Isom S, Chan MD, Miller AA, Ruiz J (2016) A phase II clinical trial of CPI-613 in patients with relapsed or refractory small cell lung carcinoma. PloS one 11 (10):e0164244. doi:10.1371/journal.pone.0164244

42. Alistar A, Morris BB, Desnoyer R, Klepin HD, Hosseinzadeh K, Clark C, Cameron A, Leyendecker J, D'Agostino Jr R, Topaloglu U (2017) Safety and tolerability of the first-in-class agent CPI-613 in combination with modified FOLFIRINOX in patients with metastatic pancreatic cancer: a single-centre, open-label, dose-escalation, phase 1 trial. The lancet oncology 18 (6):770-778. doi:10.1016/S1470-2045(17)30314-5

43. Johnston P, Kaye S (2001) Capecitabine: a novel agent for the treatment of solid tumors. Anti-cancer drugs 12 (8):639-646. doi:10.1097/00001813-200109000-00001

44. Horiuchi D, Kusdra L, Huskey NE, Chandriani S, Lenburg ME, Gonzalez-Angulo AM, Creasman KJ, Bazarov AV, Smyth JW, Davis SE, Yaswen P, Mills GB, Esserman LJ, Goga A (2012) MYC pathway activation in triple-negative breast cancer is synthetic lethal with CDK inhibition. The Journal of experimental medicine 209 (4):679-696. doi:10.1084/jem.20111512

45. Liedtke C, Mazouni C, Hess KR, André F, Tordai A, Mejia JA, Symmans WF, Gonzalez-Angulo AM, Hennessy B, Green M (2008) Response to neoadjuvant therapy and long-term survival in patients with triple-negative breast cancer. Journal of clinical oncology 26 (8):1275-1281. doi:10.1200/JCO.2007.14.4147

46. Anderton B, Camarda R, Balakrishnan S, Balakrishnan A, Kohnz RA, Lim L, Evason KJ, Momcilovic O, Kruttwig K, Huang Q (2017) MYC-driven inhibition of the glutamate-cysteine ligase promotes glutathione depletion in liver cancer. EMBO reports 18 (4):569-585. doi:10.15252/embr.201643068

47. Gao P, Tchernyshyov I, Chang TC, Lee YS, Kita K, Ochi T, Zeller KI, De Marzo AM, Van Eyk JE, Mendell JT, Dang CV (2009) c-Myc suppression of miR-23a/b enhances mitochondrial glutaminase expression and glutamine metabolism. Nature 458 (7239):762-765. doi:10.1038/nature07823

48. Camarda R, Zhou AY, Kohnz RA, Balakrishnan S, Mahieu C, Anderton B, Eyob H, Kajimura S, Tward A, Krings G, Nomura DK, Goga A (2016) Inhibition of fatty acid

oxidation as a therapy for MYC-overexpressing triple-negative breast cancer. Nature medicine 22 (4):427-432. doi:10.1038/nm.4055

49. Mitra A, Mishra L, Li S (2013) Technologies for deriving primary tumor cells for use in personalized cancer therapy. Trends in biotechnology 31 (6):347-354. doi:10.1016/j.tibtech.2013.03.006

50. Melamud E, Vastag L, Rabinowitz JD (2010) Metabolomic Analysis and Visualization Engine for LC−MS Data. Analytical Chemistry 82 (23):9818-9826. doi:10.1021/ac1021166

51. De Hoon MJ, Imoto S, Nolan J, Miyano S (2004) Open source clustering software. Bioinformatics 20 (9):1453-1454. doi:10.1093/bioinformatics/bth078

52. Saldanha AJ (2004) Java Treeview—extensible visualization of microarray data. Bioinformatics 20 (17):3246-3248. doi:10.1093/bioinformatics/bth349

53. Millard P, Letisse F, Sokol S, Portais JC (2012) IsoCor: correcting MS data in isotope labeling experiments. Bioinformatics 28 (9):1294-1296. doi:10.1093/bioinformatics/bts127

CHAPTER 4.

TARGETING SUBTYPE-SPECIFIC METABOLIC PREFERENCES IN NUCLEOTIDE BIOSYNTHESIS INHIBITS MOUSE MAMMARY TUMOR GROWTH

4.1 PREFACE

This chapter is a modified version of a primary research manuscript currently submitted for publication.

4.2 Abstract

Investigating metabolic rewiring in cancer can lead to the discovery of new treatment strategies for breast cancer subtypes that currently lack targeted therapies. Using MMTV-Myc driven tumors to model breast cancer heterogeneity, we investigated metabolic differences between two histological subtypes, the epithelial-mesenchymal transition (EMT) and the papillary subtypes, using a combination of genomic and metabolomic techniques. We identified differences in nucleotide metabolism between EMT and papillary subtypes: EMT tumors preferentially use the nucleotide salvage pathway, while papillary tumors prefer *de novo* nucleotide biosynthesis. Using CRISPR/Cas9 gene editing and mass spectrometry-based methods, we determined that targeting the preferred pathway in each subtype resulted in greater metabolic impact than targeting the non-preferred pathway. We further show that knocking out the preferred nucleotide pathway in each subtype has a deleterious effect on *in vivo* tumor growth. In contrast, knocking out the non-preferred pathway has a lesser effect or results in increased tumor growth.

4.3 Introduction

Breast cancer remains the leading cause of cancer-related mortality among women worldwide despite recent trends in decreasing mortality in high income countries [1], which can be attributed to advances in early detection and treatment [2]. Current treatment strategies for advanced breast cancer often include general chemotherapy and radiation, with the use of targeted therapies, such as endocrine therapy, for specific breast cancer subtypes [3]. These subtypes are often defined based on expression of specific receptors including the estrogen receptor (ER), progesterone receptor (PR), and human

epidermal growth factor receptor 2 (HER2), with an additional triple negative breast cancer (TNBC) subtype characterized by the absence of these markers. Breast cancer subtypes can also be classified according to gene expression patterns [4, 5] which often overlap with definitions based on receptor status and other clinical findings [3, 5] and are further able to provide valuable prognostic information [6]. However, targeted therapies are not available for all subtypes of breast cancer, and current rates of recurrence and development of resistance remain problematic [7, 8]. It is becoming increasingly clear that breast cancer subtypes have differences in metabolism, and targeting these metabolic pathways could provide new targeted therapy options [9, 10].

Metabolic rewiring is a hallmark of cancer [11], and significant efforts have been made to identify metabolic vulnerabilities in cancer and leverage these findings to develop novel treatment strategies. Early work defining this concept was performed in the 1920s by Otto Warburg, who observed that tumor cells generally upregulate glycolysis even in aerobic conditions [12] – a phenomenon now known as the Warburg effect. One of the modern consequences of the Warburg effect is that targeting aerobic glycolysis, by pharmacological inhibition of glycolytic enzymes and by limiting glucose availability through dietary restriction [13-15], is under investigation as a therapeutic strategy for many types of cancer. However, one of the challenges in using metabolic rewiring to treat cancer arises from the fact that cancer is a remarkably heterogenous disease, and few metabolic vulnerabilities are common to all cancers. This variability is clearly illustrated by breast cancer, which demonstrates heterogeneity on histologic, genetic, and metabolic levels [4, 9, 16, 17].

In addition to glycolysis, another metabolic pathway commonly targeted in cancer therapy is nucleotide biosynthesis. Nucleotides enable cellular proliferation by facilitating RNA and DNA production [18, 19]**,** and is also required to balance basal rates of RNA turnover in all cells [20]**.** Nucleotide biosynthesis occurs through two parallel metabolic pathways: 1) *de novo* nucleotide biosynthesis, which generates new nucleotides from precursors derived predominately from glucose and glutamine metabolism and is an energetically costly process, and 2) nucleotide salvage, which allows free bases derived from catabolic processes to be recycled back into nucleotides and is significantly more energetically efficient [20]**.**

In our current work, we investigate subtype-specific differences in nucleotide metabolism using two histological mouse mammary tumor subtypes derived from the MMTV-Myc mouse tumor model: 1) MMTV-Myc epithelial-mesenchymal-transition (EMT); and 2) MMTV-Myc papillary. This model system mimics the heterogeneity of human breast cancer [21], and subtypes of the MMTV-Myc model can be correlated with human cancer subtypes based on gene expression patterns: the EMT subtype strongly correlates with the claudin-low subtype, and the papillary subtype correlates more moderately with several human subtypes including basal and luminal breast cancer [22, 23]. Since the claudin-low and basal subtypes both have poor prognosis [24, 25], we decided to focus on the corresponding MMTV-Myc EMT and papillary subtypes in this study.

We have previously used cell lines derived from this model system to identify metabolic differences between subtypes [26]. Here, we build on this work by integrating genomic and metabolomic techniques to refine our understanding of the metabolic

differences between the EMT and papillary subtypes. We find striking differences in nucleotide metabolism between the two subtypes: the EMT subtype prefers nucleotide salvage pathways, while the papillary subtype prefers *de novo* nucleotide biosynthesis. We further investigate the clinical significance of expressing genes related to *de novo* purine biosynthesis and salvage pathways, and evaluate the consequences of targeting these genes in each subtype using CRISPR/Cas9 gene editing techniques [27, 28]. We find that targeting the preferred metabolic pathway of each subtype generally caused the most substantial disruption on nucleotide metabolism and had subtype-specific effects on *in vivo* tumor growth. Notably, targeting the preferred pathway significantly reduced tumor growth while targeting the non-preferred pathway either had no effect on tumor growth, or in some cases significantly increased tumor growth. These results highlight the metabolic heterogeneity of breast cancer subtypes and demonstrate the potential efficacy of tailoring therapies to inhibit subtype-specific metabolism.

4.4 Results

4.4.1 Metabolite pool sizes and gene expression patterns of MMTV-Myc mouse mammary tumors implicate differences in nucleotide metabolic pathway activity between subtypes.

To identify differences in metabolic pathway activities between EMT and papillary mouse mammary tumor subtypes, we integrated a metabolomics analysis with publicly available gene expression data [29]**.** Metabolites were extracted from flash frozen tumor sections of known histological subtype (**Figure 1A**) and quantitated using liquid chromatography tandem mass spectrometry (LC-MS/MS). We found metabolites involved in the pentose phosphate pathway (PPP) and metabolites related to nucleotide

metabolism to be significantly different between EMT and papillary tumors (**Figure 1B; Table S1**). Notably, PPP intermediates including gluconolactone, ribose 5-phosphate, ribulose 5-phosphate, and sedoheptulose phosphate are uniformly elevated in the EMT subtype compared to papillary. The PPP serves several important functions including: 1) production of ribose 5-phosphate which can be used for nucleotide biosynthesis or converted to glycolytic intermediates; 2) production of reducing equivalents in the form of NADPH; and 3) generation of erythrose 4-phosphate which can also be converted to glycolytic intermediates [30]. Several metabolites related to nucleotide metabolism are also different between the EMT and papillary tumors (**Figure 1B; Table S1**). For example, EMT tumors have higher levels of inosine monophosphate (IMP), adenine, and inosine compared to papillary tumors. Adenine and inosine are both intermediates in breakdown and salvage pathways of nucleotide metabolism, and IMP is an intermediate for purine biosynthesis. To investigate how these metabolite levels reflect differences in gene expression, we downloaded gene expression data for the EMT and papillary tumors from Gene Expression Omnibus (GEO) [31] and applied gene set enrichment analysis (GSEA) [32] using metabolism-related gene sets from the Reactome database [33]. This analysis revealed that genes involved in the PPP (**Figure 1C**) and nucleobase biosynthesis (**Figure 1C**) are both significantly enriched for *lower* expression in the EMT subtype compared to the papillary subtype. Therefore, the higher levels of PPP metabolites and IMP observed in EMT tumors (**Figure 1B**) likely reflect accumulation due to decreased flux through the PPP and nucleobase biosynthesis pathways. Together, this data agrees with our previous *in vitro* findings, where we observed lower nucleotide biosynthesis in EMT cells compared to papillary cells [26]. When considered with our previous results,

these findings further demonstrate that EMT and papillary tumors exhibit significant differences in nucleotide metabolism *in vivo*.

4.4.2 Expression of nucleotide salvage genes are increased in the EMT subtype.

To further characterize gene expression differences in nucleotide metabolism between the EMT and papillary tumors, we used the transcriptome analysis console (TAC) software. We filtered the gene list to include nucleotide metabolism and the PPP genes as denoted within the Reactome database. Based on our GSEA results (**Figure 1C-D**), we expected genes involved in *de novo* nucleotide biosynthesis and PPP to have higher expression in the papillary subtype. For the EMT subtype, we find that the gene with highest relative expression is *UPP1*, with 18-fold higher expression the EMT subtype vs. the papillary subtype (**Table S2**). *UPP1* encodes uridine phosphorylase 1, an enzyme involved in pyrimidine salvage. Together with the observation of higher nucleotide salvage pathway intermediates adenine and inosine in EMT (**Figure 1B**), this suggests the EMT subtype has higher activity of the nucleotide salvage pathway. Therefore, we decided to focus our analysis on genes involved in *de novo* nucleotide biosynthesis and nucleotide salvage pathways. Hierarchical clustering revealed two major groupings of genes as illustrated by the dendrogram in **Figure 2A**. The first, smaller group included many nucleotide salvage genes with significantly higher expression in EMT tumors and the second, larger group predominately contained *de novo* biosynthesis genes with significantly lower expression in EMT compared to papillary tumors. Therefore, EMT tumors show a relative preference for nucleotide salvage, while papillary tumors prefer *de novo* biosynthesis. We also considered GSEA results for the nucleotide salvage pathway; however, this gene set as a whole was not significantly enriched for the EMT

subtype despite several genes within this pathway having significantly higher expression in the EMT subtype (**Figure S1; Table S2**). A simplified pathway overview summarizing our results highlights the potential metabolic preferences for nucleotide biosynthesis that are specific to each subtype, with the papillary subtype preferring *de novo* biosynthesis and the EMT subtype preferring nucleotide salvage (**Figure 2B**).

4.4.3 Expression of key *de novo* and salvage genes are correlated with worse patient outcomes.

Our results thus far illustrate the possibility for distinct histological subtypes to utilize different pathways to meet the same metabolic demand for nucleotides. We next sought to determine the potential clinical relevance associated with expression of these genes in human breast cancer. We focused on genes phosphoribosyl pyrophosphate amidotransferase (*PPAT*) and adenine phosphoribosyltransferase (*APRT*) because they encode the rate limiting step for *de novo* purine biosynthesis and salvage of the purine base adenine, respectively, and our findings show that *PPAT* expression is significantly higher in the papillary subtype and *APRT* expression is significantly higher in the EMT subtype (**Figure 2B; Table S2**). We used KM plotter, which generates Kaplan-Meier curves using patient data mined from GEO datasets [34], to generate survival curves with patients stratified by relative gene expression of *PPAT* and *APRT*. We find that in general, patients with high expression of both *PPAT* and *APRT* have worse relapse-free survival (RFS) than patients with low expression of these genes (**Figure 3A**). This trend is also observed when patients are further divided according to intrinsic subtype. High expression of both *PPAT* and *APRT* is similarly significant for patients with luminal A (**Figure 3B**) and luminal B (**Figure 3C**) breast cancer. However, for patients with HER2+

(**Figure 3D**) and basal (**Figure 3E**) breast cancer, high expression of *PPAT* is no longer associated with decreased RFS, while high expression of *APRT* remains significant. These results highlight the potential importance of nucleotide metabolism in breast cancer and further suggest that *de novo* purine biosynthesis may be most important for luminal breast cancer, whereas salvage may be relevant for all breast cancer subtypes.

4.4.4 Knocking out *de novo* and salvage genes disrupts cell metabolism in a subtype-specific manner.

To further investigate the importance of nucleotide biosynthesis genes *PPAT* and *APRT* in our model, we targeted each gene using CRISPR/Cas9 gene editing [27, 28] in EMT and papillary tumor derived cell lines. We concurrently generated puromycin-resistant control cell lines for each subtype with a non-targeting scramble guide RNA. Clonal lines for each subtype, knockout (KO), and puromycin-resistant scramble control (PSC) were isolated by serial dilution, and successful gene editing was confirmed by Tracking of Indels by Decomposition (TIDE) analysis [35] (**Figures S2-S3**). Western blots were also performed to determine successful KO by protein expression (**Figure S4**). While the APRT antibody worked well, the PPAT bands were inconclusive, with multiple faint bands near the predicted molecular weight of PPAT. We therefore also performed isotope labeling studies to functionally assess how $^{13}C_6$-glucose is incorporated into purine biosynthesis in these cell lines. We reasoned that the M-5 isotopologue of ATP represents production from either pathway, since the M-5 isotopologue of ATP is predominately derived from a fully-labeled PRPP molecule with a fully-unlabeled adenine nucleobase, and both *de novo* and salvage pathways utilize PRPP as a substrate. In contrast, the M1-4 and M6-10 isotopologues require labeling of the adenine base, which

is only attained through *de novo* biosynthesis. Hence, we distinguish ATP isotopologues as unlabeled (M-0), ATP that may be derived from either *de novo* or salvage pathways (M-5), and ATP that could only be derived from *de novo* biosynthesis (M1-4 and M6-10). Using this approach, we find that, compared to controls, knocking out the salvage gene *APRT* resulted in increased labeling of isotopologues of ATP that can only be derived from *de novo* biosynthesis in both subtypes (**Figure 4; Tables S3-S4**), which is expected because a larger proportion of ATP is now derived from *de novo* biosynthesis instead of salvage. Additionally, targeting the *de novo* biosynthesis gene *PPAT* caused significantly decreased labeling of ATP isotopologues derived from *de novo* biosynthesis (**Figure 4; Tables S3-S4**). These results provide strong evidence that the metabolic activity of nucleotide salvage and *de novo* biosynthesis have been significantly decreased in the *APRT* and *PPAT* KO cell lines, respectively.

We also analyzed the abundance of a wide range of metabolites in CRISPR edited cell lines relative to the control line of each respective subtype using the targeted LC-MS/MS method described above. We found significant differences between cell lines across several metabolic pathways (**Figure S5; Tables S5-S6**). As expected, the most consistently altered metabolites include PPP related metabolites (**Figure 5A**), nucleoside triphosphates (NTPs; **Figure 5B**), and deoxynucleoside triphosphates (dNTPs; **Figure 5C**). Notably, the relative abundance of these metabolites is generally most different when the preferred metabolic pathway for each subtype has been targeted. For example, ATP (**Figure 5B**) and dATP (**Figure 5C**) levels are significantly decreased in the papillary *PPAT* KO cell line compared to the papillary control and *APRT* KO lines, while the EMT *PPAT* KO is similar to EMT control for these metabolites. Additionally, the papillary *PPAT*

KO cells have lower levels of most PPP intermediates, but significantly higher levels of phosphoribosyl pyrophosphate (PRPP; **Figure 5A**) which is used by both *de novo* biosynthesis and salvage pathways and is produced from the PPP intermediate ribose-5-phosphate. Most NTPs and dNTPs are also decreased in the papillary *PPAT* KO line compared to the control or *APRT* KO line (**Figure 5B-C)**. The exception to this is the pyrimidine uridine triphosphate (UTP), which is significantly increased in the papillary *PPAT* KO compared to control and *APRT* KO lines (**Figure 5B**). Together, these results show that targeting *PPAT* in the papillary cells creates a metabolic bottleneck by blocking *de novo* purine biosynthesis, causing: 1) decreased levels of intermediates in the PPP, the feeder pathway into nucleotide biosynthesis; and 2) increased levels of PRPP which would normally function to increase *de novo* purine and pyrimidine biosynthesis through feedforward mechanisms [20]. This PRPP-driven feedforward mechanism would also increase *de novo* pyrimidine biosynthesis in the papillary *PPAT* KO cells and explain the increased UTP levels observed in papillary *PPAT* KO cells (**Figure 5B**).

Decreased PPP intermediates, increased PRPP, and alterations in NTP and dNTP levels are not observed in the EMT *PPAT* KO cells, likely due to the metabolic preference of the EMT subtype to salvage nucleotides. Indeed, targeting the salvage pathway caused significant metabolic alterations in the EMT *APRT* KO cells compared to the control: higher levels of most nucleotides (**Figure 5B-C**) suggest that EMT *APRT* KO cells are forced to switch to *de novo* biosynthesis when their preferred means of obtaining nucleotides via salvage is inhibited. In the papillary *APRT* KO line, nucleotide levels are not significantly changed from control levels (**Figure 5B-C**). Taken together, the above results indicate that the greatest impact on nucleotide metabolism is achieved when the

preferred nucleotide biosynthesis pathway of each subtype is inhibited, while inhibiting the non-preferred pathway has minimal effects.

4.4.5 Targeting nucleotide *de novo* biosynthesis and salvage genes impact tumor growth in a subtype-specific manner.

To determine the *in vivo* effects of targeting the preferred nucleotide biosynthesis pathway for each subtype, we monitored tumor growth of KO and control cell lines injected in mice. Control or KO cells were first injected into the mammary fat pad of syngeneic mice to generate tumors, then the resulting tumors were resected, and fragments of these tumors were orthotopically implanted into new cohorts of mice to monitor tumor growth over time. This was performed because implantation of tumor fragments, rather than direct injection of tumor cells, resulted in less variability in the lag time of tumor growth. As expected, the EMT tumors grew slowest when the preferred nucleotide salvage pathway gene *APRT* is targeted: EMT *APRT* KO tumors were significantly smaller (762.8 ± 108.4 mm^2, n = 5) at 24 days post implantation as compared to the *PPAT* KO tumors (982.7 ± 116.1 mm^2, n = 5). The EMT *PPAT* KO tumors also grew slower than the PSC tumors (1344.6 ± 141.7 mm^2, n = 6), which were the largest at 24 days post implantation (**Figure 6A; Table S7**). Consistent with the reliance of the papillary subtype on *de novo* nucleotide biosynthesis, targeting *PPAT* prevented papillary cells from growing tumors *in vivo* (**Figure 6B; Table S8**). Surprisingly, targeting the non-preferred nucleotide salvage gene *APRT* caused papillary tumors to grow larger (1161.8 ± 155.8 mm^2, n = 5) than the PSC tumors (514.0 ± 114.0 mm^2, n = 5) at 24 days post implantation. Taken together, these results indicate that *de novo* nucleotide biosynthesis is a critical metabolic pathway

for papillary tumors, and further demonstrate targeting a non-preferred metabolic pathway could have the unintended side effect of increasing tumor growth.

To determine whether differences in tumor sizes are attributable to changes in proliferation or cell death, immunohistochemical (IHC) analysis was performed. Ki67 staining and terminal deoxynucleotidyl transferase dUTP nick end labeling (TUNEL) assays were performed to measure proliferation and necrosis within the tumors, respectively. As expected, Ki67 staining is directly proportional to tumor growth in each subtype. The EMT PSC tumors have significantly more $Ki67^+$ nuclei than both KOs, and the EMT *APRT* KO tumors have significantly fewer compared to *PPAT* KOs (**Figure 7A; Table S9**). This indicates that the *APRT* KO EMT tumors grow slower due to decreased proliferation. In papillary tumors, the *APRT* KOs have significantly more $Ki67^+$ nuclei than the PSC tumors (**Figure 7B; Table S10**), showing these tumors grow more quickly due to increased proliferation. TUNEL assays show that in the EMT subtype, both KOs were significantly more necrotic than the control tumors (**Figure 7C; Table S11**) In the papillary subtype, no difference in staining was observed between control and *APRT* KO tumors (**Figure 7D; Table S12**) indicating that the observed differences in tumor growth are not due to differences in tumor necrosis. Representative Ki67 staining and TUNEL assay images are in **Figures S6 and S7**, respectively**.**

To validate the monoclonal tumor growth findings, the tumor growth of additional clones for each subtype were measured (**Figure S8; Tables S7-S8**). Four additional papillary *PPAT* KO clones were tested with ATP labeling comparable to **Figure 4**, as well as one additional EMT *PPAT* KO clone (**Figure S9; Tables S13-S14**). Two additional confirmed *APRT* KO clones for each subtype were also injected into mice for *in vivo*

testing (**Figure S10**). To validate the controls, the tumor growth of an additional PSC clone and wild-type tumors of each subtype were measured. The clonal PSC tumors for the EMT subtype grew similarly and are larger than the EMT wild-type tumors at 24 days post implantation, indicating the clonal selection process may select for more aggressive clones of this subtype. Additionally, the two EMT *PPAT* KOs grew comparably and were also similar in size to the wild-type EMT tumors. However, the additional two EMT *APRT* KO clonal cell lines failed to generate tumors (**Figure S8A; Table S7**). For the papillary subtype, one *APRT* KO clone again grew more quickly than the control tumors, while the remaining clone grew similarly to the PSC and wild-type papillary tumors (**Figure S8B; Table S8**). Consistent with the results shown in **Figure 6**, the four additional papillary *PPAT* KO clonal cell lines also failed to generate tumors. Taken together, our findings demonstrate the importance of targeting subtype-specific metabolic vulnerabilities to effectively control tumor growth. In addition, inhibiting a non-preferred metabolic pathway not only fails to reduce tumor growth, but can have the detrimental effect of increasing tumor growth.

4.5 Discussion

In this study, we used a combination of genomic and metabolomic techniques to identify subtype-specific metabolic preferences in nucleotide metabolism in the EMT and papillary tumor subtypes derived from the MMTV-Myc mouse model. We discovered that the EMT subtype prefers nucleotide salvage whereas the papillary subtype relies on *de novo* nucleotide biosynthesis. We also investigated patient outcomes and identified that high expression of the nucleotide salvage gene *APRT* is correlated with worse RFS across breast cancer subtypes, while high expression of the *de novo* biosynthesis gene

PPAT is associated with worse outcomes in patients with luminal breast cancer. We further characterized the metabolic effects of targeting both the preferred and non-preferred pathway in the EMT and papillary subtypes and demonstrate the effect of knocking out these pathways on the *in vivo* tumor growth of each subtype.

Our results demonstrate that targeting the preferred metabolic pathway for nucleotide biosynthesis reduces tumor growth in both EMT and papillary tumors. Sustained proliferation is a hallmark of cancer [11], and to achieve this cancer cells have a high requirement for nucleotide biosynthesis. Indeed, targeting nucleotide metabolism has long been used as a staple of cancer therapy with early examples including the folate analog methotrexate (MTX) and the pyrimidine analog 5-fluorouracil (5FU). MTX inhibits dihydrofolate reductase and blocks one-carbon metabolism that is essential for several *de novo* biosynthetic reactions [36]**,** and 5FU inhibits thymidylate synthase, which catalyzes the *de novo* production of thymidine monophosphate [37]. Other compounds targeting *de novo* nucleotide biosynthesis including 6-mercaptopurine [38], leflunomide [39] and brequinar [40] are also currently approved or under investigation as cancer therapeutics. Notably for our model, an active metabolite of 6-mercaptopurine inhibits PPAT [38] and could prove effective at inhibiting growth of the papillary subtype. However, 6-mercaptopurine and several other *de novo* nucleotide metabolism-targeting compounds including 5FU and gemcitabine are activated by the nucleotide salvage pathway, and downregulation of this pathway could provide a potential resistance mechanism to these compounds [41, 42].

In our model, the papillary subtype has increased MYC signaling compared to the EMT subtype [29], and its metabolic preference for *de novo* nucleotide biosynthesis

highlights the role of MYC as a master regulator of nucleotide biosynthesis [43, 44]. MYC amplification is a common feature of many human cancers [45] and occurs in 15.7% of breast cancers [46]. In TNBC specifically, it has been shown that chemotherapy with doxorubicin adaptively upregulates *de novo* pyrimidine biosynthesis and co-treatment of TNBC xenografts with doxorubicin and the *de novo* pyrimidine biosynthesis inhibitor leflunomide is more effective at treating TNBC tumors than doxorubicin alone [47]. Upregulated *de novo* purine biosynthesis, directed by MYC signaling, has also been implicated as a key metabolic pathway in glioblastoma and targeting *de novo* purine biosynthesis genes improved survival and reduced tumor burden in an *in vivo* model of glioblastoma [48]. These studies and ours strongly suggest that further development of compounds targeting *de novo* nucleotide biosynthesis will be useful to treat many types of cancer.

Our results show that targeting nucleotide salvage also attenuates tumor growth in a subset of cancers that prefer this pathway, such as the EMT subtype MMTV-Myc tumors (**Figure 6A**). The EMT subtype has previously been correlated with the claudin-low subtype of human breast cancer based on gene expression patterns [22, 23], and additional studies should be performed to determine whether nucleotide salvage is also a metabolic vulnerability in claudin-low breast cancer. Nucleotides and related metabolites are abundant in the extracellular space and serve important biological functions: purines play a significant role as signaling molecules [49], and pyrimidine release by tumor-associated macrophages has been shown to mediate gemcitabine resistance in animal models of pancreatic cancer [50]. Therefore, the uptake and utilization of these metabolites should be further investigated as therapeutic targets.

Unfortunately, there are currently very few available drugs that target nucleotide salvage. Two indirect examples of salvage inhibitors are dilazep and dipyridamole. These compounds act through inhibition of equilibrative nucleoside transporters (ENTs) and function as vasodilators, prevent platelet aggregation, and are currently approved to treat cardiovascular disease [51]. ENT inhibition indirectly blocks nucleotide salvage pathways by preventing uptake of nucleosides and nucleobases. ENTs also mediate the uptake of nucleoside analogs like gemcitabine [52], which means ENT inhibition as a means to block nucleotide salvage would not be compatible for combination therapy with these drugs. Our findings support the development of therapeutic compounds to specifically target nucleotide salvage pathways. This could prove particularly beneficial for patients diagnosed with claudin-low breast cancer, which carries a poor prognosis and does not have targeted therapies [24].

Our results further reveal the concerning possibility that targeting a non-preferred pathway can cause an increase in tumor growth. Specifically, when *APRT* was targeted in the papillary subtype, two of three clones grew tumors surprisingly fast, while the remaining clone grew comparably to control tumors (**Figure 6B** and **Figure S8B)**. In our current study, we used tumors and cell lines from histologically pure samples; however, this is not always the case in spontaneous tumors. Specifically regarding the MMTV-Myc mouse model, spontaneous tumors develop with a wide variety of histologies, including mixed tumors composed of multiple subtypes in one region [29]. If we consider a possible mixed tumor that is predominately EMT with a minor papillary component, our results indicate that treating it by inhibiting nucleotide salvage alone would likely be ineffective for the papillary component and could even have the unintended side effect of increasing

the growth of the papillary portion of the tumor. One implication of this finding is that, for a mixed tumor exhibiting both EMT and papillary histologies, it may be safer to target *de novo* biosynthesis rather than the salvage pathway, because while EMT subtype cells prefer salvage, blocking *de novo* biosynthesis still has a small inhibitory effect on tumor growth (**Figure 6A**); on the other hand, blocking the salvage pathway in papillary subtype cells can have the opposite and undesirable effect of *increasing* tumor growth (**Figure 6B**).

In human breast cancer, intratumor heterogeneity can manifest in many ways, including on morphologic and genomic levels [53]. The importance of this heterogeneity is particularly notable when considering biomarker expression; for example, current recommendations report a positive finding if at least 1% of tumors cells are positive for the estrogen receptor (ER) [54]. Since the degree of ER positivity is also directly correlated with patient outcomes following anti-endocrine treatment [55], it is clear that the intratumor heterogeneity of this biomarker has important clinical implications. Based on our present findings, metabolic vulnerabilities can be used to design new treatments for breast cancer subtypes. However, the possibility of inadvertently stimulating tumor growth by improperly targeting metabolism should also be considered further, especially in recognition of the significant heterogeneity of breast cancer. Further work should be directed at determining whether subtypes of human breast cancer, which are known to exhibit different metabolic features [9], have differences in metabolic vulnerabilities, and whether targeting non-preferred pathways is detrimental.

In conclusion, our findings demonstrate that distinct histologic subtypes of breast cancer exhibit different metabolic vulnerabilities in terms of their preferred nucleotide

biosynthesis pathways, and that inhibiting the preferred pathway greatly impacts metabolism as well as *in vivo* tumor growth. Crucially, we also show that targeting the non-preferred pathway is not only less effective in controlling tumor growth but may have the opposite effect of increasing tumor growth. Our results underscore a critical need to elucidate the distinct metabolic preferences of different breast cancer subtypes in order to design effective targeted therapies for each subtype.

4.6 Methods

4.6.1 Primary mouse tumors

All animal use was performed in accordance with institutional and federal guidelines. Primary MMTV-Myc EMT and MMTV-Myc papillary tumors were acquired as a gift from Dr. Eran Andrechek and have been previously described [29]. Tumors were sectioned, formalin-fixed, and paraffin embedded for histological examination with hematoxylin and eosin staining. Wild-type EMT and papillary tumors were cryopreserved in a mixture of 90% FBS and 10% DMSO. Tumor derived cell lines were established by mechanical dissociation of primary tumors using scissors, followed by culturing tumor pieces in cell culture media [56].

4.6.2 Metabolic profiling

Unlabeled, targeted metabolomics was performed as previously described [57]. Briefly, cells were seeded in 6-well tissue culture plates at 50,000 cells/well and cultured for 48 hours. Cells were washed with saline (VWR, Radnor, Pennsylvania, 16005-092) and metabolism was quenched by addition of cold methanol. Flash frozen tumor tissue was pulverized using a liquid nitrogen cooled mortar and pestle and cold methanol and water was added to the tissue sample. The tissue samples were further processed using

a Precellys Evolution homogenizer (Bertin Instruments) operating a single 10s cycle at 10000 rpm. Extracts were then transferred to 1.5 ml Eppendorf tubes and cold chloroform was added to each tube and vortexed for 10 minutes at 4°C. The final metabolite extraction solvent ratios were methanol:water:chloroform (5:2:5). The polar phase was collected and dried under a stream of nitrogen gas. The dried metabolites were then resuspended in HPLC-grade water for analysis. LC-MS/MS analysis was performed with ion-pairing reverse phase chromatography using an Ascentis Express column (C18, 5 cm x 2.1 mm, 2.7 µm, MilliporeSigma, 53822-U) and a Waters Xevo TQ-S triple quadrupole mass spectrometer. Mass spectra were acquired using negative mode electrospray ionization operating in multiple reaction monitoring (MRM) mode. Peak processing was performed using MAVEN [58] and data for each sample was normalized to the mean signal intensity for all metabolites in the analysis. Metabolites were grouped by relationship to metabolic pathways. Heatmaps were generated using Cluster 3.0 [59] and exported using Java Treeview [60].

4.6.3 Gene expression analysis

Gene expression data for MMTV-Myc EMT and papillary data was downloaded from GEO using accession number GSE15904. The following EMT CHP datasets were downloaded: GSM399180, GSM399202, GSM399204, GSM399217, GSM399226, GSM399235, GSM399238, GSM399252, and GSM399259. The following papillary CHP datasets were downloaded: GSM399183, GSM399184, GSM399196, GSM399197, GSM399200, GSM399216, GSM399222, GSM399234, GSM399241, and GSM399245. Gene set enrichment analysis [32] was performed by converting gene expression data to the required file formats and using the GSEA software available to download from

www.gsea-msigdb.org/gsea/index.jsp. Reactome [33] metabolism gene sets were identified as all participant and sub-participant gene sets under the Reactome Metabolism pathway (stable identifier R-HSA-1430728) and were downloaded from the MSigDB canonical pathways collection [61]. Differential gene expression was determined using Transcriptome Analysis Console (TAC) 4.0 software. Sample signals and statistical measurements were exported from TAC 4.0 software. Genes measured by multiple probes were individually numbered. Clustering was performed in Cluster 3.0 using log transformed data and genes were clustered using the uncentered correlation similarity metric and average linkage settings [59]. Heatmaps were generated using JavaTreeview [60].

4.6.4 Survival Analysis

Survival curves were generated using KM Plotter for Breast Cancer [34] using probe 209434_s_AT for *PPAT* and 213892_S_AT for *APRT*. Patients were separated by upper and lower tercile of expression using the trichotomization option. Redundant samples were removed and biased arrays were excluded as per the default quality control settings.

4.6.5 Cell lines and culture conditions

EMT and papillary tumor derived cell lines were cultured in Dulbecco's Modified Eagle Medium (DMEM Corning, Corning, New York 10-017-CM) with 25 mM glucose without sodium pyruvate supplemented with 2 mM glutamine (Corning, 25-005-CI) 10% heat-inactivated fetal bovine serum (MilliporeSigma, Burlington Massachusetts, 12306C),

and 1% penicillin and streptomycin (Corning, 30-002-CI). Cells were maintained at 37°C with 5% CO_2.

4.6.6 CRISPR/Cas9

Lentivirus mediated CRISPR/Cas9 genome editing was used to achieve gene knockout. Guide RNAs targeting *APRT* or *PPAT* were designed using the CRISPR-DO web application [62]. Plasmids containing dual guide RNA, puromycin resistance, and Cas9 co-expression were acquired from VectorBuilder. Plasmids containing scramble guide RNA, puromycin resistance, and Cas9 co-expression were also acquired from VectorBuilder. *APRT* KO dual guide RNA sequences are guide A) 5'-GTCGATCTTGCCGCTGTGCG-3' and guide B) 5'-GTGTGCTCATCCGGAAACAG-3'. *PPAT* KO dual guide RNA sequences are guide A) 5'-CATACGAGGTACGCCACCAC-3' and guide B) 5'-TACGCGGTGCGAGATCCATA-3' The non-targeting puromycin-resistant scramble guide RNA sequence is 5'-GCACTACCAGAGCTAACTCA-3'. Lentiviral envelope and packaging plasmids were acquired from addgene. The VSVG plasmid was a gift from Bob Weinberg (Addgene plasmid # 8454; http://n2t.net/addgene:8454; RRID:Addgene 8454). The psPAX2 plasmid was a gift from Didier Trono (Addgene plasmid # 12260; http://n2t.net/addgene:12260; RRID:Addgene 12260). To produce lentivirus, HEK293T cells seeded in 10-cm plates were transfected using lipofectamine 3000 (ThermoFisher Scientific, L3000015) with 10.0 µg lentivirus plasmids, 0.5 µg VSVG, and 5.0 µg psPAX2 plasmids. The following morning, fresh DMEM with 15% FBS and 1% P/S was added, and cells were grown for another 48 h to generate virus. For transduction with lentivirus, the recipient EMT and papillary cells were seeded in 10-cm plates and the supernatant of transfected HEK293T was collected and passed through 0.45 um PVDF

syringe filter. 5 ml of the viral supernatant and 5 ml of fresh media were added to recipient cell plates with polybrene (Fisher Scientific, TR1003G) at a final concentration of 4 μg/ml. The cells were cultured for 24 h followed by addition of fresh DMEM medium supplemented with 10% FBS and treatment for 10 days with 2 μg/ml puromycin for selection. After transduction, cell culture media was supplemented with 50 uM nucleosides (adenosine, cytidine, guanosine, inosine, thymidine, and uridine) in DMSO across all conditions to provide extracellular nucleotides for cells with deficient *de novo* biosynthesis. The puromycin selected cells were then resuspended to a concentration of 5 cells/ml and seeded 1 cell/well on 96-well plates. Surviving clones were expanded and analyzed for successful gene knockout. Genomic DNA was extracted using DNeasy Blood and Tissue Kit (Qiagen) to check for successful gene editing. The following primer pairs were used for PCR expansion and sequencing (marked with *) of *APRT* guide A: 5'-GGGTCACTCTCCTGTCCTTG-3' and 5'-AGGACAGAGCAGAGTTCGTC-3'*, *APRT* guide B: 5'-GAGCTGTTCAGAAGGCAGGT-3'* and 5'-AGCGTTTCTGGGTGGTGTAA-3', *PPAT* guide A: 5'-CTCAGGACGGTCAAGGCTAC-3'* and 5'-AAGATGCCTTTTGTCGGAGA-3', and *PPAT* guide B: 5'-GCATACACCCCTCCTCAAGA-3'* and 5'-CATCAGAGACTGGCATAAGACG-3'. Tracking of Indels by Decomposition (TIDE) was used to evaluate successful gene editing [35].

4.6.7 Western blot analysis

Cell lysis and Western blot analysis were carried out according to standard protocols. The following dilutions of primary commercial antibodies were used as probes: 1:250 dilution of anti-APRT (Thermo Scientific, PA576741), 1:500 dilution of anti-PPAT

(Proteintech 15401-1-AP), 1:1000 dilution of anti-vinculin (Cell Signaling Technology, E1E9V). Anti-APRT and anti-vinculin antibodies were diluted in 5% bovine serum albumin and incubated overnight at 4 °C. The anti-PPAT antibody was diluted in 5% milk and incubated for 60 minutes at room temperature per manufacturer recommendations. Secondary anti-rabbit antibodies (Cell Signaling Technology, 7074S) were diluted in 5% non-fat milk at a dilution of 1:1000 and incubated at room temperature for 1 h. Blots were imaged by chemiluminescence after incubation with Clarity Western ECL substrate (Bio-Rad, 1705061) using a ChemiDoc Imaging system (Bio-Rad).

4.6.8 Isotope labeling studies

For isotope labeling experiments, DMEM without glucose or glutamine was prepared from powder (MilliporeSigma, D5030) and supplemented with $^{13}C_6$-glucose (Cambridge Isotope Laboratories, Tewksbury, Massachusetts, CLM-1396) and unlabeled glutamine (MilliporeSigma, G8540). Labeled media was prepared with 10% dialyzed FBS (Sigma-Aldrich, F0392). Cells were then seeded and cultured as described above. Fresh cell culture media without nucleoside supplementation was added to cells for 1 hour prior to switching to isotope containing media. Prior to metabolite extraction, media was switched to isotope containing media and samples were collected at T = 240 minutes. Metabolite extraction and analysis were performed as above. Labeling data was corrected for natural isotope abundance using IsoCor [63].

4.6.9 In vivo tumor studies

To generate tumors, monoclonal KO cell lines were injected in 50 µl of a 1:1 mixture of DMEM:Matrigel (Corning, 354262) at 500,000 cells/50 µl into the fourth

mammary fat pad of syngeneic 6 to 8 week old FVB mice. The resulting tumors grew to a size of 15 mm as measured by external calipers along the longest axis, at which time the tumors were harvested and fragmented into 3 mm pieces that were cryopreserved in a mixture of 90% FBS and 10% DMSO. Cryopreserved tumors were then thawed, washed in saline, and cut into 1-2mm fragments for implantation into the fourth mammary fat pad of recipient mice. These re-implanted tumors were then measured by external caliper 3 times weekly starting at 7 days post implantation until the experimental endpoint at 24 days post implantation. Tumor size was calculated as cross-sectional area using measurements from the longest and shortest axes. Mice were monitored for humane endpoints throughout the experiment according to institutional guidelines. At 24 days the tumors were collected, and a cross section of each tumor was formalin fixed for histological preparation.

4.6.10 Histological analyses

All histological preparation and immunohistochemical staining was performed by the Investigative HistoPathology Laboratory at Michigan State University. Ki67 staining was measured using multiple images taken from distinct, non-necrotic regions of each tumor and evaluated as follows. For each tumor, at least 4 color images from distinct regions were acquired using an Olympus BX41 microscope operated at 10x magnification and saved as TIFF image files. Image processing was performed in ImageJ 1.52p (Fiji distribution). The color images were first deconvoluted into H (hematoxylin) and DAB (diaminobenzidine) color channels using Color Deconvolution (‘H DAB’ deconvolution matrix). Deconvoluted H and DAB images were saved as new TIFF images. For each image, smoothing was applied 5 times, then Auto Local Threshold was performed using

Bernsen's algorithm (window size 15, contrast threshold 15) to detect stained nuclei. Stained nuclei were counted using Analyze Particles (minimum size 150, minimum circularity 0.3). The above steps were looped over all images. To check that threshold parameters were appropriate, several output images were manually inspected to confirm that visually identifiable nuclei were properly counted. The percent Ki67 + nuclei was calculated as the ratio of DAB-stained nuclei counts (representing proliferating cells) to H-stained nuclei counts (representing all cells) for each image, and averaged across all images for each experimental group. TUNEL assays were evaluated using a single image of the full tumor cross section to determine the proportion of necrotic area to non-necrotic area of each tumor. Images were acquired using a Leica M165FC stereo microscope operated at 1x magnification and saved as TIFF image files. TUNEL assay images were also processed using ImageJ. Images were duplicated and color thresholding was used to select either the TUNEL + area (image 1) or the entire tumor area (image 2). The percent TUNEL + area was calculated as the ratio of image 1 area to image 2 area for each tumor and averaged across all tumors within each experimental group.

4.6.11 Statistical analyses

Statistical analyses were performed using unpaired Student's t-test except where otherwise noted. *p* values were adjusted in R using the p.adjust() function to account for multiple hypothesis testing using the Benjamini-Hochberg procedure (metabolites) or Hommel procedure (tumor measurements). All error bars presented are standard deviation. All figures except survival curves and heatmaps were generated using GraphPad Prism.

4.7 Acknowledgments

The authors thank Deanna Broadwater, Elliot Ensink, and Hyllana Medeiros for helpful discussions and critical reading of this manuscript. The authors thank Eran Andrechek for providing primary MMTV-Myc EMT and MMTV-Myc papillary tumors. The authors also thank the MSU Mass Spectrometry and Metabolomics Core and the MSU Investigative HistoPathology Laboratory.

4.8 APPENDIX

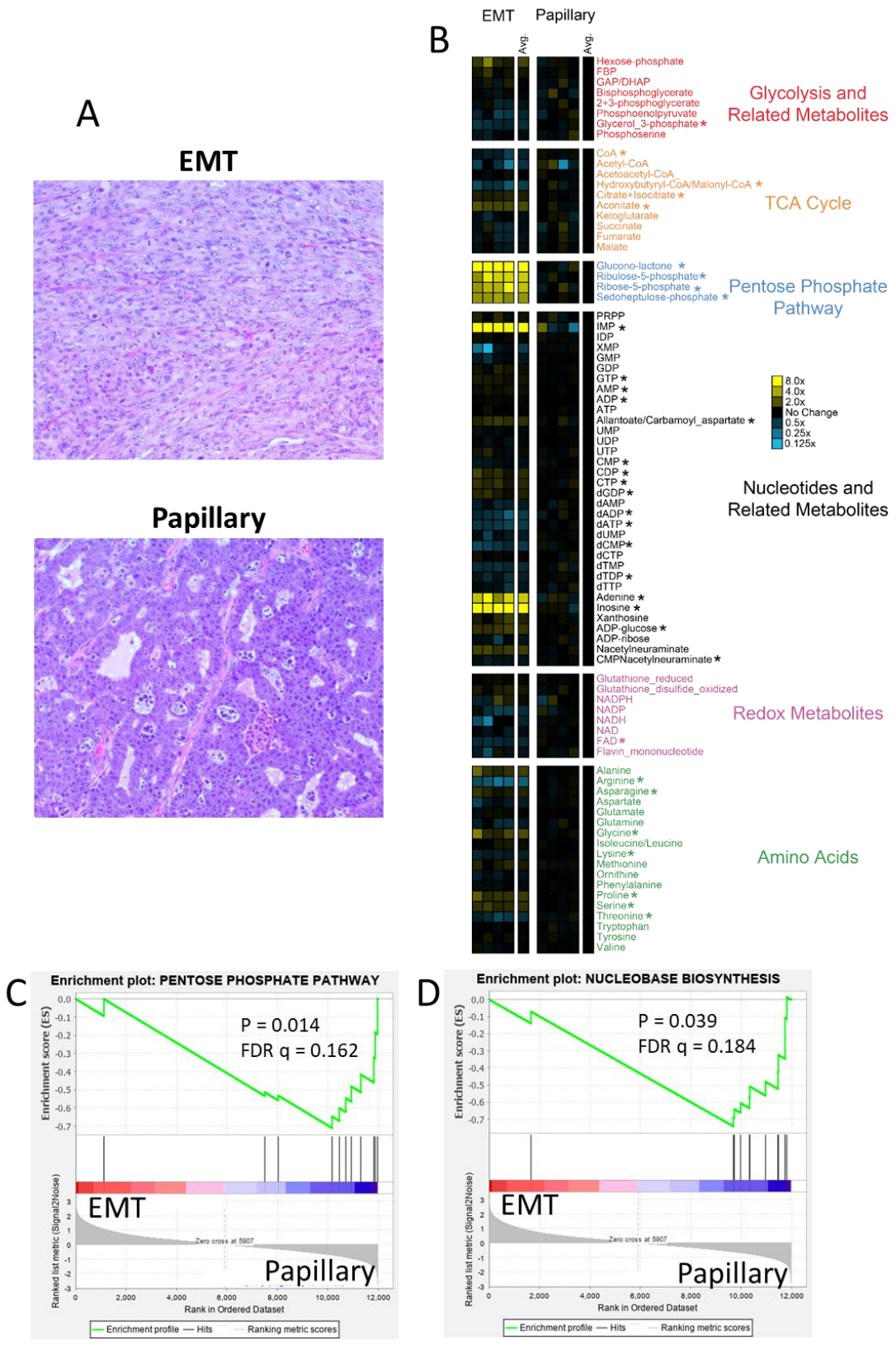

Figure 4.1 Metabolic profiles and gene expression patterns indicate differences in nucleotide metabolism between subtypes of MMTV-Myc EMT and papillary tumors.

Figure 4.1 (cont'd)
(**A**) Representative histology images of the EMT and papillary tumor subtypes. (**B**) Heatmap indicating relative metabolite differences between EMT and papillary tumors. Yellow and blue boxes indicate increased or decreased metabolite levels relative to the average of the papillary subtype, respectively. Metabolites with statistically significant differences (p-value < 0.05) are bolded and marked with asterisks (*) Statistical comparisons are listed in **Table S1**. (**C**) Gene set enrichment analysis for pentose phosphate pathway genes are significantly enriched (p-value = 0.014, FDR q-value = 0.16) for low expression in EMT tumors vs. papillary tumors. (**D**) Gene set enrichment analysis for genes involved in nucleobase biosynthesis are significantly enriched (p-value = 0.039, FDR q-value = 0.18) for low expression in EMT tumors vs. papillary tumors.

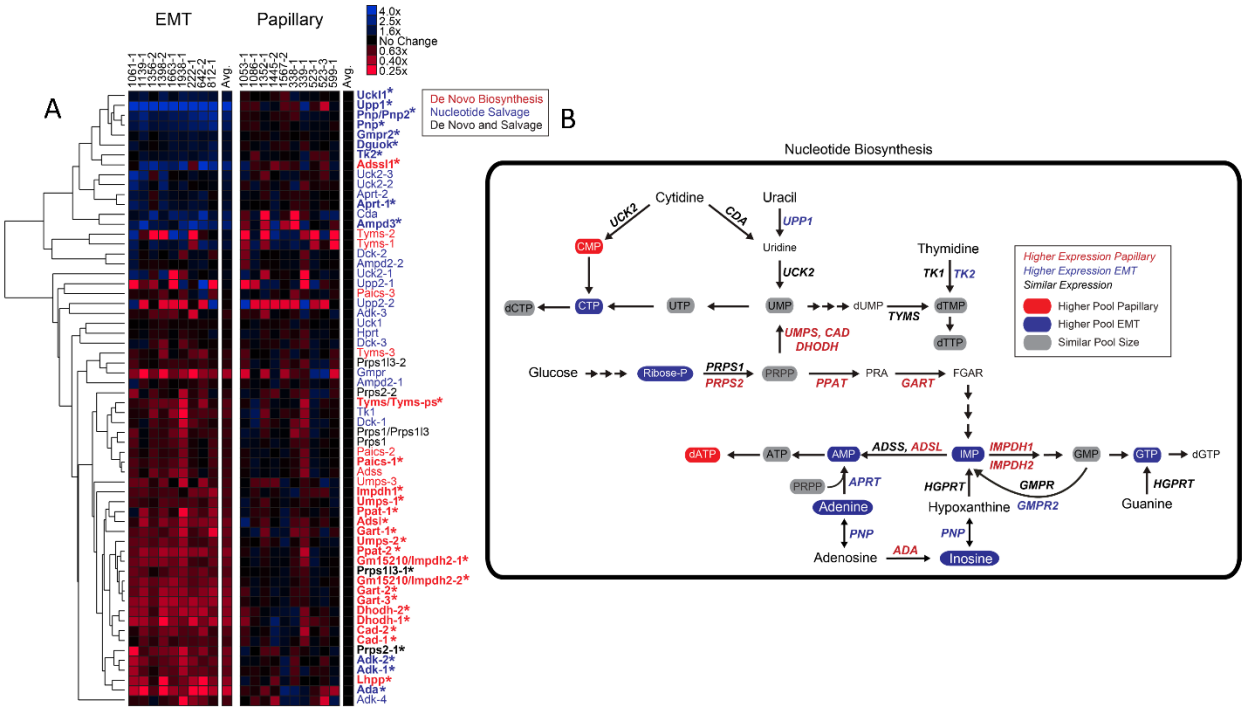

Figure 4.2 Expression of nucleotide salvage genes is higher in the EMT subtype and expression of *de novo* biosynthesis genes is higher in the papillary subtype. (**A**) Heatmap depicting expression of genes related to nucleotide metabolism. Genes are sorted by hierarchical clustering and color-coded by relationship to nucleotide metabolism pathways. Genes with statistically significant differences (FDR p-value < 0.05) are marked with asterisks (*) Statistical comparisons are listed in **Table S2**. (**B**) Summary of nucleotide biosynthesis pathway. Metabolic intermediates and genes are marked according to subtype-specific relationships.

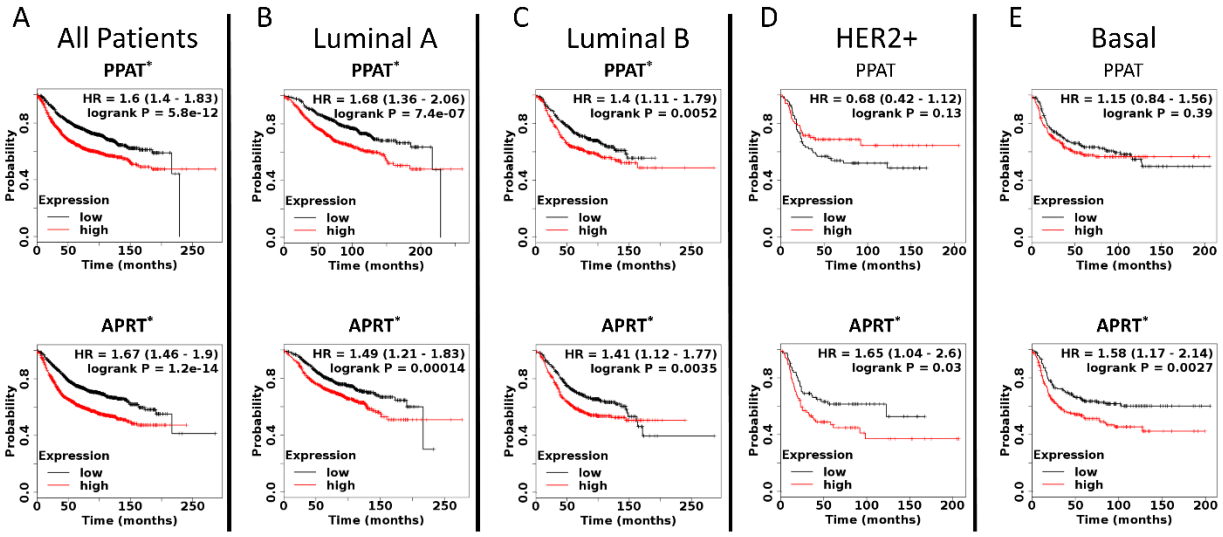

Figure 4.3 Expression of *de novo* nucleotide biosynthesis gene *PPAT* and nucleotide salvage gene *APRT* are strongly associated with relapse-free survival across breast cancer subtypes. Kaplan-Meier survival curves for (**A**) all breast cancer patients, and (**B-E**) specific breast cancer subtypes. Statistically significant relationships (p-value < 0.05) are bolded and marked with asterisks (*).

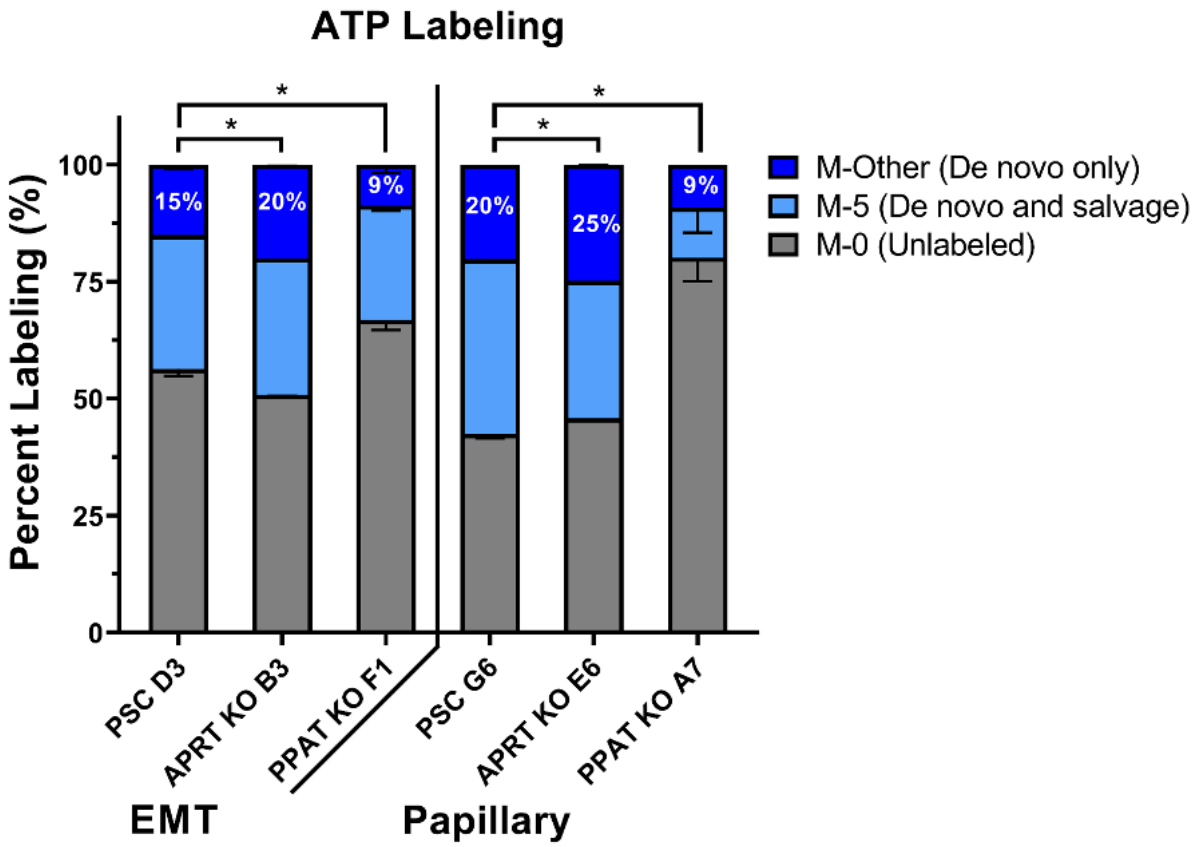

Figure 4.4 ^{13}C-Isotope incorporation from glucose into ATP biosynthesis is altered after targeting *de novo* and salvage genes. Grey boxes represent the unlabeled (M-0 isotopologue) proportion of ATP. Light blue boxes represent the M-5 isotopologue, which can be derived from either *de novo* or salvage pathways. Dark blue boxes represent the sum of all other isotopologues of ATP (M1-4 and M6-10), which are derived from *de novo* ATP biosynthesis. Data are displayed as means ± S.D., N = 3 (*p-value < 0.05). Statistical comparisons are listed in **Tables S3-S4**.

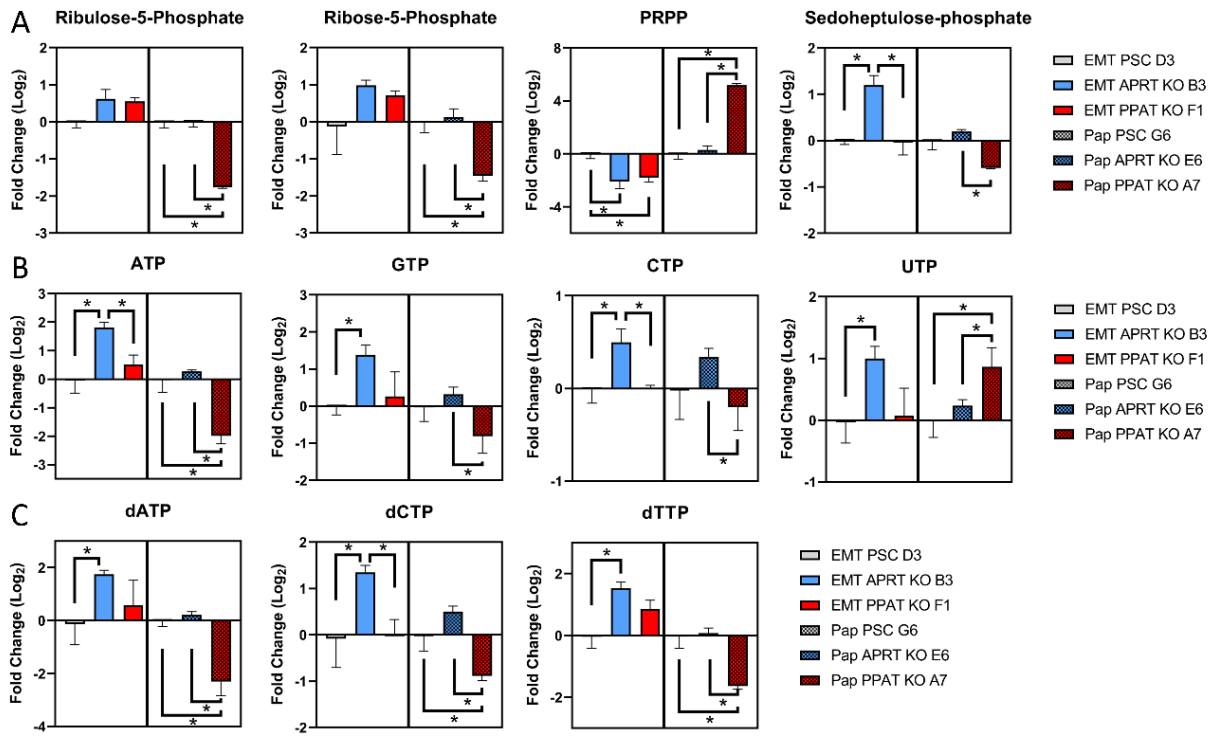

Figure 4.5 Metabolite levels are most affected by targeting the preferred nucleotide biosynthetic pathway for each subtype. The abundance of (**A**) metabolites related to the pentose phosphate pathway and (**B-C**) nucleotides are most altered within each subtype when APRT is knocked out in EMT (left half of each graph) and when PPAT is knocked out in papillary (right half of each graph). Data are displayed relative to the control for each subtype and represent means ± S.D., N = 3 (*p-value < 0.05). Statistical comparisons are listed in **Tables S5-S6**.

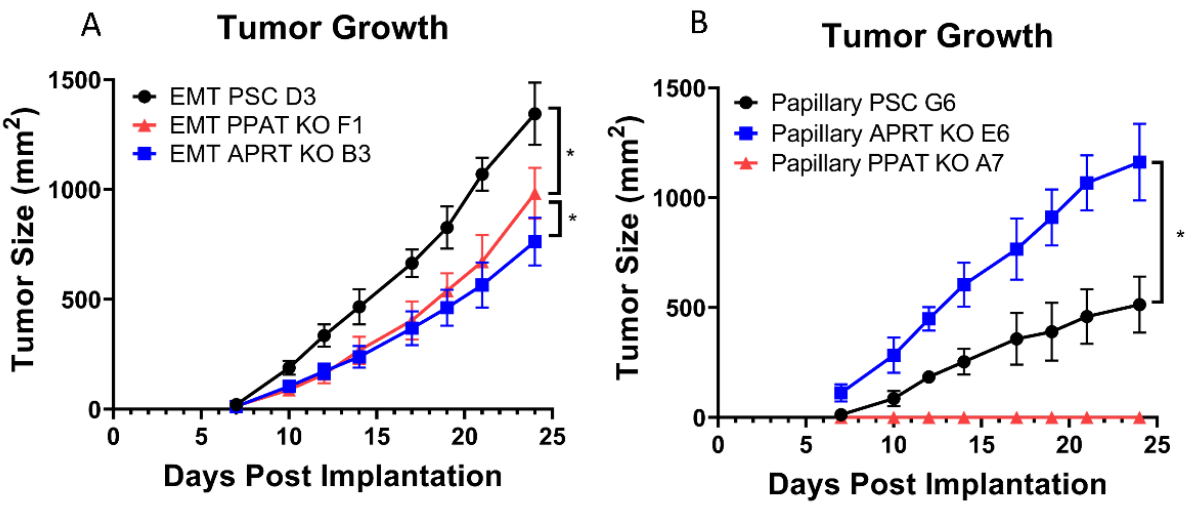

Figure 4.6 Tumor growth for each subtype is decreased after knocking out the preferred nucleotide metabolism pathway. In vivo growth curves for (A) EMT and (B) papillary tumors. Data are displayed as means ± S.D. (*p-value < 0.05). Statistical comparisons are listed in Tables S7-S8.

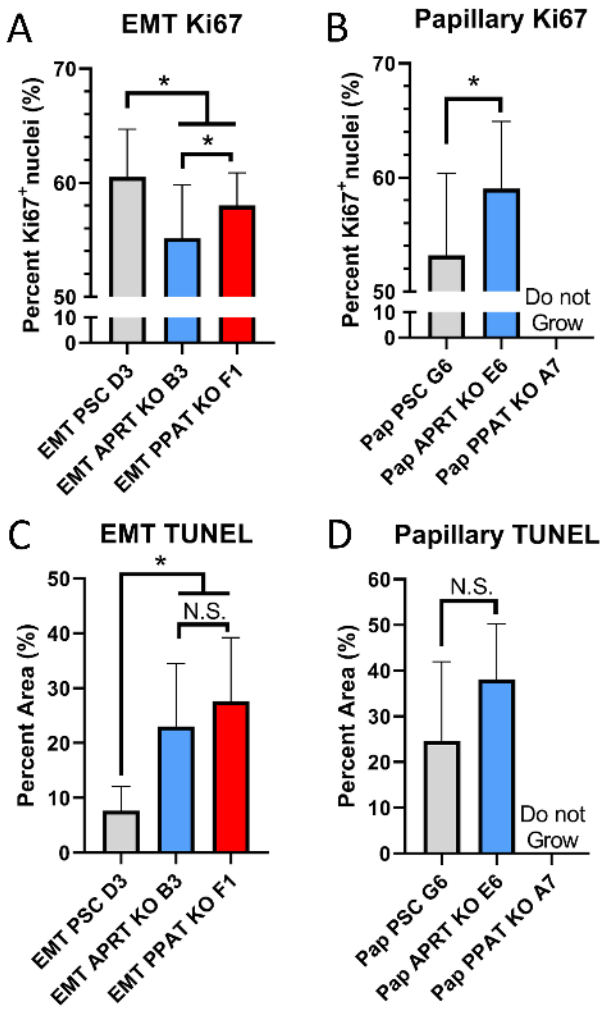

Figure 4.7 IHC analysis reveals decreased proliferation in slower growing tumors. IHC analysis for Ki67 staining in (A) EMT and (B) papillary tumors as well as TUNEL assay for (C) EMT and (D) papillary tumors. Data are displayed as means ± S.D. (*p-value < 0.05). Statistical comparisons are listed in **Tables S9-S12**.

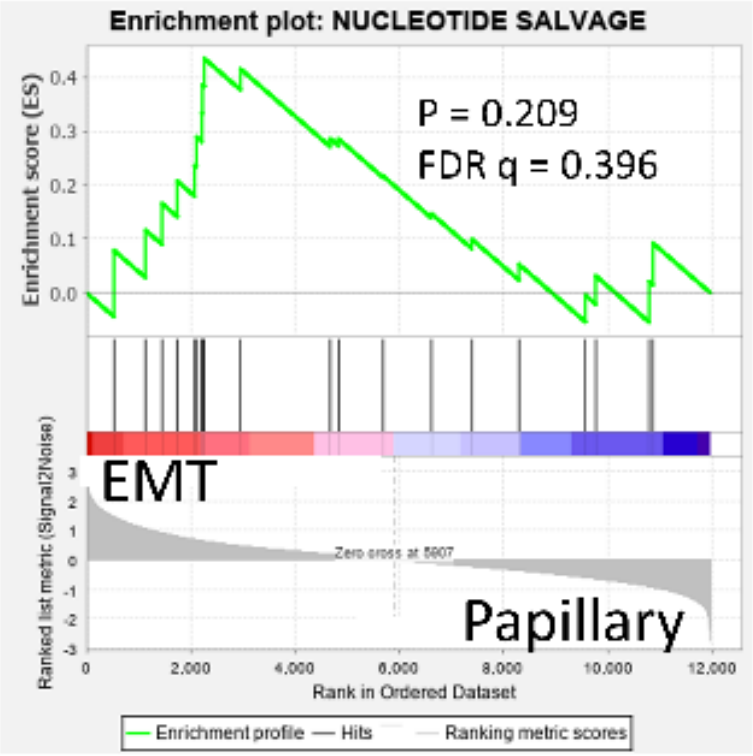

Figure S4.1 Gene set enrichment analysis for nucleotide salvage genes. GSEA for nucleotide salvage genes are not significantly enriched in the EMT subtype.

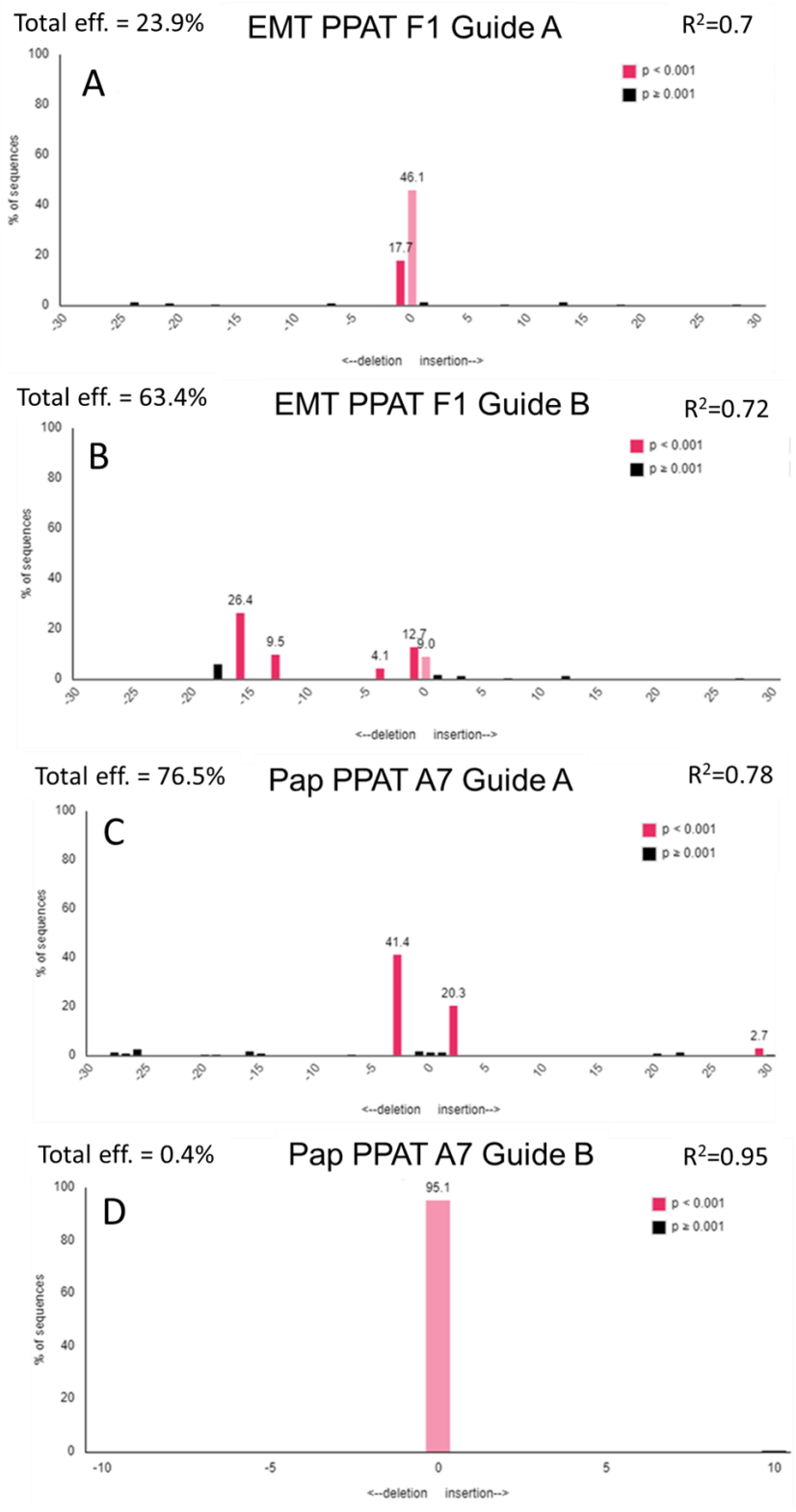

Figure S4.2 Gene editing verification of PPAT gene. Sequencing of PPAT KO cell lines was validated using TIDE analysis. Pink bars denote insertion/deletion events with high confidence ($p < 0.001$) for EMT PPAT KO clone F1 in (A) guide A and (B) guide B and for papillary PPAT KO clone A7 in (C) guide A and (D) guide B.

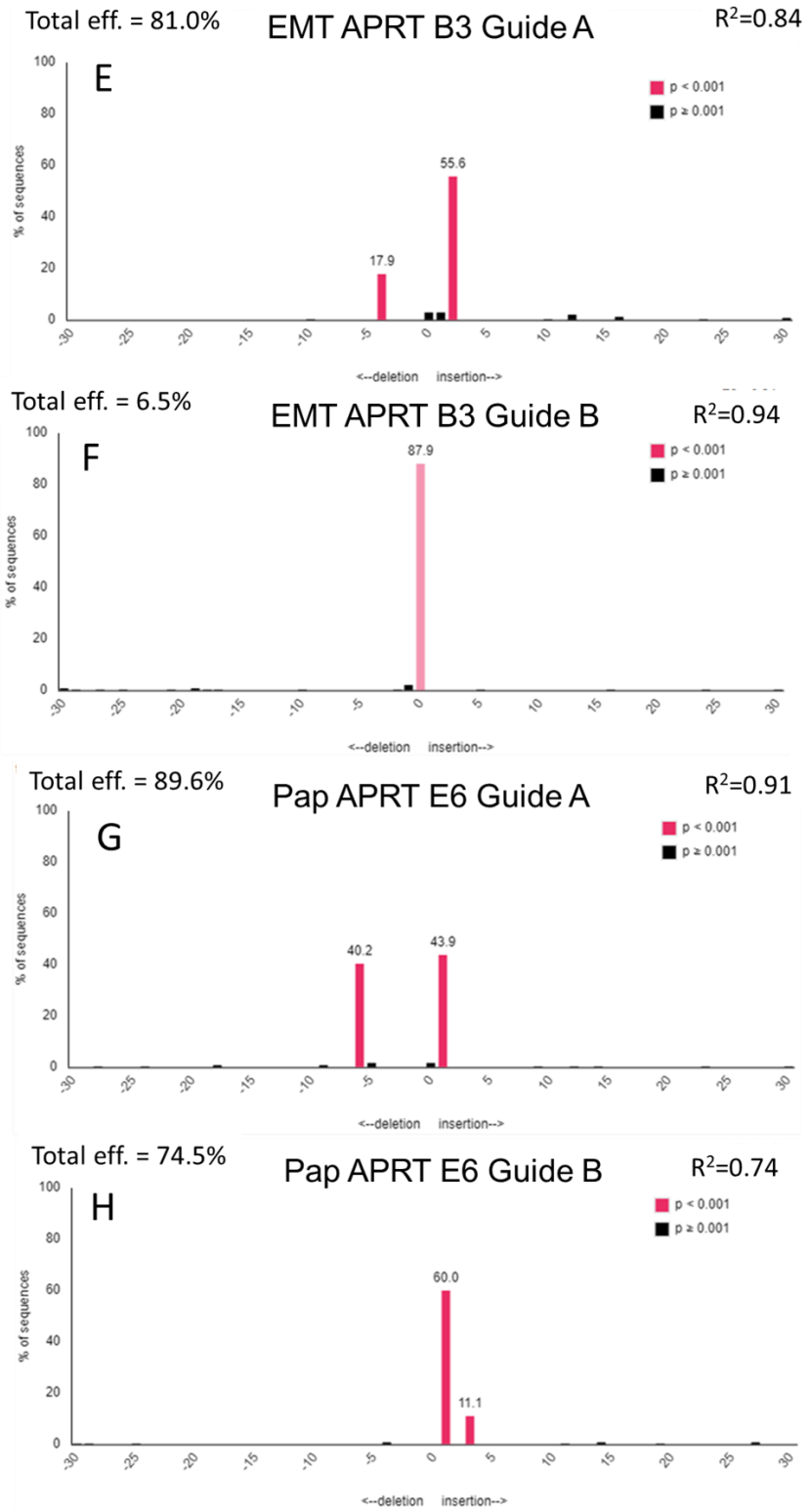

Figure S4.3 Gene editing verification of APRT gene. Sequencing of APRT KO cell lines was validated using TIDE analysis. Pink bars denote insertion/deletion events with high confidence (p <0.001) for EMT APRT KO clone B3 in (A) guide A and (B) guide B and for papillary APRT KO clone E6 in (C) guide A and (B) guide B.

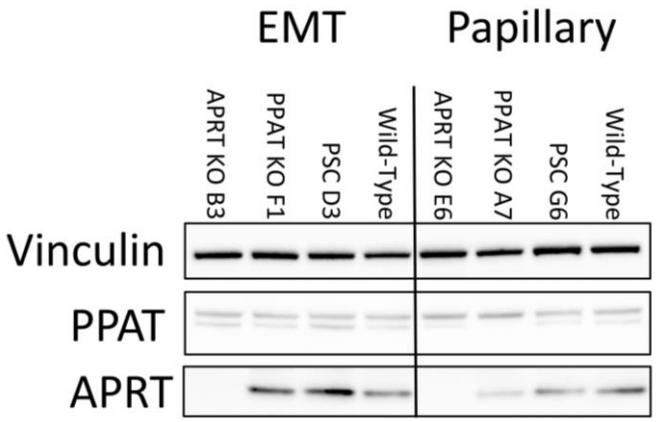

Figure S4.4 Protein level verification of KO cell lines. Western blotting was used to verify protein levels of clonal EMT lines APRT KO B3, PPAT KO F1, PSC D3, and the wild-type line. Protein levels of clonal papillary line APRT KO E6, PPAT KO A7, PSC G6, and the wild-type line were also verified.

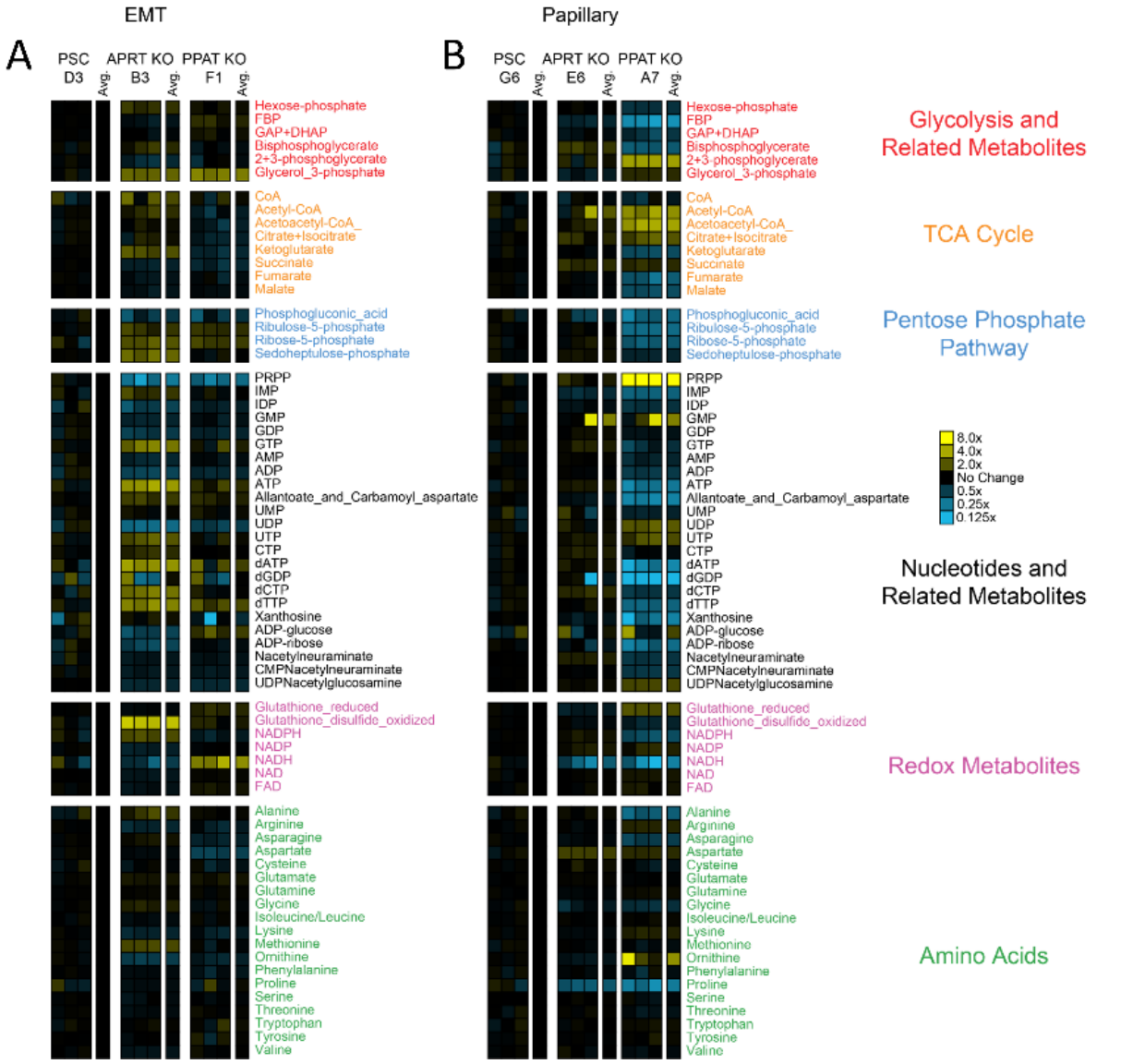

Figure S4.5 Full metabolic profiles of control and KO cell lines. Heatmap indicating relative metabolite differences between control and KO cell lines in the (A) EMT and (B) papillary subtypes. Boxes indicate metabolite levels relative to the average of the PSC control for each subtype. Statistical comparisons are listed in **Tables S5-S6**.

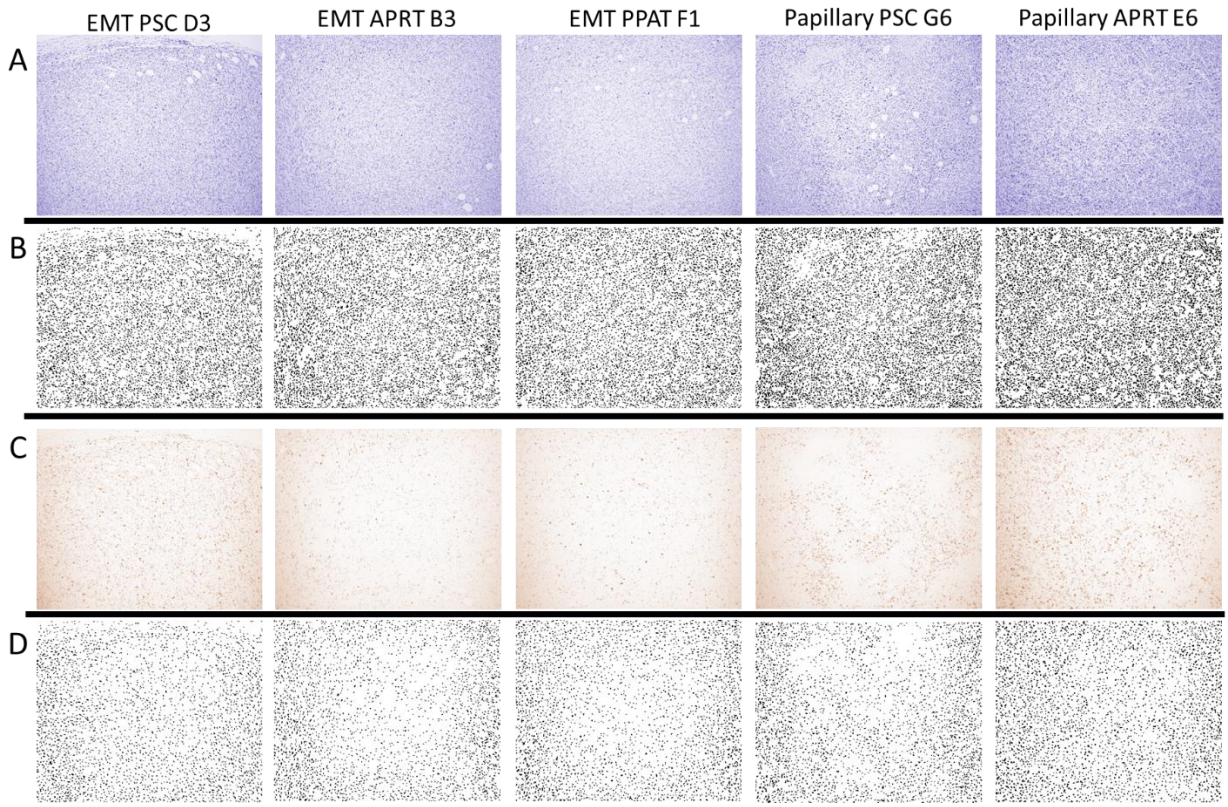

Figure S4.6 Representative Ki67 staining for EMT and papillary tumors. (A) Color deconvoluted image showing H staining and (B) color threshold image showing all nuclei as black dots. (C) Color deconvoluted image showing DAB staining and (D) color threshold image showing all Ki67 + nuclei as black dots were used to calculate the percent Ki67 + nuclei shown in **Figure 4.7 A-B**.

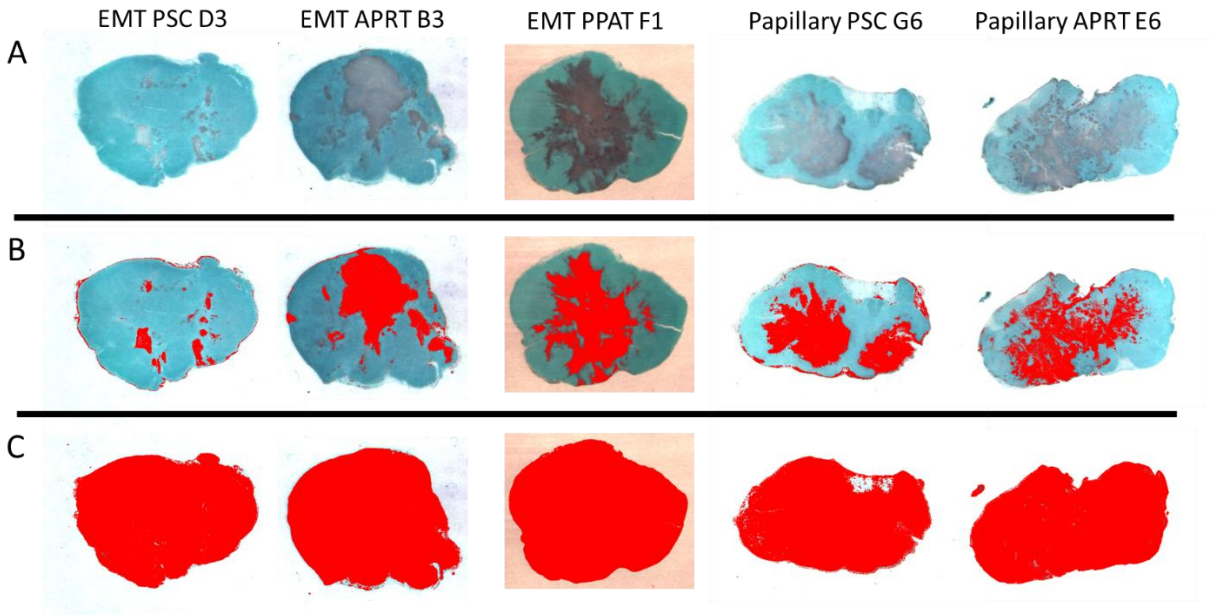

Figure S4.7 Representative TUNEL assay for EMT and papillary tumors. (A) Initial cross sectional image of EMT and papillary control and knock out tumors after TUNEL assay. Images with (B) TUNEL + area highlighted, and (C) full tumor area were used to calculate the percent area of TUNEL staining shown in **Figure 4.7 C-D**.

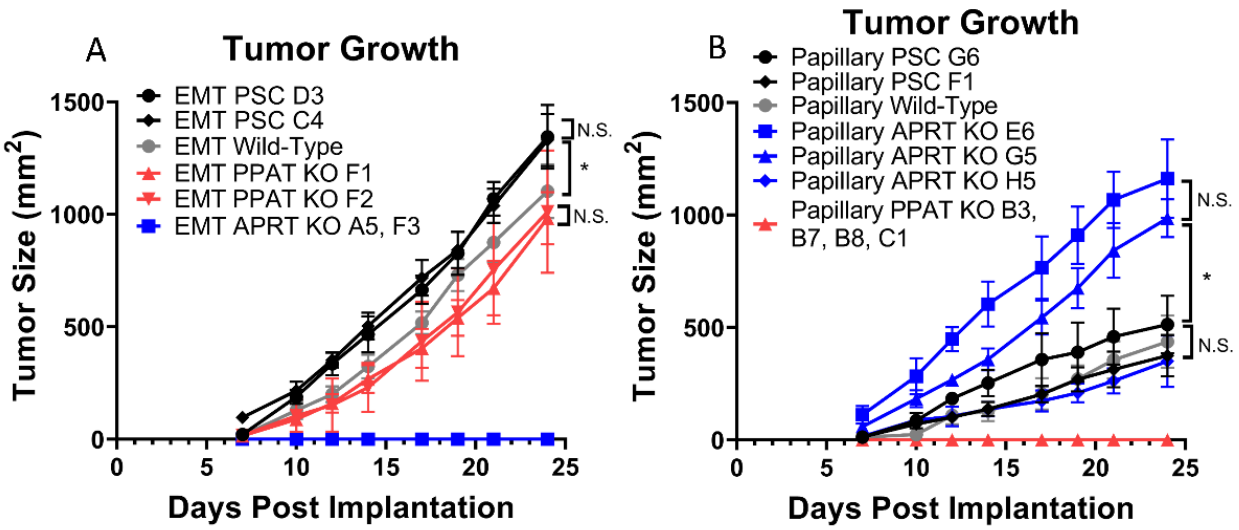

Figure S4.8 Tumor growth of additional clones. In vivo growth curves for (A) EMT and (B) papillary tumors. Data are displayed as means ± S.D. (*p-value < 0.05). Statistical comparisons are listed in **Tables S7-S8**.

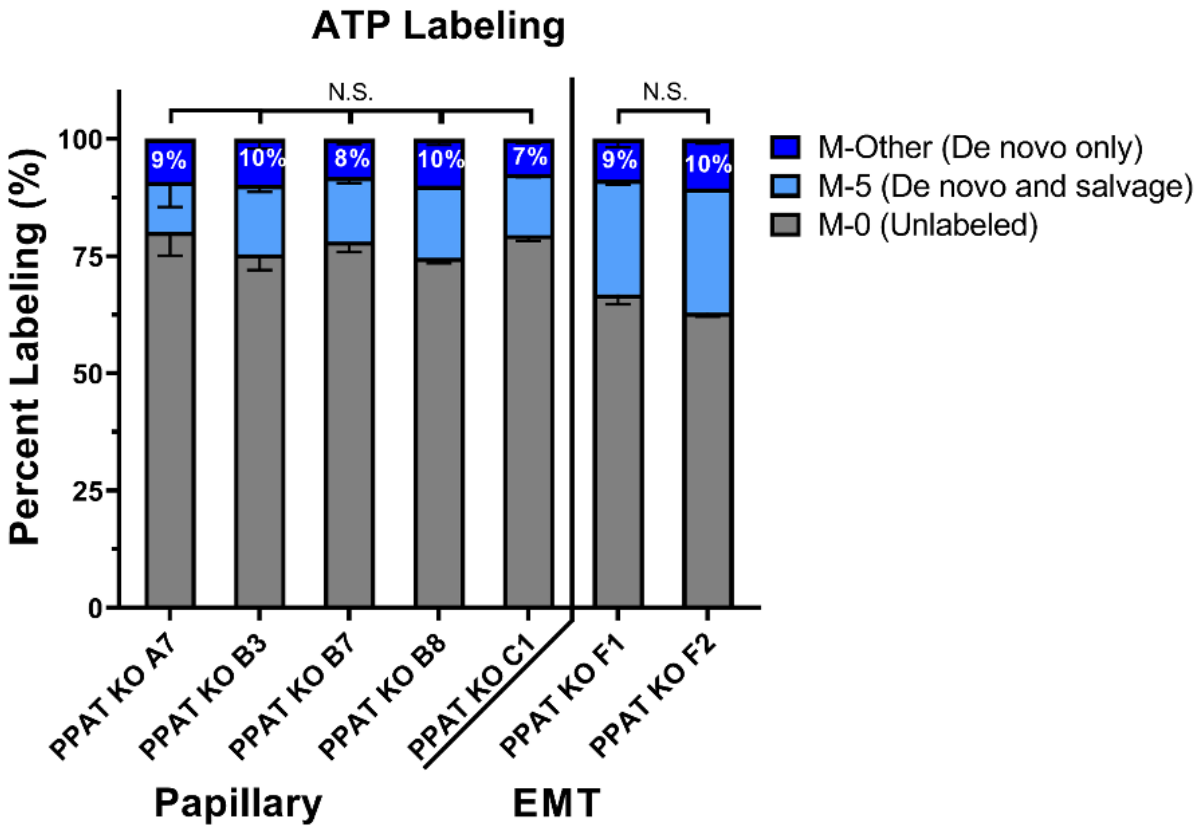

Figure S4.9 ^{13}C-Isotope incorporation from glucose into ATP biosynthesis in additional PPAT KO clones. Grey boxes represent the unlabeled (M-0 isotopologue) proportion of ATP. Light blue boxes represent the M-5 isotopologue, which can be derived from either *de novo* or salvage pathways. Dark blue boxes represent the sum of all other isotopologues of ATP (M1-4 and M6-10), which are derived from *de novo* ATP biosynthesis. Statistical comparisons are listed in **Tables S13-S14**.

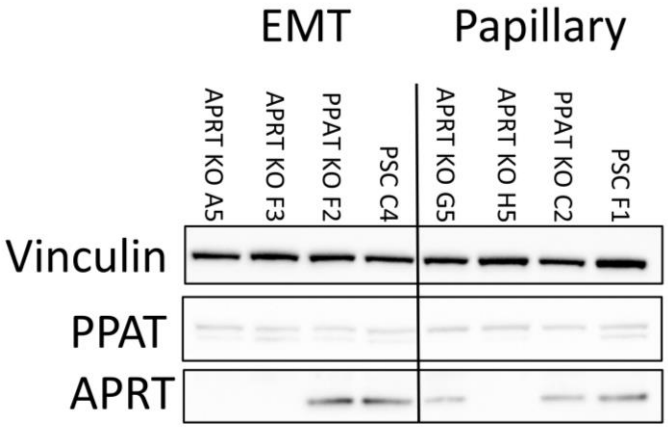

Figure S4.10 Protein level verification of additional KO cell lines. Western blotting was used to verify protein levels of clonal EMT lines APRT KO A5, APRT KO F2, PPAT KO F2, and PSC C4. Protein levels of clonal papillary line APRT KO G5, APRT KO H5, PPAT KO C2, and PSC F1 were also verified.

Metabolite	EMT Wild-Type Average (Log2 Fold Change)	EMT Wild-Type STDEV	Papillary Wild-Type Average (Log2 Fold Change)	Papillary Wild-Type STDEV	Raw P values	Adjusted P values
2+3-phosphoglycerate	-0.3	0.4	0.0	0.3	2.56E-01	3.35E-01
Acetoacetyl-CoA_	0.0	0.1	0.0	0.2	9.65E-01	9.77E-01
Acetyl-CoA	-1.0	0.8	-0.4	1.4	4.83E-01	5.35E-01
Aconitate	0.9	0.1	0.0	0.3	6.81E-04	3.92E-03
Adenine	2.3	0.5	-0.1	0.6	7.65E-04	3.92E-03
ADP	0.1	0.0	0.0	0.0	3.03E-04	2.26E-03
ADP-glucose	0.6	0.1	0.0	0.1	1.74E-04	1.43E-03
ADP-ribose	-0.4	0.4	0.0	0.2	1.47E-01	2.19E-01
Alanine	0.7	0.4	0.0	0.1	**2.57E-02**	**5.54E-02**
Allantoate_and_Carbamoyl_aspartate	0.6	0.1	0.0	0.3	1.12E-02	3.07E-02
AMP	0.2	0.1	0.0	0.1	2.71E-03	1.06E-02
Arginine	-1.6	0.3	0.0	0.1	9.43E-05	1.07E-03
Asparagine	0.4	0.2	0.0	0.2	1.30E-02	3.44E-02
Aspartate	-0.5	0.4	0.0	0.1	4.55E-02	8.74E-02
ATP	0.1	0.1	0.0	0.1	4.23E-01	4.95E-01
Bisphosphoglycerate	-0.1	0.2	-0.1	0.6	9.94E-01	9.94E-01
CDP	0.5	0.3	0.0	0.1	1.04E-02	2.94E-02
Citrate+Isocitrate	0.4	0.0	0.0	0.1	9.72E-04	4.69E-03
CMP	-0.3	0.1	0.0	0.1	2.12E-02	4.97E-02
CMPNacetylneuraminate	-0.4	0.1	0.0	0.2	9.27E-03	2.87E-02
CoA	-0.6	0.3	0.0	0.2	2.12E-02	4.97E-02
CTP	0.5	0.2	0.0	0.3	1.88E-02	4.73E-02
dADP	-1.0	0.4	0.0	0.3	9.46E-03	2.87E-02
dAMP	-0.5	0.2	0.0	0.3	3.26E-02	6.86E-02
dATP	-1.0	0.1	0.0	0.1	5.37E-05	1.07E-03
dCMP	-1.0	0.2	0.0	0.2	1.04E-03	4.72E-03
dCTP	0.1	0.1	0.0	0.2	4.60E-01	5.24E-01
dGDP	0.4	0.2	0.0	0.1	1.04E-02	2.94E-02
dTDP	-0.5	0.2	0.0	0.1	8.27E-03	2.71E-02
dTMP	-0.7	0.1	0.0	0.3	**2.36E-02**	**5.23E-02**
dTTP	-0.4	0.3	0.0	0.3	1.77E-01	2.53E-01
dUMP	-0.5	0.4	0.0	0.1	6.53E-02	1.16E-01
FAD	-0.7	0.1	0.0	0.1	9.43E-05	1.07E-03
FBP	0.3	0.3	0.0	0.2	1.88E-01	2.61E-01
Flavin_mononucleotide	-0.4	0.6	0.0	0.3	2.80E-01	3.59E-01
Fumarate	-0.4	0.3	0.0	0.3	1.79E-01	2.53E-01
GAP+DHAP	0.0	0.4	0.0	0.4	8.73E-01	8.95E-01
GDP	0.2	0.2	0.0	0.1	1.93E-01	2.64E-01
Glucono-lactone	3.2	0.1	0.0	0.4	6.40E-06	2.62E-04
Glutamate	0.0	0.2	0.0	0.0	**7.80E-01**	**8.20E-01**
Glutamine	-0.5	0.4	0.0	0.2	6.77E-02	1.18E-01

Table S4.1 Metabolite abundance with statistical significance for Figure 4.1B. Data presented relative to the average of the papillary subtype as depicted in Figure 4.1B. Data represent means and S.D. of 4 replicates. Bold values indicate Welch's t-test was used. Highlighted values are statistically significant with adjusted p value < 0.05

Table S4.1 (cont'd)

Glutathione_disulfide_oxidized	0.3	0.1	0.0	0.2	5.95E-02	1.08E-01
Glutathione_reduced	0.1	0.1	0.0	0.1	1.24E-01	1.91E-01
Glycerol_3-phosphate	-0.7	0.1	0.0	0.2	7.50E-04	3.92E-03
Glycine	0.8	0.5	0.0	0.2	1.90E-02	4.73E-02
GMP	-0.4	0.3	0.0	0.0	**8.21E-02**	**1.35E-01**
GTP	0.3	0.1	0.0	0.1	4.84E-03	1.80E-02
Hexose-phosphate	0.8	0.6	0.0	0.3	5.05E-02	9.41E-02
Hydroxybutyryl-CoA+Malonyl-CoA	-1.1	0.3	0.0	0.3	5.16E-03	1.84E-02
IDP	0.1	0.1	0.0	0.2	2.96E-01	3.67E-01
IMP	3.2	0.5	-0.5	1.3	2.20E-03	9.47E-03
Inosine	3.2	0.3	-0.1	0.5	3.60E-05	9.84E-04
Isoleucine/Leucine	0.1	0.2	0.0	0.1	2.95E-01	3.67E-01
Ketoglutarate	-0.3	0.3	0.0	0.4	3.83E-01	4.64E-01
Lysine	-0.5	0.1	0.0	0.1	1.05E-04	1.07E-03
Malate	-0.3	0.2	0.0	0.2	1.26E-01	1.91E-01
Methionine	0.3	0.2	0.0	0.2	8.09E-02	1.35E-01
Nacetylneuraminate	0.7	0.1	0.0	0.2	5.21E-04	3.56E-03
NAD	-0.2	0.2	0.0	0.1	1.00E-01	1.62E-01
NADH	-0.9	1.1	0.0	0.1	**1.99E-01**	**2.67E-01**
NADP	-0.8	0.4	0.0	0.4	3.54E-02	7.26E-02
NADPH	0.0	0.7	-0.1	0.6	8.19E-01	8.50E-01
Ornithine	-0.3	0.2	0.0	0.1	2.31E-02	5.23E-02
Phenylalanine	-0.2	0.1	0.0	0.1	4.58E-02	8.74E-02
Phosphoenolpyruvate	-0.7	0.4	0.0	0.4	7.93E-02	1.35E-01
Phosphoserine	-0.2	0.3	0.0	0.4	4.29E-01	4.96E-01
Proline	0.7	0.3	0.0	0.1	2.62E-03	1.06E-02
PRPP	0.2	0.3	0.0	0.3	3.85E-01	4.64E-01
Ribose-5-phosphate	2.2	0.5	-0.1	0.5	5.87E-04	3.70E-03
Ribulose-5-phosphate	2.4	0.5	0.0	0.3	1.55E-04	1.41E-03
Sedoheptulose-phosphate	1.8	0.1	0.0	0.1	2.10E-06	1.72E-04
Serine	0.6	0.1	0.0	0.1	8.49E-05	1.07E-03
Succinate	-0.3	0.5	-0.1	0.5	5.81E-01	6.27E-01
Threonine	-0.8	0.3	0.0	0.2	5.68E-03	1.94E-02
Tryptophan	-0.1	0.1	0.0	0.2	7.08E-01	7.54E-01
Tyrosine	0.1	0.2	0.0	0.1	5.08E-01	5.55E-01
UDP	-0.1	0.2	0.0	0.1	2.58E-01	3.35E-01
UMP	-0.2	0.1	0.0	0.1	3.99E-02	7.97E-02
UTP	0.1	0.3	0.0	0.2	4.08E-01	4.85E-01
Valine	-0.1	0.2	0.0	0.1	4.69E-01	5.27E-01
Xanthosine	0.4	0.4	0.0	0.2	1.03E-01	1.63E-01
XMP	-1.6	1.8	0.0	0.2	**1.71E-01**	**2.50E-01**

Summary Data from Transcriptome Analysis Console						
ProbeID	Gene Symbol	EMT Avg (log2)	Papillary Avg (log2)	Fold Change	P-val	FDR P-val
1448562_at	Upp1	10.04	5.86	18.1	5.17E-08	3.68E-06
1422974_at	Nt5e	8.43	5.18	9.51	9.49E-06	1.00E-04
1422184_a_at	Ak1-2	10.78	8.06	6.59	1.38E-11	3.89E-08
1436291_a_at	Dpys-3	4.31	2.47	3.58	3.43E-02	8.57E-02
1449383_at	Adssl1	8.96	7.35	3.06	3.10E-03	1.24E-02
1450939_at	Entpd1-1	7.01	5.44	2.97	3.00E-04	1.90E-03
1421204_a_at	Nudt16	7.14	5.62	2.86	5.22E-07	1.71E-05
1422573_at	Ampd3	8.48	7.13	2.55	1.80E-03	7.80E-03
1426339_at	Ak5	6.75	5.42	2.53	1.70E-03	7.60E-03
1422868_s_at	Gda	7.38	6.13	2.38	5.21E-05	5.00E-04
1423326_at	Entpd1-2	8.69	7.49	2.3	1.00E-04	9.00E-04
1432068_a_at	Entpd7-1	2.91	1.9	2.02	9.28E-02	1.88E-01
1453299_a_at	Pnp/Pnp2	9.72	8.71	2.02	2.05E-06	4.44E-05
1428164_at	Nudt9	10.11	9.29	1.76	2.70E-03	1.09E-02
1416530_a_at	Pnp	11.07	10.26	1.75	2.31E-06	4.83E-05
1423988_at	Ak1-1	4.8	4	1.74	1.10E-03	5.20E-03
1416593_at	Glrx-2	9.61	8.83	1.73	1.34E-01	2.48E-01
1420272_at	Samhd1-2	6.47	5.71	1.69	2.32E-01	3.75E-01
1416592_at	Glrx-1	9.91	9.18	1.65	2.26E-01	3.68E-01
1427357_at	Cda	5.93	5.26	1.59	3.17E-02	8.06E-02
1427810_at	Tyms-1	4.61	3.98	1.55	9.15E-02	1.86E-01
1424646_at	Uckl1	8.85	8.24	1.53	1.00E-03	4.90E-03
1425689_at	Dpys-2	3.87	3.3	1.48	9.39E-01	9.64E-01
1435625_at	Entpd7-2	6.17	5.66	1.42	3.25E-02	8.21E-02
1451703_s_at	Aprt-1	11.66	11.18	1.4	8.20E-03	2.70E-02
1435759_at	Ctps2-1	4.45	4.02	1.35	3.76E-02	9.20E-02
1425228_a_at	Dguok	8.85	8.43	1.33	8.00E-03	2.67E-02
1426909_at	Uck2-2	9.29	8.89	1.33	2.99E-02	7.67E-02
1423801_a_at	Aprt-2	11.59	11.19	1.31	5.71E-02	1.28E-01
1416356_at	Gmpr2	9.34	8.94	1.31	1.70E-03	7.70E-03
1427715_a_at	Nt5c1b	2.19	1.81	1.31	4.73E-01	6.23E-01
1417252_at	Nt5c	9.72	9.37	1.27	3.11E-02	7.92E-02
1421831_at	Ak4-4	2.51	2.18	1.26	8.20E-01	8.88E-01
1450987_a_at	Adprm	8.34	8.02	1.25	1.00E-03	4.80E-03
1448444_at	Rpe-3	4.2	3.9	1.24	8.81E-01	9.28E-01
1426100_a_at	Tk2	8.11	7.79	1.24	1.13E-02	3.51E-02
1448604_at	Uck2-3	9.31	9.02	1.22	5.63E-02	1.27E-01
1448614_at	Nt5c2-3	5.48	5.21	1.21	1.98E-01	3.33E-01
1427811_at	Tyms-2	2.6	2.33	1.21	6.86E-01	7.97E-01

Table S4.2 Gene expression with statistical significance for Figure 4.2A. Relative expression and statistical significance of all nucleotide metabolism genes from Reactome database exported using TAC. Genes are sorted by fold change. Highlighted values indicate statistical significance with FDR p value < 0.05

Table S4.2 (cont'd)

1451149_at	Pgm2	9.59	9.37	1.17	4.63E-01	6.13E-01
1424609_a_at	Cwc22/Xdh-2	11.09	10.91	1.14	5.23E-01	6.67E-01
1453767_a_at	Nt5m	8.75	8.56	1.14	3.42E-01	4.98E-01
1438250_s_at	Ak6/LOC105247169/Taf9-2	10.86	10.69	1.13	3.42E-01	4.98E-01
1427945_at	Dpyd-1	3.15	2.98	1.13	9.78E-01	9.88E-01
1424607_a_at	Cwc22/Xdh-1	10.98	10.82	1.11	4.37E-01	5.90E-01
1417137_at	Uck2-1	5.7	5.59	1.08	8.90E-01	9.34E-01
1439012_a_at	Dck-2	9.62	9.55	1.04	5.74E-01	7.09E-01
1460671_at	Gpx1	12.66	12.64	1.02	9.39E-01	9.64E-01
1433773_at	Rrm2b	8.24	8.23	1.01	6.34E-01	7.57E-01
1451548_at	Upp2-2	0	0	1	8.27E-01	8.92E-01
1448111_at	Ctps2-2	9.62	9.64	-1.02	6.69E-01	7.84E-01
1438941_x_at	Ampd2-2	10.29	10.33	-1.03	4.22E-01	5.77E-01
1422778_at	Ak6/LOC105247169/Taf9-1	11.11	11.19	-1.05	7.47E-01	8.39E-01
1417384_at	Entpd5-4	7.36	7.45	-1.06	7.16E-01	8.18E-01
1421817_at	Gsr-2	9.04	9.14	-1.07	5.88E-01	7.20E-01
1418131_at	Samhd1-1	9.21	9.3	-1.07	3.85E-01	5.41E-01
1424399_at	Uck1	8.58	8.68	-1.07	2.75E-01	4.25E-01
1448736_a_at	Hprt	10.9	10.99	-1.07	7.75E-01	8.57E-01
1449176_a_at	Dck-3	7.36	7.48	-1.08	4.05E-01	5.60E-01
1434438_at	Samhd1-4	8.62	8.78	-1.12	7.23E-01	8.22E-01
1421529_a_at	Txnrd1-2	10.52	10.71	-1.14	7.21E-02	1.54E-01
1424486_a_at	Txnrd1-3	7.36	7.55	-1.14	4.66E-02	1.10E-01
1426757_at	Ampd2-1	8.03	8.23	-1.15	5.35E-01	6.77E-01
1422126_a_at	Nudt13-1	6.7	6.9	-1.15	2.76E-01	4.26E-01
1421767_at	Adk-3	4.85	5.08	-1.17	1.48E-01	2.67E-01
1420638_at	Prps2-2	7.32	7.55	-1.18	1.91E-01	3.24E-01
1424841_s_at	Rbks-2	6.31	6.57	-1.19	4.27E-01	5.81E-01
1416705_at	Rpe-1	8.73	8.98	-1.19	5.68E-02	1.28E-01
1423706_a_at	Pgd-1	10.46	10.72	-1.2	4.06E-02	9.81E-02
1436298_x_at	Paics-3	9.98	10.26	-1.21	5.72E-01	7.08E-01
1438627_x_at	Pgd-4	11.02	11.29	-1.21	4.60E-02	1.08E-01
1420273_x_at	Samhd1-3	7.41	7.68	-1.21	7.05E-01	8.11E-01
1438690_at	Tyms-3	6.27	6.55	-1.21	5.99E-02	1.33E-01
1433903_at	Prps1l3-2	9.48	9.76	-1.21	1.83E-01	3.14E-01
1449641_at	Adk-4	4.51	4.81	-1.23	1.78E-01	3.07E-01
1417201_at	Nt5c2-1	7.69	8	-1.24	7.40E-03	2.50E-02
1423073_at	Cmpk1	11.41	11.72	-1.25	1.10E-01	2.14E-01
1424487_x_at	Txnrd1-1	5.53	5.88	-1.27	1.33E-02	4.00E-02
1428838_a_at	Dck-1	6.53	6.9	-1.29	1.46E-01	2.65E-01
1416448_at	Itpa	8.92	9.29	-1.3	1.20E-01	2.28E-01
1448808_a_at	Nme2	13.52	13.89	-1.3	1.90E-03	8.40E-03
1428943_at	Nudt13-2	6.6	6.99	-1.31	3.88E-01	5.44E-01
1436771_x_at	Pgd-2	11.72	12.12	-1.31	3.40E-03	1.34E-02
1417383_at	Entpd5-3	6.26	6.65	-1.32	8.32E-02	1.72E-01
1451509_at	Ak6/Taf9	9.99	10.4	-1.33	3.67E-02	9.03E-02
1423564_a_at	Paics-2	11.97	12.39	-1.34	3.44E-02	8.59E-02

Table S4.2 (cont'd)

1416052_at	Prps1	9.09	9.54	-1.36	2.93E-02	7.54E-02
1460713_at	Dnph1	7.39	7.84	-1.37	1.91E-02	5.36E-02
1448192_s_at	Prps1/Prps1l3	9.31	9.76	-1.37	5.73E-02	1.29E-01
1416258_at	Tk1	9.42	9.88	-1.37	3.48E-02	8.66E-02
1417722_at	Pgls	10.51	10.98	-1.39	2.30E-03	9.60E-03
1455832_a_at	Umps-1	8.29	8.77	-1.39	2.80E-03	1.14E-02
1437380_x_at	Pgd-3	11.43	11.92	-1.4	1.50E-03	6.80E-03
1416706_at	Rpe-2	9.3	9.79	-1.4	7.60E-03	2.54E-02
1452829_at	Cad-1	9	9.49	-1.41	1.56E-02	4.58E-02
1438292_x_at	Adk-1	10.69	11.19	-1.42	7.00E-04	3.90E-03
1451006_at	Xdh	9.86	10.4	-1.45	9.85E-02	1.97E-01
1425688_a_at	Dpys-1	2.18	2.72	-1.46	6.98E-01	8.06E-01
1423239_at	Impdh1	8.7	9.24	-1.46	5.10E-03	1.83E-02
1423565_at	Paics-1	11.62	12.16	-1.46	1.18E-02	3.63E-02
1434437_x_at	Rrm2-1	10.58	11.13	-1.46	1.42E-02	4.21E-02
1416798_a_at	Nme4	7.19	7.74	-1.47	5.80E-03	2.05E-02
1424435_a_at	Gart-1	8.43	8.99	-1.48	7.30E-03	2.47E-02
1451445_at	Umps-3	4.94	5.51	-1.48	3.96E-02	9.60E-02
1421816_at	Gsr-1	8.26	8.84	-1.49	2.80E-02	7.27E-02
1448226_at	Rrm2-3	9.53	10.1	-1.49	4.99E-02	1.15E-01
1449116_a_at	Dtymk-1	9.4	9.98	-1.5	2.50E-03	1.02E-02
1419270_a_at	Dut-2	9.83	10.41	-1.5	1.99E-02	5.55E-02
1460726_at	Adss	10.4	11	-1.51	2.32E-02	6.26E-02
1438177_x_at	Entpd4/Gm21685-2	8.18	8.79	-1.53	3.70E-03	1.41E-02
1424969_s_at	Upp2-1	2.08	2.71	-1.54	7.11E-01	8.15E-01
1451765_a_at	Entpd5-1	6.9	7.54	-1.56	1.45E-02	4.30E-02
1448530_at	Gmpr	7.46	8.11	-1.57	2.64E-02	6.95E-02
1428543_at	Ppat-1	7.01	7.68	-1.58	6.30E-03	2.19E-02
1434859_at	Umps-2	8.41	9.09	-1.6	6.00E-04	3.40E-03
1449190_a_at	Entpd4/Gm21685-1	7.9	8.59	-1.61	5.60E-03	1.99E-02
1418259_a_at	Entpd2	6.42	7.12	-1.62	1.87E-01	3.20E-01
1452830_s_at	Cad-2	8.6	9.33	-1.66	1.05E-02	3.31E-02
1424991_s_at	Tyms/Tyms-ps	8.77	9.49	-1.66	1.22E-02	3.73E-02
1418372_at	Adsl	8.93	9.67	-1.67	1.70E-03	7.60E-03
1429126_at	Nudt5-1	7.49	8.24	-1.67	9.60E-03	3.10E-02
1416395_at	Guk1	8.63	9.38	-1.68	2.00E-03	8.60E-03
1454814_s_at	Prps1l3-1	9.1	9.87	-1.7	6.89E-05	6.00E-04
1425933_a_at	Nt5c2-2	8.31	9.08	-1.71	4.64E-05	4.00E-04
1424840_at	Rbks-1	5.25	6.04	-1.73	9.60E-03	3.10E-02
1419269_at	Dut-1	5.96	6.8	-1.78	1.53E-01	2.75E-01

Table S4.2 (cont'd)

1420637_at	Prps2-1	7.82	8.65	-1.78	2.00E-04	1.60E-03
1416319_at	Adk-2	8.97	9.83	-1.81	7.79E-05	7.00E-04
1449349_at	Nudt1	8.43	9.29	-1.82	2.56E-05	3.00E-04
1416120_at	Rrm2-2	9.24	10.11	-1.83	2.30E-03	9.50E-03
1415878_at	Rrm1-2	10.22	11.1	-1.84	5.00E-04	3.00E-03
1421830_at	Ak4-1	7.75	8.64	-1.85	1.58E-02	4.62E-02
1415851_a_at	Gm15210/Impdh2-2	11.42	12.31	-1.85	3.08E-07	1.18E-05
1415852_at	Gm15210/Impdh2-1	11.39	12.28	-1.85	2.00E-04	1.50E-03
1452681_at	Dtymk-2	9.34	10.23	-1.86	1.10E-03	5.20E-03
1448127_at	Rrm1-1	9.71	10.61	-1.87	3.70E-03	1.43E-02
1438096_a_at	Dtymk-3	10.06	10.97	-1.88	2.00E-04	1.60E-03
1448450_at	Ak2-1	10.03	10.99	-1.94	1.20E-03	5.70E-03
1421829_at	Ak4-3	5.44	6.4	-1.94	4.94E-01	6.42E-01
1450387_s_at	Ak4-2	8.4	9.42	-2.02	1.55E-02	4.56E-02
1427946_s_at	Dpyd-2	3.16	4.19	-2.04	1.17E-01	2.24E-01
1460433_at	Entpd6	7.77	8.81	-2.06	4.03E-05	4.00E-04
1424110_a_at	Nme1-2	10.98	12.03	-2.06	1.00E-04	1.00E-03
1439443_x_at	Tkt-1	13.37	14.43	-2.08	7.25E-07	2.17E-05
1424047_at	Dera	8.98	10.05	-2.09	3.16E-06	6.10E-05
1416283_at	Gart-2	9.07	10.13	-2.09	2.54E-06	5.17E-05
1417581_at	Dhodh-1	6.76	7.87	-2.15	2.00E-04	1.20E-03
1417582_s_at	Dhodh-2	7.55	8.7	-2.2	5.54E-05	5.00E-04
1418337_at	Rpia	8.78	9.92	-2.21	1.00E-03	4.90E-03
1452831_s_at	Ppat-2	7.49	8.68	-2.28	9.19E-05	7.00E-04
1424436_at	Gart-3	7.95	9.15	-2.3	2.15E-08	2.14E-06
1452889_at	Lhpp	6.35	7.56	-2.31	1.00E-04	8.00E-04
1448651_at	Nudt5-2	8.7	9.94	-2.35	3.30E-05	3.00E-04
1448451_at	Ak2-2	9.14	10.39	-2.37	4.83E-05	4.00E-04
1417382_at	Entpd5-2	7.04	8.28	-2.37	5.00E-04	2.70E-03
1448905_at	Mrps34/Nme3	8	9.33	-2.5	2.17E-05	2.00E-04
1425129_a_at	Taldo1	11.09	12.49	-2.63	1.23E-08	1.66E-06
1417976_at	Ada	7.93	9.38	-2.73	2.00E-04	1.50E-03
1451015_at	Tkt-2	10.93	12.58	-3.12	2.95E-08	2.58E-06
1416439_at	Dctpp1	9.32	11.02	-3.23	2.35E-07	9.81E-06
1435277_x_at	Nme1-1	11.31	13.1	-3.48	4.00E-03	1.50E-02
1460244_at	Upb1	4.99	6.96	-3.93	2.28E-02	6.18E-02

							Raw P values			Adjusted P values		
Metabolite	EMT PSC D3 Average (%)	EMT PSC D3 STDEV	EMT APRT B3 Average (%)	EMT APRT B3 STDEV	EMT PPAT F1 Average (%)	EMT PPAT F1 STDEV	PSC vs APRT KO	PSC vs PPAT KO	APRT KO vs PPAT KO	PSC vs APRT KO	PSC vs PPAT KO	APRT KO vs PPAT KO
ATP M-0	56.4	2.2	50.8	0.3	66.8	3.0	**6.66E-02**	1.68E-02	**1.67E-02**	**9.98E-02**	3.50E-02	**2.17E-02**
ATP M-5	28.6	0.9	29.2	0.4	24.4	1.6	4.33E-01	3.27E-02	1.48E-02	4.33E-01	3.50E-02	2.17E-02
ATP M-OTHER	15.0	1.4	20.0	0.4	8.7	2.5	7.54E-03	3.50E-02	**2.17E-02**	2.26E-02	3.50E-02	**2.17E-02**

Table S4.3 ^{13}C-Isotope percent labeling from glucose statistical significance for figure 4.4 – EMT subtype. Data represent means and S.D. of 3 replicates. Bold values indicate Welch's t-test was used. Highlighted values are statistically significant with adjusted p value < 0.05

							Raw P values			Adjusted P values		
Metabolite	Papillary PSC G6 Average (%)	Papillary PSC G6 STDEV	Papillary APRT E6 Average (%)	Papillary APRT E6 STDEV	Papillary PPAT A7 Average (%)	Papillary PPAT A7 STDEV	PSC vs APRT KO	PSC vs PPAT KO	APRT KO vs PPAT KO	PSC vs APRT KO	PSC vs PPAT KO	APRT KO vs PPAT KO
ATP M-0	42.4	1.3	45.8	0.5	80.1	7.1	2.47E-02	1.78E-03	**2.03E-02**	2.47E-02	2.67E-03	**3.04E-02**
ATP M-5	37.4	0.7	29.4	0.5	10.7	7.6	2.14E-04	**3.69E-02**	**7.23E-02**	4.05E-04	**3.69E-02**	**7.23E-02**
ATP M-OTHER	20.2	0.5	24.8	0.1	9.2	0.5	2.70E-04	3.23E-05	2.20E-06	4.05E-04	9.69E-05	6.60E-06

Table S4.4 ^{13}C-Isotope percent labeling from glucose statistical significance for figure 4.4 – papillary subtype. Data represent means and S.D. of 3 replicates. Bold values indicate Welch's t-test was used. Highlighted values are statistically significant with adjusted p value < 0.05

Metabolite	EMT PSC D3 Average (Log2 Fold Change)	EMT PSC D3 STDEV	EMT APRT B3 Average (Log2 Fold Change)	EMT APRT B3 STDEV	EMT PPAT F1 Average (Log2 Fold Change)	EMT PPAT F1 STDEV	Raw P values			Adjusted P values		
							PSC vs APRT KO	PSC vs PPAT KO	APRT KO vs PPAT KO	PSC vs APRT KO	PSC vs PPAT KO	APRT KO vs PPAT KO
2+3-phosphoglycerate	0.0	0.2	-0.7	0.2	-0.2	0.5	1.52E-02	4.57E-01	2.12E-01	4.31E-02	7.23E-01	3.14E-01
Acetoacetyl-CoA_	0.0	0.3	0.1	0.2	-0.5	0.4	4.85E-01	1.36E-01	5.30E-02	5.41E-01	3.04E-01	9.78E-02
Acetyl-CoA	0.0	0.2	0.5	0.3	-0.5	0.4	5.22E-02	1.32E-01	2.66E-02	9.85E-02	3.04E-01	6.75E-02
ADP	-0.1	0.6	-1.1	0.1	-0.6	0.1	**1.05E-01**	**2.66E-01**	4.29E-04	**1.48E-01**	**5.14E-01**	5.70E-03
ADP-glucose	0.0	0.4	-1.1	0.2	0.7	0.4	2.07E-02	8.42E-02	1.92E-03	5.42E-02	2.49E-01	1.18E-02
ADP-ribose	-0.1	0.6	-1.1	0.2	-0.2	0.1	4.91E-02	7.74E-01	2.45E-03	9.61E-02	8.96E-01	1.19E-02
Alanine	-0.1	0.5	0.6	0.3	0.1	0.1	1.31E-01	**6.71E-01**	5.21E-02	1.72E-01	**8.30E-01**	9.78E-02
Allantoate_and_Carbamoyl_aspartate	0.0	0.1	0.7	0.2	0.4	0.2	3.98E-03	2.52E-02	9.70E-02	1.59E-02	1.32E-01	1.65E-01
AMP	0.0	0.4	-0.6	0.1	-0.2	0.2	9.58E-02	5.86E-01	2.21E-02	1.39E-01	7.81E-01	6.54E-02
Arginine	0.0	0.1	-0.6	0.1	-0.4	0.3	1.22E-03	7.68E-02	3.93E-01	9.19E-03	2.49E-01	5.14E-01
Asparagine	0.0	0.1	0.2	0.1	-0.5	0.1	6.29E-02	2.27E-03	6.04E-04	1.02E-01	3.08E-02	5.87E-03
Aspartate	0.0	0.2	-0.1	0.0	-1.0	0.1	2.51E-01	7.41E-04	8.93E-05	3.05E-01	2.52E-02	3.04E-03
ATP	0.0	0.4	1.8	0.2	0.5	0.3	2.45E-03	1.50E-01	3.86E-03	1.19E-02	3.19E-01	1.54E-02
Bisphosphoglycerate	0.0	0.3	0.5	0.3	-0.2	0.2	1.11E-01	4.06E-01	3.12E-02	1.53E-01	6.73E-01	6.75E-02
Citrate+Isocitrate	0.0	0.2	0.1	0.5	-0.5	0.2	7.52E-01	3.55E-02	1.17E-01	7.87E-01	1.61E-01	1.90E-01
CMPNacetylneuraminate	0.0	0.3	-0.4	0.1	-0.4	0.1	6.24E-02	6.15E-02	9.62E-01	1.02E-01	2.20E-01	9.62E-01
CoA	-0.1	0.7	0.8	0.8	0.0	0.6	2.27E-01	7.91E-01	2.82E-01	2.81E-01	8.96E-01	3.99E-01
CTP	0.0	0.2	0.5	0.1	0.0	0.0	1.41E-02	8.58E-01	4.52E-03	4.31E-02	9.11E-01	1.71E-02
Cysteine	0.0	0.4	-0.1	0.2	-0.3	0.4	7.89E-01	4.40E-01	5.05E-01	8.13E-01	7.13E-01	6.02E-01
dATP	-0.1	0.8	1.7	0.2	0.6	0.9	1.52E-02	3.69E-01	1.03E-01	4.31E-02	6.44E-01	1.71E-01
dCTP	-0.1	0.6	1.4	0.2	0.0	0.3	1.77E-02	8.17E-01	2.65E-03	4.80E-02	8.96E-01	1.20E-02
dGDP	-0.3	1.1	-0.6	1.8	-0.5	1.4	8.05E-01	9.03E-01	8.92E-01	8.17E-01	9.30E-01	9.19E-01
dTTP	0.0	0.4	1.5	0.2	0.9	0.3	3.28E-03	3.18E-02	2.91E-02	1.40E-02	1.54E-01	6.75E-02
FAD	0.0	0.1	-0.3	0.1	0.2	0.1	4.22E-02	5.65E-02	2.11E-03	8.97E-02	2.18E-01	1.19E-02
FBP	0.0	0.0	-0.3	0.2	0.4	0.2	**9.05E-02**	**7.30E-02**	1.02E-02	**1.34E-01**	**2.48E-01**	3.66E-02
Fumarate	0.0	0.1	-0.3	0.1	-0.2	0.4	4.47E-02	3.86E-01	7.70E-01	9.21E-02	6.56E-01	8.44E-01
GAP+DHAP	0.0	0.1	-0.1	0.2	0.2	0.2	4.04E-01	2.09E-01	1.46E-01	4.61E-01	4.30E-01	2.30E-01
GDP	0.0	0.4	-0.9	0.1	-0.6	0.1	2.82E-02	1.11E-01	2.80E-02	6.61E-02	2.79E-01	6.75E-02
Glutamate	0.0	0.2	0.2	0.0	0.2	0.1	5.55E-02	9.82E-02	7.11E-01	1.01E-01	2.77E-01	7.98E-01
Glutamine	0.0	0.1	0.1	0.0	0.0	0.1	1.26E-01	6.09E-01	7.08E-01	1.67E-01	7.81E-01	7.98E-01
Glutathione_disulfide_oxidized	0.0	0.4	2.3	0.1	0.3	0.3	7.01E-04	3.33E-01	3.73E-04	7.61E-03	5.96E-01	5.70E-03
Glutathione_reduced	0.0	0.0	-0.1	0.1	0.5	0.1	4.95E-02	1.72E-03	7.97E-04	9.61E-02	2.93E-02	6.78E-03
Glycerol_3-phosphate	0.0	0.3	1.2	0.1	1.5	0.1	2.12E-03	1.26E-03	2.63E-02	1.19E-02	2.85E-02	6.75E-02
Glycine	0.0	0.1	0.4	0.1	-0.1	0.2	5.51E-03	4.86E-01	2.90E-02	1.97E-02	7.44E-01	6.75E-02
GMP	0.0	0.3	-0.6	0.0	-0.3	0.2	**6.01E-02**	2.63E-01	8.42E-02	**1.02E-01**	5.14E-01	1.47E-01
GTP	0.0	0.2	1.4	0.3	0.3	0.7	2.34E-03	5.38E-01	5.32E-02	1.19E-02	7.61E-01	9.78E-02
Hexose-phosphate	0.0	0.0	0.6	0.1	0.2	0.1	1.61E-03	1.38E-01	1.66E-02	9.92E-03	3.04E-01	5.37E-02
IDP	-0.1	0.8	-1.1	0.3	-0.5	0.1	1.12E-01	**4.93E-01**	3.24E-02	1.53E-01	**7.44E-01**	6.75E-02
IMP	-0.1	0.5	0.6	0.2	0.0	0.3	9.04E-02	8.88E-01	3.73E-02	1.34E-01	9.29E-01	7.46E-02
Isoleucine/Leucine	0.0	0.1	-0.2	0.1	0.0	0.2	1.39E-01	9.29E-01	2.12E-01	1.78E-01	9.42E-01	3.14E-01
Ketoglutarate	0.0	0.1	0.9	0.2	-0.7	0.2	7.83E-04	3.83E-03	3.44E-04	7.61E-03	3.72E-02	5.70E-03
Lysine	0.0	0.1	-0.6	0.1	-0.4	0.3	1.47E-03	5.76E-02	4.16E-01	9.92E-03	2.18E-01	5.34E-01
Malate	0.0	0.0	-0.3	0.2	-0.2	0.1	3.02E-02	1.66E-02	2.04E-01	6.84E-02	1.02E-01	3.14E-01
Methionine	0.0	0.2	0.9	0.0	-0.1	0.3	9.22E-04	5.59E-01	**3.27E-02**	7.83E-03	7.61E-01	**6.75E-02**
Nacetylneuraminate	-0.1	0.5	-0.4	0.1	-0.3	0.1	**3.91E-01**	**5.14E-01**	2.18E-01	**4.59E-01**	**7.44E-01**	3.16E-01
NAD	0.0	0.0	-0.4	0.0	0.1	0.0	3.64E-05	7.13E-03	3.10E-05	1.24E-03	5.39E-02	2.11E-03
NADH	-0.2	1.0	-1.0	0.6	1.6	0.4	2.82E-01	3.83E-02	2.28E-03	3.37E-01	1.63E-01	1.19E-02
NADP	0.0	0.1	-0.5	0.1	0.0	0.0	3.16E-03	6.39E-01	9.37E-04	1.40E-02	8.05E-01	7.08E-03
NADPH	-0.1	0.5	0.9	0.1	-0.4	0.2	4.05E-02	3.30E-01	5.03E-04	8.88E-02	5.96E-01	5.70E-03
Ornithine	0.0	0.2	-1.0	0.1	-0.5	0.2	6.55E-04	2.01E-02	1.76E-02	7.61E-03	1.14E-01	5.44E-02
Phenylalanine	0.0	0.1	-0.2	0.0	-0.4	0.3	2.18E-02	8.31E-02	**3.19E-01**	5.48E-02	2.49E-01	**4.34E-01**
Phosphogluconic_acid	0.0	0.3	-1.0	0.5	-0.9	0.7	5.66E-02	1.05E-01	9.10E-01	1.01E-01	2.77E-01	9.24E-01
Proline	-0.1	0.7	-0.2	0.0	0.0	0.7	**8.25E-01**	8.35E-01	**6.36E-01**	**8.25E-01**	9.01E-01	**7.46E-01**
PRPP	0.0	0.3	-2.1	0.5	-1.8	0.3	4.73E-03	2.96E-03	4.63E-01	1.79E-02	3.35E-02	5.62E-01
Ribose-5-phosphate	-0.1	0.8	1.0	0.1	0.7	0.1	6.89E-02	1.34E-01	6.97E-02	1.09E-01	3.04E-01	1.25E-01
Ribulose-5-phosphate	0.0	0.2	0.6	0.3	0.6	0.1	2.34E-02	6.36E-03	7.16E-01	5.69E-02	5.39E-02	7.98E-01
Sedoheptulose-phosphate	0.0	0.1	1.2	0.2	0.0	0.3	7.07E-04	8.08E-01	3.00E-03	7.61E-03	8.96E-01	1.27E-02
Serine	0.0	0.1	-0.2	0.2	-0.1	0.1	1.64E-01	2.72E-01	4.29E-01	2.07E-01	5.14E-01	5.39E-01
Succinate	0.0	0.1	-0.5	0.1	-0.7	0.2	3.69E-04	9.10E-03	4.36E-01	7.61E-03	6.19E-02	5.39E-01
Threonine	0.0	0.1	-0.2	0.1	0.1	0.1	7.10E-02	5.59E-01	3.00E-02	1.10E-01	7.61E-01	6.75E-02
Tryptophan	0.0	0.2	0.1	0.1	0.1	0.5	6.63E-01	7.29E-01	8.90E-01	7.16E-01	8.85E-01	9.19E-01
Tyrosine	0.0	0.0	-0.1	0.1	0.0	0.6	4.07E-01	**9.86E-01**	8.82E-01	4.61E-01	**9.86E-01**	9.19E-01
UDP	-0.1	0.7	-1.7	0.1	-1.0	0.2	**5.91E-02**	1.06E-01	1.56E-03	**1.02E-01**	2.77E-01	1.06E-02
UDPNacetylglucosamine	0.0	0.0	-0.6	0.0	-0.7	0.0	6.30E-06	2.90E-06	3.66E-01	4.28E-04	1.97E-04	4.88E-01
UMP	0.0	0.3	0.1	0.2	0.1	0.2	6.93E-01	6.02E-01	8.38E-01	7.36E-01	7.81E-01	9.04E-01
UTP	0.0	0.3	1.0	0.2	0.1	0.4	1.07E-02	7.69E-01	3.01E-02	3.45E-02	8.96E-01	6.75E-02
Valine	0.0	0.1	-0.3	0.0	0.0	0.1	8.69E-03	8.06E-01	1.21E-02	2.95E-02	8.96E-01	4.12E-02
Xanthosine	-0.3	1.3	0.2	0.2	-1.3	1.9	5.64E-01	5.08E-01	**3.14E-01**	6.19E-01	7.44E-01	**4.34E-01**

Table S4.5 Metabolite abundance with statistical significance for figures 4.5 and S4.5 – EMT subtype. Data presented relative to the PSC average of the EMT subtype as depicted in

Table S4.5 (cont'd)
figures 4.5 and S4.5. Data represent means and S.D. of 3 replicates. Bold values indicate Welch's t-test was used. Highlighted values are statistically significant with adjusted p value < 0.05

							Raw P values			Adjusted P values		
Metabolite	Papillary PSC G6 Average (Log2 Fold Change)	Papillary PSC G6 STDEV	Papillary APRT E6 Average (Log2 Fold Change)	Papillary APRT E6 STDEV	Papillary PPAT A7 Average (Log2 Fold Change)	Papillary PPAT A7 STDEV	PSC vs APRT KO	PSC vs PPAT KO	APRT KO vs PPAT KO	PSC vs APRT KO	PSC vs PPAT KO	APRT KO vs PPAT KO
2+3-phosphoglycerate	-0.1	0.5	0.1	0.6	1.9	0.0	7.20E-01	**2.44E-02**	**3.18E-02**	8.60E-01	**3.95E-02**	**5.15E-02**
Acetoacetyl-CoA_	0.0	0.3	0.3	0.2	1.9	0.2	2.04E-01	7.65E-04	6.53E-04	4.86E-01	3.22E-03	1.85E-03
Acetyl-CoA	0.0	0.4	0.6	1.3	1.7	0.3	4.24E-01	3.97E-03	2.48E-01	7.01E-01	9.65E-03	2.97E-01
ADP	0.0	0.1	0.0	0.1	-0.9	0.1	6.80E-01	3.55E-04	1.36E-04	8.57E-01	1.86E-03	5.46E-04
ADP-glucose	-0.2	0.9	0.0	1.1	0.4	1.3	8.58E-01	5.71E-01	7.06E-01	9.30E-01	5.71E-01	7.27E-01
ADP-ribose	0.0	0.2	-0.4	0.5	-1.8	0.4	2.45E-01	1.99E-03	2.00E-02	5.27E-01	6.78E-03	3.67E-02
Alanine	0.0	0.4	0.1	0.1	-1.6	0.2	5.71E-01	3.37E-03	4.03E-04	8.26E-01	8.49E-03	1.25E-03
Allantoate_and_Carbamoyl_aspartat	0.0	0.1	-0.3	0.1	-2.2	0.1	4.06E-02	3.59E-05	4.54E-05	2.19E-01	4.07E-04	3.26E-04
AMP	0.0	0.1	0.0	0.0	-0.6	0.2	5.94E-01	1.09E-02	3.38E-03	8.42E-01	2.05E-02	7.40E-03
Arginine	0.0	0.1	-0.1	0.1	0.4	0.0	5.27E-01	3.10E-03	1.30E-03	7.96E-01	8.28E-03	3.32E-03
Asparagine	0.0	0.1	-0.1	0.1	-1.0	0.2	1.50E-01	8.05E-04	9.25E-04	4.57E-01	3.22E-03	2.52E-03
Aspartate	0.0	0.3	0.8	0.0	0.5	0.0	**4.91E-02**	**9.94E-02**	6.12E-05	**2.38E-01**	**1.41E-01**	3.26E-04
ATP	0.0	0.4	0.3	0.0	-2.0	0.3	**3.32E-01**	2.70E-03	1.61E-04	**5.95E-01**	7.99E-03	5.75E-04
Bisphosphoglycerate	-0.1	0.7	0.6	0.2	-1.5	0.1	1.52E-01	**7.89E-02**	3.01E-05	4.57E-01	**1.19E-01**	2.56E-04
Citrate+Isocitrate	0.0	0.2	0.4	0.3	1.0	0.3	9.72E-02	5.95E-03	8.77E-02	4.13E-01	1.35E-02	1.27E-01
CMPNacetylneuraminate	0.0	0.0	0.0	0.0	-0.9	0.0	3.48E-01	3.30E-06	4.90E-06	6.07E-01	1.12E-04	1.94E-04
CoA	0.0	0.3	-0.2	0.5	-0.5	0.5	6.41E-01	3.10E-01	5.56E-01	8.57E-01	3.67E-01	5.84E-01
CTP	0.0	0.3	0.3	0.1	-0.2	0.3	1.26E-01	4.88E-01	2.61E-02	4.57E-01	5.02E-01	4.57E-02
Cysteine	0.0	0.1	0.2	0.2	-0.3	0.2	2.89E-01	1.60E-01	8.01E-02	5.46E-01	2.02E-01	1.18E-01
dATP	0.0	0.2	0.2	0.1	-2.3	0.5	2.07E-01	2.21E-03	1.32E-03	4.86E-01	7.11E-03	3.32E-03
dCTP	0.0	0.3	0.5	0.1	-0.9	0.1	5.95E-02	1.30E-02	1.00E-04	2.70E-01	2.38E-02	4.88E-04
dGDP	0.0	0.2	-1.2	2.3	-3.3	0.5	**4.70E-01**	5.52E-04	1.98E-01	**7.27E-01**	2.50E-03	2.55E-01
dTTP	0.0	0.4	0.1	0.2	-1.6	0.1	6.81E-01	2.30E-03	1.19E-04	8.57E-01	7.11E-03	5.07E-04
FAD	0.0	0.1	0.0	0.1	0.2	0.2	7.76E-01	1.47E-01	1.88E-01	8.79E-01	1.89E-01	2.46E-01
FBP	0.0	0.1	-0.6	0.1	-2.4	0.2	1.48E-03	5.03E-05	1.19E-04	2.74E-02	4.28E-04	5.07E-04
Fumarate	0.0	0.2	-0.1	0.2	-1.5	0.4	7.11E-01	2.95E-03	2.86E-03	8.60E-01	8.28E-03	6.53E-03
GAP+DHAP	0.0	0.2	-0.2	0.2	-0.9	0.4	3.16E-01	1.89E-02	4.01E-02	5.82E-01	3.24E-02	6.19E-02
GDP	0.0	0.1	0.1	0.1	-0.3	0.1	2.04E-01	4.66E-03	7.41E-03	4.86E-01	1.09E-02	1.53E-02
Glutamate	0.0	0.1	0.1	0.0	0.0	0.0	1.55E-01	3.29E-01	2.88E-03	4.57E-01	3.79E-01	6.53E-03
Glutamine	0.0	0.1	-0.1	0.0	0.1	0.0	1.27E-01	4.82E-02	1.45E-03	4.57E-01	7.45E-02	3.52E-03
Glutathione_disulfide_oxidized	0.0	0.1	-0.1	0.1	-0.6	0.2	2.74E-01	6.27E-03	2.74E-02	5.46E-01	1.38E-02	4.57E-02
Glutathione_reduced	0.0	0.1	-0.5	0.1	0.9	0.1	6.95E-03	1.74E-04	4.85E-05	9.45E-02	1.31E-03	3.26E-04
Glycerol_3-phosphate	0.0	0.4	-0.4	0.2	0.5	0.0	1.88E-01	**1.47E-01**	**1.37E-02**	4.86E-01	**1.89E-01**	**2.67E-02**
Glycine	0.0	0.2	-0.5	0.4	-0.8	0.1	1.29E-01	3.17E-03	2.25E-01	4.57E-01	8.28E-03	2.83E-01
GMP	0.0	0.2	0.9	1.6	1.0	1.5	**4.33E-01**	**3.61E-01**	9.27E-01	**7.01E-01**	**4.02E-01**	9.27E-01
GTP	0.0	0.4	0.3	0.2	-0.8	0.5	2.30E-01	8.76E-02	1.74E-02	5.21E-01	1.27E-01	3.28E-02
Hexose-phosphate	0.0	0.1	0.0	0.1	-0.8	0.0	7.08E-01	3.56E-04	6.24E-05	8.60E-01	1.86E-03	3.26E-04
IDP	0.0	0.4	-0.2	0.1	-0.8	0.1	3.91E-01	2.27E-02	3.57E-03	6.64E-01	3.77E-02	7.58E-03
IMP	0.0	0.1	-0.7	0.1	-1.6	0.0	1.61E-03	1.83E-05	2.15E-04	2.74E-02	3.50E-04	6.97E-04
Isoleucine/Leucine	0.0	0.1	0.0	0.1	0.1	0.1	8.96E-01	3.13E-01	2.47E-01	9.52E-01	3.67E-01	2.97E-01
Ketoglutarate	0.0	0.2	-0.1	0.1	-1.2	0.1	6.47E-01	5.20E-04	3.00E-05	8.57E-01	2.50E-03	2.56E-04
Lysine	0.0	0.1	-0.1	0.0	0.4	0.1	1.71E-01	8.46E-03	1.44E-04	4.83E-01	1.74E-02	5.46E-04
Malate	0.0	0.1	-0.1	0.1	-1.2	0.1	4.63E-01	2.37E-04	5.73E-05	7.27E-01	1.59E-03	3.26E-04
Methionine	0.0	0.3	0.0	0.1	-0.2	0.2	8.61E-01	3.87E-01	2.56E-01	9.30E-01	4.21E-01	3.00E-01
Nacetylneuraminate	0.0	0.0	0.4	0.0	-0.8	0.1	7.60E-06	3.35E-05	8.00E-06	5.17E-04	4.07E-04	1.94E-04
NAD	0.0	0.2	0.0	0.1	0.3	0.0	6.66E-01	**1.20E-01**	**2.71E-02**	8.57E-01	**1.63E-01**	**4.57E-02**
NADH	0.0	0.3	-1.6	0.7	-2.3	0.9	2.23E-02	1.33E-02	3.43E-01	1.77E-01	2.38E-02	3.82E-01
NADP	0.0	0.0	0.3	0.1	0.4	0.2	3.93E-02	**1.05E-01**	4.94E-01	2.19E-01	**1.46E-01**	5.33E-01
NADPH	0.0	0.1	0.2	0.1	-1.3	0.2	3.94E-02	2.58E-04	1.98E-04	2.19E-01	1.59E-03	6.73E-04
Ornithine	0.0	0.1	-0.3	0.1	1.3	1.3	1.76E-02	**2.22E-01**	**1.59E-01**	1.77E-01	**2.72E-01**	**2.12E-01**
Phenylalanine	0.0	0.3	-0.1	0.1	-0.3	0.5	7.62E-01	5.05E-01	5.59E-01	8.79E-01	5.13E-01	5.84E-01
Phosphogluconic_acid	0.0	0.4	-0.7	0.8	-1.8	0.4	2.85E-01	8.40E-03	9.89E-02	5.46E-01	1.74E-02	1.37E-01
Proline	-0.1	0.6	-1.4	0.1	-2.0	0.4	2.35E-02	9.92E-03	5.15E-02	1.77E-01	1.93E-02	7.78E-02
PRPP	0.0	0.4	0.3	0.3	5.2	0.1	2.76E-01	2.06E-05	1.19E-05	5.46E-01	3.50E-04	1.94E-04
Ribose-5-phosphate	0.0	0.3	0.1	0.2	-1.5	0.1	5.41E-01	1.31E-03	5.27E-04	8.00E-01	4.95E-03	1.56E-03
Ribulose-5-phosphate	0.0	0.2	0.0	0.1	-1.8	0.0	9.83E-01	4.25E-05	2.51E-05	9.90E-01	4.13E-04	2.56E-04
Sedoheptulose-phosphate	0.0	0.2	0.2	0.0	-0.6	0.0	1.48E-01	**3.27E-02**	1.43E-05	4.57E-01	**5.16E-02**	1.94E-04
Serine	0.0	0.0	0.0	0.0	-0.1	0.2	2.48E-01	**4.30E-01**	2.84E-01	5.27E-01	**4.50E-01**	3.27E-01
Succinate	0.0	0.0	0.5	0.1	0.5	0.1	6.64E-04	1.65E-03	7.20E-01	2.26E-02	5.91E-03	7.31E-01
Threonine	0.0	0.3	0.0	0.1	-0.3	0.1	7.63E-01	2.24E-01	3.76E-02	8.79E-01	2.72E-01	5.95E-02
Tryptophan	0.0	0.3	0.0	0.1	0.2	0.1	9.33E-01	3.90E-01	9.66E-02	9.76E-01	4.21E-01	1.37E-01
Tyrosine	0.0	0.2	0.0	0.1	0.1	0.2	8.18E-01	4.18E-01	2.49E-01	9.12E-01	4.44E-01	2.97E-01
UDP	0.0	0.4	0.1	0.3	1.0	0.1	6.65E-01	9.92E-03	1.08E-02	8.57E-01	1.93E-02	2.15E-02
UDPNacetylglucosamine	0.0	0.0	0.1	0.0	0.8	0.0	2.07E-02	3.00E-06	1.29E-05	1.77E-01	1.12E-04	1.94E-04
UMP	-0.1	0.6	-0.1	0.9	-0.6	0.1	9.90E-01	**3.37E-01**	**4.71E-01**	9.90E-01	**3.82E-01**	**5.17E-01**
UTP	0.0	0.3	0.2	0.1	0.9	0.3	1.94E-01	1.91E-02	2.76E-02	4.86E-01	3.24E-02	4.57E-02
Valine	0.0	0.1	0.0	0.2	-0.2	0.1	9.64E-01	1.34E-01	3.42E-01	9.90E-01	1.78E-01	3.82E-01
Xanthosine	0.0	0.1	-0.3	0.2	-2.5	1.3	4.19E-02	**8.14E-02**	**1.02E-01**	2.19E-01	**1.20E-01**	**1.39E-01**

Table S4.6 Metabolite abundance with statistical significance for figures 4.5 and S4.5 – papillary subtype. Data presented relative to the PSC average of the papillary subtype as

Table S4.6 (cont'd)
depicted in figures 4.5 and S4.5. Data represent means and S.D. of 3 replicates. Bold values indicate Welch's t-test was used. Highlighted values are statistically significant with adjusted p value < 0.05

Tumor Size (Day 24)	Average	Stdev	N
EMT PSC D3	1344.6	141.7	6
EMT Wild-Type	1103.1	119.2	7
EMT PSC C4	1330.1	115.8	8
EMT PPAT F1	982.7	116.1	5
EMT PPAT F2	1012.2	271.8	5
EMT APRT B3	762.8	108.4	5

Raw P values					Adjusted P values				
PSCD3 vs WT	PSCD3 vs PSCC4	PSCC4 vs PPATF2	PPATF1 vs PPATF2	PPATF1 vs APRTB3	PSCD3 vs WT	PSCD3 vs PSCC4	PSCC4 vs PPATF2	PPATF1 vs PPATF2	PPATF1 vs APRTB3
6.58E-03	8.36E-01	1.29E-02	8.29E-01	1.48E-02	2.63E-02	8.36E-01	3.87E-02	8.36E-01	4.43E-02

Table S4.7 Tumor size statistical significance for figures 4.6A and S4.8A – EMT subtype. Data represent means and S.D. of EMT tumor size at 24 days post implantation. Highlighted values are statistically significant with adjusted p value < 0.05

Tumor Size (Day 24)	Average	Stdev	N
Pap PSC G6	514.0	114.0	5
Pap Wild-Type	437.5	100.6	4
Pap PSC F1	375.2	85.0	7
Pap APRT E6	1161.8	155.8	5
Pap APRT G5	986.0	78.1	7
Pap APRT H5	350.1	105.7	7

Raw P values						Adjusted P values					
PSCG6 vs WT	PSCG6 vs PSCF1	PSCG6 vs APRTE6	PSCG6 vs APRTG5	PSCG6 vs APRTH5	APRTE6 vs APRTG5	PSCG6 vs WT	PSCG6 vs PSCF1	PSCG6 vs APRTE6	PSCG6 vs APRTG5	PSCG6 vs APRTH5	APRTE6 vs APRTG5
3.84E-01	5.20E-02	1.51E-04	1.51E-05	4.13E-02	4.11E-02	3.84E-01	1.04E-01	7.55E-04	9.06E-05	8.27E-02	8.22E-02

Table S4.8 Tumor size statistical significance for figures 4.6B and S4.8B – papillary subtype. Data represent means and S.D. of EMT tumor size at 24 days post implantation. Highlighted values are statistically significant with adjusted p value < 0.05

IHC Analysis	EMT PSC D3 Average (%)	EMT PSC D3 STDEV	EMT APRT B3 Average (%)	EMT APRT B3 STDEV	EMT PPAT F1 Average (%)	EMT PPAT F1 STDEV
Ki67+ Nuclei (%)	60.51	4.12	55.13	4.61	58.03	2.81

Raw P values			Adjusted P values		
PSC vs APRT KO	PSC vs PPAT KO	APRT KO vs PPAT KO	PSC vs APRT KO	PSC vs PPAT KO	APRT KO vs PPAT KO
2.01E-05	7.75E-03	9.44E-03	6.03E-05	**9.44E-03**	**9.44E-03**

Table S4.9 IHC analysis statistical significance for figure 4.7A – EMT subtype. Data represent means and S.D. Bold values indicate Welch's t-test was used. Highlighted values are statistically significant with adjusted p value < 0.05

	Pap PSC G6 Average (%)	Pap PSC G6 STDEV	Pap APRT E6 Average (%)	Pap APRT E6 STDEV	PSC vs APRT KO
Ki67+ Nuclei (%)	53.18	7.06	59.05	5.78	1.85E-03

Table S4.10 IHC analysis statistical significance for figure 4.7B – papillary subtype. Data represent means and S.D. Bold values indicate Welch's t-test was used. Highlighted values are statistically significant with adjusted p value < 0.05

IHC Analysis	EMT PSC D3 Average (%)	EMT PSC D3 STDEV	EMT APRT B3 Average (%)	EMT APRT B3 STDEV	EMT PPAT F1 Average (%)	EMT PPAT F1 STDEV
Percent Area (TUNEL +)	7.69	4.04	23.07	10.23	27.66	10.36

Raw P values			Adjusted P values		
PSC vs APRT KO	PSC vs PPAT KO	APRT KO vs PPAT KO	PSC vs APRT KO	PSC vs PPAT KO	APRT KO vs PPAT KO
1.37E-02	3.48E-03	5.46E-01	2.73E-02	**1.04E-02**	**5.46E-01**

Table S4.11 IHC analysis statistical significance for figure 4.7C – EMT subtype. Data represent means and S.D. Bold values indicate Welch's t-test was used. Highlighted values are statistically significant with adjusted p value < 0.05

IHC Analysis	Pap PSC G6 Average (%)	Pap PSC G6 STDEV	Pap APRT E6 Average (%)	Pap APRT E6 STDEV	PSC vs APRT KO P Value
Percent Area (TUNEL +)	24.65	15.50	38.10	10.88	1.93E-01

Table S4.12 IHC analysis statistical significance for figure 4.7D – papillary subtype. Data represent means and S.D. Bold values indicate Welch's t-test was used. Highlighted values are statistically significant with adjusted p value < 0.05

Metabolite	EMT PPAT F1 Average (%)	EMT PPAT F1 STDEV	EMT PPAT F2 Average (%)	EMT PPAT F2 STDEV	Raw P values	Adjusted P values
ATP M-0	66.8	3.0	62.9	1.2	1.68E-01	2.52E-01
ATP M-5	24.4	1.6	26.5	0.6	1.67E-01	2.52E-01
ATP M-OTHER	8.7	2.5	10.6	1.4	4.11E-01	4.11E-01

Table S4.13 ^{13}C-Isotope percent labeling from glucose statistical significance for figure S4.9 – EMT subtype. Data represent means and S.D. of 3 replicates. Highlighted values are statistically significant with adjusted p value < 0.05

Metabolite	Papillary PPAT A7 Average (%)	Papillary PPAT A7 STDEV	Papillary PPAT B3 Average (%)	Papillary PPAT B3 STDEV	Papillary PPAT B7 Average (%)	Papillary PPAT B7 STDEV	Papillary PPAT B8 Average (%)	Papillary PPAT B8 STDEV	Papillary PPAT C1 Average (%)	Papillary PPAT C1 STDEV
ATP M-0	80.1	7.1	75.4	4.9	78.1	3.3	74.6	1.6	79.5	1.8
ATP M-5	10.7	7.6	14.7	2.1	13.7	1.9	15.4	0.8	12.9	0.9
ATP M-OTHER	9.2	0.5	9.9	2.9	8.1	1.6	10.0	1.8	7.5	1.3

	Raw P values				Adjusted P values			
Metabolite	PPAT A7 vs PPAT B3	PPAT A7 vs PPAT B7	PPAT A7 vs PPAT B8	PPAT A7 vs PPAT C1	PPAT A7 vs PPAT B3	PPAT A7 vs PPAT B7	PPAT A7 vs PPAT B8	PPAT A7 vs PPAT C1
ATP M-0	4.82E-01	7.33E-01	3.45E-01	9.09E-01	7.59E-01	7.33E-01	5.76E-01	9.09E-01
ATP M-5	5.09E-01	6.10E-01	**4.74E-01**	**7.15E-01**	7.59E-01	7.33E-01	**5.76E-01**	**9.09E-01**
ATP M-OTHER	7.59E-01	4.36E-01	5.76E-01	1.66E-01	7.59E-01	7.33E-01	5.76E-01	4.99E-01

Table S4.14 ^{13}C-Isotope percent labeling from glucose statistical significance for figure S4.9 – papillary subtype. Data represent means and S.D. of 3 replicates. Highlighted values are statistically significant with adjusted p value < 0.05

4.9 REFERENCES

REFERENCES

1. Torre LA, Siegel RL, Ward EM, Jemal A (2016) Global cancer incidence and mortality rates and trends—an update. Cancer Epidemiology and Prevention Biomarkers 25 (1):16-27

2. Althuis MD, Dozier JM, Anderson WF, Devesa SS, Brinton LA (2005) Global trends in breast cancer incidence and mortality 1973–1997. International journal of epidemiology 34 (2):405-412

3. Senkus E, Kyriakides S, Ohno S, Penault-Llorca F, Poortmans P, Rutgers E, Zackrisson S, Cardoso F (2015) Primary breast cancer: ESMO Clinical Practice Guidelines for diagnosis, treatment and follow-up. Annals of oncology 26 (suppl_5):v8-v30

4. Perou CM, Sorlie T, Eisen MB, van de Rijn M, Jeffrey SS, Rees CA, Pollack JR, Ross DT, Johnsen H, Akslen LA, Fluge O, Pergamenschikov A, Williams C, Zhu SX, Lonning PE, Borresen-Dale AL, Brown PO, Botstein D (2000) Molecular portraits of human breast tumours. Nature 406 (6797):747-752. doi:10.1038/35021093

5. Bastien RR, Rodríguez-Lescure Á, Ebbert MT, Prat A, Munárriz B, Rowe L, Miller P, Ruiz-Borrego M, Anderson D, Lyons B (2012) PAM50 breast cancer subtyping by RT-qPCR and concordance with standard clinical molecular markers. BMC medical genomics 5 (1):44

6. Coates AS, Winer EP, Goldhirsch A, Gelber RD, Gnant M, Piccart-Gebhart M, Thürlimann B, Senn H-J, Members P, André F (2015) Tailoring therapies—improving the management of early breast cancer: St Gallen International Expert Consensus on the Primary Therapy of Early Breast Cancer 2015. Annals of oncology 26 (8):1533-1546

7. Early Breast Cancer Trialists' Collaborative G (2005) Effects of chemotherapy and hormonal therapy for early breast cancer on recurrence and 15-year survival: an overview of the randomised trials. The Lancet 365 (9472):1687-1717. doi:10.1016/s0140-6736(05)66544-0

8. Gonzalez-Angulo AM, Morales-Vasquez F, Hortobagyi GN (2007) Overview of Resistance to Systemic Therapy in Patients with Breast Cancer. In: Yu D, Hung M-C (eds) Breast Cancer Chemosensitivity. Springer New York, New York, NY, pp 1-22. doi:10.1007/978-0-387-74039-3

9. Ogrodzinski MP, Bernard JJ, Lunt SY (2017) Deciphering metabolic rewiring in breast cancer subtypes. Transl Res 189:105-122. doi:10.1016/j.trsl.2017.07.004

10. Luengo A, Gui DY, Vander Heiden MG (2017) Targeting metabolism for cancer therapy. Cell chemical biology 24 (9):1161-1180. doi:10.1016/j.chembiol.2017.08.028

11. Hanahan D, Weinberg RA (2011) Hallmarks of cancer: the next generation. Cell 144 (5):646-674. doi:10.1016/j.cell.2011.02.013

12. Warburg O (1925) The metabolism of carcinoma cells. The Journal of Cancer Research 9 (1):148-163

13. Freedland SJ, Mavropoulos J, Wang A, Darshan M, Demark-Wahnefried W, Aronson WJ, Cohen P, Hwang D, Peterson B, Fields T (2008) Carbohydrate restriction, prostate cancer growth, and the insulin-like growth factor axis. The Prostate 68 (1):11-19

14. Poff A, Koutnik AP, Egan KM, Sahebjam S, D'Agostino D, Kumar NB Targeting the Warburg effect for cancer treatment: Ketogenic diets for management of glioma. In: Seminars in cancer biology, 2019. Elsevier, pp 135-148

15. Pelicano H, Martin D, Xu R, and, Huang P (2006) Glycolysis inhibition for anticancer treatment. Oncogene 25 (34):4633-4646

16. Sørlie T, Perou CM, Tibshirani R, Aas T, Geisler S, Johnsen H, Hastie T, Eisen MB, van de Rijn M, Jeffrey SS, Thorsen T, Quist H, Matese JC, Brown PO, Botstein D, Lønning PE, Børresen-Dale A-L (2001) Gene expression patterns of breast carcinomas distinguish tumor subclasses with clinical implications. Proceedings of the National Academy of Sciences of the United States of America 98 (19):10869-10874. doi:10.1073/pnas.191367098

17. Ellis I, Galea M, Broughton N, Locker A, Blamey R, Elston C (1992) Pathological prognostic factors in breast cancer. II. Histological type. Relationship with survival in a large study with long-term follow-up. Histopathology 20 (6):479-489

18. Kondo M, Yamaoka T, Honda S, Miwa Y, Katashima R, Moritani M, Yoshimoto K, Hayashi Y, Itakura M (2000) The rate of cell growth is regulated by purine biosynthesis via ATP production and G1 to S phase transition. The Journal of Biochemistry 128 (1):57-64

19. Sigoillot FD, Berkowski JA, Sigoillot SM, Kotsis DH, Guy HI (2003) Cell cycle-dependent regulation of pyrimidine biosynthesis. Journal of Biological Chemistry 278 (5):3403-3409

20. Lane AN, Fan TW-M (2015) Regulation of mammalian nucleotide metabolism and biosynthesis. Nucleic acids research 43 (4):2466-2485. doi:10.1093/nar/gkv047

21. Stewart TA, Pattengale PK, Leder P (1984) Spontaneous mammary adenocarcinomas in transgenic mice that carry and express MTV/myc fusion genes. Cell 38 (3):627-637. doi:10.1016/0092-8674(84)90257-5

22. Hollern DP, Andrechek ER (2014) A genomic analysis of mouse models of breast cancer reveals molecular features of mouse models and relationships to human breast cancer. Breast Cancer Research : BCR 16 (3):R59-R59. doi:10.1186/bcr3672

23. Hollern DP, Swiatnicki MR, Andrechek ER (2018) Histological subtypes of mouse mammary tumors reveal conserved relationships to human cancers. PLoS genetics 14 (1)

24. Prat A, Parker JS, Karginova O, Fan C, Livasy C, Herschkowitz JI, He X, Perou CM (2010) Phenotypic and molecular characterization of the claudin-low intrinsic subtype of breast cancer. Breast Cancer Research 12 (5):R68. doi:10.1186/bcr2635

25. Rakha EA, Ellis IO (2009) Triple-negative/basal-like breast cancer. Pathology 41 (1):40-47

26. Ogrodzinski MP, Lunt SY (2019) Metabolomic profiling of mouse mammary tumor derived cell lines reveals targeted therapy options for cancer subtypes. bioRxiv:DOI 10.1101/796573 (Preprint posted October 796577, 792019). doi:10.1101/796573

27. Cong L, Ran FA, Cox D, Lin S, Barretto R, Habib N, Hsu PD, Wu X, Jiang W, Marraffini LA, Zhang F (2013) Multiplex Genome Engineering Using CRISPR/Cas Systems. Science 339 (6121):819-823. doi:10.1126/science.1231143

28. Shalem O, Sanjana NE, Hartenian E, Shi X, Scott DA, Mikkelson T, Heckl D, Ebert BL, Root DE, Doench JG, Zhang F (2014) Genome-Scale CRISPR-Cas9 Knockout Screening in Human Cells. Science (New York, NY) 343 (6166):84-87. doi:10.1126/science.1247005

29. Andrechek ER, Cardiff RD, Chang JT, Gatza ML, Acharya CR, Potti A, Nevins JR (2009) Genetic heterogeneity of Myc-induced mammary tumors reflecting diverse phenotypes including metastatic potential. Proceedings of the National Academy of Sciences 106 (38):16387-16392. doi:10.1073/pnas.0901250106

30. Stincone A, Prigione A, Cramer T, Wamelink MM, Campbell K, Cheung E, Olin-Sandoval V, Grüning NM, Krüger A, Tauqeer Alam M (2015) The return of metabolism: biochemistry and physiology of the pentose phosphate pathway. Biological Reviews 90 (3):927-963

31. Barrett T, Wilhite SE, Ledoux P, Evangelista C, Kim IF, Tomashevsky M, Marshall KA, Phillippy KH, Sherman PM, Holko M (2012) NCBI GEO: archive for functional genomics data sets—update. Nucleic acids research 41 (D1):D991-D995

32. Subramanian A, Tamayo P, Mootha VK, Mukherjee S, Ebert BL, Gillette MA, Paulovich A, Pomeroy SL, Golub TR, Lander ES, Mesirov JP (2005) Gene set enrichment analysis: a knowledge-based approach for interpreting genome-wide expression profiles. Proc Natl Acad Sci U S A 102 (43):15545-15550. doi:10.1073/pnas.0506580102

33. Fabregat A, Sidiropoulos K, Garapati P, Gillespie M, Hausmann K, Haw R, Jassal B, Jupe S, Korninger F, McKay S, Matthews L, May B, Milacic M, Rothfels K, Shamovsky V, Webber M, Weiser J, Williams M, Wu G, Stein L, Hermjakob H, D'Eustachio P (2016) The Reactome pathway Knowledgebase. Nucleic Acids Research 44 (Database issue):D481-D487. doi:10.1093/nar/gkv1351

34. Győrffy B, Lanczky A, Eklund AC, Denkert C, Budczies J, Li Q, Szallasi Z (2010) An online survival analysis tool to rapidly assess the effect of 22,277 genes on breast cancer prognosis using microarray data of 1,809 patients. Breast Cancer Research and Treatment 123 (3):725-731. doi:10.1007/s10549-009-0674-9

35. Brinkman EK, Chen T, Amendola M, van Steensel B (2014) Easy quantitative assessment of genome editing by sequence trace decomposition. Nucleic acids research 42 (22):e168-e168

36. Walling J (2006) From methotrexate to pemetrexed and beyond. A review of the pharmacodynamic and clinical properties of antifolates. Investigational new drugs 24 (1):37-77

37. Longley DB, Harkin DP, Johnston PG (2003) 5-Fluorouracil: mechanisms of action and clinical strategies. Nat Rev Cancer 3 (5):330-338. doi:10.1038/nrc1074

38. Karran P, Attard N (2008) Thiopurines in current medical practice: molecular mechanisms and contributions to therapy-related cancer. Nature Reviews Cancer 8 (1):24-36

39. Fox RI, Herrmann ML, Frangou CG, Wahl GM, Morris RE, Strand V, Kirschbaum BJ (1999) Mechanism of action for leflunomide in rheumatoid arthritis. Clinical Immunology 93 (3):198-208

40. Xu X, Williams JW, Shen J, Gong H, Yin D-P, Blinder L, Elder RT, Sankary H, Finnegan A, Chong AS-F (1998) In vitro and in vivo mechanisms of action of the antiproliferative and immunosuppressive agent, brequinar sodium. The Journal of Immunology 160 (2):846-853

41. Zhang N, Yin Y, Xu S-J, Chen W-S (2008) 5-Fluorouracil: mechanisms of resistance and reversal strategies. Molecules 13 (8):1551-1569

42. Klanova M, Lorkova L, Vit O, Maswabi B, Molinsky J, Pospisilova J, Vockova P, Mavis C, Lateckova L, Kulvait V (2014) Downregulation of deoxycytidine kinase in cytarabine-resistant mantle cell lymphoma cells confers cross-resistance to nucleoside analogs gemcitabine, fludarabine and cladribine, but not to other classes of anti-lymphoma agents. Molecular cancer 13 (1):159

43. Liu Y-C, Li F, Handler J, Huang CRL, Xiang Y, Neretti N, Sedivy JM, Zeller KI, Dang CV (2008) Global regulation of nucleotide biosynthetic genes by c-Myc. PloS one 3 (7)

44. Stine ZE, Walton ZE, Altman BJ, Hsieh AL, Dang CV (2015) MYC, metabolism, and cancer. Cancer discovery 5 (10):1024-1039. doi:10.1158/2159-8290.CD-15-0507

45. Nesbit CE, Tersak JM, Prochownik EV (1999) MYC oncogenes and human neoplastic disease. Oncogene 18 (19):3004-3016

46. Deming SL, Nass SJ, Dickson RB, Trock BJ (2000) C-myc amplification in breast cancer: a meta-analysis of its occurrence and prognostic relevance. British Journal of Cancer 83 (12):1688-1695. doi:10.1054/bjoc.2000.1522

47. Brown KK, Spinelli JB, Asara JM, Toker A (2017) Adaptive Reprogramming of De Novo Pyrimidine Synthesis Is a Metabolic Vulnerability in Triple-Negative Breast Cancer. Cancer Discovery 7 (4):391

48. Wang X, Yang K, Xie Q, Wu Q, Mack SC, Shi Y, Kim LJ, Prager BC, Flavahan WA, Liu X (2017) Purine synthesis promotes maintenance of brain tumor initiating cells in glioma. Nature neuroscience 20 (5):661

49. Di Virgilio F, Adinolfi E (2017) Extracellular purines, purinergic receptors and tumor growth. Oncogene 36 (3):293-303

50. Halbrook CJ, Pontious C, Kovalenko I, Lapienyte L, Dreyer S, Lee H-J, Thurston G, Zhang Y, Lazarus J, Sajjakulnukit P (2019) Macrophage-released pyrimidines inhibit gemcitabine therapy in pancreatic cancer. Cell metabolism 29 (6):1390-1399. e1396

51. Noji T, Karasawa A, Kusaka H (2004) Adenosine uptake inhibitors. European journal of pharmacology 495 (1):1-16

52. Mackey JR, Mani RS, Selner M, Mowles D, Young JD, Belt JA, Crawford CR, Cass CE (1998) Functional nucleoside transporters are required for gemcitabine influx and manifestation of toxicity in cancer cell lines. Cancer research 58 (19):4349-4357

53. Turashvili G, Brogi E (2017) Tumor heterogeneity in breast cancer. Frontiers in medicine 4:227

54. Hammond ME, Hayes DF, Dowsett M, Allred DC, Hagerty KL, Badve S, Fitzgibbons PL, Francis G, Goldstein NS, Hayes M, Hicks DG, Lester S, Love R, Mangu PB, McShane L, Miller K, Osborne CK, Paik S, Perlmutter J, Rhodes A, Sasano H, Schwartz JN, Sweep FC, Taube S, Torlakovic EE, Valenstein P, Viale G, Visscher D, Wheeler T, Williams RB, Wittliff JL, Wolff AC (2010) American Society of Clinical Oncology/College of American Pathologists guideline recommendations for immunohistochemical testing of estrogen and progesterone receptors in breast cancer. J Clin Oncol 28. doi:10.1200/jco.2009.25.6529

55. Morgan DA, Refalo NA, Cheung KL (2011) Strength of ER-positivity in relation to survival in ER-positive breast cancer treated by adjuvant tamoxifen as sole systemic therapy. The Breast 20 (3):215-219

56. Mitra A, Mishra L, Li S (2013) Technologies for deriving primary tumor cells for use in personalized cancer therapy. Trends in biotechnology 31 (6):347-354. doi:10.1016/j.tibtech.2013.03.006

57. Ogrodzinski MP, Teoh ST, Yu L, Broadwater D, Ensink E, Lunt SY (2019) Measuring the Nutrient Metabolism of Adherent Cells in Culture. In: Fendt SM, Lunt S (eds) Methods Mol Biol, vol 1862. Methods Mol Biol. Humana Press, New York, NY, Metabolic Signaling. Methods Mol Biol, pp 37-52. doi:10.1007/978-1-4939-8769-6_3

58. Melamud E, Vastag L, Rabinowitz JD (2010) Metabolomic Analysis and Visualization Engine for LC−MS Data. Analytical Chemistry 82 (23):9818-9826. doi:10.1021/ac1021166

59. De Hoon MJ, Imoto S, Nolan J, Miyano S (2004) Open source clustering software. Bioinformatics 20 (9):1453-1454. doi:10.1093/bioinformatics/bth078

60. Saldanha AJ (2004) Java Treeview—extensible visualization of microarray data. Bioinformatics 20 (17):3246-3248. doi:10.1093/bioinformatics/bth349

61. Liberzon A, Birger C, Thorvaldsdóttir H, Ghandi M, Mesirov JP, Tamayo P (2015) The molecular signatures database hallmark gene set collection. Cell systems 1 (6):417-425

62. Ma J, Köster J, Qin Q, Hu S, Li W, Chen C, Cao Q, Wang J, Mei S, Liu Q (2016) CRISPR-DO for genome-wide CRISPR design and optimization. Bioinformatics 32 (21):3336-3338

63. Millard P, Letisse F, Sokol S, Portais JC (2012) IsoCor: correcting MS data in isotope labeling experiments. Bioinformatics 28 (9):1294-1296. doi:10.1093/bioinformatics/bts127

CHAPTER 5.

SUMMARY AND FUTURE DIRECTIONS

5.1 SUMMARY

Breast cancer heterogeneity provides significant challenges for patient care. The knowledge gained from academic research will provide clinicians with the necessary tools to treat every patient. Through my thesis work, I have contributed to our understanding of breast cancer heterogeneity by investigating metabolic vulnerabilities in histologic subtypes derived from the MMTV-Myc model. I have identified key differences in several central carbon metabolic pathways including glutathione metabolism, the TCA cycle, and nucleotide metabolism. Additionally, by integrating powerful genomic and metabolomic techniques, I was able to further identify subtype-specific preferences for parallel pathways of nucleotide biosynthesis. I have demonstrated substantial efficacy through rational targeting of vulnerable metabolic pathways specific to EMT and papillary subtypes, thus demonstrating the potential utility of targeting metabolism to guide therapy for different subtypes of breast cancer. My work has significant translational potential, as the EMT subtype derived from the MMTV-Myc mouse model correlate to the claudin-low subtype of human breast cancer, and the papillary subtype better models Myc amplification, a common feature in human breast cancer as discussed in chapters 1, 3, and 4. My work also raises several important questions including: 1) What other metabolic pathways are important for these subtypes? 2) Will targeting the pathways I have identified using approved therapeutics be sufficient to reduce tumor growth *in vivo*? And 3) How translatable are these findings to human breast cancer subtypes? Answering these questions will take considerable effort but will also further improve our understanding of how to target metabolic vulnerabilities in breast cancer subtypes.

5.2 FUTURE DIRECTIONS

5.2.1 EVALUATION WITH ADDITIONAL METABOLOMICS TECHNIQUES

There are still many known and unknown metabolites that have yet to be investigated in breast cancer subtypes. Throughout this dissertation we used a targeted mass spectrometry method that is well suited to evaluate polar compounds including nucleotides and central carbon metabolites as discussed in the preceding chapters. However, this approach is somewhat limited in that we specifically measure metabolites from a list of known compounds. Now that we have demonstrated the power of using metabolomics to identify subtype-specific metabolic vulnerabilities, we can expand upon our findings by using an untargeted metabolomics method to substantially increase the range of compounds evaluated in each sample. These experiments would be straightforward to perform, as we can easily generate additional samples from EMT and papillary cell lines or tumors, our current extraction techniques are compatible with untargeted methods, and we have access to several mass spectrometers with untargeted capabilities in the mass spectrometry and metabolomics core facility. I expect this untargeted analysis would not only validate our targeted findings but would further uncover many new metabolites of interest between the EMT and papillary subtypes – potentially revealing new metabolic pathways of interest. The main challenge of these untargeted analyses would be in developing a workflow for identifying unknown metabolites, and assigning these metabolites to specific pathways of interest. After addressing this obstacle, the same genomic and pharmacologic approaches as detailed in previous chapters could be used to test the importance of these new metabolites and pathways in EMT and papillary tumors or cell lines.

Metabolites analyzed in this work were collected from the polar phase, which precludes a wide range of potentially interesting non-polar compounds including fatty acids and lipids. As discussed in chapter 1, lipid metabolism is one area that has shown promising subtype-specific trends such as, ER+ breast cancer increasing cholesterol biosynthesis, HER2+ breast cancer increasing fatty acid biosynthesis, and TNBC increasing cholesterol uptake. In order to develop a truly comprehensive understanding of the metabolic differences between the EMT and papillary subtypes we should attempt to expand upon our current knowledge using techniques to study a wider range of metabolites.

Beyond expanding analytical techniques to measure more metabolites, we could also further develop our current findings by extracting metabolites in a more refined manner. Currently we extract metabolites from flash frozen tumor sections, which will include a mixture of both intracellular metabolites and extracellular metabolites from the tumor microenvironment. We could refine this to selectively study extracellular metabolites by centrifuging freshly collected tumor pieces over a fine mesh filter to collect an interstitial fluid filtrate, then process this filtrate using targeted and/or untargeted methods to identify compounds that are consumed and produced by EMT and papillary tumors. This could be achieved by measuring the abundance of each compound relative to serum samples from both tumor bearing and non-tumor bearing mice to establish how metabolite levels change in the tumor microenvironment and in the general circulation of the tumor bearing mouse compared to normal levels. For example, we would likely find decreased abundance of salvageable nucleosides and nucleobases in filtrates derived from the EMT subtype, reflecting the metabolic preference for nucleotide salvage in the

EMT subtype as described in chapter 4. It would also be interesting to use this approach to identify subtype-specific biomarkers. Little is currently known about metabolites/compounds that are released by EMT and papillary tumors specifically, but identifying subtype-specific metabolic biomarkers has the potential to revolutionize both cancer diagnostics and long term monitoring of patients following treatment. Studying metabolic biomarkers using mouse models could help accomplish this.

5.2.2 IN VIVO DRUG TREATMENT STUDIES

The next important direction is to follow up both *in vitro* drug treatment studies and *in vivo* gene knock-out studies with *in vivo* validation using metabolism-targeting drugs. This would ideally be done using currently approved drugs, and the compounds described in chapter 3 should serve as a starting point for future *in vivo* studies. It would also be interesting to pharmacologically inhibit nucleotide salvage based on our findings presented in chapter 4. Given the lack of drugs that target nucleotide salvage pathways, we could screen compound libraries to identify inhibitors of nucleotide salvage enzymes such as APRT and UPP1. This compound identification process may result in discovery of new therapeutics to treat cancer.

Assuming that selective inhibitors of each metabolic pathway can be identified, there are still several potential hurdles that could complicate these studies. First, it is possible that metabolic vulnerabilities identified in the *in vitro* context do not always translate *in vivo*. This is because cell culture conditions and conditions within a tumor are very different from one another, especially in terms of nutrient availability. However, *in vitro* findings are still valuable, as demonstrated by our findings regarding differences in nucleotide biosynthesis detailed in chapters 3 and 4, which are consistent between *in*

vitro and *in vivo* settings. Second, the optimal dose for each compound would need to be individually determined. The use of approved compounds would reduce this challenge by providing dosing guidelines to use as a starting point, but optimization would still be required to identify the most effective concentration for the EMT and papillary subtypes. Third, targeting a single metabolic pathway may be insufficient to inhibit tumor growth. This issue reflects the interconnected nature of metabolism, as cancer cells may upregulate a parallel metabolic pathway in response to inhibition of a preferred metabolic pathway. Addressing this concern leads to additional directions of research, as studying the reactive metabolism of drug treated cells could facilitate the development of targeted combination therapies.

5.2.3 TRANSLATION TO HUMAN DISEASE

Arguably the most important next step for this work is to investigate the translatability of these findings into human disease. As discussed in chapters 3 and 4, the greatest translational potential for these findings stems from the similarities between the EMT subtype in the MMTV-Myc mouse model and the claudin-low subtype of human breast cancer. Claudin-low breast cancer currently lacks targeted therapy options and can therefore greatly benefit from identification of novel druggable metabolic targets. Based on the findings presented in chapters 3 and 4, glutathione biosynthesis, TCA cycle metabolism, and nucleotide salvage are strong candidates for further study focused on treating claudin-low breast cancer.

The next step toward translating our findings to human disease should include examination of gene expression data of claudin-low cell lines and tumors to determine whether they exhibit expression differences in genes related to these pathways compared

to other breast cancer subtypes. Follow up experiments would examine metabolic profiles of claudin-low samples in comparison to other breast cancer subtypes to validate gene expression findings and identify any potential metabolic vulnerabilities that were not fully captured by the genomic analysis. Further experiments will evaluate the significance of these metabolic pathways in models of claudin-low breast cancer *in vitro* and *in vivo* using metabolism-targeting drugs and/or genetic manipulations as described earlier for the EMT subtype. Once fully investigated, this line of research could yield new therapeutic strategies to treat breast cancer, which are currently needed to improve our ability to provide care for patients with this deadly disease.

In conclusion, this work makes significant progress towards identification of subtype-specific metabolic vulnerabilities and demonstrates the feasibility of targeting metabolism to treat breast cancer. Subtype-specific metabolic vulnerabilities in breast cancer are not currently used to guide therapy; the work presented here demonstrates that metabolic weaknesses can be targeted to stop tumor growth and should be incorporated into therapy. This work has the potential to improve outcomes for breast cancer patients by providing a foundation for future translational research based on targeting metabolic vulnerabilities in breast cancer subtypes.